



POLITECHNIKA POZNAŃSKA
WYDZIAŁ INŻYNIERII MATERIAŁOWEJ I FIZYKI
TECHNICZNEJ

Instytut Badań Materiałowych i Inżynierii Kwantowej
Zakład Inżynierii i Metrologii Kwantowej

Marcin Suski

ROZPRAWA DOKTORSKA

*Wyznaczanie kanałów fluorescencji w atomach
terbu i europu na podstawie pomiaru stałych
struktury nadsubtelnej i czynników Landégo g_J*

Promotor: **dr hab. Bogusław Furmann, prof. PP**

Dyscyplina: Inżynieria materiałowa

Poznań, 2023

*Składam serdeczne podziękowania
mojemu promotorowi, Panu dr. hab.
Bogusławowi Furmannowi, prof. PP oraz
Pani dr hab. Danucie Stefańskiej za
wsparcie oraz pomoc okazaną w trakcie
realizacji niniejszej pracy.*

*Pragnę również podziękować
współautorom publikacji stanowiących
niniejszą rozprawę, w szczególności
mgr. inż. Maciejowi Chomskiemu, za
włożoną pracę.*

ABSTRACT

The aim of the present Ph.D. dissertation, which constitutes a collection of six scientific publications, was to determine the fluorescence channels, the A and B hyperfine structure constants and also Landé g_J factors for the known energy levels in terbium and europium atoms. These quantities are the characteristic parameters, describing the particular energy levels; they are important for the existing and potential applications, based on the fluorescent and the magnetic properties of the investigated atoms.

The investigations of the hyperfine structure and its splitting due to the Zeeman effect were carried out with the use of the laser induced fluorescence method in the hollow cathode discharge lamp, with phase-sensitive signal detection.

In four of the presented publications, concerning the terbium atom:

- the hyperfine structure constants A and B for 69 odd-parity energy levels, and Landé g_J factors for 37 energy levels, 17 of which belonged to the odd-parity configurations and 20 to the even-parity configurations, were determined,
- the values of the A and B constants were corrected for 6 even-parity energy levels, and the literature values of the g_J factors for 32 energy levels – 15 even-parity and 17 odd-parity ones, were verified.

In two publications, concerning the europium atom:

- the hyperfine structure constants A and B , and the isotope shifts for 26 even-parity energy levels, as well as Landé g_J factors for 23 energy levels, 7 of which belonged to the even-parity configurations and 16 to the odd-parity configurations, were determined,
- the hitherto available literature values of the A and B constants for 3 even-parity energy levels were slightly adjusted.

The results obtained within this work constitute a valuable extension of the available databases, concerning the structure of both investigated elements. They also increase the possibility of the use of these materials in commercial and research applications.

STRESZCZENIE

Celem niniejszej rozprawy, będącej zbiorem sześciu publikacji było poszukiwanie kanałów fluorescencji oraz wyznaczenie stałych struktury nadsubtelnej A i B , a także czynników Landégo g_J dla znanych poziomów energetycznych w atomie terbu i europu. Wielkości te stanowią charakterystyczne parametry opisujące dany poziom energetyczny, i są istotne z punktu widzenia istniejących oraz potencjalnych zastosowań obu badanych materiałów, wykorzystujących ich własności fluorescencyjne, a także magnetyczne.

Badania struktury nadsubtelnej oraz jej rozszczepienia pod wpływem efektu Zeemana prowadzono wykorzystując metodę laserowo indukowanej fluorescencji w lampie wyładowczej z katodą wnąkową, z fazoczułą detekcją sygnału.

W ramach czterech z przedłożonych publikacji, dotyczących atomu terbu:

- wyznaczono stałe struktury nadsubtelnej A i B dla 69 poziomów, należących do konfiguracji nieparzystych, oraz czynniki Landégo g_J dla 37 poziomów, z których 17 należy do konfiguracji parzystych, a 20 do nieparzystych,
- skorygowano stałe A i B dla 6 poziomów parzystych, oraz zweryfikowano dostępne w literaturze wartości czynników g_J dla 32 poziomów – 15 parzystych i 17 nieparzystych.

W dwóch pracach dotyczących atomu europu:

- wyznaczono stałe struktury nadsubtelnej A i B oraz przesunięcia izotopowe dla 26 poziomów energetycznych, należących do konfiguracji parzystych, oraz czynniki Landégo g_J dla 23 poziomów, z których 7 należy do konfiguracji parzystych, a 16 do nieparzystych,
- w niewielkim stopniu skorygowano stałe A i B dla 3 poziomów parzystych.

Uzyskane wyniki stanowią cenne rozszerzenie dostępnych baz danych struktury obu pierwiastków, a także zwiększają możliwości wykorzystania obu materiałów w zastosowaniach komercyjnych oraz badawczych.

SPIS TREŚCI

ABSTRACT.....	3
STRESZCZENIE.....	4
1. WSTĘP	6
2. METODOLOGIA	11
2.1. Laserowo indukowana fluorescencja.....	11
2.2. Badania struktury nadsubtelnej atomów	14
2.3. Badania rozszczepienia zeemanowskiego struktury nadsubtelnej.....	19
3. OPROGRAMOWANIE.....	24
3.1. Program do symulacji możliwych przejść	24
3.2. Program do rejestracji widm.....	24
3.3. Program „Fitter”	25
3.4. Program do wyznaczania czynników Landégo g_J	27
4. OPIS PRAC WCHODZĄCYCH W SKŁAD ROZPRAWY	29
4.1. Prace dotyczące atomu terbu	29
4.2. Prace dotyczące atomu europu	31
5. PODSUMOWANIE.....	34
LITERATURA	36
ZAŁĄCZNIKI	41

1. WSTĘP

Materiałami badanymi w niniejszej pracy są terb i europ – pierwiastki z grupy lantanowców. Są one zaliczane do metali ziem rzadkich, które coraz bardziej zyskują na znaczeniu jako surowce o charakterze strategicznym w gospodarce opartej na wiedzy [1].

Terb jest pierwiastkiem, znajdującym się nieco powyżej środka grupy lantanowców, występującym jako srebrzystobiały, miękki metal. Posiada tylko jeden stabilny izotop $^{159}_{65}\text{Tb}$ oraz względnie niski spin jądrowy $I = 3/2$. Wartości magnetycznego momentu dipolowego oraz elektrycznego momentu kwadrupolowego jądra europu wynoszą odpowiednio: $\mu = +2,014(4) \text{ nm}$ i $Q = +1,432(8) \text{ b}$ [2].

Ze względu na swoje właściwości fluorescencyjne terb jest wykorzystywany przede wszystkim do produkcji zielonych luminoforów do lamp i wyświetlaczy [1]. Natomiast właściwości magnetyczne terbu umożliwiają jego zastosowanie w elementach wykonawczych (aktuatorach), sonarach czy różnego rodzaju czujnikach. Oprócz zastosowań komercyjnych, terb może być wykorzystany także w nauce i medycynie – w formie biochemicznych sond fluorescencyjnych [3] lub radioizotopów w celach diagnostycznych i terapeutycznych [4]. Obecnie trwają badania nad możliwością zastosowania terbu w komputerach kwantowych. W roku 2020 ukazała się praca autorstwa R. L. Smitha *et al.* [5], w której zaproponowano możliwość wpływania na spin jądra domieszki terbu w pojedynczej molekułe poprzez wykorzystanie dynamicznego efektu Starka na strukturze nadsubtelnej. W zakresie inżynierii kwantowej terb może być potencjalnym kandydatem do realizowania chłodzenia laserowego i pułapkowania w pułapkach magnetoptycznych (*MOT*), oraz badania dryfu czasowego stałej α .

Zarówno terb jak i europ mogą być wykorzystywane jako domieszki fluorescencyjne w banknotach, chroniące je przed fałszerstwem. Domieszki europu są już z powodzeniem używane jako zabezpieczenie banknotów euro, gdzie pod wpływem promieniowania UV emitują światło czerwone. Rozwinięciem tego pomysłu mogłoby być wzbudzenie charakterystycznych linii widmowych danego pierwiastka za pomocą specjalnie do nich dostrojonych wiązek laserowych. Tym samym osoba kontrolująca dany banknot miałaby pewność, że jest on domieszkowany konkretnym pierwiastkiem, co jeszcze bardziej utrudniłoby próby fałszerstwa.

Początki badań nad strukturą nadsubtelną atomu terbu można datować na lata 60te XX wieku. Pierwszą istotną pracą była publikacja S. P. Davisa, w której zbadano rozszczepienie nadsubtelne 232 linii widmowych [6]. Następnie ukazało się opracowanie

C. Arnoult i S. Gerstenkorna, gdzie wyznaczono stałe struktury nadsubtelnej dla 3 poziomów energetycznych, należących do konfiguracji $4f^9 6s^2$ [7]. Bardzo istotne okazały się trzy prace autorstwa W. J. Childsa [8-10], z których pierwsza wydana została w roku 1970. Zawierały one wyznaczone eksperymentalnie stałe struktury nadsubtelnej dla kilkunastu najniższych leżących poziomów energetycznych. W tym samym roku ukazała się również praca, w której skorygowany został błędnie dotychczas wyznaczony poziom podstawowy [11]. Powyższe pozycje stanowiły dobrą bazę do dalszych badań struktury nadsubtelnej atomu terbu, jednak dostępna wiedza nie została w żaden istotny sposób poszerzona aż do roku 2015, w którym temat został podjęty przez zespół badawczy, którego autor niniejszej rozprawy jest obecnie częścią.

Pierwsze próby wyznaczania czynników Landégo g_J na podstawie analizy efektu Zeemana przypadają mniej więcej na ten sam okres, co pierwsze pomiary stałych struktury nadsubtelnej. W pracach I. Bendera *et al.* oraz C. Arnoulta, opublikowanych w latach odpowiednio 1963 i 1966 [7, 12], przedstawione zostały wartości czynników g_J dla 17 poziomów energetycznych z dokładnością do trzeciego miejsca po przecinku. Precyzja wyznaczenia tych wartości została następnie zwiększona do piątego miejsca po przecinku w dwóch publikacjach W. J. Childsa, wydanych kilka lat później [8, 13]. Istotna była również seria sześciu prac P. F. Klinkenberga i E. Meinders, gdzie wyznaczono czynniki Landégo dla 46 poziomów energetycznych [14-19].

Europ, podobnie jak terb, również należy do pierwiastków z szeregu lantanowców i znajduje się w środku szeregu. Europ ma formę srebrzystobiałego metalu. Posiada dwa stabilne izotopy: $^{151}_{63}\text{Eu}$ oraz $^{153}_{63}\text{Eu}$, których naturalne występowanie jest równe odpowiednio 47,8% i 52,2%. Spin jądrowy obu izotopów wynosi $I = 5/2$. Magnetyczny moment dipolowy jądra izotopu ^{151}Eu ma wartość $3,4717(6) \text{ nm}$, natomiast jądra izotopu ^{153}Eu $1,5324(3) \text{ nm}$ [2]. W przypadku elektrycznych momentów kwadrupolowych, rozrzut tych wartości jest znaczny, w zależności od sposobu ich wyznaczenia. Zakłada się jednak, że stosunek wartości $Q(^{153}\text{Eu})/Q(^{151}\text{Eu})$ wynosi $2,5516(12)$.

Do popularnych zastosowań europu należą wyświetlacze ciekłokrystaliczne, oświetlenie fluorescencyjne oraz diagnostyka medyczna [1] – gdzie wykorzystywany jest w scyntylatorach. Jak wspomniano wcześniej, domieszki europu stanowią również zabezpieczenia banknotów euro. Ze względu na duży przekrój czynny na pochłanianie neutronów, europ używany jest w prętach kontrolnych w reaktorach jądrowych. Możliwe

jest także pułapkowanie atomów europu we wspomnianych już pułapkach magnetoptycznych, którego realizacja opisana jest w pracach [20, 21]. Ponadto, w ubiegłym roku ukazała się praca [22], w której przedstawiono kryształy molekularne europu jako obiecujący materiał do uzyskania interfejsu foton-spin do zastosowania w komputerach kwantowych.

Na przestrzeni ostatniego wieku ukazało się ponad 100 prac dotyczących badań struktury atomu europu. Pierwsze prace eksperymentalne, w których wyznaczono wartości stałych struktury nadsubtelnej ukazały się na początku lat 70-tych. Przykładem może być praca J. Kuhla [23] z roku 1971, gdzie wyznaczone zostały wartości stałych A i B dla jednego poziomu energetycznego w obu stabilnych izotopach wykorzystując absorpcję w strumieniu atomowym w sferycznym interferometrze Fabry-Perot.

Duża część prac zorientowana była na wyznaczanie wartości przesunięć izotopowych. Ważną okazała się publikacja J. Bauche i R. J. Champeau [24], w której zaproponowano parametryzację przesunięć i badania efektów drugiego rzędu (*CSO – Crossed Second-Order*) wykorzystując współczynniki kątowe, otrzymane na podstawie analizy struktury subtelnej. W przypadku poziomów, gdzie nie dochodzi do mieszania konfiguracji, wartości przesunięć izotopowych i parametrów *CSO* wyznaczone w ten sposób wykazywały dużą zgodność z wartościami obliczonymi metodą *ab initio*.

Do przypisania poziomu energetycznego do danej konfiguracji zazwyczaj wykorzystuje się wartości czynników Landégo g_J i stałe struktury nadsubtelnej, jednak niekiedy bywa to niewystarczające, szczególnie w przypadku poziomów, dla których dane wartości są do siebie zbliżone. W pierwiastkach posiadających kilka izotopów parzystych, a nie posiadających izotopów nieparzystych, lub w których rozszczepienie nadsubtelne było zanedbywalnie małe, wykorzystywano w tym celu przesunięcie izotopowe. Takie rozwiązanie zostało zaproponowane w pracy D. Skroka i R. Winklera do próby klasyfikacji poziomów należących do konfiguracji parzystych w europie [25], jednak ze względu na ograniczenia metody eksperymentalnej oraz wynikające z braku danych empirycznych w ówczesnym czasie nie dawało ono w pełni wiarygodnych rezultatów. Metoda ta została w późniejszym czasie rozwinięta o analizę semi-empiryczną w pracy [26].

W przeciwieństwie do badań struktury nadsubtelnej i przesunięć izotopowych w atomie europu, prac dotyczących wyznaczania czynników Landégo g_J jest stosunkowo niewiele. Zdecydowana większość wartości wyznaczonych eksperymentalnie znajduje

się w opracowaniu G. Smitha i F. S. Tomkinsa [27], zawierającym dane dla ponad 200 parzystych poziomów energetycznych oraz poziomu podstawowego.

Obserwowany w ostatnich latach niezwykle dynamiczny rozwój metod laserowego chłodzenia i pułapkowania jonów oraz atomów umożliwia potraktowanie schłodzonej i uwięzionej w pułapce chmury atomów lub jonów jako nowej klasy materiału kwantowego. Taki materiał może zostać wykorzystany na przykład jako „wahadło” w zegarach atomowych. Podobnie jak o dokładności klasycznego zegara z wahadłem decyduje mała rozszerzalność termiczna materiału, z którego wykonane jest wahadło, na dokładność zegara atomowego zasadniczy wpływ będą mieć: częstotliwość przejścia wykorzystywanego jako wzorzec, szerokość naturalna linii, stopień schłodzenia atomów (jonów). Wszystkie te parametry wynikają z pomiarów podstawowych właściwości poziomów elektronowych takich jak energia poziomu, czynnik Landégo g_J , stałe struktury nadsubtelnej A i B , przesunięcie izotopowe jeżeli pierwiastek ma więcej niż jeden izotop oraz czas życia. Poszukiwanie optymalnych „przejsć zegarowych” jest zatem zagadnieniem bardzo złożonym i wymaga jak najpełniejszej informacji o strukturze poziomów elektronowych.

Schłodzona chmura jonów jest też jednym z typowych materiałów do budowy komputera kwantowego. Również w tym wypadku jakość obliczeń kwantowych zależy w dużej mierze od parametrów poziomów elektronowych użytych do chłodzenia i adresowania kubitów (bitów kwantowych). Podobna jest rola atomów w pamięciach kwantowych realizowanych w oparciu o zjawisko optycznie wymuszonej przezroczystości, w wytwarzaniu kondensatu Bosego-Einsteina czy konstrukcji koherentnego źródła fal atomowych (atomowego odpowiednika lasera).

Celem niniejszej pracy było poszukiwanie kanałów fluorescencji i eksperymentalne wyznaczenie stałych struktury nadsubtelnej A i B oraz dodatkowo czynników Landégo g_J znanych poziomów energetycznych atomów obu pierwiastków poprzez badania te same struktury oraz jej rozszczepienia pod wpływem efektu Zeemana. Oba pierwiastki posiadają bardzo bogatą strukturę nadsubtelną, a uzyskane dane są niezbędne do wytwarzania materiałów kwantowych na bazie badanych atomów. Są one także istotne z punktu widzenia istniejących, oraz potencjalnych możliwości wykorzystania badanych materiałów, w szczególności w oparciu o ich właściwości fluorescencyjne, jak i magnetyczne. Ponadto, stanowią one znaczące poszerzenie dostępnej wiedzy o strukturze atomowej obu pierwiastków, która pomimo zauważalnego postępu w badaniach nadal pozostaje daleka od kompletnej. Stałe struktury nadsubtelnej

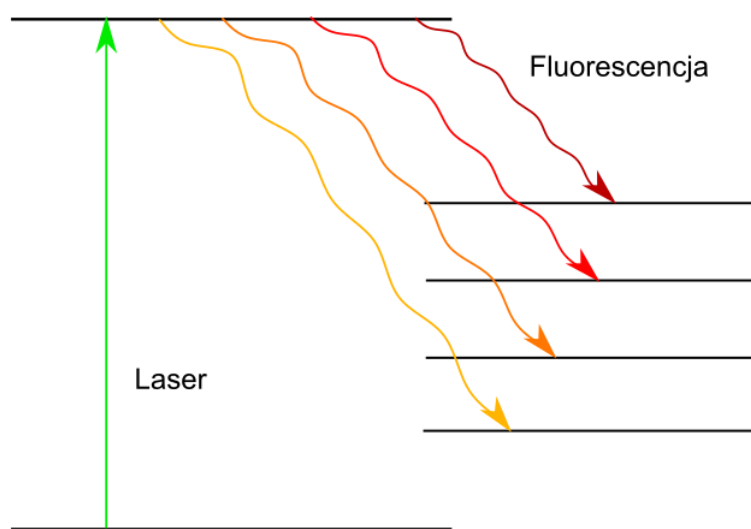
i czynniki Landégo, a także wartości przesunięć izotopowych są charakterystycznymi parametrami opisującymi dany poziom energetyczny. Dodatkowo znacząco ułatwiają poprawne przypisanie poziomu do określonej konfiguracji. Powiększanie istniejących baz danych ma duże znaczenie dla dalszego rozwoju prac badawczych, prowadzonych w zakresie inżynierii i metrologii kwantowej – zarówno doświadczalnych, których przykłady podano powyżej, jak i teoretycznych, takich jak semi-empiryczny opis struktury atomowej. Do tego typu analiz niezbędna jest jak największa ilość danych eksperymentalnych, zwłaszcza w przypadku pierwiastków takich jak lantanowce, w których na skutek kolapsu funkcji falowej orbitalu $4f$ wiele poziomów w różnych konfiguracjach ma zbliżone wartości energii. Ponadto, gdy dochodzi do mieszania konfiguracji, wykorzystanie obliczeń semi-empirycznych do parametryzacji przesunięć izotopowych i parametrów CSO pozwala na uzyskanie dużo bardziej precyzyjnych wyników niż metoda *ab initio*. Szczegółowa wiedza na temat struktury atomu danego pierwiastka jest także istotna z punktu widzenia astrofizyki, gdzie wykorzystywana jest np. do określania składu gwiazd. Jeżeli pierwiastek posiada strukturę nadsubtelną, jest to widoczne w liniach widma absorpcyjnego danej gwiazdy.

W ramach sześciu publikacji przedłożonych jako niniejsza rozprawa prowadzono badania struktury nadsubtelnej terbu i europu wykorzystując metodę laserowo indukowanej fluorescencji w lampie wyładowczej z katodą wnękową. Bardziej szczegółowe opisy stosowanej techniki i używanej aparatury pomiarowej znajdują się w kolejnych rozdziałach pracy. W rezultacie na podstawie analizy zarejestrowanych linii widmowych wyznaczono wartości stałych nadsubtelnych A i B oraz czynników Landégo g_J dla kilkudziesięciu poziomów energetycznych obu parzystości, z czego dla większości po raz pierwszy. Ponadto, dla europu wyznaczono także wartości przesunięć izotopowych. Szczegółowe informacje przedstawione są w rozdziale dotyczącym opisu zawartości prac wchodzących w skład rozprawy.

2. METODOLOGIA

2.1. Laserowo indukowana fluorescencja

Zjawiskiem fizycznym wykorzystywanym do detekcji zmian absorpcji próbki w ramach prowadzonych badań była laserowo indukowana fluorescencja (*Laser Induced Fluorescence – LIF*). Jest to metoda polegająca na wzbudzeniu za pomocą lasera wybranych przejść elektronowych w atomie, a następnie obserwacji zachodzącej spontanicznie fluorescencji. Schematyczne przedstawienie powyższego procesu ukazane jest na rysunku 1.

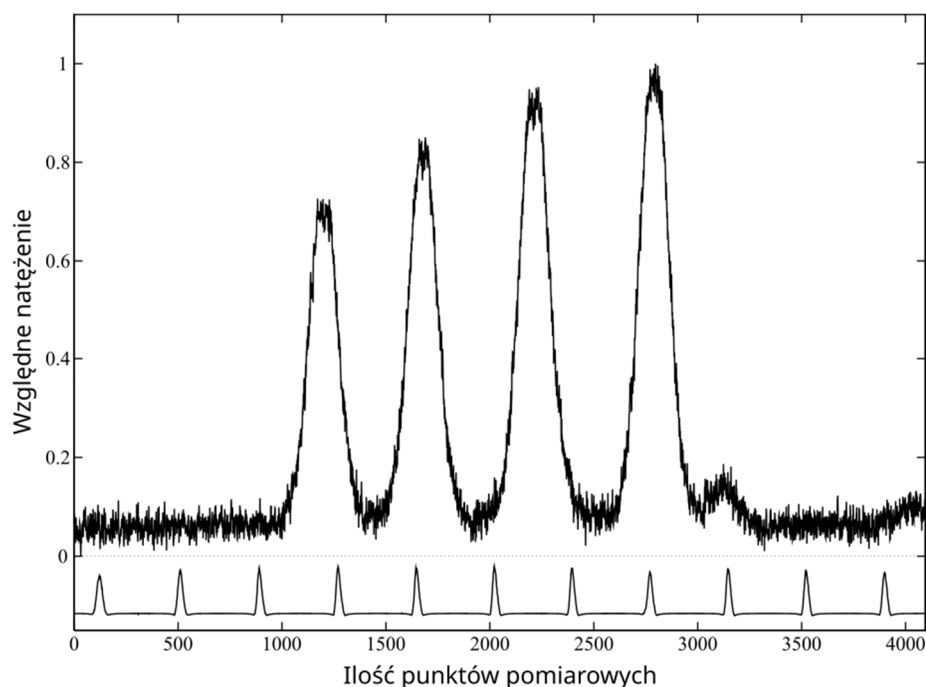


Rys. 1. Schematyczne przedstawienie metody laserowo indukowanej fluorescencji.

W ramach badanego przejścia, elektrony z niżej leżącego poziomu energetycznego, określanego jako dolny, są wzbudzone przez wiązkę laserową i obsadzają wyżej leżący poziom (górnny). Długość fali lasera musi być równa różnicy pomiędzy wartościami energii poziomu górnego i dolnego. Następnie, na skutek procesu relaksacji dochodzi do depopulacji poziomu górnego, czyli obsadzenia niżej leżących poziomów energetycznych poprzez dozwolone przez reguły wyboru przejścia promieniste, tzw. kanały fluorescencji. Sygnał fluorescencji jest następnie rejestrowany przez fotonowielacz lub matrycę CCD, natomiast selekcja wybranego kanału fluorescencji realizowana jest przy użyciu przyrządów dyspersyjnych, np. monochromatora.

Metoda ta pozwala na analizę struktury nadsubtelnej wybranych poziomów energetycznych danego pierwiastka poprzez rejestrację linii widmowej stanowiącej przejście, w którym dany poziom bierze udział. Na podstawie zmian natężenia sygnału

fluorescencji, proporcjonalnego do absorpcji przez linię wzbudzającą możliwe jest wyznaczenie położenia i względnych natężeń składowych struktury nadsubtelnej. Przykład linii widmowej, zarejestrowanej podczas badań atomu terbu pokazany jest na rysunku 2.



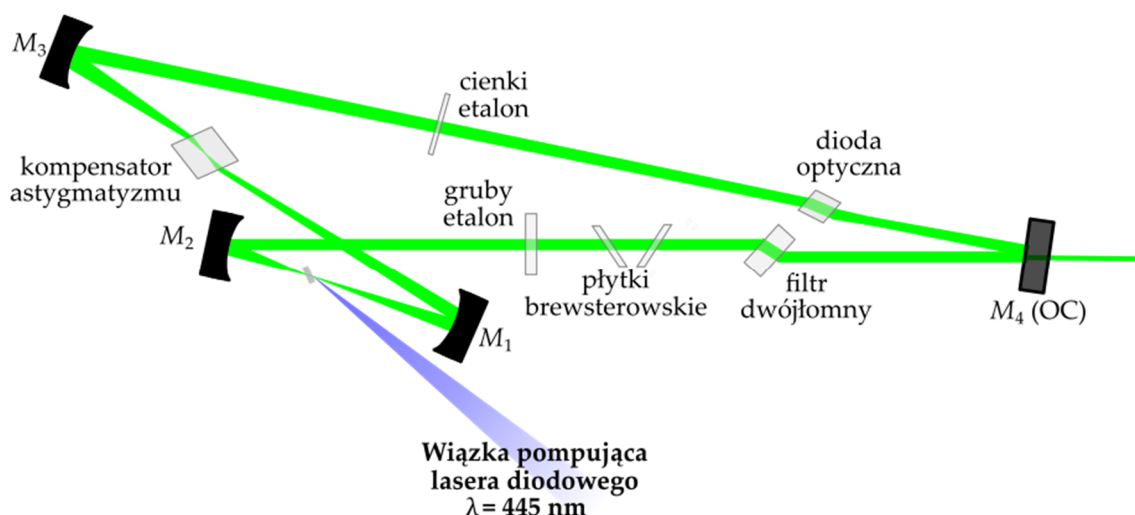
Rys. 2. Zarejestrowana linia widmowa $18145,16 \text{ cm}^{-1}$ ($\lambda=550,958 \text{ nm}$) wraz z sygnałem znacznika częstości. Przejście pomiędzy poziomami $462,08 \text{ cm}^{-1} J=15/2$ oraz $18607,24 \text{ cm}^{-1} J=13/2$ w atomie terbu.

Szerokość struktur w przypadku linii widmowych, rejestrowanych w prowadzonych badaniach zawierała się w granicach od kilku do kilkudziesięciu gigaherców w skali częstotliwości. Do obserwacji całej struktury niezbędne było wykorzystanie laserów przestrajalnych, czyli takich, które umożliwiają płynną zmianę częstotliwości generowanej wiązki. Do wzbudzania możliwych przejść zastosowano trzy jednomodowe przestrajalne lasery barwnikowe o pracy ciągłej z rezonatorem pierścieniowym. Schemat rezonatora, wraz z zaznaczonymi elementami lasera znajduje się na rysunku 3. W dwóch przypadkach były to zmodyfikowane wersje modelu Coherent CR 699-21, natomiast rezonator trzeciego lasera był projektowany na wzór wspomnianego modelu, jednak w oparciu o szkielet mechaniczny lasera liniowego Coherent CR 599. Jako ośrodki czynne wykorzystywane były roztwory czterech różnych barwników, tj.

- kumaryna 498, umożliwiająca generację wiązki o długości fali w zakresie 481 – 540 nm,
- mieszanina kumaryny 498 i Pyrromethene 556, umożliwiająca generację w zakresie długości fali 535 – 565 nm,

- rodamina 6G, umożliwiająca generację w zakresie długości fali 565 – 620 nm,
- DCM, umożliwiający generację w zakresie długości fali 615 – 679 nm.

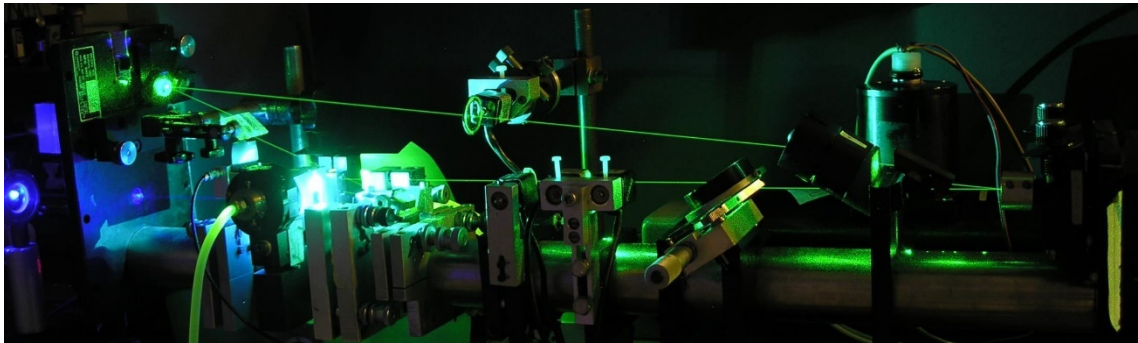
W początkowej fazie prac dostępne były roztwory jedynie trzech z nich – kumaryna 498, rodamina 6G i DCM. Do pompowania optycznych roztworów barwników rodaminy 6G i DCM używano lasera Nd:YVO₄ firmy Coherent (model Verdi V10) o długości fali 532 nm i nominalnej mocy wyjściowej 10 W. Roztwór kumaryny 498 oraz mieszanina kumaryny 498 i Pyrromethene 556 były pompowane za pomocą lasera diodowego. Początkowo był to model Lasever Inc. LSR445SD-4W (445 nm, 4 W), następnie po jego awarii Lasertack GmbH LDM-445-5000-C (445 nm, 5,5 W). Warto wspomnieć, że było to pierwsze na świecie opublikowane wykorzystanie lasera diodowego do pompowania lasera barwnikowego, stosowanego w spektroskopii o dużej zdolności rozdzielczej [28], w którego realizacji autor niniejszej pracy brał czynny udział.



Rys. 3. Schemat rezonatora zmodyfikowanego lasera barwnikowego Coherent CR 699-21 [29].
Literą M z odpowiednią cyfrą w indeksie oznaczone są poszczególne zwierciadła rezonatora.

W późniejszych etapach badań podjęto próbę poszerzenia możliwego do uzyskania zakresu spektralnego o obszar pomiędzy długofalową granicą generacji kumaryny 498 i krótkofalową granicą generacji rodaminy 6G, tj. w przybliżeniu 540 – 565 nm. Należy zaznaczyć, że jest to niezwykle trudny do uzyskania zakres widmowy, gdyż jest on niemożliwy do osiągnięcia za pomocą pojedynczego, komercyjnie dostępnego lasera. W tym celu wykorzystano efekt transferu energii wzbudzenia w laserach barwnikowych (*Energy transfer dye lasers*). Opiera się ono na rezonansie Förstera, czyli bezpromienistym przekazaniu energii wzbudzenia w roztworze mieszaniny dwóch lub więcej barwników (układ donor – akceptor). Innymi słowy, polega to na wzbudzeniu laserem pompującym jednego z barwników w mieszaninie (donora), który następnie

przekazuje energię do drugiego barwnika (akceptora), w którym zachodzi emisja wymuszona. Generacja wiązki laserowej może nastąpić częściowo za pośrednictwem donora i akceptora lub wyłącznie za pośrednictwem akceptora. Przy doborze barwników ważne jest, by widmo emisji donora jak najbardziej przekrywało się z widmem absorpcji akceptora, tj. by całka przekrywania była jak największa. Badania zrealizowano we współpracy z Zakładem Mikro- i Nanostruktur Instytutu Badań Materiałowych i Inżynierii Kwantowej na Wydziale Inżynierii Materiałowej i Fizyki Technicznej, w których autor niniejszej rozprawy również miał znaczny udział. Ich efektem było uzyskanie generacji w zakresie 535 – 565 nm przez zastosowanie mieszaniny kumaryny 498 i Pyrromethene 556 i pompowanie tej mieszaniny za pomocą lasera diodowego [30]. Umożliwiło to wykorzystanie pełnego zakresu spektralnego od 481 nm do 679 nm do wzbudzania przejść badanych w ramach realizowanych prac.



Rys. 4. Zmodyfikowany przestrajalny laser barwnikowy z rezonatorem pierścieniowym Coherent CR 699-21. Autor: dr Andrzej Jarosz.

2.2. Badania struktury nadsubtelnej atomów

Struktura nadsubtelna atomu (*hyperfine structure* – oznaczona skrótowo *hfs*) jest efektem oddziaływania jądra atomowego z powłokami elektronowymi. Na skutek oddziaływań magnetycznych dipolowych i elektrycznych kwadrupolowych dochodzi do rozszczepienia poziomów energetycznych o określonej wartości całkowitego elektronowego momentu pędu J na szereg podpoziomów o całkowitym atomowym momencie pędu F , mogącym przybierać wartości [31, 32]:

$$F = J + I, J + I - 1, \dots, |J - I|, \quad (1)$$

gdzie I to spin jądra. Możliwa ilość podpoziomów, na które może rozszczepić się dany poziom energetyczny uzależniona jest od liczb kwantowych I oraz J , i przybiera ona wartość $2I + 1$, gdy $J \geq I$ lub $2J + 1$, jeżeli $J < I$ [31]. Zjawisko to zostało

schematycznie zobrazowane na rysunku 5. Energia danego podpoziomu opisana jest równaniem [31]:

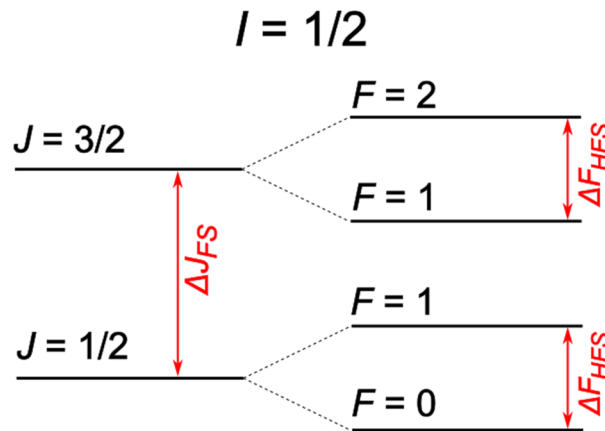
$$E^{hfs} = h \left(\frac{1}{2} KA + \frac{3/4K(K+1) - I(I+1)J(J+1)}{2I(2I-1)J(2J-1)} B \right) \quad (2)$$

$$= h(\alpha A + \beta B),$$

gdzie h jest stałą Plancka, A i B to stałe struktury nadsubtelnej (odpowiednio magnetyczna dipolowa i elektryczna kwadrupolowa) natomiast $K = F(F+1) - J(J+1) - I(I+1)$, $|J-I| \leq F \leq |J+I|$. Znając wartości stałych A i B , możliwe jest wyznaczenie położenia składowych struktury nadsubtelnej. Przedstawia to równanie:

$$\nu = \nu_{cg} + \alpha_g A_g + \beta_g B_g - \alpha_d A_d - \beta_d B_d, \quad (3)$$

gdzie ν_{cg} to środek ciężkości linii, natomiast indeksy dolne g i d opisują poziom górny i dolny, biorące udział w danym przejściu. Wykorzystując powyższą relację, możliwe jest zatem wyznaczenie wartości stałych A i B na podstawie eksperymentalnie określonych położzeń składowych struktury nadsubtelnej.

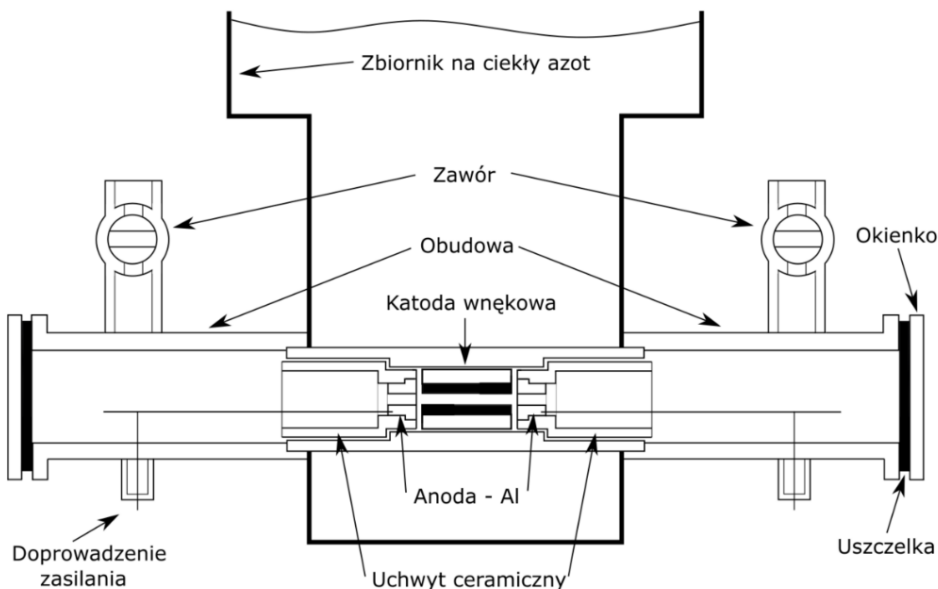


Rys. 5. Schematyczne przedstawienie powstawania struktury nadsubtelnej. ΔJ_{FS} obrazuje rozszczepienie subtelne, ΔF_{HFS} nadsubtelne.

W przypadku pierwiastków posiadających więcej niż jeden stabilny izotop, takich jak europ, pojawia się zjawisko przesunięcia izotopowego. Objawia się ono przesunięciem pomiędzy środkami ciężkości linii danych izotopów, obserwowanych przy przejściach pomiędzy tymi samymi poziomami energetycznymi. Na przesunięcie izotopowe składają się dwa efekty: efekt masy oraz efekt pola. Efekt masy zależy od masy jądra (normalny efekt masy) oraz od oddziaływań pomiędzy funkcjami falowymi elektronów (specyficzny efekt masy), natomiast efekt pola uzależniony jest od struktury jądra. W przypadku

pierwiastków ciężkich o dużej liczbie atomowej Z dominujący jest efekt pola, zaś w przypadku lekkich – efekt masy [33].

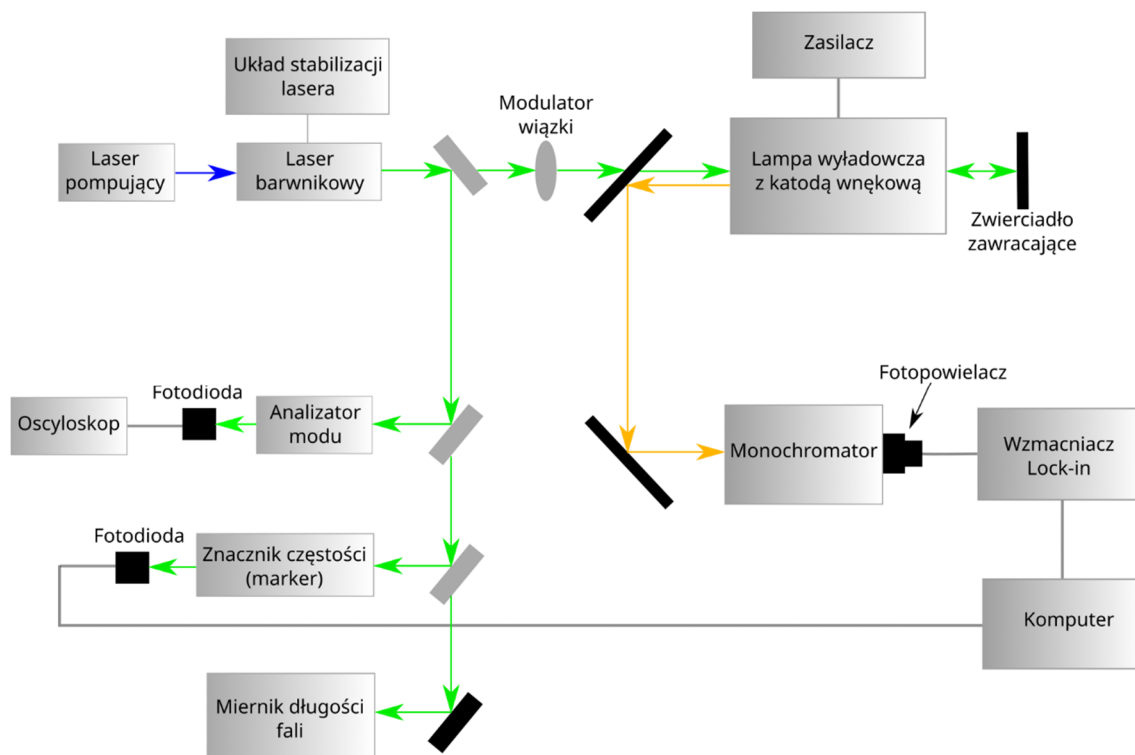
Badania struktury nadsubtelnej opierają się na rejestrowaniu i późniejszej analizie sygnału fluorescencji, uzyskanego metodą *LIF*, opisaną w rozdziale 2.1. Źródłem swobodnych atomów była lampa wyładowcza z katodą wnąkową. Główną część lampy stanowi szklano-metalowa obudowa. Szklane ramiona przytwierdzone są do metalowego korpusu, połączonego ze zbiornikiem na ciekły azot. Przy ramionach znajdują się zawory próżniowe, umożliwiające odpompowanie powietrza z układu i wpuszczenie gazu buforowego, oraz kontakty pozwalające na doprowadzenie zasilania do wywołania wyładowania w gazie. Okienka na końcach ramion, utrzymywane na miejscu przez podciśnienie, zamykają szczelnie cały układ. W środku lampy znajduje się wkręcona w metalowy korpus katoda wnąkowa, stanowiąca niewielki miedziany cylinder, na którego wewnętrznych ściankach osadzony jest badany materiał w formie stałej. W niewielkiej odległości od katody (ok. 0,5 – 1 mm) umieszczone są anody aluminiowe, połączone z kontaktami elektrycznymi, osadzone w izolujących obudowach ceramicznych. Wewnątrz katody oraz anod musi znajdować się otwór przepuszczający wiązkę laserową.



Rys. 6. Schemat lampy wyładowczej z katodą wnąkową.

Początkowo lampa wyładowcza jest odpompowywana za pomocą pompy rotacyjnej do ciśnienia rzędu 10^{-3} mbar. Następnie do środka włączany jest argon, pełniący funkcję gazu buforowego, podwyższając ciśnienie w układzie do 10^{-1} mbar. Przyłożony do połączonych z anodami kontaktów prąd o natężeniu rzędu kilkudziesięciu miliamperów

powoduje pojawienie się wyładowania i zjonizowanie gazu buforowego. Częsteczki powstałej plazmy argonowej powodują wybijanie atomów badanego pierwiastka z wnętrza katody wnekowej, tworząc chmurę atomową. Dodatkowo, wybite z katody atomy, na skutek zderzeń z jonami argonu, są wzbudzone na wyższe poziomy energetyczne. Aby zapobiec przegrzaniu, całość układu chłodzona była ciekłym azotem. Dokładne wartości ciśnienia gazu buforowego oraz natężenia prądu wyładowania podane są w poszczególnych pracach, stanowiących niniejszą rozprawę.



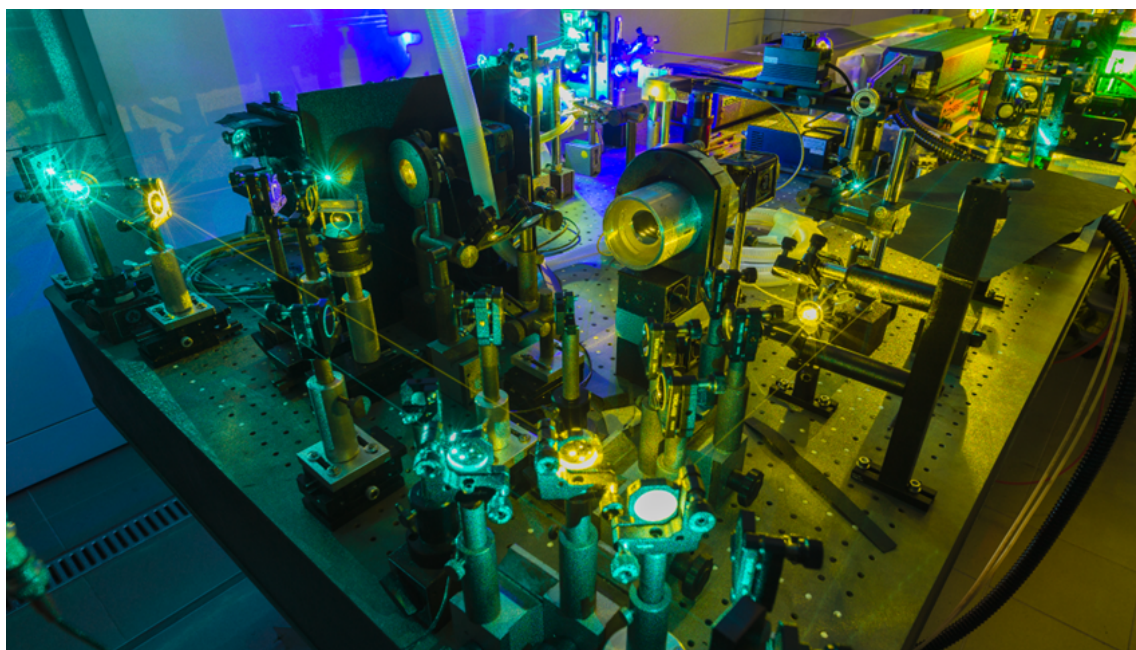
Rys. 7. Schemat układu do badań struktury nadsubtelnej.

Do wzbudzania konkretnych przejść pomiędzy wybranymi poziomami energetycznymi wykorzystywane były lasery, omówione szerzej w podrozdziale 2.1. Wzbudzenie następuje podczas przejścia wiązki laserowej przez chmurę atomową wewnątrz katody wnekowej. Wstępna długość fali ustawiana była na środek szerokości potencjalnej linii widmowej, na podstawie odczytu z miernika długości fali Burleigh WA-1500. Podczas rejestrowania sygnału fluorescencji, częstotliwość (długość fali) lasera była przestrajana w zakresie kilkudziesięciu gigaherców, tak by na widmie widoczna była cała struktura nadsubtelna. Każdy z laserów posiadał układ stabilizacji częstotliwości, zapewniający płynne przestrajanie bez przeskoków międzymodowych. Dodatkowo, jednomodowa praca lasera kontrolowana była za pomocą analizatora modów. Do uzyskania skali częstotliwości dla rejestrowanych skanów wykorzystywano

stabilizowany interferometr Fabry-Perot o wartości $FSR=1500$ MHz, pełniący funkcję znacznika częstości (markera). Jego sygnał był rejestrowany równoległe z sygnałem fluorescencji.

Układ detekcji sygnału *LIF* oparty jest o wykorzystanie metody fazoczułej. Po wyborze kanału fluorescencji za pomocą monochromatora Carl Zeiss Jena SPM-2, sygnał trafiał do fotopowielacza Hamamatsu R-375, a następnie był wzmacniany przez wzmacniacz fazoczuły. Umożliwia on poprawę stosunku sygnału do szumu poprzez modulację sygnału fluorescencji referencyjnym sygnałem sinusoidalnym o określonej częstotliwości, a następnie wyodrębnienie go i odfiltrowanie szumów, niezawierających składowych modulowanych. Do modulacji wiązki laserowej użyto tzw. choppera, połączonego ze wzmacniaczem Lock – in. Jest to modulator mechaniczny, którego kluczowym elementem jest obrotowa tarcza z otworami, przerywająca wiązkę z określoną częstotliwością. Niekiedy, podczas obserwacji słabych linii o małym natężeniu wykorzystywano zwierciadło zawracające, ustawione za lampą wyładowczą. Umożliwiało ono powtórne przejście wiązki laserowej przez katodę wnękową, a tym samym zwiększenie natężenia sygnału fluorescencji.

Każda badana linia widmowa była rejestrowana ok. 10 – 20 razy, w zależności od siły sygnału, a poszczególne skany były następnie uśredniane. Do dalszej analizy i wyznaczania stałych struktury nadsubtelnej wykorzystywano program „Fitter”, którego działanie opisano w rozdziale 3.3.

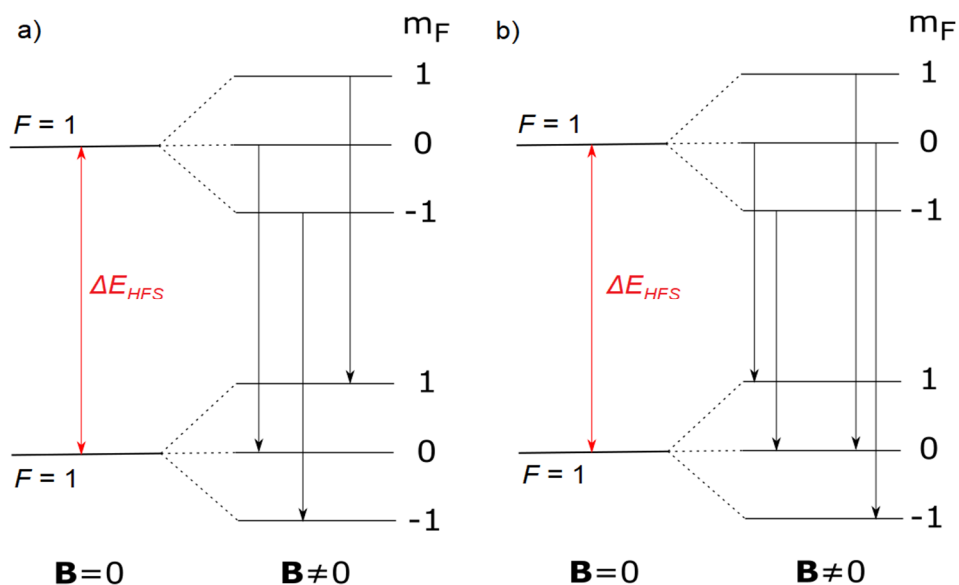


Rys. 8. Fragment układu eksperymentalnego – lasery i układ kontrolny.
Źródło: archiwum Zakładu Inżynierii i Metrologii Kwantowej.

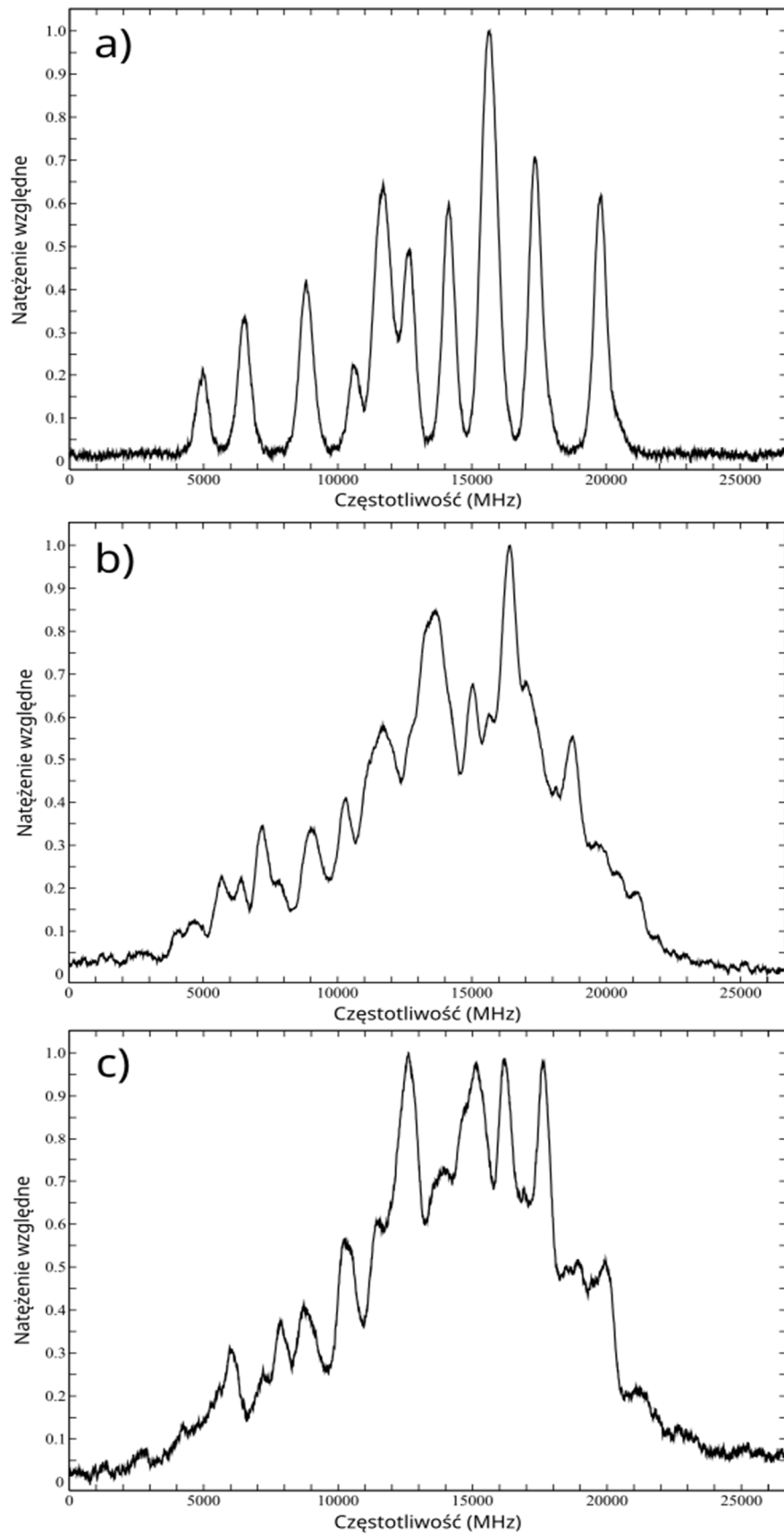
2.3. Badania rozszczepienia zeemanowskiego struktury nadsubtelnej

Pod wpływem działania zewnętrznego pola magnetycznego poziomy struktury nadsubtelnej mogą ulec rozszczepieniu na kolejne możliwe podpoziomy. Jeżeli wartość indukcji pola magnetycznego jest niewielka, tj. gdy wartość energii oddziaływania pomiędzy momentami magnetycznymi jądra i elektronów jest mniejsza niż wartość sprzężenia zeemanowskiego pomiędzy spinowym momentem elektronowym a zewnętrznym polem magnetycznym, dochodzi do rozszczepienia poziomu o całkowitym momencie pędu $F = 1$ na trzy podpoziomy, opisane liczbą kwantową $m_F = 0, \pm 1$. Jest to tzw. anomalny efekt Zeemana [34]. Na widmie jest to obserwowane jako rozszczepienie i rozsuniecie składowych struktury nadsubtelnej, których wielkość zależy od natężenia zewnętrznego pola magnetycznego oraz czynników Landégo g_J poziomów, biorących udział w danym przejściu. Przykładowe widmo, zarejestrowane w atomie europu znajduje się na rysunku 10.

Przejścia promieniste pomiędzy poziomami zeemanowskimi, dozwolone przez reguły wyboru, są zależne także od ustawienia płaszczyzny polaryzacji wiązki laserowej w stosunku do linii pola magnetycznego. Jeżeli płaszczyzna liniowo spolaryzowanej wiązki jest równoległa do linii pola, jest to tzw. polaryzacja π i przejścia zachodzą pomiędzy poziomami o $\Delta m_F = 0$. W odwrotnym przypadku, tj. gdy płaszczyzna polaryzacji wiązki jest prostopadła do linii pola, przejścia zachodzą pomiędzy poziomami o $\Delta m_F = \pm 1$, i jest to tzw. polaryzacja σ . Zostało to schematycznie zobrazowane na poniższym rysunku:

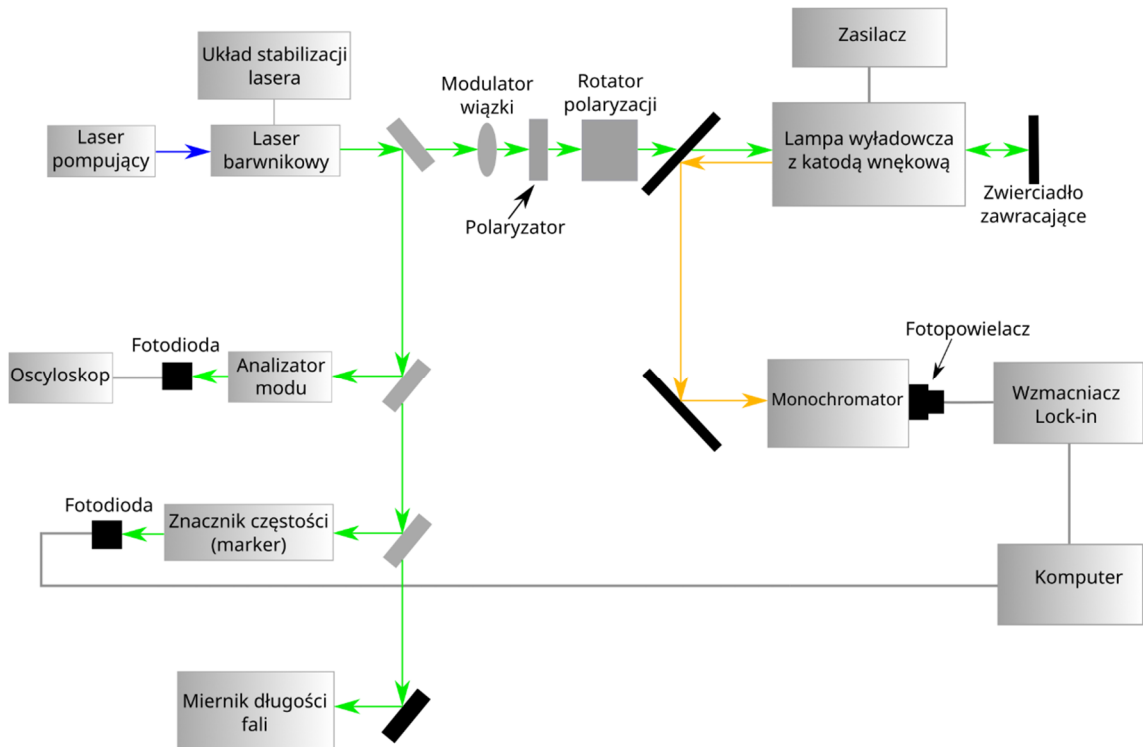


Rys. 9. Schematyczne przedstawienie rozszczepienia Zeemana struktury nadsubtelnej: a) polaryzacja π , b) polaryzacja σ .



Rys. 10. Rozszczepienie zeemanowskie linii widmowej $15288,63 \text{ cm}^{-1}$ ($\lambda=653,900 \text{ nm}$). Przejście pomiędzy poziomami $19273,24 \text{ cm}^{-1}$ $J=9/2$ i $34561,87 \text{ cm}^{-1}$ $J=7/2$ w atomie europu: a) struktura nadsubtelna, b) polaryzacja π , c) polaryzacja σ .

Układ do badania rozszczepienia struktury nadsubtelnej pod wpływem efektu Zeemana nie różni się znacząco od wykorzystywanego do badania samej struktury. W okolicy katody wnekowej umieszczono parę magnesów neodymowych, natomiast w bieg wiązki laserowej wstawiono rotator polaryzacji oraz polaryzator.

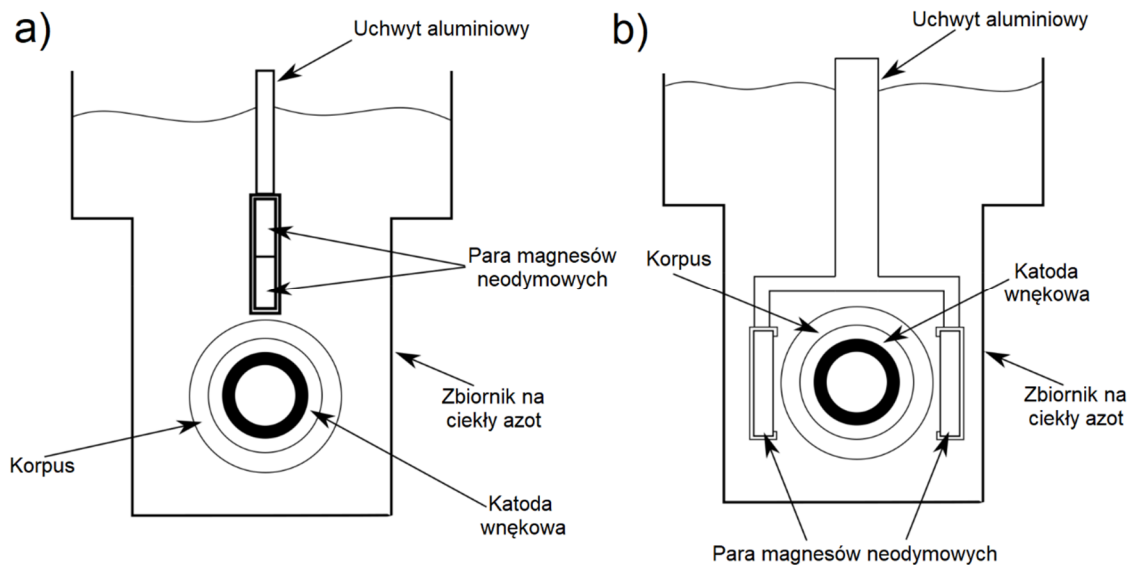


Rys. 11. Schemat układu do badania rozszczepienia struktury nadsubtelnej pod wpływem efektu Zeemana.

Rotator polaryzacji umożliwiał zmianę płaszczyzny polaryzacji wiązki laserowej tak, by możliwa była obserwacja przejść π oraz σ . Wiązka generowana przez wykorzystywane lasery była spolaryzowana liniowo w około 99 %. Zastosowanie polaryzatora pozwoliło na odfiltrowanie niepożądanego domieszki polaryzacji, a tym samym zminimalizowanie efektu szczątkowego przenikania polaryzacji π do polaryzacji σ i na odwrót. Rozszczepienie zeemanowskie uzyskano za pomocą pary trwałych magnesów neodymowych, umieszczonych w bliskiej odległości korpusu z katodą wnekową. Stosowane były układy w dwóch konfiguracjach, widocznych na rysunku 12.

W pierwszym układzie oba magnesy znajdowały się jeden nad drugim w uchwycie aluminiowym, zamocowanym bezpośrednio nad katodą wnekową. Zmierzona wartość indukcji pola magnetycznego to około 50 – 60 mT (500 – 600 Gs). W drugiej konfiguracji uchwyt umożliwiał umocowanie po jednym magnecie po obu stronach katody. W tym przypadku wartość indukcji wynosiła ok. 190 – 200 mT (1900 – 2000 Gs). Wartości te zmierzono za pomocą czujnika Halla, dzięki pomocy dr. inż. Semira El-Ahmara

z Zakładu Fizyki Powierzchni i Nanotechnologii Instytutu Fizyki na Wydziale Inżynierii Materiałowej i Fizyki Technicznej Politechniki Poznańskiej.



Rys. 12. Możliwe konfiguracje ustawienia pary magnesów w pobliżu katody wnąkowej. W układzie a) indukcja pola wynosiła 50 – 60 mT, w układzie b) 190 – 200 mT.

Do pomiarów efektu Zeemana struktury nadsubtelnej w atomie europu wykorzystano konfigurację pierwszą. Mogłoby się wydawać, że lepiej sprawdzi się układ drugi, gdyż ustawienie magnesu po obu stronach katody zapewnia znacznie bardziej jednorodne pole magnetyczne wewnątrz obszaru, w którym znajduje się chmura atomowa, natomiast większa wartość indukcji spowoduje mocniejsze rozszczepienie składowych widma i ich wyraźniejsze rozsuniecie. Problemem okazał się jednak wpływ pola magnetycznego na samą chmurę atomów. Ze względu na zbyt silne pole, chmura ulegała odchyleniu, powodując osadzanie się atomów badanego pierwiastka na uchwytach ceramicznych, izolujących anody aluminiowe od katody. W efekcie dochodziło do zwarcia, co z kolei wymagało czasochłonnego rozbierania i czyszczenia układu. Zastosowanie układu z dwoma magnesami umieszczonymi nad katodą wnąkową, pomimo mniej jednorodnego pola, umożliwiło prowadzenie prac przez wymagany czas, natomiast uzyskane wyniki wartości czynników Landégo g_J nie różniły się zauważalnie od tych, uzyskanych przy użyciu konfiguracji drugiej. Zostało to potwierdzone w publikacji dotyczącej wyznaczenia czynników g_J w atomie holmu [35], gdzie wykorzystywany był ten sam układ pomiarowy.

W przypadku badań prowadzonych w atomie terbu używano naprzemiennie obu konfiguracji magnesów. Spowodowane to było zjawiskiem ekranowania pola

magnetycznego na skutek przejść fazowych w terbie. Poniżej temperatury 218 K terb jest ferromagnetykiem. Powyżej tej wartości przechodzi on do fazy antyferromagnetycznej, która utrzymuje się do temperatury Néela, wynoszącej 230 K, natomiast punkt Curie terbu to 237 K. W efekcie, skrajne części katody wnękowej, chłodzone ciekłym azotem znajdowały się w fazie ferromagnetycznej, natomiast część środkowa, ogrzewana przez prąd wyładowania pozostawała w fazie paramagnetycznej. Skutkiem była znacząco obniżona wartość indukcji pola magnetycznego w obszarze chmury atomowej. W przypadku wielu badanych przejść aby zaobserwować rozszczepienie zeemanowskie, niezbędne było użycie konfiguracji magnesów zapewniające większą wartość pola magnetycznego. Ponadto, zaobserwowano, że efekt ekranowania jest ściśle związany z wartością natężenia prądu wyładowania. Podczas obserwacji tej samej linii widmowej otrzymywano różny stopień rozszczepienia dla różnych wartości natężenia prądu. Zatem, by jak najbardziej zminimalizować ten efekt, starano się utrzymywać stałą wartość natężenia prądu wyładowania w trakcie prowadzenia prac pomiarowych.

Rzeczywiste wartości indukcji pola magnetycznego wewnątrz katody wnękowej wyznaczono na podstawie pomiarów rozszczepienia zeemanowskiego linii argonu o znanych z dużą dokładnością wartościach czynników g_J dla obu poziomów, biorących udział w przejściu. W tym celu wykorzystano program do wyznaczania czynników Landégo, opisany w rozdziale 3.4. Do zarejestrowanych eksperymentalnie linii argonu dopasowywane były funkcje, dla których znane wartości czynników g_J przyjęto jako stałe, natomiast wartością szukaną była indukcja pola magnetycznego. Linie argonu były rejestrowane wielokrotnie w ciągu każdego dnia pomiarów.

Podobnie jak w przypadku badań struktury nadsubtelnej, widma danej linii były rejestrowane wielokrotnie, osobno dla każdej z obu polaryzacji, a następnie uśredniane. W celu wyznaczania wartości czynników Landégo g_J na podstawie zarejestrowanych widm wykorzystano wspomniany program, opisany w rozdziale 3.4.

3. OPROGRAMOWANIE

3.1. Program do symulacji możliwych przejść

Program do symulacji możliwych przejść w badanych atomach został napisany przez dr. hab. Bogusława Furmanna, prof. PP., będącego promotorem niniejszej rozprawy. Jako dane wejściowe wprowadzane są zestawienia znanych poziomów energetycznych, należących do konfiguracji parzystych i nieparzystych oraz zestawienie sklasyfikowanych linii widmowych. Na ich podstawie program generuje listę możliwych przejść, dozwolonych przez reguły wyboru. Dla każdego poziomu górnego podawane są wartości energii poziomów dolnych, z których możliwe są przejścia, oraz wartości liczb falowych linii widmowych. Ponadto, na podstawie zaimplementowanej krzywej kalibracyjnej, program wyznacza ustawienia szczeliny monochromatora, dla których powinien się pojawić sygnał fluorescencji. Aby umożliwić szybkie znalezienie tych kanałów fluorescencji, które są najsilniejsze, program przeszukuje też zestawienie sklasyfikowanych linii widmowych, wybiera te linie dla których długość fali jest zbliżona z długością fali danego kanału fluorescencji i wypisuje je obok danych kanału łącznie z wartością natężenia linii

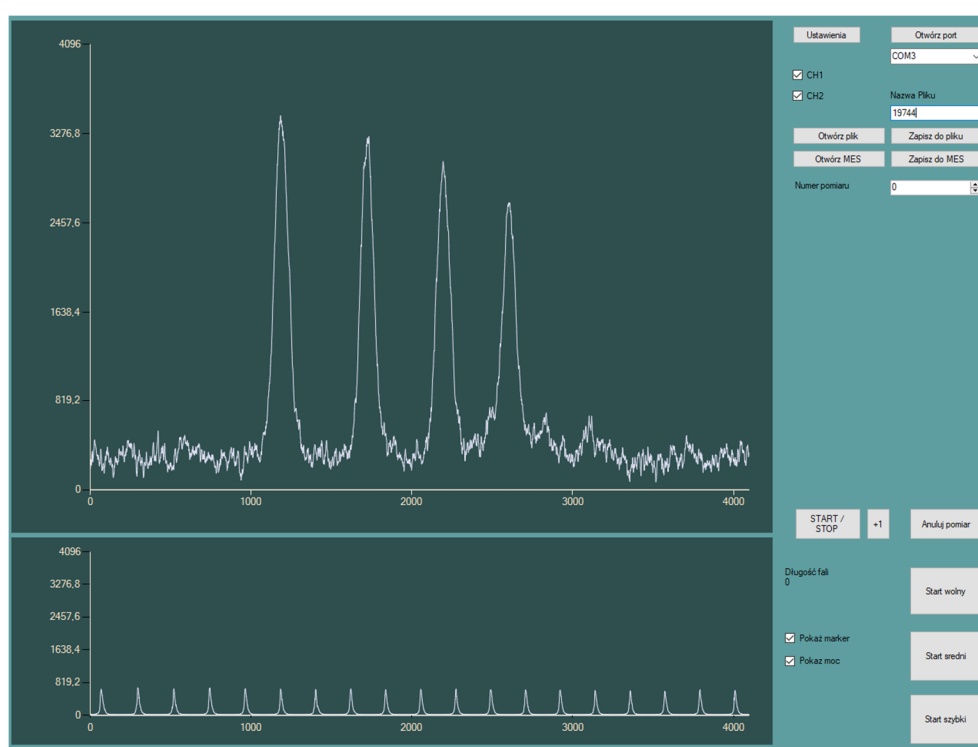
W oparciu o tak przygotowaną listę wybierane są poziomy energetyczne, dla których istnieje możliwość wzbudzenia przejść w zakresie spektralnym, uzyskiwanym przez posiadane lasery. Następnie wszystkie potencjalne przejścia są weryfikowane w ramach prowadzonego eksperymentu i rejestrowane z zastosowaniem detekcji metodą *LIF*.

3.2. Program do rejestracji widm

Rejestrację badanych linii widmowych oraz sygnału znacznika częstości (markera) umożliwił program napisany przez mgr. inż. Patryka Gałczyka w ramach realizowanej pracy magisterskiej, której promotorem był dr hab. Bogusław Furmann, prof. PP.

Program wykorzystuje dedykowany układ elektroniczny, składający się z przetworników: analogowo – cyfrowego i cyfrowo – analogowego, sterowanych przez mikrokontroler ATMEGA32U4 o architekturze AVR. Na podstawie wartości napięcia na fotodiodzie ustawionej za markerem i natężenia fotoprądu fotopowielacza wzmocnionego za pomocą przedwzmacniacza i wzmacniacza fazoczułego, program generuje jednocześnie widmo fluorescencji i sygnał interferencji markera w postaci graficznej w trakcie skanu lasera. Po zarejestrowaniu widma możliwy jest jego zapis do pliku w formacie obsługiwanym przez pozostałe wykorzystywane programy.

W programie możliwe jest także ustawienie szybkości przestrajania lasera (skanu). Jest to realizowane poprzez trzy parametry: akumulację, czas przestoju i rozdzielczość skanu. Akumulacja odpowiada za ilość próbek na dany krok pomiarowy, która jest następnie uśredniana. Czas przestoju to czas pomiędzy podaniem napięcia wyjściowego a wykonaniem kroku pomiaru, natomiast rozdzielczość skanu odpowiada za ilość kroków pomiarowych. Na ich podstawie generowany jest analogowy sygnał napięciowy, przesyłany do skrzyni kontrolnej lasera, określający szybkość obrotu elementów selektywnych. Dla wygody zostały przygotowane 3 profile, w których możliwa jest zmiana wartości parametrów skanu, nazwane: szybki, średni i wolny.



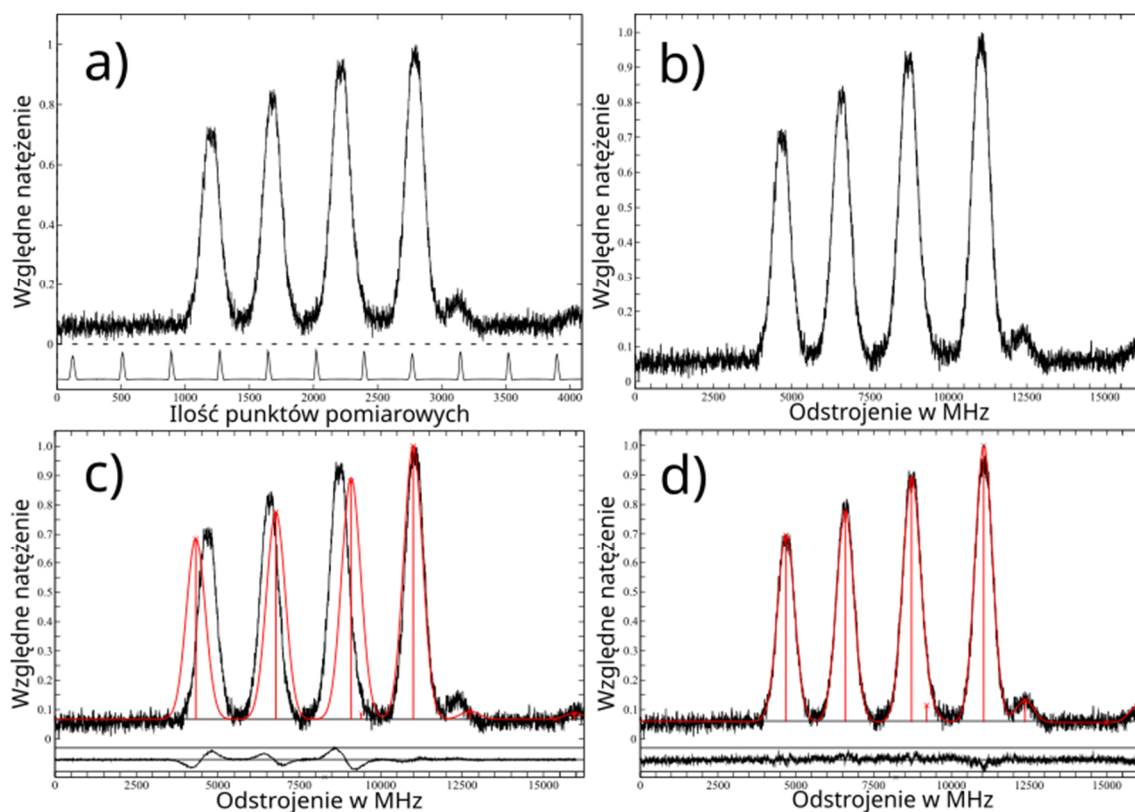
Rys. 13. Interfejs programu do rejestracji widm.

3.3. Program „Fitter”

Do wyznaczania stałych struktury nadsubtelnej A i B wykorzystywano program „Fitter”, opracowany przez grupę prof. G. H. Guthöhrleina w Hamburgu. Umożliwia on wyznaczenie wartości stałych na podstawie dopasowania funkcji do eksperymentalnie zarejestrowanego widma.

Opracowanie danych w programie „Fitter” składa się z dwóch etapów. Pierwszym jest tzw. linearyzacja widma. Program nanosi odpowiednią skalę częstotliwości na podstawie sygnału znacznika częstotliwości (markera), rejestrowanego równoległe z widmem, oraz wartości parametru FSR tegoż znacznika. Kolejnym krokiem jest dopasowanie

funkcji do linii widmowej. Wstępnie dopasowana krzywa teoretyczna generowana jest na podstawie zadanych parametrów opisujących oba poziomy energetyczne, biorące udział w analizowanym przejściu, takich jak: wartości liczb kwantowych J , stałe struktury nadsubtelnej A i B jednego z poziomów, szerokości profili Gaussa i Lorentza. Następnie program dopasowuje krzywą teoretyczną do widma poprzez iteracyjną zmianę wartości zadanych parametrów. Po osiągnięciu najlepszego dopasowania możliwe jest jego wyświetlenie w formie graficznej, oraz tworzony jest plik, zawierający wartości wyznaczonych stałych struktury nadsubtelnej. Możliwe jest jednoczesne dopasowywanie stałych A i B dla obu poziomów, biorących udział w przejściu, jednak uzyskane wyniki mogą okazać się nieprecyzyjne. Dlatego zalecane jest, by stałe przynajmniej jednego poziomu były znane z dużą dokładnością i podstawione w programie jako wartości niezmiennicze.



Rys. 14. Przedstawienie procedury dopasowywania w programie „Fitter” na przykładzie linii widmowej $18145,16 \text{ cm}^{-1}$ ($\lambda=550,958 \text{ nm}$) pomiędzy poziomami $462,08 \text{ cm}^{-1} J=15/2$ oraz $18607,24 \text{ cm}^{-1} J=13/2$ w atomie terbu: a) zarejestrowane widmo, b) linearyzacja widma, c) wstępne dopasowanie krzywej teoretycznej, d) ostateczne dopasowanie krzywej teoretycznej.

Linie widmowe, zarejestrowane w trakcie badań eksperymentalnych wykazują poszerzenie naturalne oraz Dopplerowskie, opisane odpowiednio profilem Lorentza oraz Gaussa. „Fitter” pozwala na wybór profili dopasowywanych w ramach krzywej

teoretycznej: Gaussa, Lorentza oraz Voigta, będącego złożeniem obu profili. Poszerzenie Dopplera jest zdecydowanie większe niż poszerzenie naturalne, dlatego najczęściej korzystano z dopasowania profili Gaussa, a następnie Voigta jeżeli następowało zauważalne polepszenie jakości dopasowania.

Ponadto, „Fitter” pozwala także na uwzględnienie oraz zminimalizowanie wpływu efektu nasycenia, objawiającego się zmniejszeniem natężenia niektórych składowych w stosunku do pozostałych na rejestrowanym widmie. Odbywa się to poprzez sprzęganie ze sobą odpowiednich grup składowych. Dodatkowo, możliwe jest także dopasowywanie osobnych krzywych do kilku izotopów danego pierwiastka jednocześnie. Było to szczególnie ważne przy wyznaczaniu stałych struktury nadsubtelnej i przesunięć izotopowych w atomie europu.

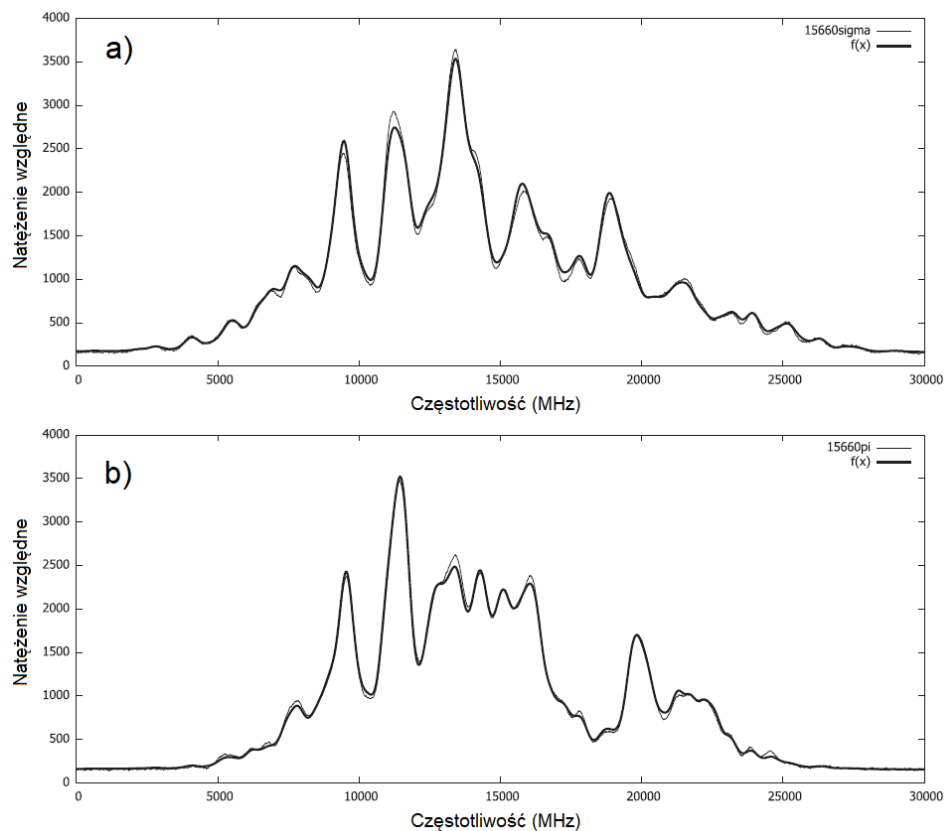
3.4. Program do wyznaczania czynników Landégo g_J

Program do wyznaczania wartości czynników Landégo g_J na podstawie badań efektu Zeemana struktury nadsubtelnej został napisany przez dr. hab. Bogusława Furmanna, prof. PP oraz dr. hab. Jarosława Ruczkowskiego z wydziału Automatyki, Robotyki i Elektrotechniki Politechniki Poznańskiej.

Program, podobnie jak „Fitter”, dopasowuje funkcję do eksperymentalnie zarejestrowanego widma polaryzacji π lub σ i na jej podstawie wyznacza wartości czynników g_J . Początkowo należy nanieść skalę częstotliwości na widmo w programie „Fitter”, następnie generowana jest funkcja opisująca krzywą teoretyczną (osobno dla każdej polaryzacji). W tym celu program dokonuje diagonalizacji hamiltonianu, opisującego energię atomu w zewnętrznym polu magnetycznym. Wyznaczane są względne energie podpoziomów zeemanowskich obu poziomów, biorących udział w danym przejściu. Na podstawie otrzymanych wartości i wektorów własnych, określone są względne położenia na skali częstotliwości oraz natężenia poszczególnych składowych. Wygenerowana w ten sposób funkcja jest dopasowywana do widma wykorzystując algorytm Marquardt’a. Metoda ta została opracowana w oparciu o tę, przedstawioną w pracy [36]. Do parametrów, niezbędnych przy tworzeniu funkcji zaliczają się wartości, charakteryzujące oba poziomy energetyczne, takie jak: liczba kwantowa J , stałe struktury nadsubtelnej A i B , oraz czynniki Landégo g_J , a także wartość indukcji pola magnetycznego oraz wstępnie dobrane szerokości profili Gaussa i Lorentza. Następnie podczas dopasowywania krzywej program dobiera odpowiednie wartości zadanych parametrów i wyznacza szukaną wartość czynnika g_J . Przy generowaniu

funkcji program wykorzystuje zależność, że jeżeli analizowane są zmiany wartości funkcji w niewielkim przedziale, to każda funkcja zmienia się w przybliżeniu liniowo. Dlatego wartości czynników g_J , uzyskane z dopasowania będą poprawne, gdy różnica między wartością początkową a końcową nie będzie duża. W innym wypadku należy ponownie wygenerować funkcję, podstawiając odpowiednio zbliżoną wartość początkową czynnika g_J , a następnie powtórzyć dopasowanie. Podobnie jak podczas wyznaczania stałych A i B za pomocą programu „Fitter”, możliwe jest jednoczesne wyznaczanie czynników Landégo obu poziomów, biorących udział w przejściu, lecz dokładność otrzymanych wartości jest dużo niższa niż w przypadku, gdy parametr g_J dla jednego z poziomów jest znany z dużą dokładnością. Wartości czynników Landégo, wyznaczone osobno dla polaryzacji π oraz σ są następnie odpowiednio uśredniane, dając ostateczną wartość czynnika dla konkretnego poziomu w badanym przejściu.

Program umożliwia również uwzględnienie wspomnianego już efektu nasycenia. Jest on opisany parametrami, których zmiana powoduje zmniejszenie jego wpływu na otrzymane wartości wyznaczanych czynników. W podobny sposób uwzględniono także efekt szczątkowego przenikania jednej polaryzacji do drugiej.



Rys. 15. Zarejestrowana w atomie europu linia widmowa $15660,34 \text{ cm}^{-1}$ ($\lambda=638,379 \text{ nm}$) pomiędzy poziomami $15137,72 \text{ cm}^{-1} J=3/2$ oraz $30798,06 \text{ cm}^{-1} J=3/2$, wraz z dopasowaną w programie krzywą teoretyczną: a) polaryzacja π , b) polaryzacja σ .

4. OPIS PRAC WCHODZĄCYCH W SKŁAD ROZPRAWY

4.1. Prace dotyczące atomu terbu

4.1.1. Hyperfine structure studies of the odd-parity electronic levels of the terbium atom

B. Furmann, D. Stefańska, M. Chomski, **M. Suski**, S. Wilman

Journal of Quantitative Spectroscopy & Radiative Transfer 237, 106613, 2019

W niniejszej pracy poddano analizie 43 poziomy energetyczne w atomie terbu, należące do konfiguracji nieparzystych. Na podstawie 73 zarejestrowanych linii widmowych wyznaczono stałe struktury nadsubtelnej A i B dla tychże poziomów.

Dla 41 poziomów energetycznych stałe zostały wyznaczone eksperymentalnie po raz pierwszy, natomiast dla pozostałych 2 zostały skorygowane w stosunku do wartości wcześniej dostępnych w literaturze.

Ponadto, w ramach badań skorygowano także stałe struktury nadsubtelnej dla dwóch poziomów energetycznych, należących do konfiguracji parzystych.

Pomiary przeprowadzono wykorzystując metodę laserowo indukowanej fluorescencji w lampie wyładowczej z katodą wnękową. Linie zarejestrowano w zakresie ok. 535 – 616 nm. Do ich wzbudzenia użyto dwóch laserów barwnikowych, pracujących na roztworach mieszaniny kumaryny 498 i Pyrromethene 556, oraz rodaminy 6G.

4.1.2. Hyperfine structure investigations of the odd-parity electronic levels of the terbium atom

M. Suski, B. Furmann, M. Chomski, S. Mieloch, P. Głowacki, D. Stefańska

Journal of Quantitative Spectroscopy & Radiative Transfer 298, 108492, 2023

Praca ta jest kontynuacją badań nieparzystych poziomów energetycznych w atomie terbu. W jej ramach wyznaczono stałe struktury nadsubtelnej A i B dla 26 poziomów na podstawie analizy 62 zarejestrowanych linii widmowych.

Dla wszystkich badanych poziomów energetycznych stałe zostały eksperymentalnie wyznaczone po raz pierwszy.

Dodatkowo, skorygowane zostały wartości stałych struktury nadsubtelnej dla 4 parzystych poziomów energetycznych, opublikowanych we wcześniejszych pracach.

Podobnie jak w poprzedniej publikacji, wykorzystywaną metodą była laserowo indukowana fluorescencja w lampie wyładowczej z katodą wnękową. Badania wykonano w zakresie widmowym ok. 483 – 538 nm, wykorzystując laser barwnikowy, pracujący na roztworze kumaryny 498.

4.1.3. Landé g_J factors of the even-parity electronic levels of the terbium atom

M. Suski, M. Chomski, B. Furmann, J. Ruczkowski, D. Stefańska

Journal of Quantitative Spectroscopy & Radiative Transfer 288, 108270, 2022

Na podstawie badań efektu Zeemana struktury nadsubtelnej w atomie terbu wyznaczono wartości czynników Landégo g_J dla 17 poziomów energetycznych, należących do konfiguracji parzystych. Wyniki uzyskano na podstawie analizy 47 linii widmowych.

Wartości czynników Landégo, uzyskane dla 17 poziomów parzystych zostały wyznaczone eksperymentalnie po raz pierwszy. Wykazały one zgodność w granicach niepewności z wartościami wyznaczonymi teoretycznie, w oparciu o analizę semi-empiryczną.

Przeprowadzono także weryfikację dostępnych w literaturze wartości czynników g_J dla 17 nieparzystych poziomów energetycznych, występujących jako poziomy dolne w badanych przejściach. Rezultaty uzyskane dla 15 poziomów były zgodne w granicach niepewności z wartościami literaturowymi, wyznaczonymi na podstawie analizy widma Fouriera. W przypadku pozostałych dwóch poziomów wartości literaturowe czynników Landégo uniemożliwiały poprawne dopasowanie funkcji do eksperymentalnie zarejestrowanych widm. Istnieje podejrzenie, że wartości czynników g_J dla tych poziomów zostały wyznaczone błędnie, w związku z czym wyznaczono nowe wartości.

W badaniach zastosowano metodę laserowo indukowanej fluorescencji w lampie wyładowczej z katodą wnękową w stałym polu magnetycznym. Analizowane linie widmowe zostały zarejestrowane w zakresie ok. 490 – 609. Dla każdej linii polaryzacje π i σ rejestrowano osobno, a ich selekcję umożliwiło wykorzystanie rotatora polaryzacji. Do wzbudzenia użyto dwóch laserów barwnikowych, wykorzystujących jako ośrodek czynny roztwory kumaryny 490 i rodaminy 6G.

4.1.4. Landé g_J factors of the odd-parity electronic levels of the terbium atom determined by laser spectroscopy

M. Suski, B. Furmann, M. Chomski, J. Ruczkowski, D. Stefańska, S. Mieloch
Journal of Quantitative Spectroscopy & Radiative Transfer 291, 108342, 2022

Niniejsza praca stanowi bezpośrednią kontynuację publikacji przedstawionej w poprzednim punkcie. Wyznaczono w niej wartości czynników Landégo g_J dla 20 nieparzystych poziomów energetycznych w atomie terbu na podstawie analizy efektu Zeemana struktury nadsubtelnej dla 32 linii widmowych.

Wszystkie uzyskane wartości czynników g_J zostały wyznaczone eksperymentalnie po raz pierwszy. W niektórych z badanych przejść, jako poziomy dolne brały udział poziomy, których wartości czynników Landégo zostały opublikowane w pracy opisanej w punkcie 5.1.3. W związku z tym, wykorzystano te wartości do procedury dopasowywania funkcji do widm eksperymentalnych,

Ponadto, dokonano weryfikacji literaturowych wartości czynników Landégo g_J dla 15 poziomów z konfiguracji parzystych, biorących udział w badanych przejściach jako poziomy dolne. Wszystkie uzyskane wartości były zgodne z literaturowymi w granicach niepewności.

Pomiary zostały wykonane stosując metodę laserowo indukowanej fluorescencji w lampie wyładowczej z katodą wnątkową w stałym zewnętrznym polu magnetycznym. Ponownie wykorzystano dwa lasery barwnikowe, pracujące na roztworach kumaryny 498 i rodaminy 6G, wzbudzając przejścia w zakresie widmowym ok. 492 – 609 nm. Widma polaryzacji π i σ dla każdej linii rejestrowano osobno.

4.2. Prace dotyczące atomu europu

4.2.1. Investigations of the hyperfine structure and isotope shifts in the even-parity level system of atomic europium

B. Furmann, M. Chomski, **M. Suski**, S. Wilman, D. Stefańska
Journal of Quantitative Spectroscopy & Radiative Transfer 251, 107070, 2020

W tej pracy przedstawiono wyznaczone w atomie europu wartości stałych struktury nadsubtelnej A i B oraz przesunięć izotopowych dla 26 poziomów energetycznych, należących do konfiguracji parzystych, leżących w zakresie

energii 28000-40000 cm^{-1} . Obliczenia były prowadzone dla obu stabilnych izotopów europu jednocześnie. W tym celu przeanalizowano 73 linie widmowe, znajdujące się w dwóch zakresach widmowych: 480 – 560 nm oraz 625 – 680 nm.

Wartości stałych A i B oraz przesunięć izotopowych dla 10 spośród badanych poziomów zostały eksperymentalnie wyznaczone po raz pierwszy. Dodatkowo, dla 3 z pozostałych poziomów wartości wspomnianych parametrów zostały wyznaczone z większą precyzją w stosunku do tych, opublikowanych w jednej z wcześniejszych pracach.

Podobnie jak w przypadku pozostałych badań struktury nadsubtelnej, zastosowano metodę laserowo indukowanej fluorescencji w lampie wyładowczej z katodą wnąkową. Do wzbudzania wybranych przejść wykorzystano dwa lasery barwnikowe, pracujące na roztworach mieszaniny kumaryny 498 i Pyromethene 556, oraz DCM.

W pracy zamieszczono także zestawienie 110 poziomów parzystych, dla których znane są wartości stałych struktury nadsubtelnej oraz przesunięć izotopowych. Tam, gdzie to możliwe przedstawiono także wartości czynników Landégo g_J .

4.2.2. Landé g_J factors of the electronic levels of the europium atom

B. Furmann, J. Ruczkowski, M. Chomski, **M. Suski**, S. Wilman, D. Stefańska
Journal of Quantitative Spectroscopy & Radiative Transfer 255, 107258, 2020

W pracy przedstawiono wyniki badań efektu Zeemana struktury nadsubtelnej w atomie europu. Wyznaczono wartości czynników Landégo g_J dla 23 poziomów energetycznych na podstawie analizy 54 linii widmowych. 16 z badanych poziomów należało do konfiguracji nieparzystych, pozostałe 7 zaś do parzystych.

Wartości czynników g_J dla wszystkich badanych poziomów nieparzystych i 4 poziomów parzystych zostały wyznaczone eksperymentalnie po raz pierwszy, oraz porównane z dostępnymi w literaturze wartościami wyznaczonymi semi-empirycznie. Uzyskane eksperymentalnie wartości są zgodne z przewidywaniami teoretycznymi, jednak w wielu przypadkach różnice przekraczają niepewności pomiarowe.

Dla pozostałych 3 poziomów parzystych wartości czynników Landégo zostały nieco skorygowane. Wartości czynników g_J dla dwóch z tych poziomów,

zaprezentowane w niniejszej pracy mieszczą się w granicach niepewności pomiarowych tych, dostępnych w literaturze. W przypadku wartości literaturowej czynnika Landégo dla ostatniego poziomu możliwe jest, że doszło do pomyłki w druku, gdyż wartość opublikowana wcześniej byłaby zgodna z nowo wyznaczoną, gdyby zamienić miejscami dwie ostatnie cyfry.

Pomiary wykonano wykorzystując metodę laserowo indukowanej fluorescencji w lampie wyładowczej z katodą wnątkową w stałym zewnętrznym polu magnetycznym. Badania prowadzone były w zakresie widmowym 511 – 662 nm, w związku z czym w laserach barwnikowych stosowano wszystkie cztery dostępne roztwory barwników, tj. kumaryny 498, mieszaniny kumaryny 498 i Pyrromethene 556, rodaminy 6G, oraz DCM. Dla 67 z tych poziomów, stałe A i B zostały wyznaczone po raz pierwszy, natomiast dla pozostałych dwóch zostały one skorygowane w stosunku do wcześniej opublikowanych.

5. PODSUMOWANIE

W niniejszej pracy, będącej zbiorem sześciu spójnych tematycznie publikacji zawarto rezultaty badań struktury nadsubtelnej oraz jej rozszczepienia pod wpływem efektu Zeemana w atomie terbu i europu. Na ich podstawie dla wielu poziomów energetycznych obu pierwiastków wyznaczono wartości stałych struktury nadsubtelnej: magnetycznej dipolowej A oraz elektrycznej kwadrupolowej B , a także wartości czynników Landégo g_J , opisujących liczbowo rozszczepienie zeemanowskie. Badania prowadzone były z wykorzystaniem metody laserowo indukowanej fluorescencji w lampie wyładowczej z katodą wnąkową, która stanowiła źródło wolnych atomów.

Dla atomu terbu, stałe struktury nadsubtelnej zostały wyznaczone dla 69 poziomów energetycznych, należących do konfiguracji nieparzystych. W tym celu zarejestrowano i przeanalizowano w sumie 135 linii widmowych, znajdujących się w zakresie spektralnym pomiędzy 483 a 616 nm. Ponadto, skorygowane zostały także stałe dla 6 poziomów, należących do konfiguracji parzystych.

Czynniki Landégo g_J wyznaczono dla 37 poziomów energetycznych, z których 17 należy do konfiguracji parzystych, a pozostałe 20 do nieparzystych. Dla wszystkich poziomów wartości czynników g_J zostały wyznaczone eksperymentalnie po raz pierwszy. Zbadanych zostało 79 linii widmowych w zakresie 490 – 609 nm. Zweryfikowane zostały także wartości czynników Landégo dla kolejnych 32 poziomów (17 nieparzystych i 15 parzystych). Dla dwóch poziomów nieparzystych zaproponowano nowe wartości, natomiast w przypadku pozostałych były one zgodne z literaturowymi w granicach błędów pomiarowych.

W ramach badań atomu europu, na podstawie 73 zarejestrowanych linii widmowych wyznaczono wartości stałych nadsubtelnych A i B oraz wartości przesunięć izotopowych dla 26 poziomów energetycznych, należących do konfiguracji parzystych. Wartości te dla 10 spośród badanych poziomów zostały wyznaczone po raz pierwszy, dla 3 kolejnych – nieco bardziej precyzyjnie niż w przypadku opublikowanych we wcześniejszej pracy, będącej w dorobku niniejszej grupy badawczej.

Wyznaczono także wartości czynników Landégo g_J dla 23 poziomów energetycznych, w oparciu o analizę 54 linii widmowych. Dla 16 poziomów nieparzystych i 7 parzystych wartości te zostały wyznaczone po raz pierwszy. W niewielkim stopniu korygowano także wartości dla kolejnych 3 poziomów, należących do konfiguracji parzystych.

Celem prowadzonych badań było poszukiwanie kanałów fluorescencji oraz eksperymentalne wyznaczenie wymienionych parametrów pod kątem poszerzenia wiedzy o strukturze atomu obu materiałów. Jest to bezpośrednio związane ze zwiększeniem potencjalnych możliwości wykorzystania terbu i europu w oparciu o ich właściwości fluorescencyjne, a także magnetyczne. Zarówno terb i europ są materiałami szeroko wykorzystywanymi w zastosowaniach konwencjonalnych, takich jak luminofory, lampy, ekrany telewizorów, itd. ale są także potencjalnymi kandydatami na materiały kwantowe, wykorzystywane np. w komputerach i pamięciach kwantowych. Jak przytoczono we wstępie, badania na tym polu wciąż trwają. Poszerzenie baz danych struktury pierwiastków jest niezwykle istotne dla realizacji eksperymentów z zakresu inżynierii kwantowej, wymagających pułapkowania czy chłodzenia atomów. Do osiągnięcia takiego stanu wykorzystuje się określone przejścia pomiędzy poziomami energetycznymi, spełniającymi niezbędne kryteria. Zarówno stałe struktury nadsubtelnej A i B , jak i czynniki Landégo g_J stanowią swego rodzaju „odcisk palca” – są to charakterystyczne parametry, opisujące dany poziom energetyczny. Na ich podstawie możliwe było jednoznaczne sklasyfikowanie badanych linii widmowych. Wzbogacanie dostępnych baz danych o nowe wartości eksperymentalne tych parametrów oraz klasyfikacja obserwowanych linii widmowych stwarza zatem dodatkowe możliwości w poszukiwaniu pożądaných przejść. Wyznaczenie stałych A i B oraz czynników g_J umożliwia pełniejszy opis funkcji falowych sprzężenia pośredniego. To z kolei pozwala na lepsze oszacowanie prawdopodobieństw przejść między poziomami, czyli natężenia kanałów fluorescencji, które są proporcjonalne do tych prawdopodobieństw. Ponadto, wspiera to także teoretyczny opis struktury danego pierwiastka. Dla pierwiastków, w których dochodzi do mieszania konfiguracji, takich jak terb i europ, a także pozostałe lantanowce, opis semi-empiryczny pozwala na uzyskanie lepszych rezultatów niż obliczenia *ab initio*. Jednak aby opis był jak najbardziej dokładny, niezbędne jest możliwie jak najwięcej danych eksperymentalnych. W przypadku terbu, w dalszym ciągu nie udało się przeprowadzić takiego opisu dla konfiguracji nieparzystych, ze względu na duży stopień złożoności tego układu.

Wyniki badań, opublikowane w przedłożonych pracach stanowią znaczące rozwinięcie dostępnych baz danych struktury atomów terbu i europu. Mogą one przyczynić się do rozwinięcia istniejących oraz potencjalnych zastosowań obu materiałów, zarówno konwencjonalnych, jak i kwantowych, a także dalszą analizę teoretyczną ich struktury.

LITERATURA

- [1] M. Burchard-Dziubińska, *Strategiczna rola metali ziem rzadkich w gospodarce opartej na wiedzy*, *Gospodarka w Praktyce i Teorii* 1(34), 2014, URI: <http://hdl.handle.net/11089/11867>
- [2] N. J. Stone, *Table of nuclear magnetic dipole and electric quadrupole moments*, *At. Data Nucl. Data Tables* 90, 75–176, 2005, DOI: <https://doi.org/10.1016/j.adt.2005.04.001>
- [3] G. Yonuschot, G. W. Mushrush, *Terbium as a fluorescent probe for DNA and chromatin*, *Biochemistry* 14 (8), 1677-1681, 1975, DOI: <https://doi.org/10.1021/bi00679a020>
- [4] C. Müller, K. A. Domnanich, C. A. Umbrecht, N.P. van der Meulen, *Scandium and terbium radionuclides for radiotheranostics: current state of development towards clinical application*, *Br J Radiol.* 91(1091), 20180074, 2018, DOI: <https://doi.org/10.1259/bjr.20180074>
- [5] R. L. Smith, A. L. Wysocki, K. Park, *Electrically tuned hyperfine spectrum in neutral Tb(II)(Cp^{iPr5})₂ single-molecule magnet*, *Physical Chemistry Chemical Physics* 22(38), 21793–21800, 2020, DOI: <https://doi.org/10.1039/D0CP04056H>
- [6] S. P. Davis, *Hyperfine structure, Zeeman effects, and separation of lines in terbium spectra*, *Astrophys. J.* 2, 486–492, 1960, DOI: <https://www.doi.org/10.1086/146946>
- [7] C. Arnoult, S. Gerstenkorn, *Experimental and theoretical hyperfine structure of low-lying levels of terbium 4f⁸5d6s² configuration; quadrupole moment of ¹⁵⁹Tb*, *J Opt Soc Am* 56(2), 177–81, 1966, DOI: <https://doi.org/10.1364/JOSA.56.000177>
- [8] W. J. Childs, *Hyperfine structure of many atomic levels of Tb¹⁵⁹ and the Tb¹⁵⁹ nuclear electric-quadrupole moment*, *Phys Rev A* 2, 316–336, 1970, DOI: <https://doi.org/10.1103/PhysRevA.2.316>
- [9] W. J. Childs, L. S. Goodman, *Assignment of unclassified lines in Tb I through high-resolution laser-fluorescence measurements of hyperfine structure*, *J Opt Soc Am* 69, 815–819, 1979, DOI: <https://doi.org/10.1364/JOSA.69.000815>
- [10] W. J. Childs, *Use of atomic-beam laser radio-frequency double resonance for interpretation of complex spectra: Tb I as a test case*, *J Opt Soc Am B* 9, 191–196, 1992, DOI: <https://doi.org/10.1364/JOSAB.9.000191>
- [11] P. F. A. Klinkenberg, T. A. M. Van Kleef, *The ground state of the terbium atom*, *Physica (Utrecht)* 50, 625–628, 1970, DOI: <https://doi.org/10.1016/0031-8914%2870%2990218-1>
- [12] I. Bender, S. Penselin, K. Schlüpmann, *Zur frage des grundzustandes im Tb I spektrum*, *Z Phys* 179(1), 4–8, 1964, DOI: <https://doi.org/10.1007/BF01379209>

- [13] W. J. Childs, L. S. Goodman, *Hyperfine structure and g_J values of low levels of ^{159}Tb* . J Opt Soc Am 59(7), 875, 1969,
DOI: <https://doi.org/10.1364/JOSA.59.000875>
- [14] P. F. A. Klinkenberg, *Structure of the spectrum of neutral terbium, Tb I*, Physica (Utrecht) 32, 1113–47, 1966,
DOI: <https://doi.org/10.1016/0031-8914%2866%2990147-9>
- [15] P. F. A. Klinkenberg, E. Meinders, *Structure of the spectrum of neutral terbium, Tb I. Part II*, Physica (Utrecht) 32, 1617–32, 1966,
DOI: <https://doi.org/10.1016/0031-8914%2866%2990077-2>
- [16] P. F. A. Klinkenberg, *Structure of the spectrum of neutral terbium, Tb I. Part III: levels having extreme values of J* , Physica (Utrecht) 37, 197–214, 1967,
DOI: <https://doi.org/10.1016/0031-8914%2867%2990151-6>
- [17] E. Meinders, P. F. A. Klinkenberg, *Structure of the spectrum of neutral terbium, Tb I. Part IV*, Physica (Utrecht) 38, 253–74, 1968,
DOI: <https://doi.org/10.1016/0031-8914%2868%2990149-3>
- [18] P. F. A. Klinkenberg, E. Meinders, *Structure of the spectrum of neutral terbium, Tb I. Part V: the configuration $4f^8 5d^2 6s$* , Physica (Utrecht) 42, 213–41, 1969,
DOI: <https://doi.org/10.1016/0031-8914%2869%2990014-7>
- [19] P. F. A. Klinkenberg, *Structure of the spectrum of neutral terbium, Tb I. Part VI: the sextet system of $4F^8(^7F)5d6s^2$* , Physica (Utrecht) 57, 594–615, 1972,
DOI: <https://doi.org/10.1016/0031-8914%2872%2990048-1>
- [20] J. Kim, B. Friedrich, D. P. Katz, D. Patterson, J. D. Weinstein, R. DeCarvalho, *et al.*, *Buffer-gas loading and magnetic trapping of atomic europium*, Phys Rev Lett 78, 3665–8, 1997, DOI: <https://doi.org/10.1103/PhysRevLett.78.3665>
- [21] R. Inoue, Y. Miyazawa, M. Kozuma, *Magneto-optical trapping of optically pumped metastable europium*, Phys Rev A 97, 061607, 2018,
DOI: <https://doi.org/10.1103/PhysRevA.97.061607>
- [22] D. Serrano, S. K. Kuppasamy, B. Heinrich, *et al.*, *Ultra-narrow optical linewidths in rare-earth molecular crystals*, Nature 603, 241–246, 2022,
DOI: <https://doi.org/10.1038/s41586-021-04316-2>
- [23] J. Kuhl, *Hyperfeinstrukturuntersuchungen mit einem sphärischen Fabry-Perot-Interferometer mit internem Absorptionsatomstrahl im Tm I- und Eu I-Spektrum*, Zeitschrift für Physik A Hadrons and nuclei, 242, 66–85, 1971,
DOI: <https://doi.org/10.1007/BF01395380>
- [24] J. Bauche, R.-J. Champeau, *Recent Progress in the Theory of Atomic Isotope Shift*, Advances in Atomic and Molecular Physics, 12, 39-86, 1976,
DOI: <https://doi.org/10.1016/S0065-2199%2808%2960042-1>

- [25] D. Skrok, R. Winkler, *Level classification in the configurations $4f^6 5d 6s^2$ and $4f^7 5d 6p$ of $^{151}, ^{153}\text{Eu-I}$ by isotope shift measurements*, Physica B+C, 85(1), 214-218, 1976, DOI: <https://doi.org/10.1016/0378-4363%2876%2990116-9>
- [26] B. Furmann, D. Stefańska, *Isotope shift and hyperfine structure in even configurations of neutral europium*, J. Phys. B: At. Mol. Opt. Phys., 44, 225005, 2011, DOI: <https://doi.org/10.1088/0953-4075/44/22/225005>
- [27] G. Smith, F. S. Tomkins, G. W. R. Stephen, *The absorption spectrum of europium*, Phil Trans R Soc A 283, 345–65, 1976, DOI: <https://doi.org/10.1098/rsta.1976.0089>
- [28] D. Stefańska, M. Suski, B. Furmann, *Tunable continuous wave single-mode dye laser directly pumped by a diode laser*, Laser Phys Lett 14(4), 045701, 2017, DOI: <https://doi.org/10.1088/1612-202X/aa5f00>
- [29] D. Stefańska, M. Suski, B. Furmann, *Diode laser optical pumping of a tunable single-mode dye laser*, Workshop on Current Problems in Physics, 16-19 October 2017, Zielona Góra
- [30] D. Stefańska, M. Suski, A. Zygmunt, J. Stachera, B. Furmann, *Tunable single-mode cw energy-transfer dye laser directly optically pumped by a diode laser*, Opt Laser Technol 120, 105673, 2019, DOI: <https://doi.org/10.1016/j.optlastec.2019.105673>
- [31] I. I. Sobelman, *Atomic Spectra and Radiative Transitions*, Springer-Verlag, Berlin Heidelberg New York, 1979, ISBN 3-540-09082-7
- [32] H. Haken, H. C. Wolf, *Atomy i kwanty. Wprowadzenie do współczesnej spektroskopii atomowej*, Wydawnictwo Naukowe PWN, Warszawa, 1997, ISBN 83-01-12135-1
- [33] J. E. Mack, H. Arroe, *Isotope shift in atomic spectra*, Annual Review of Nuclear Science, 6(1), 117-128, 1956, DOI: <https://doi.org/10.1146/annurev.ns.06.120156.001001>
- [34] W. Demtröder, *Atoms, Molecules and Photons. An Introduction to Atomic-, Molecular- and Quantum-Physics*, Springer-Verlag, Berlin Heidelberg, 2010, ISBN 978-3-642-10297-4
- [35] M. Chomski, B. Furmann, J. Ruczkowski, M. Suski, D. Stefańska, *Landé g_J factors of the electronic levels of the holmium atom*, J Quant Spectrosc Radiat Transfer 274, 107865, 2021, DOI: <https://doi.org/10.1016/j.jqsrt.2021.107865>
- [36] D. Grabowski, R. Drozdowski, J. Kwela, J. Heldt, *Hyperfine structure and Zeeman effect studies in the $6p^7p-6p^7s$ transitions in Bi II*, Zeitschrift Für Physik D Atoms, Molecules and Clusters, 38(4), 289–293, 1996, DOI: <https://doi.org/10.1007/s004600050093>

Pozostałe publikacje współautorskie

1. D. Stefańska, **M. Suski**, B. Furmann, *Tunable continuous wave single-mode dye laser directly pumped by a diode laser*, *Laser Physics Letters* 14, 045701 (7pp), 2017, DOI: <https://doi.org/10.1088/1612-202X/aa5f00>
2. B. Furmann, D. Stefańska, **M. Suski**, S. Wilman, *Identification of new electronic levels in the holmium atom and investigation of their hyperfine structure*, *Journal of Quantitative Spectroscopy and Radiative Transfer* 219, 117-126, 2018, DOI: <https://doi.org/10.1016/j.jqsrt.2018.08.005>
3. B. Furmann, D. Stefańska, **M. Suski**, S. Wilman, M. Chomski, *Hyperfine structure studies of the odd-parity electronic levels of the holmium atom. I: Levels with known energies*, *Journal of Quantitative Spectroscopy and Radiative Transfer*, 234, 115–123, 2019, DOI: <https://doi.org/10.1016/j.jqsrt.2019.05.028>
4. B. Furmann, D. Stefańska, S. Wilman, M. Chomski, **M. Suski**, *Hyperfine structure studies of the odd-parity electronic levels in the holmium atom. II: New levels*, *Journal of Quantitative Spectroscopy and Radiative Transfer*, 235, 70–80, 2019, DOI: <https://doi.org/10.1016/j.jqsrt.2019.06.005>
5. D. Stefańska, **M. Suski**, A. Zygmunt, J. Stachera, B. Furmann, *Tunable single-mode cw energy-transfer dye laser directly optically pumped by a diode laser*, *Optics & Laser Technology*, 120, 105673, 2019, DOI: <https://doi.org/10.1016/j.optlastec.2019.105673>
6. D. Stefańska, B. Furmann, J. Ruczkowski, M. Elantkowska, P. Głowacki, M. Chomski, **M. Suski**, S. Wilman, *Investigations of the possible second-stage laser cooling transitions for the holmium atom magneto-optical trap*, *Journal of Quantitative Spectroscopy and Radiative Transfer*, 246, 106915, 2020, DOI: <https://doi.org/10.1016/j.jqsrt.2020.106915>
7. M. Elantkowska, J. Ruczkowski, S. Wilman, **M. Suski**, *Semi-empirical determination of the nuclear quadrupole moment of ^{109}Sn* , *European Physical Journal Plus*, 136(3), 330, 2021, DOI: <https://doi.org/10.1140/epjp/s13360-021-01231-3>
8. M. Chomski, B. Furmann, J. Ruczkowski, **M. Suski**, D. Stefańska, *Landé g_J factors of the electronic levels of the holmium atom*, *Journal of Quantitative Spectroscopy and Radiative Transfer*, 274, 107865, 2021, DOI: <https://doi.org/10.1016/j.jqsrt.2021.107865>
9. M. Chomski, **M. Suski**, S. Wilman, B. Furmann, J. Ruczkowski, D. Stefańska, *Landé g_J factors of odd-parity electronic levels of the holmium atom*, *Journal of Quantitative Spectroscopy and Radiative Transfer*, 279, 108045, 2022, DOI: <https://doi.org/10.1016/j.jqsrt.2021.108045>

10. M. Chomski, B. Furmann, **M. Suski**, P. Głowacki, D. Stefańska, S. Mieloch, *Determination of the energies of new electronic levels of the holmium atom and investigation of their hyperfine structure*, Journal of Quantitative Spectroscopy and Radiative Transfer, 297, 108480, 2023,
DOI: <https://doi.org/10.1016/j.jqsrt.2022.108480>

ZAŁĄCZNIKI

Poznań, 5.07.2023r.

mgr inż. Marcin Suski
Instytut Badań Materiałowych i Inżynierii Kwantowej,
Wydział Inżynierii Materiałowej i Fizyki Technicznej,
Politechnika Poznańska
ul. Piotrowo 3
60-965 Poznań
e-mail: marcin.j.suski@doctorate.put.poznan.pl, **tel.** +48 61 665 3229

Oświadczenie współautora artykułów naukowych

Oświadczam, że jestem współautorem następujących prac, składanych jako spójny tematycznie cykl publikacji naukowych w ramach mojej pracy doktorskiej:

1. B. Furmann, D. Stefańska, M. Chomski, M. Suski, S. Wilman, „*Hyperfine structure studies of the odd-parity electronic levels of the terbium atom*”, *Journal of Quantitative Spectroscopy & Radiative Transfer*, 2019, vol. 237 (106613).
2. M. Suski, B. Furmann, M. Chomski, S. Mieloch, P. Głowacki, D. Stefańska, „*Hyperfine structure investigations of the odd-parity electronic levels of the terbium atom*”, *Journal of Quantitative Spectroscopy & Radiative Transfer*, 2023, vol. 298 (108492).
3. M. Suski, M. Chomski, B. Furmann, J. Ruczkowski, D. Stefańska, „*Landé g_J factors of the even-parity electronic levels of the terbium atom*”, *Journal of Quantitative Spectroscopy & Radiative Transfer*, 2022, vol. 288 (108270).
4. M. Suski, B. Furmann, M. Chomski, J. Ruczkowski, D. Stefańska, S. Mieloch, „*Landé g_J factors of the odd-parity electronic levels of the terbium atom determined by laser spectroscopy*”, *Journal of Quantitative Spectroscopy & Radiative Transfer*, 2022, vol. 291 (108342).
5. B. Furmann, M. Chomski, M. Suski, S. Wilman, D. Stefańska, „*Investigations of the hyperfine structure and isotope shifts in the even-parity level system of atomic europium*”, *Journal of Quantitative Spectroscopy & Radiative Transfer*, 2020, vol. 251 (107070).
6. B. Furmann, J. Ruczkowski, M. Chomski, M. Suski, S. Wilman, D. Stefańska, „*Landé g_J factors of the electronic levels of the europium atom*”, *Journal of Quantitative Spectroscopy & Radiative Transfer*, 2020, vol. 255 (107258).

Mój udział w niniejszych pracach polegał na:

- Ad. 1. Udziale w badaniach, analizie formalnej, pomocy w opracowaniu wyników prac badawczych.
- Ad. 2. Udziale w badaniach, analizie formalnej, opracowaniu wyników badań, redakcji manuskryptu oraz przygotowaniu odpowiedzi dla recenzentów.
- Ad. 3. Udziale w badaniach, analizie formalnej, opracowaniu wyników badań, redakcji manuskryptu oraz przygotowaniu odpowiedzi dla recenzentów.
- Ad. 4. Udziale w badaniach, analizie formalnej, opracowaniu wyników badań, redakcji manuskryptu oraz przygotowaniu odpowiedzi dla recenzentów

Ad. 5. Udziale w badaniach, analizie formalnej, pomocy w opracowaniu wyników prac badawczych.

Ad. 6. Udziale w badaniach, analizie formalnej, pomocy w opracowaniu wyników prac badawczych.

Suski

.....
(podpis współautora)

Poznań, 5.07.2023r.

dr hab. Bogusław Furmann, prof. PP
Instytut Badań Materiałowych i Inżynierii Kwantowej,
Wydział Inżynierii Materiałowej i Fizyki Technicznej,
Politechnika Poznańska
ul. Piotrowo 3
60-965 Poznań
e-mail: boguslaw.furmann@put.poznan.pl, tel. +48 61 665 3226

Oświadczenie współautora artykułów naukowych

Oświadczam, że opublikowałem z mgr. inż. Marcinem Suskim następujące prace:

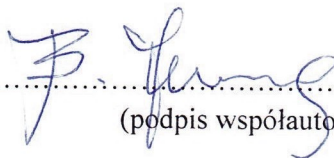
1. B. Furmann, D. Stefańska, M. Chomski, M. Suski, S. Wilman, „*Hyperfine structure studies of the odd-parity electronic levels of the terbium atom*”, Journal of Quantitative Spectroscopy & Radiative Transfer, 2019, vol. 237 (106613).
2. M. Suski, B. Furmann, M. Chomski, S. Mieloch, P. Głowacki, D. Stefańska, „*Hyperfine structure investigations of the odd-parity electronic levels of the terbium atom*”, Journal of Quantitative Spectroscopy & Radiative Transfer, 2023, vol. 298 (108492).
3. M. Suski, M. Chomski, B. Furmann, J. Ruczkowski, D. Stefańska, „*Landé g_J factors of the even-parity electronic levels of the terbium atom*”, Journal of Quantitative Spectroscopy & Radiative Transfer, 2022, vol. 288 (108270).
4. M. Suski, B. Furmann, M. Chomski, J. Ruczkowski, D. Stefańska, S. Mieloch, „*Landé g_J factors of the odd-parity electronic levels of the terbium atom determined by laser spectroscopy*”, Journal of Quantitative Spectroscopy & Radiative Transfer, 2022, vol. 291 (108342).
5. B. Furmann, M. Chomski, M. Suski, S. Wilman, D. Stefańska, „*Investigations of the hyperfine structure and isotope shifts in the even-parity level system of atomic europium*”, Journal of Quantitative Spectroscopy & Radiative Transfer, 2020, vol. 251 (107070).
6. B. Furmann, J. Ruczkowski, M. Chomski, M. Suski, S. Wilman, D. Stefańska, „*Landé g_J factors of the electronic levels of the europium atom*”, Journal of Quantitative Spectroscopy & Radiative Transfer, 2020, vol. 255 (107258).

Mój udział w niniejszych pracach polegał na:

- Ad. 1. Konceptualizacji prac badawczych, nadzorowaniu oraz udziale w badaniach, opracowaniu i walidacji wyników prac badawczych, analizie formalnej, wizualizacji wyników, zgromadzeniu funduszy, redakcji manuskryptu oraz przygotowaniu odpowiedzi dla recenzentów.
- Ad. 2. Pomocy w opracowaniu wyników badań oraz analizie formalnej, nadzorowaniu oraz udziale w pracach badawczych, przygotowaniu oprogramowania, zgromadzeniu funduszy oraz pomocy w redakcji manuskryptu.
- Ad. 3. Pomocy w opracowaniu wyników badań oraz analizie formalnej, nadzorowaniu oraz udziale w pracach badawczych, przygotowaniu oprogramowania, zgromadzeniu funduszy oraz pomocy w redakcji manuskryptu.

- Ad. 4. Pomocy w opracowaniu wyników badań oraz analizie formalnej, nadzorowaniu oraz udziale w pracach badawczych, przygotowaniu oprogramowania, zgromadzeniu funduszy oraz pomocy w redakcji manuskryptu.
- Ad. 5. Konceptualizacji prac badawczych, nadzorowaniu oraz udziale w badaniach, opracowaniu i walidacji wyników prac badawczych, analizie formalnej, wizualizacji wyników, zgromadzeniu funduszy, redakcji manuskryptu oraz przygotowaniu odpowiedzi dla recenzentów.
- Ad. 6. Konceptualizacji prac badawczych, nadzorowaniu oraz udziale w badaniach, opracowaniu i walidacji wyników prac badawczych, analizie formalnej, wizualizacji wyników, zgromadzeniu funduszy, redakcji manuskryptu oraz przygotowaniu odpowiedzi dla recenzentów.

Wyrażam zgodę na przedłożenie wyżej wymienionych prac przez mgr. inż. Marcina Suskiego jako części rozprawy doktorskiej w formie spójnego tematycznie zbioru artykułów naukowych.


.....
(podpis współautora)

Poznań, 5.07.2023r.

dr hab. Jarosław Ruczkowski
Instytut Robotyki i Inteligencji Maszynowej,
Wydział Automatyki, Robotyki i Elektrotechniki,
Politechnika Poznańska
ul. Piotrowo 3
60-965 Poznań
e-mail: jaroslaw.ruczkowski@put.poznan.pl, tel. +48 61 665 3228

Oświadczenie współautora artykułów naukowych


Oświadczam, że opublikowałem z mgr. inż. Marcinem Suskim następujące prace:

1. M. Suski, M. Chomski, B. Furmann, J. Ruczkowski, D. Stefańska, „*Landé g_J factors of the even-parity electronic levels of the terbium atom*”, *Journal of Quantitative Spectroscopy & Radiative Transfer*, 2022, vol. 288 (108270).
2. M. Suski, B. Furmann, M. Chomski, J. Ruczkowski, D. Stefańska, S. Mieloch, „*Landé g_J factors of the odd-parity electronic levels of the terbium atom determined by laser spectroscopy*”, *Journal of Quantitative Spectroscopy & Radiative Transfer*, 2022, vol. 291 (108342).
3. B. Furmann, J. Ruczkowski, M. Chomski, M. Suski, S. Wilman, D. Stefańska, „*Landé g_J factors of the electronic levels of the europium atom*”, *Journal of Quantitative Spectroscopy & Radiative Transfer*, 2020, vol. 255 (107258)

Mój udział w niniejszych pracach polegał na:

- Ad. 1. Udziale w analizie formalnej, przygotowaniu oprogramowania, redakcji części manuskryptu.
- Ad. 2. Udziale w analizie formalnej, przygotowaniu oprogramowania, redakcji części manuskryptu.
- Ad. 3. Konceptualizacji prac badawczych, przygotowaniu oprogramowania, redakcji części manuskryptu.

Wyrażam zgodę na przedłożenie wyżej wymienionych prac przez mgr. inż. Marcina Suskiego jako części rozprawy doktorskiej w formie spójnego tematycznie zbioru artykułów naukowych.


.....
(podpis współautora)

Poznań, 5.07.2023r.

dr hab. Danuta Stefańska

Instytut Badań Materiałowych i Inżynierii Kwantowej,

Wydział Inżynierii Materiałowej i Fizyki Technicznej,

Politechnika Poznańska

ul. Piotrowo 3

60-965 Poznań

e-mail: danuta.stefanska@put.poznan.pl, **tel.** +48 61 665 3232

Oświadczenie współautora artykułów naukowych

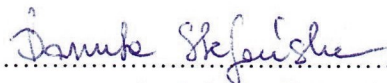
Oświadczam, że opublikowałam z mgr. inż. Marcinem Suskim następujące prace:

1. B. Furmann, D. Stefańska, M. Chomski, M. Suski, S. Wilman, „*Hyperfine structure studies of the odd-parity electronic levels of the terbium atom*”, *Journal of Quantitative Spectroscopy & Radiative Transfer*, 2019, vol. 237 (106613).
2. M. Suski, B. Furmann, M. Chomski, S. Mieloch, P. Głowacki, D. Stefańska, „*Hyperfine structure investigations of the odd-parity electronic levels of the terbium atom*”, *Journal of Quantitative Spectroscopy & Radiative Transfer*, 2023, vol. 298 (108492).
3. M. Suski, M. Chomski, B. Furmann, J. Ruczkowski, D. Stefańska, „*Landé g_J factors of the even-parity electronic levels of the terbium atom*”, *Journal of Quantitative Spectroscopy & Radiative Transfer*, 2022, vol. 288 (108270).
4. M. Suski, B. Furmann, M. Chomski, J. Ruczkowski, D. Stefańska, S. Mieloch, „*Landé g_J factors of the odd-parity electronic levels of the terbium atom determined by laser spectroscopy*”, *Journal of Quantitative Spectroscopy & Radiative Transfer*, 2022, vol. 291 (108342).
5. B. Furmann, M. Chomski, M. Suski, S. Wilman, D. Stefańska, „*Investigations of the hyperfine structure and isotope shifts in the even-parity level system of atomic europium*”, *Journal of Quantitative Spectroscopy & Radiative Transfer*, 2020, vol. 251 (107070).
6. B. Furmann, J. Ruczkowski, M. Chomski, M. Suski, S. Wilman, D. Stefańska, „*Landé g_J factors of the electronic levels of the europium atom*”, *Journal of Quantitative Spectroscopy & Radiative Transfer*, 2020, vol. 255 (107258).

Mój udział w niniejszych pracach polegał na:

- Ad. 1. Udziale w badaniach, pomocy w opracowaniu i walidacji wyników prac badawczych, udziale w analizie formalnej, pomocy w redakcji i edycji manuskryptu.
- Ad. 2. Udziale w pracach badawczych, pomocy w redakcji i edycji manuskryptu.
- Ad. 3. Udziale w pracach badawczych, pomocy w redakcji i edycji manuskryptu.
- Ad. 4. Udziale w pracach badawczych, pomocy w redakcji i edycji manuskryptu.
- Ad. 5. Udziale w pracach badawczych, pomocy w redakcji i edycji manuskryptu.
- Ad. 6. Udziale w pracach badawczych, pomocy w redakcji i edycji manuskryptu.

Wyrażam zgodę na przedłożenie wyżej wymienionych prac przez mgr. inż. Marcina Suskiego jako części rozprawy doktorskiej w formie spójnego tematycznie zbioru artykułów naukowych.



(podpis współautora)

Poznań, 5.07.2023r.

dr inż. Przemysław Głowacki
Instytut Badań Materiałowych i Inżynierii Kwantowej,
Wydział Inżynierii Materiałowej i Fizyki Technicznej,
Politechnika Poznańska
ul. Piotrowo 3
60-965 Poznań
e-mail: przemyslaw.glowacki@put.poznan.pl, tel. +48 61 665 3222

Oświadczenie współautora artykułów naukowych


Oświadczam, że opublikowałem z mgr. inż. Marcinem Suskim następującą pracę:

M. Suski, B. Furmann, M. Chomski, S. Mieloch, P. Głowacki, D. Stefańska, „*Hyperfine structure investigations of the odd-parity electronic levels of the terbium atom*”, *Journal of Quantitative Spectroscopy & Radiative Transfer*, 2023, vol. 298 (108492).

Mój udział w niniejszej pracy polegał na:

Udziale w badaniach, pomocy w opracowaniu wyników badań.

Wyrażam zgodę na przedłożenie wyżej wymienionej pracy przez mgr. inż. Marcina Suskiego jako części rozprawy doktorskiej w formie spójnego tematycznie zbioru artykułów naukowych.


.....
(podpis współautora)

mgr inż. Maciej Chomski

Instytut Badań Materiałowych i Inżynierii Kwantowej,

Wydział Inżynierii Materiałowej i Fizyki Technicznej,

Politechnika Poznańska

ul. Piotrowo 3

60-965 Poznań

e-mail: maciej.s.chomski@doctorate.put.poznan.pl, tel. +48 61 665 3229

Oświadczenie współautora artykułów naukowych

Oświadczam, że opublikowałem z mgr. inż. Marcinem Suskim następujące prace:

1. B. Furmann, D. Stefańska, M. Chomski, M. Suski, S. Wilman, „*Hyperfine structure studies of the odd-parity electronic levels of the terbium atom*”, *Journal of Quantitative Spectroscopy & Radiative Transfer*, 2019, vol. 237 (106613).
2. M. Suski, B. Furmann, M. Chomski, S. Mieloch, P. Głowacki, D. Stefańska, „*Hyperfine structure investigations of the odd-parity electronic levels of the terbium atom*”, *Journal of Quantitative Spectroscopy & Radiative Transfer*, 2023, vol. 298 (108492).
3. M. Suski, M. Chomski, B. Furmann, J. Ruczkowski, D. Stefańska, „*Landé g_J factors of the even-parity electronic levels of the terbium atom*”, *Journal of Quantitative Spectroscopy & Radiative Transfer*, 2022, vol. 288 (108270).
4. M. Suski, B. Furmann, M. Chomski, J. Ruczkowski, D. Stefańska, S. Mieloch, „*Landé g_J factors of the odd-parity electronic levels of the terbium atom determined by laser spectroscopy*”, *Journal of Quantitative Spectroscopy & Radiative Transfer*, 2022, vol. 291 (108342).
5. B. Furmann, M. Chomski, M. Suski, S. Wilman, D. Stefańska, „*Investigations of the hyperfine structure and isotope shifts in the even-parity level system of atomic europium*”, *Journal of Quantitative Spectroscopy & Radiative Transfer*, 2020, vol. 251 (107070).
6. B. Furmann, J. Ruczkowski, M. Chomski, M. Suski, S. Wilman, D. Stefańska, „*Landé g_J factors of the electronic levels of the europium atom*”, *Journal of Quantitative Spectroscopy & Radiative Transfer*, 2020, vol. 255 (107258).

Mój udział w niniejszych pracach polegał na:

- Ad. 1. Udziały w badaniach, analizie formalnej, pomocy w opracowaniu wyników prac badawczych.
- Ad. 2. Udziały w badaniach, analizie formalnej, pomocy w opracowaniu wyników prac badawczych.
- Ad. 3. Udziały w badaniach, analizie formalnej, pomocy w opracowaniu wyników prac badawczych.
- Ad. 4. Udziały w badaniach, analizie formalnej, pomocy w opracowaniu wyników prac badawczych.

Ad. 5. Udziale w badaniach, analizie formalnej, pomocy w opracowaniu wyników prac badawczych.

Ad. 6. Udziale w badaniach, analizie formalnej, pomocy w opracowaniu wyników prac badawczych.

Wyrażam zgodę na przedłożenie wyżej wymienionych prac przez mgr. inż. Marcina Suskiego jako części rozprawy doktorskiej w formie spójnego tematycznie zbioru artykułów naukowych.

.....
Chomski Maciej

(podpis współautora)

Poznań, 5.07.2023r.

mgr inż. Szymon Mieloch

Instytut Badań Materiałowych i Inżynierii Kwantowej,

Wydział Inżynierii Materiałowej i Fizyki Technicznej,

Politechnika Poznańska

ul. Piotrowo 3

60-965 Poznań

e-mail: szymon.mieloch@doctorate.put.poznan.pl, tel. +48 61 665 3229

Oświadczenie współautora artykułów naukowych

Oświadczam, że opublikowałem z mgr. inż. Marcinem Suskim następujące prace:

1. M. Suski, B. Furmann, M. Chomski, S. Mieloch, P. Głowacki, D. Stefańska, „*Hyperfine structure investigations of the odd-parity electronic levels of the terbium atom*”, Journal of Quantitative Spectroscopy & Radiative Transfer, 2023, vol. 298 (108492).
2. M. Suski, B. Furmann, M. Chomski, J. Ruczkowski, D. Stefańska, S. Mieloch, „*Landé g_J factors of the odd-parity electronic levels of the terbium atom determined by laser spectroscopy*”, Journal of Quantitative Spectroscopy & Radiative Transfer, 2022, vol. 291 (108342).

Mój udział w niniejszych pracach polegał na:

Ad. 1. Udziale w badaniach, analizie formalnej oraz pomocy w opracowaniu wyników badań.

Ad. 2. Udziale w badaniach oraz pomocy w opracowaniu wyników badań.

Wyrażam zgodę na przedłożenie wyżej wymienionych prac przez mgr. inż. Marcina Suskiego jako części rozprawy doktorskiej w formie spójnego tematycznie zbioru artykułów naukowych.



.....
(podpis współautora)

Poznań, 5.07.2023r.

mgr inż. Sebastian Wilman

Instytut Badań Materiałowych i Inżynierii Kwantowej,

Wydział Inżynierii Materiałowej i Fizyki Technicznej,

Politechnika Poznańska

ul. Piotrowo 3

60-965 Poznań

e-mail: sebastian.b.wilman@doctorate.put.poznan.pl, **tel.** +48 61 665 3229

Oświadczenie współautora artykułów naukowych

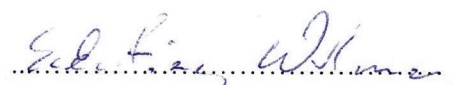
Oświadczam, że opublikowałem z mgr. inż. Marcinem Suskim następujące prace:

1. B. Furmann, D. Stefańska, M. Chomski, M. Suski, S. Wilman, „*Hyperfine structure studies of the odd-parity electronic levels of the terbium atom*”, *Journal of Quantitative Spectroscopy & Radiative Transfer*, 2019, vol. 237 (106613).
2. B. Furmann, M. Chomski, M. Suski, S. Wilman, D. Stefańska, „*Investigations of the hyperfine structure and isotope shifts in the even-parity level system of atomic europium*”, *Journal of Quantitative Spectroscopy & Radiative Transfer*, 2020, vol. 251 (107070).
3. B. Furmann, J. Ruczkowski, M. Chomski, M. Suski, S. Wilman, D. Stefańska, „*Landé g factors of the electronic levels of the europium atom*”, *Journal of Quantitative Spectroscopy & Radiative Transfer*, 2020, vol. 255 (107258).

Mój udział w niniejszych pracach polegał na:

- Ad. 1. Udziale w badaniach, analizie formalnej, pomocy w opracowaniu wyników prac badawczych.
- Ad. 2. Udziale w badaniach, analizie formalnej, pomocy w opracowaniu wyników prac badawczych.
- Ad. 3. Udziale w badaniach, analizie formalnej, pomocy w opracowaniu wyników prac badawczych.

Wyrażam zgodę na przedłożenie wyżej wymienionych prac przez mgr. inż. Marcina Suskiego jako części rozprawy doktorskiej w formie spójnego tematycznie zbioru artykułów naukowych.


(podpis współautora)



Hyperfine structure studies of the odd-parity electronic levels of the terbium atom

B. Furmann*, D. Stefańska, M. Chomski, M. Suski, S. Wilman

Institute of Materials Research and Quantum Engineering, Faculty of Technical Physics, Poznan University of Technology, Piotrowo 3, 60–965 Poznan, Poland



ARTICLE INFO

Article history:

Received 15 July 2019

Revised 18 August 2019

Accepted 20 August 2019

Available online 21 August 2019

Keywords:

Atomic structure

Laser spectroscopy

Hyperfine structure

Terbium

ABSTRACT

In this work the hyperfine structure of 43 odd-parity levels of the terbium atom was investigated with the method of laser induced fluorescence in a hollow cathode discharge. Altogether 73 spectral lines were examined, with the odd-parity levels involved as the upper levels. For 41 levels the constants A and B were determined for the first time, and for the remaining two levels improved values could be obtained due to the supplementary measurements performed. As a by-product, also the hyperfine structure constants for two lower even-parity levels could be corrected. The obtained results concerning the odd-parity levels contributed to considerable extension of the available database of the hyperfine structure constants for the atomic terbium; they would be included in the semi-empirical analysis of the fine and the hyperfine structure for the odd-parity configurations system, planned in our research group.

© 2019 Elsevier Ltd. All rights reserved.

1. Introduction

Terbium is a lanthanide element located close to the middle of the series. Until recently it belonged to the elements with very scarcely investigated electronic levels' structure. A series of experimental works were published already in 1960-ies [1–4]; however, due to the unusually low energy of the first even-parity level it was first mistakenly interpreted as the terbium atom ground state, and the actual odd-parity ground state was correctly identified only in 1970 [5].

With its only stable isotope $^{159}_{65}\text{Tb}$, characterized with a low nuclear spin value $I = 3/2$, terbium exhibits relatively simple hyperfine structure of its electronic levels, but until recently the hfs constants were determined only for a limited number of the lowest-lying levels of both parities [6–8]. In our earlier works the hfs constants A and B were determined for numerous higher-lying levels: 61 even-parity [9–11] and 223 odd-parity ones [12]. The present work is a continuation of investigations concerning the hyperfine structure of the odd-parity electronic levels of atomic terbium, performed within the last work cited.

Despite the essential progress achieved, atomic terbium still belongs to the elements, for which the knowledge of the electronic levels' structure is far from being complete. Extension of this knowledge would certainly be important from the point of view of the theory of complex atoms. In one of our earlier works [11] a

successful semi-empirical analysis of the fine- and the hyperfine structure for the even-parity configuration system was performed - the known A and B constants were reproduced to within a few per cent, thus confirming the correctness of the intermediate-coupling eigenvectors assumed. A similar analysis is also planned for the odd-parity configuration system. However, this system is much more complex, due to the particularly strong overlap of various configurations on the energy scale, and the resulting strong configuration mixing; this issue was pointed out in our earlier work concerning the hfs of the odd-parity levels [12]. Nevertheless systematic extension of the experimental database available may help to solve this nontrivial problem.

More complete description of the electronic levels' structure of the terbium atom is also desired because of the possible applications, among them in quantum engineering and metrology, such as e.g. the measurements of the temporal drift of the fine structure constant α (according to the proposal [13], but possibly with a more suitable pair of levels), or perhaps laser cooling in a magneto-optical trap (with the use of a method developed for lanthanide elements [14], hitherto successfully applied for erbium, thulium, dysprosium and holmium) - if a suitable levels' scheme can be found. Since the only terbium isotope is bosonic, the further perspective of achieving condensation may perhaps also be considered.

2. Experimental details

As in our earlier works concerning the hyperfine structure of electronic levels in the terbium atom, investigations within this

* Corresponding author.

E-mail address: boguslaw.furmann@put.poznan.pl (B. Furmann).

work were performed with the method of laser induced fluorescence (LIF) in a hollow cathode discharge. The important feature of the applied variant of the method is the spectral selection of various decay channels from the excited electronic levels - this is particularly important in investigations of the lanthanides' spectra, where various excitation transitions, involving often very different pairs of electronic levels, overlap in frequency domain.

The experimental setup used in this work was described in more detail in the earlier works concerning this element; in the most recent work on devoted to the odd-parity electronic levels [12] the setup scheme was also presented. Thus the fundamental features of the setup are only briefly reviewed in the following, and only the modifications introduced are described in more detail.

The hollow cathode lamp was the same device as used in our earlier experiments on terbium; the buffer gas used was argon at a pressure of $3.0 - 5.5 \cdot 10^{-1}$ mbar, typical discharge currents of several tens of mA were applied. Further details were described in our earlier work [11].

As the source of light for excitation of the transitions studied, single-mode tunable dye lasers were applied (Coherent model CR 699-21 with modified frequency selection system). Most of the lines were excited with the laser operated on the dye Rhodamine 6G, optically pumped at $\lambda = 532$ nm by a frequency-doubled Nd³⁺:YVO₄ laser (Coherent model Verdi V-10). The remaining transitions, positioned in more short-wavelength regions, were excited by a recently set up energy-transfer dye laser operated on the mixture of Coumarin 498 (donor) and Pyrromethene 556 (acceptor), optically pumped at $\lambda = 445$ nm by a diode laser (Lasever Inc., China, model LSR445SD-4W) [15].

As mentioned, in detection various fluorescence transitions (commonly referred to as the fluorescence channels) were recorded separately; these were selected by a grating monochromator (Carl Zeiss Jena, model SPM-2), occasionally additionally supported by the use of color glass filters.

The transitions' wavenumbers were controlled by a wavemeter (Burleigh, model WA-1500). The exciting laser beam was intensity-modulated by a mechanical chopper and phase-sensitive (lock-in) detection of induced fluorescence was applied; thus the signal-to-noise ratio could be improved. Moreover, the beam exiting the discharge lamp was retroreflected in order to increase the effective interaction path; for a few lines this allowed observation of saturation effects - the resulting Lamb dips on top of the strong components (with $\Delta F = \Delta J$) facilitated determination of the components' positions.

Typically at least 10 (up to several tens) frequency scans were performed, the particular number dependent on the observed quality of the spectra.

3. Results

3.1. General remarks

Altogether 73 spectral lines were investigated, all of them involving even-parity lower levels with *hfs* constants *A* and *B* determined in earlier studies (performed in our research group [11] or by other authors [6–8,16]) and odd-parity upper levels with hitherto unknown *hfs* constants (in two cases - earlier determined constants requiring verification). Altogether 43 odd-parity levels were involved, 41 investigated for the first time. Two spectral lines, investigated earlier under less favorable experimental conditions, were remeasured.

Three examples of the *hfs* patterns of the spectral lines recorded are presented in Fig. 1. For the first line depicted the Lamb dips on top of the $\Delta F = \Delta J$ components can be noticed.

3.2. Values of the *hfs* constants

The spectra were fitted with the use of the program "Fitter" (developed in the research group of Prof. Guthöhrlein in Hamburg). In order to estimate the constants' values, first the patterns averaged over all recorded scans of a particular transition were fitted; further, the *A* and *B* constants were determined from either single scans or groups of a few subsequent scans, and the resulting values were averaged. The final values obtained from analysis of individual spectral lines are compiled in Table 1.

In the majority of cases the known (reliable) *hfs* constants of the lower levels were fixed in the least-squares fitting procedure and only the interesting upper levels' constants were fitted as adjustable parameters. In a few cases, however, lower levels investigated in our earlier work [9] in single lines only were involved. We found that the *hfs* constants for two of such levels need to be reevaluated; the details are discussed in Section 4.

Table 1 is arranged as follows: in columns 2 and 3 the relevant information on the transitions investigated is provided (wavelengths and wavenumbers, respectively); columns 4–7 contain the information on the transitions' lower (even-parity) levels (energies, *J* quantum numbers, the known *hfs* constants *A* and *B*), the respective references being listed in column 8, while the analogous data concerning the upper (odd-parity) levels are included in columns 9–12; the reference information concerning the constants of the upper levels (see above) is included in column 13.

The final values of the *A* and *B* constants for the odd-parity levels are compiled in Table 2. For 25 levels, for which the *hfs* constants were determined from the analysis of single spectral lines, these were adopted directly from Table 1. For the remaining 18 levels, examined in multiple spectral lines, the final values were calculated as means from the values obtained for individual transitions.

3.3. Uncertainties of the *hfs* constants

The uncertainties quoted in Table 1 are of statistical nature only - these are single mean standard deviations. Of course, since the *hfs* *A* and *B* constants of one of the levels involved in a particular line were fixed (this mostly concerned the lower even-parity levels), the respective uncertainties were taken into account when calculating the uncertainties for the *hfs* constants of the other level, evaluated in by the program "Fitter". The standard formula for error propagation ($\sigma = \sqrt{\sigma_1^2 + \sigma_2^2}$, where the subscripts refer to the statistical uncertainties concerning the fixed constant and the relevant fitted constant) was used in these cases.

For the levels investigated in multiple spectral lines the final uncertainties reflect the scattering of the results obtained for individual lines (these were calculated as simple mean standard deviations). Such uncertainties are believed to account also for some of the possible systematic uncertainties, which may shift somewhat the values obtained from a particular line with respect to those obtained from another one, although certainly not all the effects could be revealed in this way.

For the *hfs* constants evaluated from the analysis of single lines the uncertainties were recalculated to account also for the evident systematic factors; this procedure was adopted in our earlier works concerning the holmium atom and described in the first work in that series [17], but it perhaps requires some more detailed description in the case of investigations reported in the present work. There are certainly several conceivable sources of systematic uncertainties in this kind of experiment - the most important of them are discussed below.

No significant scan nonlinearities at the accuracy level of a few MHz was observed - no scattering of the intervals between the marker maxima, used as a kind of "ruler" to generate the relative

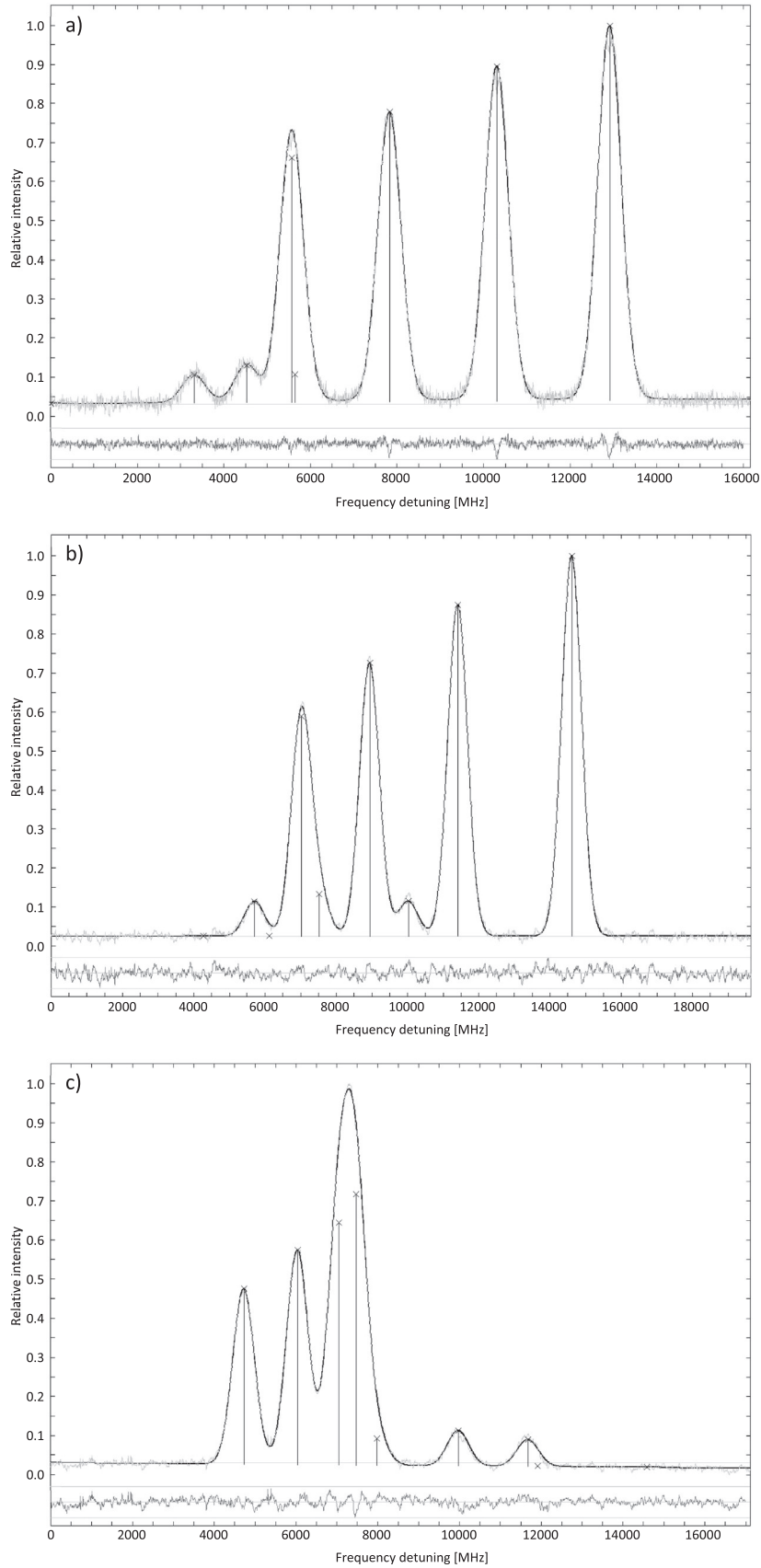


Fig. 1. Examples of the recorded hfs patterns of spectral lines involving odd-parity levels in the terbium atom as the upper levels, along with the components fitted by program “Fitter” (marked with vertical lines): a) $\lambda = 552.412$ nm (line 10 in Table 1: 509.85 cm^{-1} , $J = 11/2 \rightarrow 18607.24$ cm^{-1} , $J = 13/2$ - Lamb dips on top of $\Delta F = \Delta J$ are observed), b) $\lambda = 578.759$ nm (line 32 in Table 1: 5829.86 cm^{-1} , $J = 9/2 \rightarrow 23103.41$ cm^{-1} , $J = 11/2$), c) $\lambda = 596.790$ nm (line 58 in Table 1: 6351.75 cm^{-1} , $J = 13/2 \rightarrow 23103.41$ cm^{-1} , $J = 11/2$). The lower traces, representing the deviations of the experimental data from the respective theoretical curves (scaling factors: 0.5500, 1.5315 and 1.3721, respectively), show the quality of the fit. The horizontal lines at the value of relative intensity close to 0 represent the fitted background.

Table 1

Spectral lines of the terbium atom, investigated in order to determine the hyperfine structure constants for the upper odd-parity levels, along with the A and B values obtained. In most cases the hfs constants of the lower even-parity levels involved in the spectral lines were fixed at the available values in the least-squares fit procedure; the respective citations are given in a separate column. For some spectral lines, involving two particular lower even-parity levels (10680.17 cm^{-1} and 10997.85 cm^{-1}), the hfs constants of these levels were determined instead (for details see text, Section 4.2). The energies of both the lower and the upper levels were taken from the NIST Atomic Spectra Database [18]).

No	Line		Lower level						Upper level				
	λ_{air} (nm)	k_{vac} (cm^{-1})	E (cm^{-1})	J	A (MHz)	B (MHz)	Ref.	E (cm^{-1})	J	A (MHz)	B (MHz)	Ref.	
1	2	3	4	5	6	7	8	9	10	11	12	13	
1	535.488	18669.37	462.08	15/2	472.643 (0.002)	1154.239 (0.017)	[6]	19131.45	17/2	906.1 (0.8)	1411.7 (6.0)		
2	541.424	18464.69	5425.06	15/2	459.627 (0.001)	1724.243 (0.010)	[7]	23889.75	15/2	775.4 (0.5)	1209.2 (5.2)		
3	542.815	18417.37	6351.75	13/2	438.5 (2.2)	1122 (29)	[11]	24769.12	13/2	659.0 (2.3)	694 (30)		
4	542.845	18416.36	7824.19	9/2	621.5 (2.1)	790.1 (3.5)	[11]	26240.55	11/2	397.1 (0.5)	404 (10)		
5	545.648	18321.74	285.50	13/2	532.204 (0.002)	928.861 (0.030)	[6]	18607.24	13/2	843.1 (0.1)	855.3 (2.1)		
6	547.014	18275.98	7767.02	15/2	509.0 (0.9)	2048 (15)	[11]	26043.00	13/2	692.8 (1.0)	1059 (16)		
7	547.265	18267.60	7824.19	9/2	621.5 (2.1)	790.1 (3.5)	[11]	26091.79	11/2	684.5 (0.5)	560.0 (9.0)		
8	550.713	18153.22	3719.71	13/2	354.454 (0.003)	72.183 (0.015)	[6]	21872.93	11/2	765.5 (0.7)	-26.3 (6.0)		
9	550.958	18145.16	462.08	15/2	472.643 (0.002)	1154.239 (0.017)	[6]	18607.24	13/2	842.9 (0.1)	867.3 (1.0)		
10	552.412	18097.40	509.85	11/2	577.465 (0.002)	989.917 (0.030)	[6]	18607.24	13/2	843.3 (0.1)	869.8 (0.4)		
11	553.612	18058.18	285.50	13/2	532.204 (0.002)	928.861 (0.030)	[6]	18343.68	11/2	681.8 (1.2)	368 (17)		
12	559.989	17852.54	8190.46	15/2	948.5 (1.1)	699 (31)	[11]	26043.00	13/2	690.2 (1.1)	1015 (32)		
13	565.488	17678.93	8994.66	7/2	710.991 (0.003)	966.85 (0.003)	[8]	26673.59	9/2	-74.9 (0.3)	1272.0 (4.1)		
14	565.753	17670.66	12906.60	13/2	831.0 (1.1)	820 (17)	[11]	30577.26	15/2	572.2 (1.2)	1275 (18)		
15	565.914	17665.64	5353.37	11/2	267.2 (1.0)	-448.7 (9.8)	[11]	23019.01	9/2	308.2 (1.1)	266 (10)		
16	566.588	17644.60	12932.66	15/2	294.2 (1.8)	406 (24)	[11]	30577.26	15/2	570.9 (1.9)	1299 (25)		
17	567.639	17611.93	9145.23	9/2	1069.3 (0.3)	1088.8 (7.5)	[10]	26757.16	9/2	1113.9 (0.4)	593.7 (9.0)		
18	568.199	17594.59	9897.73	9/2	1109.4 (0.2)	537.3 (3.7)	[10]	27492.32	11/2	395.6 (0.3)	558.7 (4.3)		
19	569.552	17552.79	9897.73	9/2	1109.4 (0.2)	537.3 (3.7)	[10]	27450.52	9/2	564.0 (0.3)	421.4 (4.0)		
20	570.032	17538.00	6351.75	13/2	438.5 (2.2)	1122 (29)	[11]	23889.75	15/2	778.8 (2.3)	1193 (30)		
21	570.186	17533.27	10920.18	3/2	1001.8 (3.2)	-133 (19)	[11]	28453.45	1/2	-213.3 (3.3)			
22	570.574	17521.35	11260.41	11/2	919.9 (2.3)	309 (13)	[11]	28781.76	9/2	473.9 (2.4)	117 (14)		
23	571.088	17505.59	9986.73	9/2	636.719 (0.003)	367.994 (0.003)	[8]	27492.32	11/2	402.4 (0.1)	454.8 (0.4)		
24	571.217	17501.64	10030.35	5/2	783.5 (0.1)	515.4 (9.7)	[9]	27531.99	7/2	677.7 (0.4)	-433 (13)		
25	571.408	17495.79	6351.75	13/2	438.5 (2.2)	1122 (29)	[11]	23847.54	13/2	691.7 (2.3)	675 (30)		
26	574.213	17410.31	2840.17	9/2	441.771 (0.005)	158.750 (0.040)	[6]	20250.48	11/2	474.1 (0.3)	393.5 (4.2)		
27	575.040	17385.27	10680.17	9/2	332.6 (0.1)	-342.3 (1.1)		28065.44	11/2	578.6 (0.1)	680.0 (0.8)	*	
28	575.055	17384.83	5483.98	3/2	-177.8 (7.6)	-504 (23)	[11]	22868.81	3/2	291.7 (8.0)	-367 (24)		
29	576.530	17340.35	2419.48	7/2	591.564 (0.007)	733.233 (0.070)	[6]	19759.83	5/2	708.1 (0.5)	-204.1 (3.8)		
30	576.732	17334.26	7441.03	9/2	509.843 (0.003)	547.483 (0.003)	[8]	24775.29	9/2	518.2 (0.4)	264.2 (2.2)		
31	578.169	17291.18	5353.37	11/2	267.2 (1.0)	-448.7 (9.8)	[11]	22644.55	13/2	755.1 (1.1)	324 (11)		
32	578.759	17273.55	5829.86	9/2	271.2 (0.7)	-349.8 (6.8)	[11]	23103.41	11/2	653.4 (0.8)	40.7 (7.0)		
33	579.988	17236.95	6488.28	7/2	114.9 (0.3)	-498.7 (0.7)	[9]	23725.23	9/2	300.0 (0.5)	109.6 (3.2)		
34	580.004	17236.48	8994.66	7/2	710.991 (0.003)	966.85 (0.003)	[8]	26231.14	5/2	416.7 (0.2)	-302.3 (1.6)		
35	580.576	17219.49	5425.06	15/2	459.626 (0.001)	1724.249 (0.010)	[7]	22644.55	13/2	754.9 (0.1)	268.8 (2.0)		
36	581.058	17205.21	9897.73	9/2	1109.4 (0.2)	537.3 (3.7)	[10]	27102.94	11/2	433.8 (0.3)	159.0 (4.0)		
37	581.601	17189.15	5829.86	9/2	271.2 (0.7)	-349.8 (6.8)	[11]	23019.01	9/2	314.7 (0.8)	304.7 (9.1)		

(continued on next page)

Table 1 (continued)

Line			Lower level					Upper level				
No	λ_{air} (nm)	κ_{vac} (cm^{-1})	E (cm^{-1})	J	A (MHz)	B (MHz)	Ref.	E (cm^{-1})	J	A (MHz)	B (MHz)	Ref.
1	2	3	4	5	6	7	8	9	10	11	12	13
38	582.135	17173.38	6674.15	11/2	527.6 (1.2)	528.4 (1.4)	[11]	23847.54	13/2	687.7 (1.3)	697.2 (2.0)	
39	582.600	17159.67	8932.12	11/2	456.1 (3.1)	589.1 (3.4)	[10]	26091.79	11/2	684.8 (3.2)	586.4 (4.0)	
40	583.741	17126.15	1371.05	9/2	602.219 (0.003)	1267.267 (0.030)	[6]	18497.20	9/2	560.0 (0.2)	224.9 (1.4)	
41	584.080	17116.21	9986.73	9/2	636.719 (0.003)	367.994 (0.003)	[8]	27102.94	11/2	440.2 (0.1)	123.0 (0.4)	
42	585.743	17067.59	10997.85	11/2	498.2 (0.1)	1059.5 (1.1)		28065.44	11/2	578.6 (0.1)	680.0 (0.8)	*
43	586.311	17051.08	6674.15	11/2	527.6 (1.2)	528.4 (1.4)	[11]	23725.23	9/2	298.0 (1.3)	30.2 (3.4)	
44	587.226	17024.49	9763.02	13/2	469.4 (0.8)	1480 (11)	[11]	26787.51	13/2	948.9 (0.9)	803 (12)	
45	589.021	16972.63	1371.05	9/2	602.219 (0.003)	1267.267 (0.030)	[6]	18343.68	11/2	686.4 (0.3)	487.0 (1.1)	
46	589.654	16954.41	10997.85	11/2	498.9 (0.7)	1124 (38)	**	27952.26	9/2	387.1 (0.8)	-185 (39)	
47	589.971	16945.30	9763.02	13/2	469.4 (0.8)	1480 (11)	[11]	26708.32	15/2	673.3 (0.9)	1745 (12)	
48	591.302	16907.16	509.85	11/2	577.465 (0.002)	989.917 (0.030)	[6]	17417.01	9/2	1004.1 (0.1)	334.2 (2.2)	
49	591.925	16889.34	1371.05	9/2	602.219 (0.003)	1267.267 (0.030)	[6]	18260.38	7/2	655.2 (0.4)	-173.9 (3.1)	
50	592.976	16859.43	9897.73	9/2	1109.4 (0.2)	537.3 (3.7)	[10]	26757.16	9/2	1115.4 (1.7)	517 (24)	
51	593.287	16850.57	10997.85	11/2	500.1 (0.8)	1124.6 (6.4)		27848.42	13/2	328.7 (0.7)	399.0 (6.0)	*
52	593.899	16833.21	5829.86	9/2	271.2 (0.7)	-349.8 (6.8)	[11]	22663.07	9/2	550.9 (0.8)	89.7 (8.2)	
53	594.018	16829.85	7059.90	13/2	519.5 (0.7)	1179.7 (2.7)	[11]	23889.75	15/2	776.1 (0.8)	1196.6 (3.2)	
54	594.643	16812.15	10680.17	9/2	329.3 (3.6)	-264 (54)		27492.32	11/2	399.1 (3.5)	506 (53)	*
55	594.651	16811.94	1371.05	9/2	602.219 (0.003)	1267.267 (0.030)	[6]	18182.98	11/2	503.1 (1.7)	646 (32)	
56	595.761	16780.61	5483.98	3/2	-177.8 (7.6)	-504 (23)	[11]	22264.59	1/2	-829.5 (8.0)		
57	596.123	16770.43	9986.73	9/2	636.719 (0.003)	367.994 (0.003)	[8]	26757.16	9/2	1114.6 (0.2)	577.8 (1.5)	
58	596.790	16751.66	6351.75	13/2	438.5 (2.2)	1122 (29)	[11]	23103.41	11/2	656.9 (2.3)	37 (30)	
59	596.860	16749.72	1371.05	9/2	602.219 (0.003)	1267.267 (0.030)	[6]	18120.77	7/2	709.2 (0.9)	-112.3 (5.8)	
60	600.341	16652.60	8932.12	11/2	456.1 (3.1)	589.1 (3.4)	[10]	25584.72	9/2	696.6 (3.2)	524.2 (4.0)	
61	600.813	16639.50	11425.94	13/2	672.5 (0.4)	75.4 (9.9)	[11]	28065.44	11/2	578.6 (0.5)	680 (10)	
62	601.890	16609.72	6259.09	1/2	-1762.5 (8.9)		[11]	22868.81	3/2	298.2 (9.1)	-366.5 (6.3)	
63	602.604	16590.06	8994.66	7/2	710.991 (0.003)	966.85 (0.003)	[8]	25584.72	9/2	700.1 (0.2)	508.5 (3.0)	
64	602.678	16588.01	11260.41	11/2	919.9 (2.3)	309 (13)	[11]	27848.42	13/2	328.0 (2.4)	393 (14)	
65	603.685	16560.35	14016.91	17/2	648.9 (2.3)	669.5 (3.5)	[11]	30577.26	15/2	573.4 (2.4)	1222.8 (4.0)	
66	605.175	16519.56	5353.37	11/2	267.2 (1.0)	-448.7 (9.8)	[11]	21872.93	11/2	767.1 (1.1)	-33 (11)	
67	606.096	16494.47	10997.85	11/2	498.3 (3.6)	1188 (54)		27492.32	11/2	399.1 (3.5)	506 (53)	*
68	608.742	16422.77	10680.17	9/2	328.9 (2.3)	-262 (30)		27102.94	11/2	438.1 (2.2)	115 (28)	*
69	608.753	16422.48	11425.94	13/2	672.5 (0.4)	75.4 (9.9)	[11]	27848.42	13/2	329.4 (0.5)	404 (11)	
70	610.476	16376.13	6351.75	13/2	438.5 (2.2)	1122 (29)	[11]	22727.88	13/2	817.2 (2.3)	-359 (30)	
71	613.434	16297.15	2310.09	11/2	405.106 (0.003)	-92.638 (0.050)	[6]	18607.24	13/2	846.1 (0.2)	861.1 (5.0)	
72	613.598	16292.80	6351.75	13/2	438.5 (2.2)	1122 (29)	[11]	22644.55	13/2	757.2 (2.3)	247 (30)	
73	615.292	16247.94	5483.98	3/2	-177.8 (7.6)	-504 (23)	[11]	21731.92	3/2	-238.4 (8.0)	-563 (24)	

* A and B constants of the upper levels fixed at the values determined from the analysis of the hitherto investigated lines involving them, except for the lines with the lower levels 10680.17 cm^{-1} or 10997.85 cm^{-1} (for detailed description see text, 4.2); the following lines were taken into account in obtaining the constants' values for the particular upper levels: 27102.94 cm^{-1} : lines No 36 and 41, 27492.32 cm^{-1} : lines No 18 and 23, 27848.42 cm^{-1} : lines No 64 and 69, 28065.44 cm^{-1} : line No 61 ** A and B constants of the lower level fixed at the averages calculated from the values obtained for the remaining lines investigated in this work.

Table 2

Compilation of the hyperfine structure constants A and B for the odd-parity levels in the terbium atom investigated in this work. For two levels, examined before in our earlier works under inferior experimental conditions, supplementary data were obtained in the present work; the earlier results mentioned are presented for comparison (no other experimental literature data are available). In parentheses the full uncertainties (in MHz) are quoted.

Level		<i>hfs</i> constants (this work)		<i>hfs</i> constants (earlier works)		
J	E (cm ⁻¹)	A (MHz)	B (MHz)	A (MHz)	B (MHz)	Ref.
1	2	3	4	5	6	7
1/2	22264.59	-830 (10) ^b				
	28453.45	-213.3(6.3) ^b				
3/2	21731.92	-238 (11) ^b	-563 (30) ^b			
	22868.81	295.1(3.1) ^a	-366.8(0.3) ^a			
5/2	19759.83	708.1(2.1) ^b	-204 (17) ^b			
	26231.14	416.7(1.8) ^b	-302 (15) ^b			
7/2	18120.77	709.2(1.8) ^b	-112 (17) ^b			
	18260.38	655.2(1.3) ^b	-174 (15) ^b			
	27531.99	677.7(2.7) ^b	-433 (31) ^b			
9/2	17417.01	1004.1(0.8) ^b	334 (13) ^b			
	18497.20	560.0(1.5) ^b	225 (15) ^b			
	22663.07	550.9(2.1) ^b	90 (21) ^b			
	23019.01	311.5(3.3) ^a	287 (18) ^a			
	23725.23	299.0(1.0) ^a	70 (40) ^a			
	24775.29	518.2(1.7) ^b	264 (15) ^b			
	25584.72	698.3(1.8) ^a	516.5(7.5) ^a			
	26673.59	-74.9(2.0) ^b	1272 (24) ^b			
	26757.16	1114.6(0.5) ^a	563 (24) ^a			
	27450.52	564.0(2.6) ^b	421 (28) ^b			
	27952.26	387.1(1.7) ^b	-185 (52) ^b			
	28781.76	473.9(3.7) ^b	117 (34) ^b			
	11/2	18182.98	503.1(2.5) ^b	646 (45) ^b		
18343.68		684.1(2.3) ^a	428 (60) ^a			
20250.48		474.1(1.0) ^b	394 (16) ^b			
21872.93		766.3(0.8) ^a	-29.5(3.5) ^a			
23103.41		655.2(1.8) ^a	40.5(0.5) ^a			
26091.79		684.7(0.2) ^a	573 (13) ^a			
26240.55		397.1(1.5) ^b	400 (24) ^b			
27102.94		437.0(2.0) ^a	134 (13) ^a	440.4(1.5)	64.2(5.5)	[9]
27492.32		399.1(1.4) ^a	506 (22) ^a			
28065.44		578.6(1.2) ^b	680 (25) ^b			
13/2		18607.24	843.9(0.8) ^a	863.3(3.3) ^a		
	22644.55	755.7(0.8) ^a	281 (23) ^a			
	22727.88	817.2(3.9) ^b	-360 (55) ^b			
	23847.54	689.7(2.0) ^a	688.5(8.5) ^a			
	24769.12	659.0(3.5) ^b	694 (50) ^b			
	26043.00	691.5(1.3) ^a	1037 (22) ^a			
	26787.51	948.9(2.4) ^b	803 (36) ^b			
	27848.42	328.7(0.4) ^a	398.5(3.2) ^a			
15/2	23889.75	776.7(1.1) ^a	1198.6(5.7) ^a			
	26708.32	673.3(1.5) ^b	1745 (27) ^b			
	30577.26	572.2(0.8) ^a	1266 (23) ^a	574.5(1.2)	1243(30)	[11]
17/2	19131.45	906.1(1.6) ^b	1412 (25) ^b			

^a A and B constants determined as the averages from all investigated lines involving the level considered (excluding the lines involving the lower even-parity levels: 10680.17 cm⁻¹ and 10997.85 cm⁻¹); the uncertainties are single standard mean deviations, reflecting the scattering of the results between the lines.

^b A and B constants determined from single lines (for the level 28065.44 cm⁻¹ only the line No 61 from Table 1 was applied); the uncertainties were evaluated taking into account the systematic factors (as described in Section 3.3).

frequency scale, was detected by the program "Fitter". The FSR of the frequency marker, approximately 1500 MHz, was calibrated in our earlier experiments with the use of transitions with precisely known hyperfine structure; the respective wavelength-corrected precise FSR values were used, as mentioned in Section 2. The possible overlap of the signal from other transitions located in the same wavenumber region and with similar fluorescence detection wavelength could not be absolutely excluded, although in the cases examined no evidence of such an effect was found; nevertheless, es-

timation of its possible influence on the results obtained was not considered feasible under our experimental circumstances.

Thus we considered only one possible systematic effect, which was evident and relatively easy to model; this was concerned with the spectral resolution of the data acquisition system used. The total frequency scan was divided into 4096 steps (12-bit DAC was applied); thus the frequency increment value (the frequency step) was dependent on the scan width and amounted up to ca. 10 MHz. The uncertainty of determination of the frequency intervals

between the individual *hfs* components was found not to exceed one frequency step, and this value was taken as the uncertainty of the parts related with the *hfs* constants *A* and *B* in each interval. In order to estimate the influence of such an uncertainty on the constants *A* or *B*, the assumed interval frequency uncertainty (frequency step width) was divided by the relevant differences of the Casimir coefficients for *A* or *B* constants. The latter are considerably more affected, since the Casimir coefficients for the constants *B* (and thus also their differences) are much smaller than those concerning the constants *A*. The intervals corresponding to the change of the *F* values for the level under study were only considered – their values depend only on the *hfs* constants of this level; the values obtained for various intervals were then averaged. Of course taking into account that the model assumed is very simple, only a rough estimate of this kind of systematic uncertainty can be expected.

Finally, after the systematic uncertainties mentioned were estimated, their values were added to the statistical uncertainties given in Table 1 to yield the uncertainty values presented in Table 2.

4. Discussion

4.1. Hyperfine structure constants for the odd-parity levels

Among 43 odd-parity levels investigated in this work, 41 were examined for the first time.

Out of this number, 24 levels could be investigated in single lines only, but 10 of them were the lines involving the lower levels with very precisely known *hfs* constants, determined by Childs et al. by ABMR or ABMR-LIRF techniques [6–8]. In the remaining 14 lines the lower levels had their *hfs* constants determined in our studies, but from the analysis of multiple spectral lines, which makes them also reliable (although obviously less precise). If any further possibilities of experimental investigation of such levels arise (e.g. through the extension of the available spectral range of the exciting laser radiation), attempts of confirmation of the *hfs* constants will be undertaken.

17 remaining odd-parity levels, which were hitherto not investigated, were now examined in at least two (in some cases three or four) transitions; the *hfs* constants obtained from individual transitions proved mutually consistent, except for the lines involving two particular lower levels: 10680.17 cm⁻¹ (*J* = 9/2) and 10997.85 cm⁻¹ (*J* = 11/2). This issue deserves separate discussion, presented below, in Section 4.2.

Since some of the currently investigated lines were used to evaluate the constants for the lower levels mentioned rather than the respective upper levels involved, for one of such upper odd-parity levels, 28065.44 cm⁻¹ (*J* = 11/2), only one line could be applied for determination of its constants *A* and *B*. Thus the number of the odd-parity levels, whose *hfs* were based on the investigation of single lines in this work, amounts to 25, and for altogether 18 levels (16 studied for the first time) the *hfs* constants were evaluated on the basis of multiple lines.

For two odd-parity levels: 27102.94 cm⁻¹, *J* = 11/2, and 30577.26 cm⁻¹, *J* = 15/2, investigated in our earlier works [9,11] under less favorable experimental conditions in single spectral lines only, new results were obtained. Apart from new spectral lines, also the previously examined lines $\lambda = 584.080$ nm (17116.21 cm⁻¹, line No 41 in Table 1) and $\lambda = 565.753$ nm (17670.66 cm⁻¹, line No 14 in Table 1) were recorded with improved signal-to-noise ratio. The *hfs* constants *A* and *B* obtained in the present work can be compared with the earlier values, also quoted in Table 2 (and in compilation in [12]). For the first level, 27102.94 cm⁻¹, the former and the current value of the constant *A* agree quite well, while the current (certainly more reliable)

value of the constant *B* is by ca. 70 MHz higher than the previous one. Nevertheless, this apparently large difference falls within the maximum statistical uncertainty limits. For the second level, 30577.26 cm⁻¹, both the constants *A* and *B* are fully consistent with the earlier results.

4.2. Corrected hyperfine structure constants for the selected even-parity levels

The constants *A* and *B* for the mentioned levels 10680.17 cm⁻¹ and 10997.85 cm⁻¹, and also for some other levels, could be determined in our earlier works from single spectral lines only. Since at that time only very scarce data on the *hfs* of the electronic levels of the terbium atom were available, indirect verification of the results, through the values concerning the other levels involved in the spectral lines considered, was not always possible – these were often also determined exclusively from the same lines. Nevertheless, usually such *hfs* constants could be confirmed in further studies. It should be stressed that in our early works on terbium no estimates of any systematic uncertainties were made, and the error values quoted are single mean standard deviations, also for the levels examined in single lines.

However, for the levels 10680.17 cm⁻¹ and 10997.85 cm⁻¹ the earlier constants *A* and *B* proved somewhat doubtful: in the lines involving the lower level 10680.17 cm⁻¹ the constants *A* of the upper levels were somewhat higher (by ca. 10–15 MHz) than in other lines; the same applied to the constants *B* in the lines involving the lower level 10997.85 cm⁻¹ (the difference of ca. 100–150 MHz was noted in this case). Thus it was decided to verify the *hfs* constants for both the lower levels in question.

In order to obtain improved *hfs* constants, the following procedure was applied. First we checked the upper levels of the transitions involving the considered lower levels (lines No 27, 54 and 68 for the level 10680.17 cm⁻¹, and the lines No 42, 46, 51 and 67 for the level 10997.85 cm⁻¹). In all the cases, except for the level 27952.26 cm⁻¹ (*J* = 9/2), involved in line No 46, the *A* and *B* constants of the upper levels could be independently determined in a standard way, from the lines involving other lower levels. Then the averages of the resulting constants for the upper levels (marked with single asterisks in Table 1) were fixed in the fitting procedure in order to evaluate the new constants' values for the lower levels 10680.17 cm⁻¹ and 10997.85 cm⁻¹. For the latter level the average constants' values (marked with double asterisk in Table 1) were fixed in the analysis of line No 46 in order to determine the constants of the level 27952.26 cm⁻¹.

The new corrected *hfs* constants for the lower even-parity levels discussed are presented below, compared to the former values based on examination of single lines:

10680.17 cm⁻¹ (*J* = 9/2):

A = 330.2(1.2) MHz, *B* = –289(27) MHz (this work),

A = 351.9(1.2) MHz, *B* = –229.5(7.8) MHz [9];

10997.85 cm⁻¹ (*J* = 11/2):

A = 498.9(0.7) MHz, *B* = 1124(38) MHz (this work),

A = 500.3(2.0) MHz, *B* = 1262.5(2.5) MHz [9].

Although the present uncertainties are somewhat higher than the earlier purely statistical errors reflecting the scattering of the results for one line only in each case, the present values of the *hfs* are certainly more reliable, since generally good consistency of the values obtained from various lines was found.

For the first level the corrected constant *A* differs from the previously reported one by ca. 20 MHz, which is more than the total statistical error limit, while the values of the constants *B* can be considered mutually consistent. For the second level the constants *A* agree very well, while for the constants *B* the difference of almost 140 MHz is observed, which slightly exceeds the total statistical error limit. It has to be emphasized, that the earlier values could

not be verified at the time of their publication, since the available data on the hyperfine structure for the terbium atom were insufficient. In contradiction to the former unfavorable situation, currently a much extended experimental database for both the even- and odd-parity levels can be exploited, which makes indirect verification of results based on investigation of single lines possible.

It should also be mentioned that taking into account systematic effects for the previous results in the same way as for our current investigations would considerably reduce the discrepancies observed. As already mentioned, the two levels considered should be regarded as exceptional - for most levels investigated in our earlier works the supplementary results for the hfs constants A and B proved reasonably consistent with the initial values, and were only used to obtain their insignificant correction.

4.3. Remarks on the accuracy of the hfs constants determined

It should be stressed that the main factor influencing the accuracy of the hfs constants determined was the possibility to fix the respective constants for the other levels involved in the investigated transitions. For any hfs patterns encountered (except for very poorly resolved ones, which were not considered in this work), such constraints assure reasonable reproducibility and relatively low scattering of the results obtained, regardless of the starting parameters assumed in the least-squares fitting procedure. The quality of the previously known hfs , which are fixed, is decisive; in the cases where very precise constants A and B from ABMR or ABMR-LIRF studies are available for the lower levels [6–8], usually small absolute scattering of the respective constants determined for the upper levels from various spectral lines is observed (although not always within the total statistical uncertainty limits).

It was found, by testing various model curve profiles in the least-squares fitting procedure, that the dominating line broadening mechanism was Doppler broadening reflecting the effective discharge temperature, dependent on the discharge current (typically 90 – 95% Gaussian contribution in the Voigt profiles). Thus, for some relatively poorly resolved lines, where the fitting procedure could possibly partially “compensate” for the frequency shifts resulting from the hyperfine splitting with changes of the fitted linewidth of the hfs components, the latter parameter was carefully controlled and its consistency with the linewidths obtained for other lines recorded with the same discharge current (taking into account the relevant wavelength correction) was always checked. Moreover, the relative intensities of the hfs components were coupled according to the theoretical ratios within the groups with the same ΔF ; this assured protection against the possible compensation by uncontrolled variation of the intensities.

5. Conclusions

In this work the hyperfine structure of 43 odd-parity levels of the terbium atom was investigated by laser induced fluorescence in a hollow cathode discharge; for 41 levels the hfs constants A and B were determined for the first time; in the case of two levels, investigated in our earlier works in single lines only, additional data were currently obtained and improved values of the hfs constants could be evaluated.

For the odd-parity levels investigated in multiple lines, generally mutual consistency of the hfs constants' values obtained in individual cases was observed. For the remaining levels the A and B values obtained can also be considered reliable (within the quoted uncertainty limits), since the constants of the lower levels involved

in the transitions, fixed in the fitting procedure, were either very precisely known from ABMR or ABMR-LIRF studies by other authors, or determined in our studies from multiple lines.

For two previously investigated even-parity levels the hfs constants were slightly corrected.

The results obtained in this work considerably enriched the available experimental database concerning the hfs constants of the odd-parity levels of the terbium atom (hitherto including ca. 230 levels, mostly investigated in our earlier works for the first time). They can be included in semi-empirical analysis of the fine- and the hyperfine structure of the odd-parity configuration system of the atomic terbium, considered in our research group.

Acknowledgements

The research within this work was financially supported by the Ministry of Science and Higher Education within the Project 06/65/SBAD/1953, realized at Faculty of Technical Physics, Poznan University of Technology.

The authors would like to express their gratitude to Prof. Guthöhrlein for making the program “Fitter” accessible.

Many thanks are due to Dr. Magdalena Elantkowska, as well as Dr. Jarosław Ruczkowski from Institute of Control, Robotics and Information Engineering, Faculty of Electrical Engineering, Poznan University of Technology, for numerous fruitful discussions.

References

- [1] Klinkenberg PFA. Structure of the spectrum of neutral terbium, tb i. *Physica (Utrecht)* 1966;32:1113–47.
- [2] Klinkenberg PFA, Meinders E. Structure of the spectrum of neutral terbium, tb I. Part II. *Physica (Utrecht)* 1966;32:1617–32.
- [3] Klinkenberg PFA. Structure of the spectrum of neutral terbium, tb I. Part III: levels having extreme values of j . *Physica (Utrecht)* 1967;37:197–214.
- [4] Klinkenberg PFA, Meinders E. Structure of the spectrum of neutral terbium, tb i. part v: the configuration $4f^8 5d^2 6s$. *Physica (Utrecht)* 1969;42:213–41.
- [5] Klinkenberg PFA, Van Kleef TAM. The ground state of the terbium atom. *Physica (Utrecht)* 1970;50:625–8.
- [6] Childs WJ. Hyperfine structure of many atomic levels of Tb^{159} and the Tb^{159} nuclear electric-quadrupole moment. *Phys Rev A* 1970;2:316–36.
- [7] Childs WJ, Goodman LS. Assignment of unclassified lines in tb I through high-resolution laser-fluorescence measurements of hyperfine structure. *J Opt Soc Am* 1979;69:815–19.
- [8] Childs WJ. Use of atomic-beam laser radio-frequency double resonance for interpretation of complex spectra: tb I as a test case. *J Opt Soc Am B* 1992;9:191–6.
- [9] Furmann B, Stefańska D, Krzykowski A. Hyperfine structure of the $4f^8 5d 6s^2$ configuration of the tb atom. *Spectrochim Acta, Part B* 2015;111:38–45.
- [10] Furmann B, Stefańska D, Krzykowski A. Hyperfine structure of the $4f^8 5d^2 6s$ configuration in the tb atom. *J Phys B* 2016;49:025001.
- [11] Stefańska D, Elantkowska M, Ruczkowski J, Furmann B. Fine- and hyperfine structure investigations of even configuration system of atomic terbium. *J Quant Spectrosc Radiat Transf* 2017;189:441–56.
- [12] Stefańska D, Furmann B. Hyperfine structure of the odd parity level system in the terbium atom. *J Phys B* 2017;50:175002.
- [13] Angstmann EJ, Dzuba VA, Flambaum VV, Nevsky AY, Karshenboim SG. Narrow atomic transitions with enhanced sensitivity to variation of the fine structure constant. *J Phys B* 2006;39(8):1937.
- [14] McClelland JJ, Hanssen JL. Laser cooling without repumping: a magneto-optical trap for erbium atoms. *Phys Rev Lett* 2006;96:143005.
- [15] Stefańska D, Suski M, Zygmunt A, Stachera J, Furmann B. Tunable single-mode cw energy-transfer dye laser directly optically pumped by a diode laser. *Opt Laser Technol* 2019;120:105673.
- [16] Childs WJ, Crosswhite H, Goodman LS, Pfeufer V. Hyperfine structure of $4f^6 6s^2$ configurations in ^{159}Tb , $^{161,163}Dy$, and ^{169}Tm . *J Opt Soc Am B* 1984;1(1):22–9.
- [17] Stefańska D, Furmann B. Hyperfine structure investigations for the odd-parity configuration system in atomic holmium. *J Quant Spectrosc Radiat Transf* 2018;206:286–95.
- [18] Kramida A, Ralchenko Y, Reader J, and NIST ASD Team. NIST atomic spectra database (ver. 5.3), [Online]. Available: <http://physics.nist.gov/asd> [2015]. National institute of standards and technology, Gaithersburg, MD.; 2015.



Hyperfine structure investigations of the odd-parity electronic levels of the terbium atom



M. Suski*, B. Furmann, M. Chomski, S. Mieloch, P. Głowacki, D. Stefańska

Institute of Materials Research and Quantum Engineering, Faculty of Materials Engineering and Technical Physics, Poznan University of Technology, Piotrowo 3A, Poznan 60-965, Poland

ARTICLE INFO

Article history:

Received 9 December 2022

Revised 15 January 2023

Accepted 16 January 2023

Available online 20 January 2023

Keywords:

Atomic structure

Laser spectroscopy

Hyperfine structure

Terbium

ABSTRACT

In the present work the hyperfine structure constants A and B were determined for 26 odd-parity energy levels of the terbium atom. Altogether 62 spectral lines in the spectral range between 483 - 538 nm were examined, using the method of laser induced fluorescence in a hollow cathode discharge lamp. All the results are presented for the first time. Additionally, the constants for 4 even-parity energy levels, previously reported by our research group, were reevaluated and slightly corrected.

© 2023 Elsevier Ltd. All rights reserved.

1. Introduction

Terbium is an element possessing only one single isotope ^{159}Tb . It belongs to lanthanides and is positioned slightly above the middle of the series. Due to the low nuclear spin value $I=3/2$, the number of the hyperfine sublevels is restricted to a maximum of 4, which in consequence limits the number of occurring hyperfine components in the spectral lines to 9 - 10. Although the structure of the spectral lines of terbium is less complex than in many other lanthanides, the density of electronic levels, related to its placement in the series, is extremely high, and the mean energies of different configurations are nearly the same due to wavefunction collapse of the 4f orbital, which results in the overlap of electronic configurations in the energy scale. These issues cause significant difficulties in experimental investigations, as well as theoretical calculations of the atomic structure. Due to these reasons, more thoroughly described in our recent works concerning determination of Landé g_J factors in terbium [1,2], the knowledge of the hyperfine structure (hfs) constants for the terbium atom is still far from complete.

The first significant work, concerning the determination of hfs constants in atomic terbium, is dated to 1970 [3]. This work, along with two subsequent works [4,5], provided the hfs constants for a limited number of the lowest-lying energy levels of both parities. It is also worth mentioning, that the actual ground state of the terbium atom was not correctly identified until 1970 [6]. Apart from

the mentioned works, no further data on hfs constants was reported until 2015, when the topic was undertaken by our research group. Within the series of 5 works [7-11] the values of the hfs constants were determined for 61 even-parity and 264 odd-parity energy levels.

This research is a continuation of those investigations, concerning the hyperfine structure of terbium. Within the present work, the hfs constants' values for 26 odd-parity energy levels were experimentally determined, based on the investigations of 62 recorded spectral lines. All of the values were determined for the first time. Moreover, the values for 4 even-parity levels, previously reported in our works [8,10], were reevaluated and slightly corrected.

As stated in our previous works, hfs constants are one of the most characteristic parameters of the electronic levels. Comprehensive knowledge on that matter can greatly facilitate the studies of the structure of the terbium atom. It provides the data required for the semi-empirical calculations. For atoms which possess electronic configurations with several open shells, *ab initio* calculations of various parameters, regarding the energy-levels, are highly imprecise and usually differ from experimental values. Therefore, in such cases semi-empirical calculations are the only feasible method of theoretical analysis. Moreover, the hfs constants greatly improve the proper assignment of the electronic levels to the particular configurations.

The more thorough description of the terbium structure enhances its application potential. In quantum engineering and metrology it may be a possible candidate for e.g. quantum computing [12], laser cooling and confinement in magneto-optical traps

* Corresponding author.

E-mail address: marcin.j.suski@doctorate.put.poznan.pl (M. Suski).

(MOT), or investigations of the temporal variation of the fine structure constant α . There are also various applications, based on its fluorescence properties, such as green phosphores in fluorescent lamps, or biochemical probes, screens, or even in banknotes as a safeguard to help protect against counterfeiting.

2. Experimental details

The experimental method and setup, applied in this research, is generally the same as in our previous works, concerning the hyperfine structure investigations of the terbium atom [7–11], where a detailed description can be found. Therefore, only a brief overview is presented below.

The measurements were carried out by laser induced fluorescence (LIF) in a hollow cathode discharge lamp. The experimental conditions for the discharge lamp remained nearly unchanged, compared to the previously reported in the mentioned works. The pressure of argon, used as the buffer gas, was kept at approximately 0.4 mbar, and the discharge current of 50–60 mA was applied.

The laser light, used to optically excite the investigated transitions, was generated by a single-mode tunable ring dye laser - a modified Coherent CR 699-21 model. The laser was operated on Coumarin 498 dye solution, optically pumped by a diode laser at $\lambda=445$ nm [13] (the diode laser is currently Lasertack GmbH, model LDM-445-5000-C). The available spectral range was approx. 481–540 nm, which corresponds to the blue-green region of the spectrum. The precise value of the exciting wavelength was determined based on the readings from Burleigh WA-1500 wavemeter, whereas a mode analyzer was applied to ensure the single mode operation. The frequency of the laser radiation was scanned over the range up to 35 GHz, dependent on the spectral width of the *hfs* pattern, around the center of gravity of the spectral line. The relative frequency scale was based on the signal from a temperature-stabilized Fabry-Perot interferometer (FSR=1500 MHz), recorded along with the LIF signal during the frequency scan.

The fluorescence signal was directed to a SPM-2 grating monochromator, which enables the spectral selection of the decay transitions from the excited levels (referred to as fluorescence channels). This method is particularly helpful in investigations of the atoms with quasi-continuous spectrum, such as terbium. The fluorescence light emitted in the selected channel was recorded by a Hamamatsu R-375 photomultiplier (operated in photocurrent mode) with preamplifier. The recorded signal was further enhanced by a phase sensitive amplifier, with a mechanical chopper used for the modulation of the exciting beam.

Dependent on the signal-to-noise ratio, 10–15 frequency scans were recorded for each investigated transition.

3. Results

In this work altogether 62 spectral lines were investigated, for which the *hfs* constants A and B for the upper odd-parity energy levels were determined. The results are presented in Table 1.

In order to calculate the values of the *hfs* constants the program "Fitter", developed in the group of Prof. Guthöhrlein in Hamburg, was applied. For the recorded spectral lines, two types of broadening occur - Doppler broadening and natural broadening resulting from the lifetimes of the lower and the upper energy level, involved in the transition. The former is described by the Gaussian profile, whereas the latter - by the Lorentzian profile. Therefore, to properly fit the spectra, in most cases Voigt function was applied, which is the convolution of both aforementioned profiles. In some cases, when the individual components of the *hfs* spectrum are not separated, simultaneous determination of the widths of Gaussian and Lorentzian profiles, as well as the intervals between the

components, might be somewhat problematic. For that reason, the same width for each component of the spectral lines was applied by the "Fitter" program. Additionally, within this work the assumption was adopted that for the scans recorded at the same values of the discharge current and the pressure of the buffer gas, and at similar wavelengths, the Doppler broadening is the same.

Furthermore, the saturation effects may interfere with calculations of the intervals between not properly separated components. In the case of the hyperfine structure, the saturation effects manifest in the fact that firstly: intensity ratios between the groups of components with different ΔF values differ from the ratios predicted by the selection rules, and secondly: the intensities of the strongest components in the strongest group ($\Delta F = \Delta J$) are decreased. To minimize the negative influence of the saturation effects on the obtained results, mutual coupling of the components, available in "Fitter" program, was applied. The intensities of the components with the same ΔF value were fitted together, while the intensity ratios between the groups of components with different ΔF values were fitted freely by the program. Additionally, the intensities of the strongest components were fitted freely as well.

These fitting procedures were previously tested in our laboratory for different elements, based on comparison of the experimental results with Doppler broadening and limited Doppler broadening (obtained with LIF method on an atomic beam), and were found to provide the most consistent outcome of the calculations.

The values for the lower even-parity energy levels, involved in the investigated transitions, were taken from earlier studies of our research group [7,10] or the works of other authors [3,5]. For each line the groups containing several averaged recorded scans were fitted separately, and the results were then averaged. Some examples of the recorded scans with the fitted *hfs* patterns are presented in Figs. 1, 2, 3 and 4.

At first, in all cases the *hfs* constants for the lower energy-levels were fixed, and only the constants of the upper levels were fitted as adjustable parameters. The results, obtained for individual spectral lines, were further averaged for each particular even-parity energy level. For some levels the *hfs* constants could be determined only from a single spectral line in each case. The A and B constants' values, obtained for 26 odd-parity energy levels are listed in Table 2.

For several lines, involving the lower levels $7839.85 \text{ cm}^{-1} J=7/2$, $8097.88 \text{ cm}^{-1} J=9/2$, $9145.23 \text{ cm}^{-1} J=9/2$ and $9897.73 \text{ cm}^{-1} J=9/2$, it was noticed, that the results obtained for the upper levels noticeably differ from other values, concerning the same upper levels, obtained from the remaining lines - in the case of the A constant up to 10 MHz. For that matter, the previously reported *hfs* constants for the mentioned even-parity levels were believed to be somewhat doubtful; in Section 4 the possible reasons of systematic shifts of the values evaluated before are discussed in more detail. Thus it was decided that the constants for these four levels need to be reevaluated.

In this case, the procedure described in the previous step, was reversed. In the transitions from the investigated even-parity levels, the mean values of the A and B constants, obtained from the remaining lines for the involved upper energy levels were fixed, and the values for the lower levels were fitted. The results were further averaged for each particular level. The recalculated values for the four mentioned levels are presented in the second part of Table 2. Finally, the reevaluated constants were used to calculate the *hfs* constants of the involved odd-parity levels once again.

Table 1 is arranged as follows: columns 2 and 3 contain the information concerning the investigated transition, i. e. its wavelength and wavenumber respectively. In columns 4–7, information about the lower even-parity energy levels is provided, namely their energy values, J quantum numbers and *hfs* constants A and B . The

Table 1

Spectral lines of the terbium atom, investigated in order to determine the hyperfine structure constants for the upper odd-parity levels, along with the A and B values obtained. In most cases the hfs constants of the lower even-parity levels involved in the spectral lines were fixed at the available values in the least-squares fit procedure; the respective citations are given in a separate column. For some spectral lines, involving four particular lower even-parity levels (7839.85 cm^{-1} , 8097.88 cm^{-1} , 9145.23 cm^{-1} and 9897.73 cm^{-1}), the hfs constants of these levels were determined independently (for details see text, Section 3 and 4). The energies of both the lower and the upper levels were taken from NIST Atomic Spectra Database [15]

No	Line		Lower Level							Upper Level					
	λ_{air} (nm)	κ_{vac} (cm^{-1})	E (cm^{-1})	J	A (MHz)	B (MHz)	ref.	E (cm^{-1})	J	A (MHz)	B (MHz)				
1	2	3	4	5	6	7	8	9	10	11	12				
1	537.594	18596.24	285.50	13/2	532.204	(0.002)	928.861	(0.030)	[3]	18881.74	15/2	653.74	(0.05)	547.9	(2.3)
2	536.964	18618.05	462.08	15/2	472.643	(0.002)	1154.239	(0.017)	[3]	19080.13	15/2	1087.21	(0.03)	1590.3	(0.5)
3	531.919	18794.63	285.50	13/2	532.204	(0.002)	928.861	(0.030)	[3]	19080.13	15/2	1086.70	(0.07)	1600.5	(0.9)
4	530.820	18833.55	2840.17	9/2	441.771	(0.005)	158.750	(0.040)	[3]	21673.72	11/2	955.50	(0.03)	716.1	(0.4)
5	492.408	20302.68	1371.05	9/2	602.219	(0.003)	1267.267	(0.030)	[3]	21673.72	11/2	955.35	(0.08)	734.3	(0.6)
6	512.831	19494.16	3719.71	13/2	354.454	(0.003)	72.183	(0.030)	[3]	23213.87	15/2	826.7	(0.3)	343.4	(4.4)
7	523.984	19079.25	6674.15	11/2	527.6	(1.2)	528.4	(1.4)	[10]	25753.40	11/2	465.4	(1.3)	350.4	(7.1)
8	501.779	19923.54	5829.86	9/2	271.2	(0.7)	-349.8	(6.8)	[10]	25753.40	11/2	468.9	(0.8)	145.5	(7.3)
9	490.059	20400.03	5353.37	11/2	267.2	(1.0)	-448.7	(9.8)	[10]	25753.40	11/2	467.8	(1.1)	222.7	(9.9)
10	514.781	19420.31	6488.28	7/2	114.9	(0.3)	-498.7	(0.7)	[7]	25908.59	7/2	491.2	(0.8)	251.8	(7.1)
11	497.901	20078.73	5829.86	9/2	271.2	(0.7)	-349.8	(6.8)	[10]	25908.59	7/2	490.7	(0.8)	79.6	(8.6)
12	514.572	19428.20	7059.90	13/2	519.5	(0.7)	1179.7	(2.7)	[10]	26488.10	13/2	667.6	(0.8)	656.4	(3.4)
13	512.697	19499.28	6988.82	11/2	446.7	(0.3)	739	(15)	[10]	26488.10	13/2	668.2	(0.4)	686	(16)
14	504.554	19813.95	6674.15	11/2	527.6	(1.2)	528.4	(1.4)	[10]	26488.10	13/2	669.1	(1.3)	725.2	(4.1)
15	496.476	20136.35	6351.75	13/2	438.5	(2.2)	1122	(29)	[10]	26488.10	13/2	671.8	(2.3)	664	(30)
16	521.966	19153.02	7441.03	9/2	509.843	(0.003)	547.483	(0.003)	[5]	26594.05	7/2	583.5	(0.5)	234.3	(4.0)
17	505.092	19792.86	6801.19	5/2	-123.7	(2.8)	-286	(15)	[10]	26594.05	7/2	581.9	(2.9)	163	(16)
18	497.231	20105.77	6488.28	7/2	114.9	(0.3)	-498.7	(0.7)	[7]	26594.05	7/2	585.2	(0.4)	290.8	(1.6)
19	506.228	19748.43	7059.90	13/2	519.5	(0.7)	1179.7	(2.7)	[10]	26808.33	11/2	702.5	(1.0)	499	(70)
20	504.413	19819.51	6988.82	11/2	446.7	(0.3)	739	(15)	[10]	26808.33	11/2	704.3	(0.4)	335	(16)
21	496.529	20134.18	6674.15	11/2	527.6	(1.2)	528.4	(1.4)	[10]	26808.33	11/2	706.4	(1.3)	465.3	(4.0)
22	488.704	20456.58	6351.75	13/2	438.5	(2.2)	1122	(29)	[10]	26808.33	11/2	706.4	(2.3)	377	(30)
23	522.713	19125.64	8277.04	13/2	981.2	(2.6)	820	(24)	[10]	27402.68	11/2	341.0	(2.7)	259	(25)
24	510.622	19578.49	7824.19	9/2	621.5	(2.1)	790.1	(3.5)	[10]	27402.68	11/2	338.3	(2.2)	281.8	(4.4)
25	500.821	19961.65	7441.03	9/2	509.843	(0.003)	547.483	(0.003)	[5]	27402.68	11/2	342.4	(0.2)	299.2	(4.4)
26	489.727	20413.86	6988.82	11/2	446.7	(0.3)	739	(15)	[10]	27402.68	11/2	340.1	(0.4)	276	(16)
27	496.365	20140.84	7441.03	9/2	509.843	(0.003)	547.483	(0.003)	[5]	27581.87	9/2	533.7	(0.4)	-283.0	(8.6)
28	485.465	20593.05	6988.82	11/2	446.7	(0.3)	739	(15)	[10]	27581.87	9/2	535.4	(2.7)	-311	(44)
29	513.354	19474.30	8190.46	15/2	948.5	(1.1)	699	(31)	[10]	27664.77	13/2	593.3	(1.2)	1089	(32)
30	485.187	20604.87	7059.90	13/2	519.5	(0.7)	1179.7	(2.7)	[10]	27664.77	13/2	592.9	(0.8)	1002.7	(3.7)
31	483.519	20675.95	6988.82	11/2	446.7	(0.3)	739	(15)	[10]	27664.77	13/2	592.2	(0.4)	951	(16)

(continued on next page)

Table 1 (continued)

No	Line		Lower Level						Upper Level					
	λ_{air} (nm)	k_{vac} (cm^{-1})	E (cm^{-1})	J	A (MHz)	B (MHz)	ref.	E (cm^{-1})	J	A (MHz)	B (MHz)			
1	2	3	4	5	6	7	8	9	10	11	12			
32	498.006	20074.48	7839.85	7/2	609.7	(0.2)	429.8	(3.4)	27914.33	7/2	821.4	(0.7)	219	(12)
33	488.305	20473.30	7441.03	9/2	509.843	(0.003)	547.483	(0.003)	27914.33	7/2	821.7	(0.6)	225.0	(5.3)
34	518.289	19288.88	8646.21	11/2	984.255	(0.003)	925.956	(0.003)	27935.09	13/2	621.4	(0.2)	501.3	(1.9)
35	508.556	19658.05	8277.04	13/2	981.2	(2.6)	820	(24)	27935.09	13/2	619.0	(2.7)	527	(25)
36	506.326	19744.63	8190.46	15/2	948.5	(1.1)	699	(31)	27935.09	13/2	619.0	(1.2)	533	(32)
37	524.100	19075.01	9145.23	9/2	1067.5	(0.6)	1086	(17)	28220.24	7/2	467.0	(1.0)	122.2	(8.0)
38	490.531	20380.39	7839.85	7/2	610.2	(0.6)	404	(17)	28220.24	7/2	468.2	(0.7)	155	(12)
39	521.752	19160.85	9145.23	9/2	1066.2	(0.8)	1079.6	(5.3)	28306.08	7/2	885.4	(1.0)	118.1	(7.8)
40	495.515	20175.40	8130.68	5/2	874.4	(4.8)	411	(25)	28306.08	7/2	886.7	(4.9)	110	(26)
41	494.710	20208.21	8097.88	9/2	230.6	(0.8)	-397.5	(4.9)	28306.08	7/2	885.4	(1.2)	126.9	(2.9)
42	488.473	20466.23	7839.85	7/2	611.5	(0.8)	436.5	(5.0)	28306.08	7/2	882.4	(0.7)	117	(12)
43	488.100	20481.89	7824.19	9/2	621.5	(2.1)	790.1	(3.5)	28306.08	7/2	885.6	(2.2)	138.2	(5.1)
44	506.805	19725.97	8646.21	11/2	984.255	(0.003)	925.956	(0.003)	28372.18	13/2	998.52	(0.08)	346.7	(3.5)
45	497.494	20095.14	8277.04	13/2	981.2	(2.6)	820	(24)	28372.18	13/2	998.1	(2.8)	278	(29)
46	495.360	20181.71	8190.46	15/2	948.5	(1.1)	699	(31)	28372.18	13/2	996.7	(1.2)	358	(32)
47	518.618	19276.66	9145.23	9/2	1065.4	(2.1)	1049.8	(4.6)	28421.89	7/2	658.0	(1.0)	774.9	(8.4)
48	491.891	20324.02	8097.88	9/2	232.7	(2.0)	-392.0	(3.3)	28421.89	7/2	654.0	(1.2)	769.8	(3.2)
49	504.162	19829.36	9897.73	9/2	1112.4	(2.3)	416	(87)	29727.09	11/2	593.0	(1.6)	223	(49)
50	485.729	20581.86	9145.23	9/2	1067.7	(2.3)	1079	(87)	29727.09	11/2	597.5	(1.1)	397	(12)
51	503.342	19861.68	9867.65	7/2	903.5	(2.5)	533	(23)	29729.33	7/2	417.3	(2.6)	-60	(25)
52	485.676	20584.10	9145.23	9/2	1070.4	(2.1)	1053	(18)	29729.33	7/2	413.4	(1.1)	-54	(15)
53	528.623	18911.81	10920.18	3/2	1001.8	(3.2)	-133	(19)	29831.99	3/2	861.5	(3.3)	194	(20)
54	515.977	19375.32	10456.67	5/2	912.9	(6.9)	149	(35)	29831.99	3/2	855.3	(7.0)	250	(36)
55	513.641	19463.43	10456.67	5/2	912.9	(6.9)	149	(35)	29920.10	5/2	538.4	(7.0)	-1121	(37)
56	491.246	20350.70	9897.73	9/2	1113.9	(0.8)	516	(16)	30248.43	9/2	478.1	(1.5)	260	(48)
57	525.420	19027.08	11331.14	19/2	876.3	(3.8)	1460	(20)	30358.22	19/2	888.7	(3.9)	-1240	(22)
58	500.351	19980.39	10456.67	5/2	912.9	(6.9)	149	(35)	30437.06	7/2	778.8	(7.0)	117	(36)
59	486.735	20539.33	9897.73	9/2	1109.5	(1.2)	572	(50)	30437.06	7/2	780.4	(1.8)	19	(47)
60	518.820	19269.13	11425.94	13/2	672.5	(0.4)	75.4	(9.9)	30695.07	11/2	756.3	(0.8)	836	(18)
61	514.401	19434.66	11260.41	11/2	919.9	(2.3)	309	(13)	30695.07	11/2	758.1	(2.4)	734	(14)
62	507.544	19697.22	10997.85	11/2	500.3	(2.0)	1262.5	(2.5)	30695.07	11/2	755.7	(2.1)	770.7	(7.1)

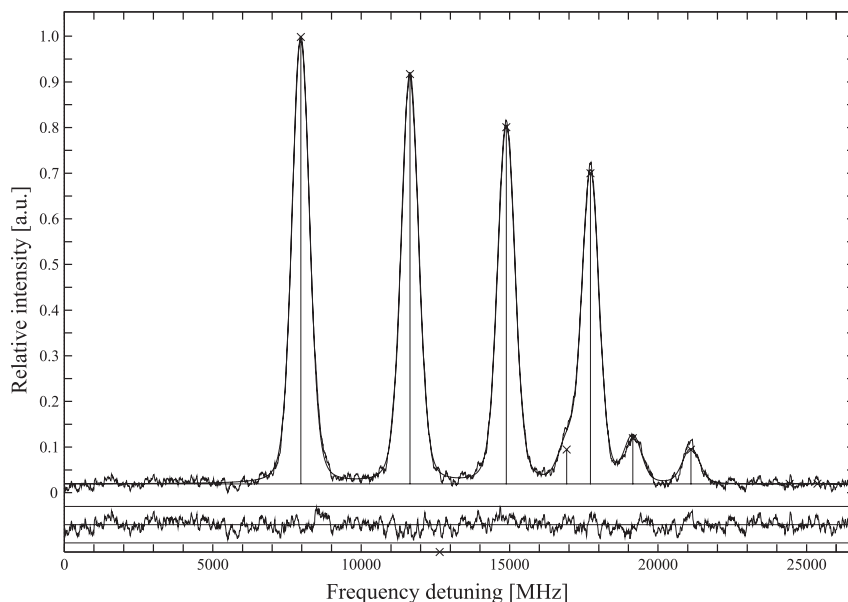


Fig. 1. Recorded *hfs* pattern of spectral line $\lambda = 506.326$ nm ($k=19744.63$ cm^{-1} , transition between the levels 8190.46 cm^{-1} , $J=15/2$ and 27935.09 cm^{-1} , $J=13/2$) in the terbium atom (Table 1, No. 36), along with the components fitted with the program "Fitter" (vertical lines). The lower trace represents deviations of the experimental data from the fitted theoretical curve.

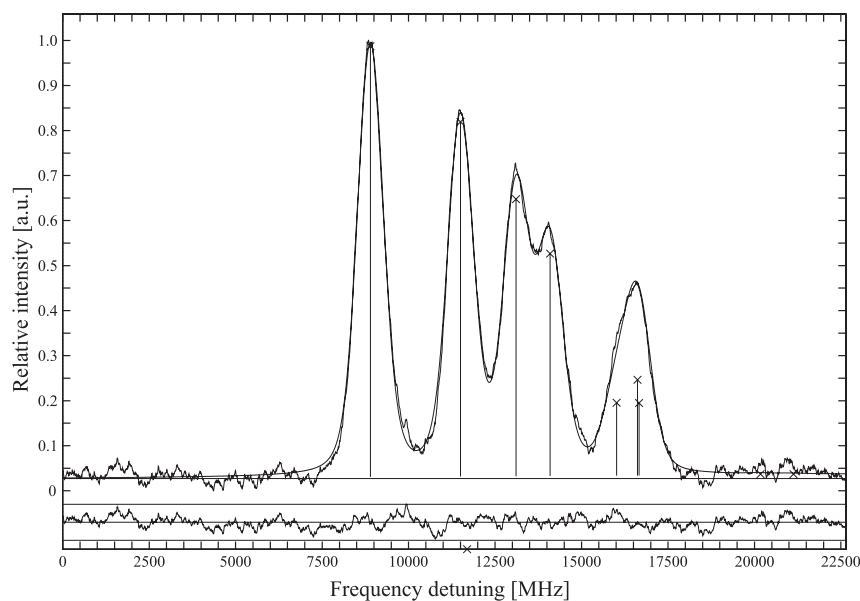


Fig. 2. Recorded *hfs* pattern of spectral line $\lambda = 521.752$ nm ($k=19160.85$ cm^{-1} , transition between the levels 9145.23 cm^{-1} , $J=9/2$ and 28306.08 cm^{-1} , $J=7/2$) in the terbium atom (Table 1, No. 39), along with the components fitted with the program "Fitter" (vertical lines). The lower trace represents deviations of the experimental data from the fitted theoretical curve.

source of the *hfs* constants for the particular lower level is indicated in column 8. For the reevaluated levels, no reference is given. In columns 9–12 the analogous information concerning the upper energy levels is presented.

In Table 2 the final results for 26 odd-parity and 4 reevaluated even-parity levels are presented. In columns 1 and 2, J quantum numbers and energy values of the investigated levels are given. The number of spectral lines recorded, used for averaging, is presented in column 3. Columns 4 and 5 contain the *hfs* constants determined within this work. Additionally, the previously reported constants' values for the reevaluated even-parity levels, along with the reference, are indicated in columns 6–8 for comparison.

The uncertainties, presented in parentheses next to each particular A and B constant, were estimated according to the method adopted in the first work, concerning investigation of the holmium atom [14]. Some further description is provided in our latest research on *hfs* structure of atomic terbium [11]. For each individual spectral line, the uncertainty is the combination of mean standard deviation of the averaged value for the investigated upper energy level and the uncertainty of the fixed value for the lower energy level, and is calculated according to the formula: $\sigma = \sqrt{\sigma_1^2 + \sigma_2^2}$. The final uncertainties for the levels, where the constants were evaluated from more than one line, are mean standard deviations of the values averaged from the respective spectral lines, whereas

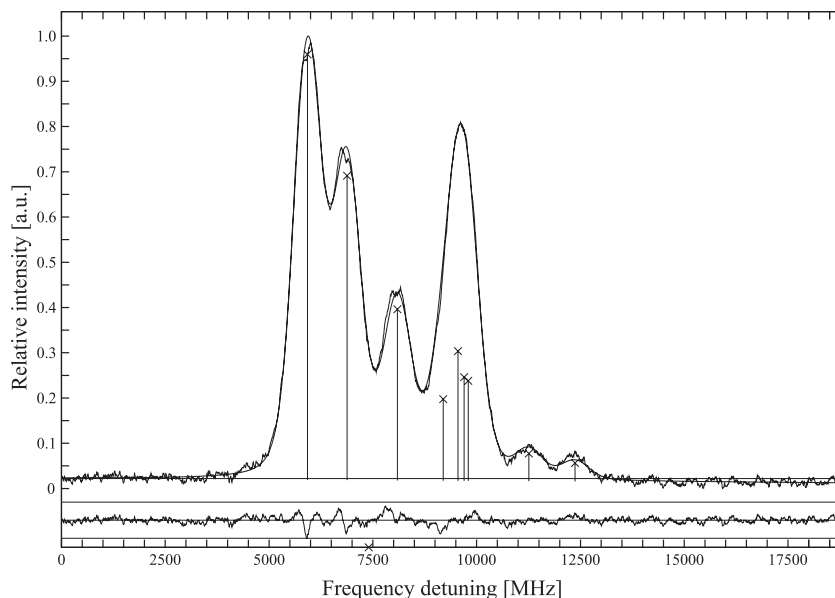


Fig. 3. Recorded *hfs* pattern of spectral line $\lambda = 515.977$ nm ($k=19375.32$ cm^{-1} , transition between the levels 10456.67 cm^{-1} , $J=5/2$ and 29831.99 cm^{-1} , $J=3/2$) in the terbium atom (Table 1, No. 54), along with the components fitted with the program "Fitter" (vertical lines). The lower trace represents deviations of the experimental data from the fitted theoretical curve.

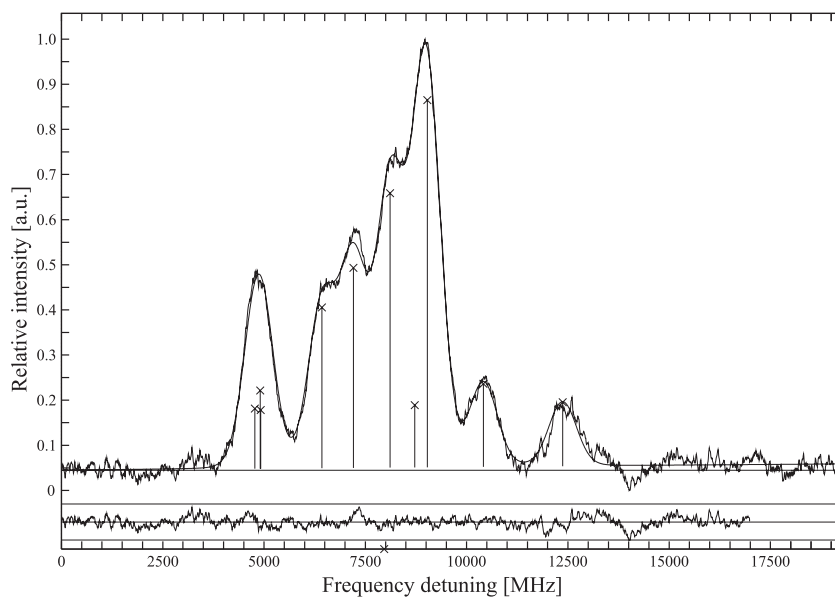


Fig. 4. Recorded *hfs* pattern of spectral line $\lambda = 498.006$ nm ($k=20074.48$ cm^{-1} , transition between the levels 7839.85 cm^{-1} , $J=7/2$ and 27914.33 cm^{-1} , $J=7/2$) in the terbium atom (Table 1, No. 32), along with the components fitted with the program "Fitter" (vertical lines). The lower trace represents deviations of the experimental data from the fitted theoretical curve.

in case of the levels, where the *hfs* constants were determined from single lines, both statistical and systematic errors are involved.

4. Discussion

All of the *hfs* *A* and *B* constants, determined for 26 odd-parity energy levels, are presented for the first time.

Among this number, 5 energy levels were investigated in single spectral lines each. For two of these levels, namely 18881.74 cm^{-1} $J=15/2$ and 23213.87 cm^{-1} $J=15/2$, investigated transitions involved the lower levels, for which the *hfs* constants were determined with high precision by Childs [3] using ABMR technique. Therefore,

the values obtained for these levels are considered to be precise. The results for the remaining 3 levels, i.e. 29920.10 cm^{-1} $J=7/2$, 30248.43 cm^{-1} $J=9/2$ and 30358.22 cm^{-1} $J=19/2$, may be somewhat less accurate. In all cases, further research may be beneficial.

For all of the presented 26 odd-parity energy levels the results obtained from different transitions are consistent - in majority of the cases the uncertainty of the *A* constant remains below 1 MHz. Only for one level, 29831.99 cm^{-1} $J=3/2$, the uncertainty slightly exceeds 3 MHz. The constants' values for this level were determined from two spectral lines: 18911.81 cm^{-1} and 19375.32 cm^{-1} (No. 53 and 54 in Table 1). It can be noticed, that the results differ between these lines, although within the uncertainty limit. However, one can see that the uncertainties are relatively high,

Table 2

Compilation of the hyperfine structure constants A and B for the odd-parity levels in the terbium atom investigated in this work. Reevaluated values for four previously reported even-parity levels are also provided; the earlier results are presented for comparison. In parentheses the uncertainties (in MHz), calculated as described in Section 3, are quoted

J	Level		hfs constants (this work)		hfs constants (earlier works)		
	E (cm ⁻¹)	No. of lines	A (MHz)	B (MHz)	A (MHz)	B (MHz)	ref.
1	2	3	4	5	6	7	8
odd-parity	levels						
3/2	29831.99	2	858.4(3.1)	222 (29)			
7/2	25908.59	2	491.0(0.3)	166 (87)			
	26594.05	3	583.5(1.0)	229 (37)			
	27914.33	2	821.5(0.2)	221.8(3.3)			
	28220.24	2	467.6(0.6)	139 (17)			
	28306.08	5	885.1(0.8)	122.0(4.9)			
	28421.89	2	656.0(2.0)	772.4(2.6)			
	29729.33	2	415.4(2.0)	-57.0(2.6)			
	29920.10	1	538.4(1.9)	-1121 (17)			
	30437.06	2	779.6(0.8)	68 (50)			
9/2	27581.87	2	534.6(0.9)	-297 (14)			
	30248.43	1	478.2(2.1)	260 (23)			
11/2	21673.72	2	955.42(0.09)	725.2(9.1)			
	25753.40	3	467.4(1.1)	240 (60)			
	26808.33	4	704.9(1.0)	419 (39)			
	27402.68	4	340.5(0.9)	279.0(8.3)			
	29727.09	2	595.3(2.3)	310 (87)			
	30695.07	3	756.7(0.8)	780 (30)			
13/2	26488.10	4	669.2(1.0)	683 (16)			
	27664.77	3	592.8(0.4)	1014 (41)			
	27935.09	3	619.8(0.9)	520.4(9.7)			
	28372.18	3	997.8(0.6)	327 (26)			
15/2	18881.74	1	653.7(0.6)	548 (12)			
	19080.13	2	1087.0(0.3)	1595.4(5.2)			
	23213.87	1	826.7(1.3)	343 (27)			
19/2	30358.22	1	888.7(0.6)	-1240 (16)			
even-parity	levels						
7/2	7839.85	3	610.5(0.6)	423 (11)	606.2(0.7)	428.7(0.4)	[7]
9/2	8097.88	2	231.7(1.1)	-394.8(2.8)	229.1(1.7)	-398.8(6.4)	[10]
	9145.23	5	1067.4(0.9)	1069.5(7.6)	1069.3(0.3)	1088.8(7.5)	[8]
	9897.73	3	1111.9(1.4)	501 (46)	1109.4(0.2)	537.3(3.7)	[8]

compared to other spectral lines. In this case, they are dominated mostly by the high uncertainties of the lower energy levels, involved in these transitions, which is one of the possible reasons of such discrepancies. Some further investigations may be favourable, when other spectral regions become available for the exciting laser radiation.

As stated in Section 3, the hfs constants for the aforementioned 4 even-parity levels (7839.85 cm⁻¹ $J=7/2$, 8097.88 cm⁻¹ $J=9/2$, 9145.23 cm⁻¹ $J=9/2$ and 9897.73 cm⁻¹ $J=9/2$), presented in our previous works, were considered inaccurate. The results obtained for spectral lines, in which these levels were involved as the lower levels, were inconsistent with those from other lines for particular upper levels. The corrected constants, reevaluated according to the procedure described also in Section 3, and further fixed in the fitting procedure significantly reduced the inconsistency of the constants for the upper levels, and only typical discrepancies, characteristic for our investigations, were observed. Differences between the values obtained within this work and those previously reported are noticeably higher than the estimated uncertainties, as can be seen in Table 2. The main cause is the already mentioned scarcity of knowledge of the hfs structure of terbium. The very precise values of the hfs constants (to the third decimal place), determined by Childs et al. using ABMR or ABMR-LIRF techniques [3–5], are avail-

able only for a limited number of the lowest lying energy levels. In many cases these levels cannot be exploited, even if the possible transitions exist, as it is highly limited by the spectral range covered by the lasers available in our laboratory. The hfs constants for the discussed even-parity levels, presented in [8,10], were obtained by performing the fitting procedure simultaneously for both levels, involved in the investigated transitions time, as no experimental data was available for the respective odd-parity energy levels. Simultaneous calculations of the hfs constants for both levels are possible, however such an approach decreases the accuracy, as one may notice in this particular case.

5. Conclusions

Within this work, hfs constants were determined for 26 odd-parity energy levels on the basis of investigations of 62 spectral lines with the method of laser induced fluorescence in a hollow cathode discharge lamp. All of the results are presented for the first time.

Additionally, hfs constants for 4 energy levels, belonging to even-parity configurations, previously reported in our older works [8,10], were reevaluated. The constants' values obtained for the spectral lines, where the levels with reevaluated constants were

involved as the lower levels, are now consistent with the results from other lines associated with a given upper odd-parity level.

The results presented in this work constitute a further extension of the available experimental database of the hyperfine structure of the terbium atom. It may greatly facilitate the semi-empirical analysis of the fine- and hyperfine structure of the odd-parity configuration system, which is still difficult due to the complexity of this system, resulting from strong configuration mixing. Additionally, the data provided within this work, along with our previous works, concerning both hfs constants and Landé g_J factors, may be valuable from the point of view of possible applications of terbium. Even though the investigated unclassified spectral lines are rather weak, they can be successfully excited with precisely tuned laser beam, which is favourable for some exemplary applications, mentioned in Section 1, such as the safeguard in the banknotes.

Declaration of Competing Interest

The authors declare that they have no known competing financial interests or personal relationships that could have appeared to influence the work reported in this paper.

CRediT authorship contribution statement

M. Suski: Data curation, Investigation, Formal analysis, Writing – original draft, Writing – review & editing. **B. Furmann:** Data curation, Formal analysis, Investigation, Software, Funding acquisition, Writing – review & editing, Supervision. **M. Chomski:** Data curation, Investigation, Formal analysis. **S. Mieloch:** Data curation, Investigation, Formal analysis. **P. Głowacki:** Data curation, Investigation. **D. Stefańska:** Investigation, Writing – review & editing.

Data Availability

No data was used for the research described in the article.

Acknowledgements

The authors would like to express their gratitude to Prof. Guthöhrlein for making the program "Fitter" accessible. Many thanks are due to Dr. Magdalena Elantkowska, as well as Dr. Jarosław Ruczkowski from Institute of Control, Robotics and Information Engineering, Faculty of Electrical Engineering, Poznan University of Technology, for valuable discussions. Dr. Andrzej

Krzykowski is greatly acknowledged for his expert help in technical aspects of this work. The research within this work was financially supported by the Ministry of Education and Science, Poland within the project 0511/SBAD/2251 at Faculty of Materials Engineering and Technical Physics, Poznan University of Technology.

References

- [1] Suski M, Chomski M, Furmann B, Ruczkowski J, Stefańska D. Landé g_J factors of the even-parity electronic levels of the terbium atom. *J Quant Spectrosc Radiat Transfer* 2022;288:108270. doi:10.1016/j.jqsrt.2022.108270.
- [2] Suski M, Furmann B, Chomski M, Ruczkowski J, Stefańska D, Mieloch S. Landé g_J factors of the odd-parity electronic levels of the terbium atom determined by laser spectroscopy. *J Quant Spectrosc Radiat Transfer* 2022;291:108342. doi:10.1016/j.jqsrt.2022.108342.
- [3] Childs WJ. Hyperfine structure of many atomic levels of Tb¹⁵⁹ and the Tb¹⁵⁹ nuclear electric-quadrupole moment. *Phys Rev A* 1970;2:316–36. doi:10.1103/PhysRevA.2.316.
- [4] Childs WJ, Goodman LS. Assignment of unclassified lines in Tb I through high-resolution laser-fluorescence measurements of hyperfine structure. *J Opt Soc Am* 1979;69:815–19. doi:10.1364/JOSA.69.000815.
- [5] Childs WJ. Use of atomic-beam laser radio-frequency double resonance for interpretation of complex spectra: Tb I as a test case. *J Opt Soc Am B* 1992;9:191–6. doi:10.1364/JOSAB.9.000191.
- [6] Klinkenberg PFA, Van Kleef TAM. The ground state of the terbium atom. *Physica (Utrecht)* 1970;50:625–8. doi:10.1016/0031-8914(70)90218-1.
- [7] Furmann B, Stefańska D, Krzykowski A. Hyperfine structure of the 4f⁸5d6s² configuration of the Tb atom. *Spectrochim Acta B* 2015;111:38–45. doi:10.1016/j.sab.2015.06.016.
- [8] Furmann B, Stefańska D, Krzykowski A. Hyperfine structure of the 4f⁸5d²6s configuration in the Tb atom. *J Phys B: At Mol Opt Phys* 2015;49:025001. doi:10.1088/0953-4075/49/2/025001.
- [9] Stefanska D, Furmann B. Hyperfine structure of the odd parity level system in the terbium atom. *J Phys B: At Mol Opt Phys* 2017;50(17):175002. doi:10.1088/1361-6455/aa8370.
- [10] Stefanska D, Elantkowska M, Ruczkowski J, Furmann B. Fine- and hyperfine structure investigations of even configuration system of atomic terbium. *J Quant Spectrosc Radiat Transfer* 2017;189:441–56. doi:10.1016/j.jqsrt.2016.10.008.
- [11] Furmann B, Stefanska D, Chomski M, Suski M, Wilman S. Hyperfine structure studies of the odd-parity electronic levels of the terbium atom. *J Quant Spectrosc Radiat Transfer* 2019;237:106613. doi:10.1016/j.jqsrt.2019.106613.
- [12] Smith RL, Wysocki AL, Park K. Electrically tuned hyperfine spectrum in neutral Tb(II)(Cp^{1Pr5})₂ single-molecule magnet. *Phys Chem Chem Phys* 2020;22:21793–800. doi:10.1039/D0CP04056H.
- [13] Stefanska D, Suski M, Furmann B. Tunable continuous wave single-mode dye laser directly pumped by a diode laser. *Laser Phys Lett* 2017;14(4):045701. doi:10.1088/1612-202x/aa5f00.
- [14] Stefanska D, Furmann B. Hyperfine structure investigations for the odd-parity configuration system in atomic holmium. *J Quant Spectrosc Radiat Transfer* 2018;206:286–95. doi:10.1016/j.jqsrt.2017.11.019.
- [15] Kramida A., Yu. Ralchenko, Reader J., and NIST ASD Team. NIST Atomic Spectra Database (ver. 5.9), [Online]. Available: <http://physics.nist.gov/asd> [2021]. National Institute of Standards and Technology, Gaithersburg, MD.; 2021. 10.18434/T4W30F



Landé g_j factors of the even-parity electronic levels of the terbium atom



M. Suski^{a,*}, M. Chomski^a, B. Furmann^a, J. Ruczkowski^b, D. Stefańska^a

^a Institute of Materials Research and Quantum Engineering, Faculty of Materials Engineering and Technical Physics, Poznan University of Technology, Piotrowo 3A, Poznan 60-965, Poland

^b Institute of Robotics and Machine Intelligence, Faculty of Control, Robotics and Electrical Engineering, Poznan University of Technology, Piotrowo 3A, Poznan 60-965, Poland

ARTICLE INFO

Article history:

Received 25 April 2022

Revised 17 May 2022

Accepted 17 May 2022

Available online 19 May 2022

Keywords:

Atomic structure

Laser spectroscopy

Zeeman effect

Hyperfine structure

Landé factors

Terbium

ABSTRACT

In the present work Landé g_j factors for 17 even-parity electronic levels of the terbium atom are presented. The spectra of the Zeeman splitting of the hyperfine structure were recorded with the method of laser spectroscopy in a hollow cathode discharge lamp in a constant magnetic field, with laser induced fluorescence detection. The analysis of 47 spectral lines of terbium in the spectral range between 490 and 609 nm enabled the determination of the g_j factors for the presented even-parity levels for the first time. Moreover, verification of the g_j factor values for 17 odd-parity levels, previously reported by other authors from the analysis of Fourier transform spectra.

© 2022 Elsevier Ltd. All rights reserved.

1. Introduction

Terbium is a rare-earth element, located roughly in the middle of the lanthanides series. It possesses a single stable isotope ^{159}Tb with relatively low nuclear spin value of $I=3/2$, and its values of magnetic dipole and electric quadrupole moments amount to $\mu=+2.014(4)$ nm and $Q=+1.432(8)$ b, respectively [1]. Due to its fluorescent properties, terbium is widely used in green phosphores, which are applicable in commercial devices, such as fluorescent lamps, as well as in fundamental research, e.g. biochemical probes. The magnetic properties of terbium make it a favorable candidate to be used in production of electronic and magnetomechanical devices, such as actuators, sonar systems, etc.

Until recently the knowledge of the electronic levels' structure of terbium was vastly limited. One of the main reasons is the extremely high density of electronic levels, even in comparison with other lanthanides, which is the cause of certain difficulties in both experimental investigations and theoretical interpretation. This feature is related to the placement of terbium in the middle of the lanthanides series and its electronic configurations with several open shells. For such configurations, the results of *ab initio* calculations, concerning the values of energy levels, Landé g_j fac-

tors, A and B hyperfine structure (*hfs*) constants and other parameters, are highly imprecise and often differ significantly from the experimental values. Moreover, due to the wavefunction collapse of the $4f$ orbital, the mean energies of different configurations are nearly the same, hence the spectrum of the terbium atom is quasi-continuous. For the analysis of such atoms, semi-empirical methods are favorable, although they require a significant amount of experimental data. Additionally, for semi-empirical calculations to be considered to be reliable, it is necessary to properly determine the wavefunctions of the intermediate coupling. This can be greatly facilitated by the proper assignment of electronic levels with characteristic values of parameters. In most elements, to properly assign a certain level to a particular configuration, either *hfs* constants or Landé g_j factors were used. For the terbium atom, due to its aforementioned low nuclear spin, the number of the *hfs* components is limited to at most 10. Moreover, the differences between A and B *hfs* constants of various levels are also relatively small. Therefore, reliable identification of the energy levels involved in the unclassified spectral lines requires the determination of both Landé g_j factors and *hfs* constants.

The first significant works concerning the determination of Landé g_j factors were published in 1960-ies, where values for 17 energy levels were reported with precision of the third decimal place [2,3]. It was followed by two works by Childs in 1969 and 1970, where the precision of the values for the previously determined levels was improved to the fifth decimal place [4,5]. Be-

* Corresponding author. Tel.: +48 616653229.

E-mail address: marcin.j.suski@doctorate.put.poznan.pl (M. Suski).

tween 1966 and 1972 a series of six works was published by Klinkenberg and Meinders, where the values of Landé factors for 46 even energy levels were reported with accuracy to the third decimal place [6–11]. Currently, there are 106 even-parity and 493 odd-parity energy levels known according to Martin, Zalubas and Hagan [12], and NIST Atomic Spectra Database [13], for which 65 and 380 g_j factors are reported, respectively.

The begin of investigations of the *hfs* constants of terbium levels are dated roughly to the same time as for Landé factors. The already mentioned work by Childs, published in 1970, provided data concerning *A* and *B* constants of 17 energy levels [5]. No further data concerning *hfs* was reported until, after more than twenty years later, the topic was undertaken by our research group. This resulted in a series of five published works, providing experimental data for numerous electronic levels of both even- and odd-parity [14–18].

Apart from experimental investigations, also attempts of interpretation of the energy levels' structure of the terbium atom were undertaken. An extensive analysis of some even-parity configurations was reported in the following works [5,14,19,20]. As stated before, to further improve such interpretations, new experimental data are required.

Despite the progress achieved, the knowledge of the electronic levels' structure is far from being complete - especially considering the scarcity of data on Landé g_j factors, which are one of the most characteristic parameters of electronic levels. More extensive experimental data on the g_j factors would certainly provide the essential knowledge important from the point of view of the theory of complex atoms, but also required for the potential applications, such as laser cooling in magneto-optical traps (MOT), quantum computers and memories.

The aim of this research is firstly to enrich the available knowledge necessary for the semi-empirical interpretation of the electronic levels' system of the terbium atom. Secondly, it provides the experimental data which can possibly facilitate the aforementioned quantum engineering applications and quantum optics. Within this work the experimental values of Landé g_j factors for 17 even-parity electronic levels in the atomic terbium are presented for the first time. Moreover, the g_j factors values of 17 odd-parity electronic levels published earlier by other authors [12], are verified. The investigations were performed by observation of laser-induced fluorescence (LIF) in a hollow cathode discharge lamp, which was previously used in determination of Landé g_j factors in holmium and europium atoms [21–23].

2. Experimental details

In order to properly determine the Landé g_j factors, Zeeman splitting of the hyperfine structure was employed. This method was successfully adapted from the group from University of Gdansk, in cooperation with Graz University of Technology [24–29]. Both the method and the experimental setup are thoroughly described in our previous works, concerning the investigations of Landé factors in other elements [21–23,30]. In general, it requires recording of the hyperfine structure of the spectral lines split in a magnetic field. The spectra are recorded for two different linear polarization directions of the exciting laser beam in relation to the magnetic field direction - the σ component is observed for perpendicular orientation, and the π component for the parallel one.

The method applied was laser spectroscopy with laser induced fluorescence detection in a hollow cathode discharge lamp, which was the source of free atoms. The external magnetic field was provided by neodymium magnets, placed in close vicinity of the terbium cathode. The desired transitions were excited by single-mode tunable dye lasers. For the selection of the mentioned polarization components, a polarization rotator was used.

The experimental conditions were similar to those presented in our already mentioned previous works. The lamp was cooled with liquid nitrogen and the discharge occurred in the presence of argon as buffer gas. The pressure in the discharge lamp was kept at approximately 0.4 mbar. The discharge current value was relatively stable during a single experimental run at ca. 40 mA. For the weakest spectral lines, the value of the current was increased to 50 mA.

The appropriate magnetic field inside the hollow cathode was ensured by one of two sets of magnets - in the first configuration two magnets were located above the cathode, and in the second one other two magnets were placed on both sides of the cathode. The estimated magnetic field value for the former configuration is approximately 500–600 G, and 1900–2000 G for the latter. However, the actual field in the cathode was found to be significantly different from the given values, and it occurred to be correlated to the value of the electric current required for the discharge. For different values of the current, different Zeeman splittings were observed for any investigated spectral line, which implies that there were changes in the magnetic field. It was attributed to the series of magnetic phase transitions of solid terbium. Below the temperature of 218 K terbium is in ferromagnetic phase. Above this point it reaches the antiferromagnetic state, which persists to the Néel temperature of 230 K, whereas its paramagnetic Curie point is 237 K [31]. The most external parts of the hollow cathode, cooled by the liquid nitrogen, remained in the ferromagnetic state, whereas the internal part, heated by the discharge current, behaved paramagnetic. Such situation resulted in a screening effect that affected the magnetic field, depended on the value of the electric current. Hence, to minimize the magnetic field drift, a value of discharge current as constant as possible was kept during a single measurement run, as already mentioned.

The actual value of the magnetic field was determined by recording spectral lines of argon, namely transitions between electronic levels, for which the g_j factors values are known with high precision. The recorded lines were 17059.2145 cm^{-1} , $\lambda_{\text{air}}=586.031$ nm (104102.0990 cm^{-1} , $J=1$, $g_j=1.985 \rightarrow 121161.3135$ cm^{-1} , $J=1$, $g_j=1.271$) for the long wavelength region, and 19365.8743 cm^{-1} , $\lambda_{\text{air}}=516.228$ nm (104102.0990 cm^{-1} , $J=1$, $g_j=1.985 \rightarrow 123467.9733$ cm^{-1} , $J=1$, $g_j=1.22$) for the short wavelength region. However, due to the mentioned screening effect, the splitting of the π components of the argon spectral lines was too low for reliable determination of the magnetic field strength, therefore spectral lines of terbium, for which the Landé factors for both lower and upper level were known, were used as well. For the same reason as for the argon lines, only the σ components were taken for evaluation of the magnetic field value. The uncertainties of the magnetic field values estimated for the π components were relatively high, in some cases exceeding the difference between the magnetic field strength for π and σ polarizations. Therefore, for calculating the weighted mean values of the g_j factors for the upper energy levels of the investigated transitions, the weights for the results, obtained from the recorded σ polarization scans, were higher than those obtained for π components. For example, for the long wavelength region the line 17191.09 cm^{-1} , $\lambda_{\text{air}}=581.535$ nm (4646.83 cm^{-1} , $J=17/2$, $g_j=1.40626 \rightarrow 21837.92$ cm^{-1} , $J=17/2$, $g_j=1.43$) was used [5,12], and for the short wavelength region the line 20224.03 cm^{-1} , $\lambda_{\text{air}}=494.323$ nm (6801.190 cm^{-1} , $J=5/2$, $g_j=1.80 \rightarrow 27025.22$ cm^{-1} , $J=5/2$, $g_j=1.45$) was exploited [12]. Such lines were recorded several times during each session day. An exemplary spectrum of the σ polarization of the line 17191.09 cm^{-1} is presented in Fig. 1.

To optically excite the terbium atoms, two modified frequency-stabilized Coherent CR 699-21 ring dye lasers were used, both operating in continuous wave regime. The first laser operated on the solution of Coumarin 498 dye, covering the blue-green region of the spectrum (approx. 490–525 nm), optically pumped

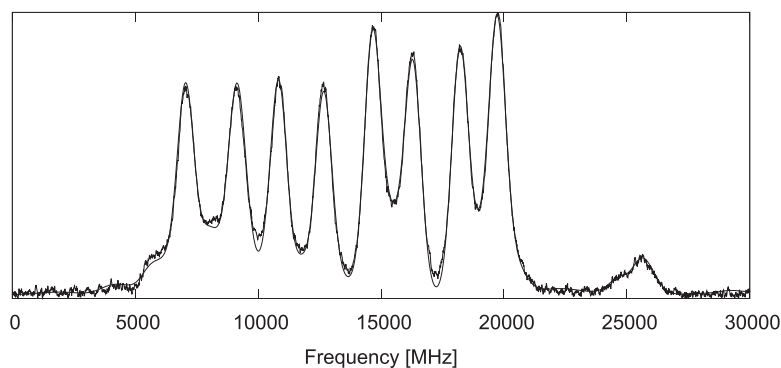


Fig. 1. Recorded Zeeman-hfs patterns of the σ polarization of the spectral line $\lambda = 581.535$ nm ($k=17191.09$ cm^{-1} , transition between the levels 4646.83 cm^{-1} , $J=17/2$ and 21837.92 cm^{-1} , $J=17/2$) in the terbium atom, used for determination of the magnetic field value. The obtained field strength value is $444.3(19.3)$ G.

by a diode laser emitting at 445 nm (Lasever Inc., China, model LSR445SD-4W) [32]. The second dye laser covered the yellow-orange region of the spectrum (approx. 570–610 nm), exploiting Rhodamine 6G dye solution as a lasing medium. A frequency doubled Nd:YVO₄ laser (Coherent Verdi V-10) was used as a pump source. The precise value of the laser wavelength was controlled with the wavemeter readings (Burleigh WA-1500), while the single mode operation was ensured by a mode analyzer.

The fluorescence light from decay transitions was directed to a SPM-2 grating monochromator and, after spectral selection, to a Hamamatsu R-375 photomultiplier with preamplifier, where the photocurrent signal was generated. The signal-to-noise ratio was enhanced by a phase-sensitive amplifier, with a mechanical chopper used for the periodic interruption of the laser beam. The signal was further directed to the computer for scan recording. The frequency scale for the scans was obtained by recording the transmission signal of a temperature-stabilized Fabry-Perot interferometer (FSR=1500 MHz) simultaneously with the measured spectrum.

To apply the frequency scale based on the marker signal, the "Fitter" program was used, which has been exploited in our calculations of both hfs and Landé factors for many years.

3. Determination of g_j values

3.1. Hyperfine structure and Zeeman splitting

When an atom is placed in an external magnetic field H_{mag} , its eigenstates constitute linear combinations of the form:

$$|\psi M_F\rangle = \sum_F C_{M_F F} |\gamma J I F M_F\rangle. \quad (1)$$

The eigenvector amplitudes $C_{M_F F}$ can be derived by means of diagonalization of the Hamiltonian matrix:

$$H_{F M_F, F' M_F'} = \delta_{F F'} \left(A \frac{C}{2} + B \frac{3C(C+1) - I(I+1)J(J+1)}{2I(2I-1)J(2J-1)} \right) + \mu_B g_j H_{mag} (-1)^{F-M_F+J+I+F'+1} \sqrt{(2F+1)(2F'+1)J(J+1)(2J+1)} \times \begin{pmatrix} F & 1 & F' \\ -M_F & 0 & M_F' \end{pmatrix} \begin{Bmatrix} F & 1 & F' \\ J & I & J \end{Bmatrix}, \quad (2)$$

where $C = F(F+1) - J(J+1) - I(I+1)$, μ_B is the Bohr magneton and g_j is the Landé factor.

The intensity of an individual radiative transition between two Zeeman sublevels M_F and M_F' is proportional to the related transition probability. The line shape observed experimentally is the envelope of all individual Zeeman components, each having a line profile determined by Doppler- and other broadening mechanisms and by instrumental effects.

3.2. Computational procedures

As the first step of our computational procedures, the Zeeman sublevels energies, relative to the fine structure energy $E(J)$, for both the upper and the lower level of the studied transition, are determined by means of diagonalization of the Hamiltonian expressed by Eq. (2). The required input data, concerning values of the magnetic field H_{mag} , nuclear spin I and electronic shell angular momentum J quantum numbers, the hyperfine structure A and B constants, as well as the initial values of Landé g_j factors for two energy levels involved, are loaded from an appropriate input file. The obtained eigenvalues and eigenvectors are adopted for determination of the relative positions of the Zeeman components on the frequency scale, and their intensities, separately for σ and π transitions.

Afterwards, the intensity distribution function is derived as a sum of intensities for each abscissa value of the final pattern, with the use of evaluated splitting constants and line profile parameters. In an iterative procedure, this function is fitted to the experimentally observed line profile stored in the digital form, where values of Landé g_j factors for the upper and the lower levels are adjustable parameters. In the calculations the Marquardt's algorithm [33] is applied. There is also a possibility to fine-tune the values of hfs constants, which is important in particular when these constants are determined earlier with considerable experimental uncertainties.

In order to include saturation effects, an additional parameter A_s (saturation rate) was introduced in the fitting procedure. The calculated decay rate of each Zeeman component (A_v) of frequency ν was modified according to the following expression [34]:

$$A_v^{sat} = \frac{A_v}{1 + A_v/A_s} \quad (3)$$

4. Results

In this work altogether 49 spectral lines of the terbium atom were investigated for determination of Landé g_j factors. All of the lines are presented in Table 1.

In order to properly calculate the g_j factor of the lower or the upper energy level of a transition, the value of the magnetic field has to be known. Also, the knowledge of the g_j factor of one of the energy levels, participating in this transition, is favourable, as it significantly increases the precision of the calculations. However, calculations of g_j factors for both energy levels simultaneously are also possible, though the accuracy of the obtained results might be decreased.

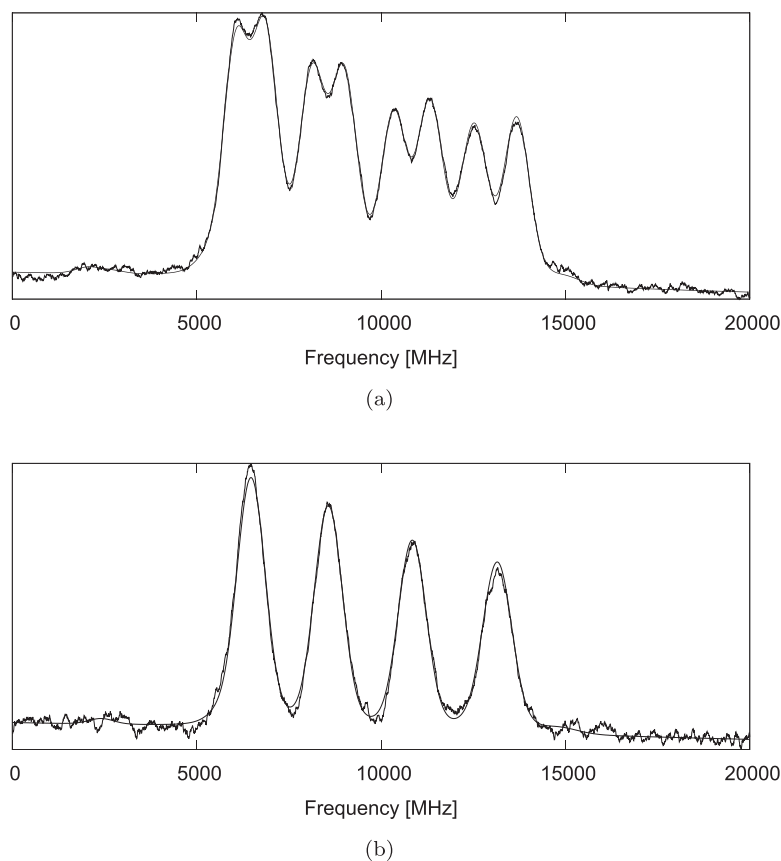


Fig. 2. Recorded Zeeman- hfs patterns of the spectral line $\lambda = 596.490$ nm ($k=16760.11$ cm^{-1} , transition between the levels 12628.67 cm^{-1} , $J=15/2$ and 29388.78 cm^{-1} , $J=15/2$) in the terbium atom (Table 1, No 24), along with the least-squares fitted curves for a) polarization σ , and b) polarization π at the magnetic field strength 240.8 G.

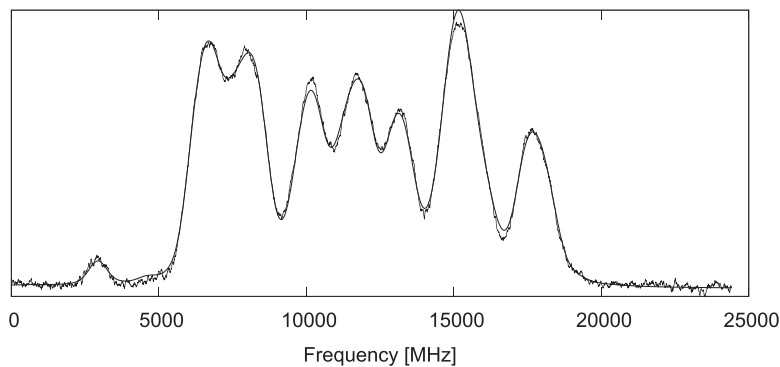
Determination of the magnetic field strength exploits recording of transitions between energy levels with precisely known g_j values in argon, as presented in our previous works. In that case, the standard calculation procedure had to be reversed. However, as mentioned in Section 2, due to the magnetic field screening effect, resulting from phase transition in terbium, the data obtained from recorded argon lines were insufficient because the splitting of the π components was too small. Therefore, additionally σ components of the spectral lines between energy levels in terbium, for which Landé factors are already known, were exploited.

First iteration of the calculations concerned the determination of the g_j factors for the lower even-parity energy levels, with the g_j factors of the upper odd-parity levels fixed at the available literature values. The obtained results were further averaged for each particular even-parity energy level. Secondly, the g_j factors of the upper energy levels were recalculated by reversing the procedure and using the averaged values for the lower levels, obtained in the previous step. Finally, the g_j factors of the lower levels were calculated once again, with improved average values for the upper levels. Such an approach enabled the reduction of the uncertainties for the lower even-parity levels and the verification of the g_j values of the odd-parity levels, which were obtained by other authors from a Fourier spectrum. The values, obtained for individual spectral lines, are summarized in Table 1. The first set of columns (2 and 3) provide the information on the transition, namely the wavelengths and wavenumbers. In columns 4–6 data concerning the lower energy levels is presented - energies, J quantum numbers, the experimental values of the g_j factors, calculated as weighted means of the values obtained for π and σ components. The last group of columns contains similar information for

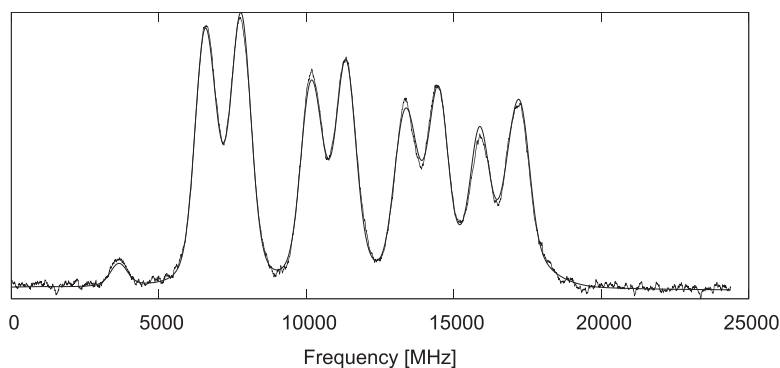
the upper energy levels. Examples of the recorded spectra with the fitted Zeeman- hfs patterns are presented in Figs. 2 - 4.

The final g_j factors for particular energy levels were obtained by averaging the partial values concerning those levels. Hence, the values for 17 even-parity (lower) energy levels were determined, and the values for 17 odd-parity (upper) energy levels were re-evaluated and compared with the values from the literature. The results, arranged by the parity of the energy levels, are presented in Table 2. For even-parity levels the semi-empirically predicted values of the g_j factors are presented, whereas for odd-parity levels available experimental literature g_j factors are also provided. The number of lines recorded, used for averaging, is given for each energy level. In case of 5 even-parity levels and 4 odd-parity levels, the Landé g_j factors were obtained from only one line in each case. These are the even-parity levels 11956.25 cm^{-1} ($J=9/2$), 12296.45 cm^{-1} ($J=5/2$), 12932.66 cm^{-1} ($J=15/2$), 13277.23 cm^{-1} ($J=7/2$), 13666.46 cm^{-1} ($J=11/2$) and the odd-parity levels 29210.56 cm^{-1} ($J=9/2$), 32015.99 cm^{-1} ($J=15/2$), 32163.47 cm^{-1} ($J=9/2$), 33638.32 cm^{-1} ($J=9/2$), respectively.

The experimental uncertainties of the calculated Landé g_j factors consist of separate mean standard deviations for the fitted g_j factors of both energy levels involved in a transition and the uncertainty concerning the fluctuations of the magnetic field. Concerning the latter, the mean standard deviation for the average magnetic field value, was estimated from the investigation of transitions between levels with known g_j factors, for π and σ components, separately. The actual contribution was determined to be the difference of the g_j factors calculated for the underestimated and the overestimated values of the magnetic field, divided by 2. Hence, the total uncertainty for single energy levels is calculated

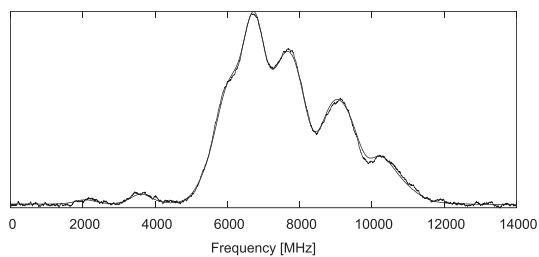


(a)

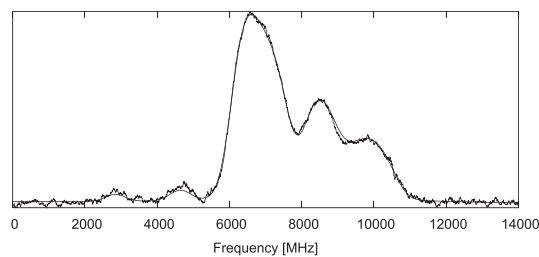


(b)

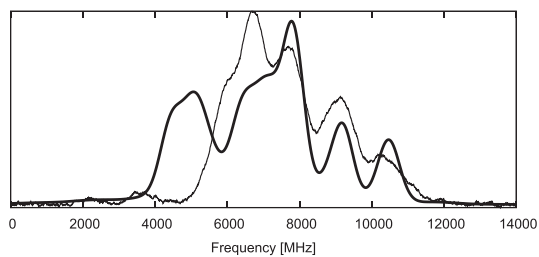
Fig. 3. Recorded Zeeman-*hfs* patterns of the spectral line $\lambda = 573.446$ nm ($k=17433.59$ cm^{-1} , transition between the levels 13116.48 cm^{-1} , $J=13/2$ and 30550.07 cm^{-1} , $J=13/2$) in the terbium atom (Table 1, No 45), along with the least-squares fitted curves for a) polarization σ , and b) polarization π at the magnetic field strength 444.3 G.



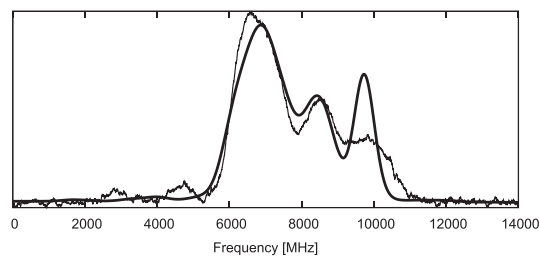
(a)



(b)



(c)



(d)

Fig. 4. Recorded Zeeman-*hfs* patterns of the spectral line $\lambda = 592.126$ nm ($k=16883.61$ cm^{-1} , transition between the levels 13666.46 cm^{-1} , $J=11/2$ and 30550.07 cm^{-1} , $J=13/2$) in the terbium atom (Table 1, No 47), along with the least-squares fitted curves for a) polarization σ , and b) polarization π at the magnetic field strength 444.3 G. Pictures c) and d) present an attempt to match the literature value of the g_J factor [7] for the upper energy level for σ and π polarization, respectively. The thin solid line is the recorded pattern, while the bold solid line is the least-squares fitted curve. The experimental literature value of the Landé g_J factor doesn't fit to the recorded spectra.

Table 1

Spectral lines of the terbium atom experimentally investigated in this work for the purpose of determination of the Landé g_j factors. For all lines the g_j factors for the upper odd-parity levels and the lower even-parity levels were determined independently.

No	Line		Lower level			Upper level		
	λ_{air} (nm)	k_{vac} (cm^{-1})	E (cm^{-1})	J	$g_{J,av}$	E (cm^{-1})	J	$g_{J,av}$
1	2	3	4	5	6	7	8	9
1	585.920	17062.46	11425.94	13/2	1.566(56)	28488.40	15/2	1.331(62)
2	572.438	17464.30	11425.94	13/2	1.572(62)	28890.24	13/2	1.453(47)
3	571.492	17493.20	11425.94	13/2	1.548(45)	28919.14	11/2	1.529(58)
4	591.282	16907.72	11580.68	15/2	1.517(36)	28488.40	15/2	1.331(33)
5	577.555	17309.56	11580.68	15/2	1.484(42)	28890.24	13/2	1.509(41)
6	572.030	17476.75	11956.25	9/2	1.071(31)	29433.01	9/2	1.412(43)
7	598.964	16690.86	12228.28	9/2	1.756(42)	28919.14	11/2	1.471(33)
8	581.074	17204.73	12228.28	9/2	1.745(34)	29433.01	9/2	1.401(32)
9	501.600	19930.65	12228.28	9/2	1.709(39)	32158.93	7/2	1.633(36)
10	592.414	16875.42	12250.99	7/2	1.917(33)	29126.41	9/2	1.412(43)
11	502.172	19907.94	12250.99	7/2	1.925(37)	32158.93	7/2	1.593(51)
12	503.321	19862.48	12296.45	5/2	1.562(56)	32158.93	7/2	1.584(65)
13	608.211	16437.10	12453.14	11/2	1.550(51)	28890.24	13/2	1.434(51)
14	599.596	16673.27	12453.14	11/2	1.502(34)	29126.41	9/2	1.439(43)
15	578.394	17284.47	12453.14	11/2	1.479(46)	29737.61	11/2	1.545(53)
16	574.088	17414.10	12453.14	11/2	1.500(15)	29867.24	13/2	1.362(41)
17	607.978	16443.40	12475.74	13/2	1.520(42)	28919.14	11/2	1.467(31)
18	591.096	16913.04	12475.74	13/2	1.489(48)	29388.78	15/2	1.383(33)
19	585.754	17067.27	12475.74	13/2	1.500(15)	29543.01	13/2	1.402(17)
20	579.151	17261.87	12475.74	13/2	1.491(32)	29737.61	11/2	1.519(28)
21	574.834	17391.50	12475.74	13/2	1.500(19)	29867.24	13/2	1.345(20)
22	568.724	17578.33	12475.74	13/2	1.506(26)	30054.07	11/2	1.370(27)
23	568.263	17592.61	12475.74	13/2	1.502(17)	30068.35	15/2	1.418(19)
24	596.490	16760.11	12628.67	15/2	1.430(82)	29388.78	15/2	1.367(60)
25	591.050	16914.34	12628.67	15/2	1.454(15)	29543.01	13/2	1.406(27)
26	579.934	17238.57	12628.67	15/2	1.446(17)	29867.24	13/2	1.360(28)
27	515.657	19387.32	12628.67	15/2	1.458(46)	32015.99	15/2	1.372(31)
28	606.021	16496.51	12714.05	7/2	1.428(63)	29210.56	9/2	1.466(62)
29	514.131	19444.88	12714.05	7/2	1.439(51)	32158.93	7/2	1.587(61)
30	589.414	16961.30	12776.31	9/2	1.484(37)	29737.61	11/2	1.471(33)
31	578.618	17277.76	12776.31	9/2	1.418(23)	30054.07	11/2	1.389(31)
32	515.782	19382.62	12776.31	9/2	1.451(35)	32158.93	7/2	1.584(41)
33	515.662	19387.16	12776.31	9/2	1.439(68)	32163.47	9/2	1.348(58)
34	606.548	16482.18	12906.60	13/2	1.563(58)	29388.78	15/2	1.354(47)
35	593.977	16831.01	12906.60	13/2	1.563(43)	29737.61	11/2	1.499(49)
36	583.015	17147.47	12906.60	13/2	1.556(28)	30054.07	11/2	1.371(33)
37	582.530	17161.75	12906.60	13/2	1.529(16)	30068.35	15/2	1.447(24)
38	583.416	17135.69	12932.66	15/2	1.440(26)	30068.35	15/2	1.419(63)
39	599.847	16666.31	13071.30	11/2	1.535(42)	29737.61	11/2	1.496(25)
40	595.217	16795.94	13071.30	11/2	1.553(15)	29867.24	13/2	1.340(21)
41	588.669	16982.77	13071.30	11/2	1.555(25)	30054.07	11/2	1.362(26)
42	596.823	16750.76	13116.48	13/2	1.536(19)	29867.24	13/2	1.344(23)
43	590.239	16937.59	13116.48	13/2	1.515(27)	30054.07	11/2	1.396(28)
44	589.742	16951.87	13116.48	13/2	1.531(21)	30068.35	15/2	1.428(22)
45	573.446	17433.59	13116.48	13/2	1.544(15)	30550.07	13/2	1.332(24)
46	490.996	20361.09	13277.23	7/2	1.527(52)	33638.32	9/2	1.518(45)
47	592.126	16883.61	13666.46	11/2	1.518(14)	30550.07	13/2	1.340(43)

as follows:

$$\Delta g_j = \sqrt{(SD_1)^2 + (SD_2)^2 + (\Delta g_{j,B})^2} \quad (4)$$

where $SD_{1,2}$ are the mean standard deviations for g_j of the upper and the lower energy level and the last term is the contribution of the magnetic field fluctuation to the total error.

5. Discussion

The Landé g_j factors determined for the even-parity levels within this work are presented for the first time, hence they cannot be compared to any earlier experimental works. In comparison with the predicted values, one can learn that the results are consistent within the limits of the measurement uncertainties. The highest difference, which exceeds 5%, is observed for the level 12714.05 cm^{-1} ($J=7/2$), based on two lines.

Concerning the verification of the g_j factors of the 17 odd-parity levels, the values of the g_j factors for 15 investigated levels agree with the already published values [12] within the uncertainty limits. For the remaining two levels, i.e. 30550.07 cm^{-1} ($J=13/2$) and 32015.99 cm^{-1} ($J=15/2$), the least-squares fitted curves didn't match the recorded spectra for the reference g_j factors of these levels. It is possible that these values were previously determined incorrectly. The new experimental values are included in Table 2. The attempt to fit the least-squares curve using the reference g_j factor for the line 16883.61 cm^{-1} (13666.46 cm^{-1} , $J=11/2 \rightarrow 30550.07 \text{ cm}^{-1}$, $J=13/2$) is presented in Fig. 4.

Some differences between the results are observable for π and σ components of the particular spectral lines, as well as between average values of g_j factors of various lines with the same lower or upper level, contributing to the increase of the calculated uncertainties. The main factor is the magnetic field screening by terbium in the ferromagnetic phase, which negatively affects the precision

Table 2

Values of the Landé g_j factors of the electronic levels of the terbium atom, determined in this work from the measurements of the Zeeman effect in the hyperfine structure; available literature data and theoretically predicted values are presented for comparison.

No	E(cm ⁻¹)	J	No of lines	g_j^{mean}	g_j^{pred} [17]	g_j^{lit}
1	2	3	4	5	6	7
even-parity levels						
1	11425.94	13/2	3	1.562(37)	1.570	
2	11580.68	15/2	2	1.501(39)	1.519	
3	11956.25	9/2	1	1.071(31)	1.104	
4	12228.28	9/2	3	1.737(27)	1.729	
5	12250.99	7/2	2	1.921(20)	1.931	
6	12296.45	5/2	1	1.562(62)	1.524	
7	12453.14	11/2	4	1.508(27)	1.475	
8	12475.74	13/2	7	1.501(15)	1.510	
9	12628.67	15/2	4	1.447(25)	1.459	
10	12714.05	7/2	2	1.433(48)	1.519	
11	12776.31	9/2	4	1.448(24)	1.465	
12	12906.60	13/2	4	1.553(19)	1.543	
13	12932.66	15/2	1	1.440(35)	1.468	
14	13071.30	11/2	3	1.548(17)	1.571	
15	13116.48	13/2	4	1.532(14)	1.516	
16	13277.23	7/2	1	1.526(52)	1.525	
17	13666.46	11/2	1	1.518(19)	1.533	
odd-parity levels						
1	28488.40	15/2	2	1.331(23)		1.34(2) [12]
2	28890.24	13/2	3	1.465(36)		1.500(5) [6]
3	28919.14	11/2	3	1.489(36)		1.48(2) [12]
4	29126.41	9/2	2	1.426(30)		1.400(5) [6]
5	29210.56	9/2	1	1.466(63)		1.46(2) [12]
6	29388.78	15/2	3	1.368(33)		1.385(5) [8]
7	29433.01	9/2	2	1.407(24)		1.41(2) [6]
8	29543.01	13/2	2	1.404(11)		1.40(2) [12]
9	29737.61	11/2	5	1.506(25)		1.50(2) [12]
10	29867.24	13/2	5	1.350(11)		1.36(2) [6]
11	30054.07	11/2	5	1.378(17)		1.35(2) [12]
12	30068.35	15/2	4	1.428(14)		1.43(2) [12]
13	30550.07	13/2	2	1.336(10)		1.66(2) [7]
14	32015.99	15/2	1	1.372(42)		1.91(2) [12]
15	32158.93	7/2	5	1.596(29)		1.59(2) [6]
16	32163.47	9/2	1	1.348(64)		1.37(2) [7]
17	33638.32	9/2	1	1.518(45)		1.53(2) [11]

of the magnetic field determination. Moreover, the screening effect decreases the value of the magnetic field itself, hence the Zeeman splitting of the hfs components is smaller. Due to that fact, the precision of determination of intervals between split components is reduced. This is especially noticeable for π polarization, where the Zeeman splitting is significantly smaller than for σ polarization.

6. Conclusions

In this work experimental results of Landé g_j factors for 17 even-parity electronic levels are presented, which were obtained for the first time. The values are close to those predicted theoretically within the experimental uncertainties. The estimated uncertainties are dominated by the contribution of the high uncertainties of the magnetic field, resulting from the screening effect, mentioned in Section 2, as well as the high uncertainties for the literature values of g_j factors of the upper odd-parity energy levels, used for initial calculations. The deviations from the predicted values are estimated on average at 1.5% for nominal values. Therefore, the consistency of the results may be considered very good.

Moreover, the values of g_j factors for 17 levels belonging to the odd-parity configurations, already available in the literature [12], were verified. The results for most of the investigated levels are consistent with the reference values within the uncertainty limits, dominated mostly by the same aspects, as the g_j factors of the even-parity levels. For two of the odd-parity levels significantly different g_j values are introduced, as the previously reported values don't fit to the spectra recorded within the present work.

The new results obtained within this work constitute a significant extension of the available database of Landé g_j factors' values of atomic terbium and may contribute to notable improvement of the semi-empirical analysis of the fine structure of this element.

Declaration of Competing Interest

The authors declare that they have no known competing financial interests or personal relationships that could have appeared to influence the work reported in this paper.

CRediT authorship contribution statement

M. Suski: Data curation, Investigation, Formal analysis, Writing – original draft, Writing – review & editing. **M. Chomski:** Data curation, Investigation, Formal analysis. **B. Furmann:** Data curation, Formal analysis, Investigation, Software, Funding acquisition, Writing – review & editing, Supervision. **J. Ruczkowski:** Formal analysis, Software, Writing – original draft. **D. Stefańska:** Investigation, Writing – review & editing.

Acknowledgments

The authors would like to express their gratitude to Dr. Sci. Magdalena Elantkowska for her valuable remarks concerning the development of the software for g_j factors' calculation, as well as Dr. Andrzej Krzykowski, Dr. Eng. Semir El-Ahmar and M.Sc. Eng. Sebastian Wilman for their professional help in realization of the

technical part of the work. Dr. Sławomir Werbowy from the University of Gdańsk is greatly acknowledged for his essential contribution to the transfer of the idea of measuring the Zeeman effect of the hyperfine structure to our group.

Financial support of this work by the Ministry of Science and Higher Education, Poland within the projects realized at Poznan University of Technology: 0511/SBAD/2251 at Faculty of Materials Engineering and Technical Physics, (M.S., M.C., B.F. and D.S.), 0711/SBAD/4560 at Institute of Electric Power Engineering (J.R.) is also acknowledged.

References

- [1] Stone N. Table of nuclear magnetic dipole and electric quadrupole moments. At Data Nucl Data Tables 2005;90(1):75–176. doi:10.1016/j.adt.2005.04.001.
- [2] Bender I, Penselin S, Schlüpmann K. Zur frage des grundzustandes im Tb I-spektrum. Z Phys 1964;179(1):4–8. doi:10.1007/BF01380687.
- [3] Arnoult C, Gerstenkorn S. Experimental and theoretical hyperfine structure of low-lying levels of terbium $4f^8 5d 6s^2$ configuration; quadrupole moment of ^{159}Tb . J Opt Soc Am 1966;56(2):177–81. doi:10.1364/JOSA.56.000177.
- [4] Childs WJ, Goodman LS. Hyperfine structure and g_J values of low levels of ^{159}Tb . J Opt Soc Am 1969;59(7):875. doi:10.1364/JOSA.59.000875.
- [5] Childs WJ. Hyperfine structure of many atomic levels of Tb^{159} and the Tb^{159} nuclear electric-quadrupole moment. Phys Rev A 1970;2:316–36. doi:10.1103/PhysRevA.2.316.
- [6] Klinkenberg PFA. Structure of the spectrum of neutral terbium, Tb I. Physica (Utrecht) 1966;32:1113–47. doi:10.1016/0031-8914(66)90147-9.
- [7] Klinkenberg PFA, Meinders E. Structure of the spectrum of neutral terbium, Tb I. Part II. Physica (Utrecht) 1966;32:1617–32. doi:10.1016/0031-8914(66)90077-2.
- [8] Klinkenberg PFA. Structure of the spectrum of neutral terbium, Tb I. Part III: levels having extreme values of J . Physica (Utrecht) 1967;37:197–214. doi:10.1016/0031-8914(67)90151-6.
- [9] Meinders E, Klinkenberg PFA. Structure of the spectrum of neutral terbium, Tb I. Part IV. Physica (Utrecht) 1968;38:253–74. doi:10.1016/0031-8914(68)90149-3.
- [10] Klinkenberg PFA, Meinders E. Structure of the spectrum of neutral terbium, Tb I. Part V: the configuration $4f^8 5d^2 6s$. Physica (Utrecht) 1969;42:213–41. doi:10.1016/0031-8914(69)90014-7.
- [11] Klinkenberg PFA. Structure of the spectrum of neutral terbium, Tb I. Part VI: the sextet system of $4f^8 ({}^7F) 5d 6s^2$. Physica (Utrecht) 1972;57:594–615. doi:10.1016/0031-8914(66)90147-9.
- [12] Martin WC, Zalubas R, Hagan L. Atomic energy levels – the rare-earth elements. Nat. Stand. Ref. Data Ser., NSRDS-NBS 60. US: Nat Bur Stand; 1978. <https://nvlpubs.nist.gov/nistpubs/Legacy/NSRDS/nbsnsrds60.pdf>
- [13] Kramida A., Yu. Ralchenko, Reader J., and NIST ASD Team. NIST Atomic Spectra Database (ver. 5.9), [Online]. Available: <http://physics.nist.gov/asd> [2021]. National Institute of Standards and Technology, Gaithersburg, MD.; 2021. 10.18434/T4W30F
- [14] Furmann B, Stefańska D, Krzykowski A. Hyperfine structure of the $4f^8 5d 6s^2$ configuration of the Tb atom. Spectrochim Acta B 2015;111:38–45. doi:10.1016/j.sab.2015.06.016.
- [15] Furmann B, Stefańska D, Krzykowski A. Hyperfine structure of the $4f^8 5d^2 6s$ configuration in the Tb atom. J Phys B: At Mol Opt Phys 2015;49:025001. doi:10.1088/0953-4075/49/2/025001.
- [16] Stefanska D, Furmann B. Hyperfine structure of the odd parity level system in the terbium atom. J Phys B: At Mol Opt Phys 2017;50(17):175002. doi:10.1088/1361-6455/aa8370.
- [17] Stefanska D, Elantkowska M, Ruczkowski J, Furmann B. Fine- and hyperfine structure investigations of even configuration system of atomic terbium. J Quant Spectrosc Radiat Transfer 2017;189:441–56. doi:10.1016/j.jqsrt.2016.10.008.
- [18] Furmann B, Stefanska D, Chomski M, Suski M, Wilman S. Hyperfine structure studies of the odd-parity electronic levels of the terbium atom. J Quant Spectrosc Radiat Transfer 2019;237:106613. doi:10.1016/j.jqsrt.2019.106613.
- [19] Bauche-Arnoult C, Sinzelle J, Bachelier A. Extensive theoretical analysis of the f^d and f^d configurations. application to $4f^8 5d 6s^2$ in Tb I. J Opt Soc Am 1978;68(3):368–74. doi:10.1364/JOSA.68.000368.
- [20] Elantkowska M, Ruczkowski J, Sikorski A, Dembczyński J. Construction of the energy matrix for complex atoms. Part VIII: hyperfine structure HPC calculations for terbium atom. Eur Phys J Plus 2017;132:455. doi:10.1140/epjp/i2017-11725-0.
- [21] Furmann B, Ruczkowski J, Chomski M, Suski M, Wilman S, Stefańska D. Lande g_J factors of the electronic levels of the europium atom. J Quant Spectrosc Radiat Transfer 2020;255:107258. doi:10.1016/j.jqsrt.2020.107258.
- [22] Chomski M, Furmann B, Ruczkowski J, Suski M, Stefańska D. Lande g_J factors of the electronic levels of the holmium atom. J Quant Spectrosc Radiat Transfer 2021;274:107865. doi:10.1016/j.jqsrt.2021.107865.
- [23] Chomski M, Suski M, Wilman S, Furmann B, Ruczkowski J, Stefańska D. Lande g_J factors of odd-parity electronic levels of the holmium atom. J Quant Spectrosc Radiat Transfer 2022;279:108045. doi:10.1016/j.jqsrt.2021.108045.
- [24] Grabowski D, Drozdowski R, Kwela J, Heldt J. Hyperfine structure and Zeeman effect studies in the $6p^2 6p^3$ transitions in Bi II. Z Phys D 1996;38:289–93. doi:10.1007/s004600050093.
- [25] Werbowy S, Güney C, Windholz L. Experimental investigations of the Zeeman effect of new fine structure levels of lanthanum and praseodymium. Spectrochim Acta Part B 2016;116(Supplement C):16–20. doi:10.1016/j.sab.2015.11.003.
- [26] Werbowy S, Güney C, Windholz L. Studies of Landé g_J -factors of singly ionized lanthanum by laser-induced fluorescence spectroscopy. J Quant Spectrosc Radiat Transfer 2016;179(Supplement C):33–9. doi:10.1016/j.jqsrt.2016.03.009.
- [27] Sobolewski Ł, Windholz L, Kwela J. Laser induced fluorescence spectroscopy used for the investigation of Landé g_J - factors of praseodymium energy levels. J Quant Spectrosc Radiat Transfer 2017;194(Supplement C):24–30. doi:10.1016/j.jqsrt.2017.03.021.
- [28] Sobolewski Ł, Windholz L, Kwela J. Determination of Lande g_J - factors of La I levels using laser spectroscopic methods: complementary investigations. J Quant Spectrosc Radiat Transfer 2017;201(Supplement C):30–4. doi:10.1016/j.jqsrt.2017.06.030.
- [29] Sobolewski Ł, Windholz L, Kwela J. Zeeman structure of red lines of lanthanum observed by laser spectroscopy methods. J Quant Spectrosc Radiat Transfer 2017;201(Supplement C):180–3. doi:10.1016/j.jqsrt.2017.07.013.
- [30] Stefańska D, Furmann B, Ruczkowski J, Elantkowska M, Glowacki P, Chomski M, Suski M, Wilman S. Investigations of the possible second-stage laser cooling transitions for the holmium atom magneto-optical trap. J Quant Spectrosc Radiat Transfer 2020;246:106915. doi:10.1016/j.jqsrt.2020.106915.
- [31] Thoburn WC, Legvold S, Spedding FH. Magnetic properties of terbium metal. Phys Rev 1958;112:56. doi:10.1103/PhysRev.112.56.
- [32] Stefanska D, Suski M, Furmann B. Tunable continuous wave single-mode dye laser directly pumped by a diode laser. Laser Phys Lett 2017;14(4):045701. doi:10.1088/1612-202x/aa5f00.
- [33] Marquardt DW. An algorithm for least-squares estimation of nonlinear parameters. J Soc Ind App Math 1963;11(2):431–41. <http://www.jstor.org/stable/2098941>
- [34] Sobolewski L, Windholz L, Kwela J. Landé g_J - factors of Nb I levels determined by laser spectroscopy. J Quant Spectrosc Radiat Transfer 2020;249:107015. doi:10.1016/j.jqsrt.2020.107015.



Landé g_j factors of the odd-parity electronic levels of the terbium atom determined by laser spectroscopy



M. Suski^{a,*}, B. Furmann^a, M. Chomski^a, J. Ruczkowski^b, D. Stefańska^a, S. Mieloch^a

^aInstitute of Materials Research and Quantum Engineering, Faculty of Materials Engineering and Technical Physics, Poznan University of Technology, Piotrowo 3A, Poznan 60-965, Poland

^bInstitute of Robotics and Machine Intelligence, Faculty of Control, Robotics and Electrical Engineering, Poznan University of Technology, Piotrowo 3A, Poznan 60-965, Poland

ARTICLE INFO

Article history:

Received 12 July 2022

Revised 4 August 2022

Accepted 4 August 2022

Available online 6 August 2022

Keywords:

Atomic structure

Laser spectroscopy

Zeeman effect

Hyperfine structure

Landé factors

Terbium

ABSTRACT

In the present work the experimentally determined values of Landé g_j factors for 20 odd-parity electronic levels of atomic terbium are presented. The Zeeman splitting of the hyperfine structure was investigated using the method of laser induced fluorescence in a hollow cathode discharge lamp in a constant magnetic field. All of the values were determined for the first time, by the analysis of 32 spectral lines, recorded in the spectral range between 492 and 609 nm. Moreover, the g_j factors for 15 even-parity energy levels, reported in the available literature, were verified.

© 2022 Elsevier Ltd. All rights reserved.

1. Introduction

Terbium is an element belonging to the lanthanides, possessing one stable isotope $^{159}_{65}\text{Tb}$. It is characterized by nuclear spin $I = 3/2$ and the magnetic dipole and electric quadrupole moments' values of $\mu = +2.014(4)$ nm and $Q = +1.432(8)$ b, respectively [1]. Terbium exhibits distinctive fluorescent and magnetic features, applicable in various fields, both scientific and commercial. It is used in green phosphores, implemented in fluorescent lamps or biochemical probes, as well as in production of electronic and magnetomechanical devices, such as actuators and sonar systems, to name only a few.

Landé g_j factors belong to the most characteristic parameters of the electronic levels; this work, being a continuation of recently published research on g_j factors for the even-parity levels of terbium [2], focuses on determination of g_j factors for the odd-parity levels. Some of the even-parity energy levels, for which the experimentally determined values of the g_j factors were presented in the previous work for the first time, are involved in the transitions investigated within this study, and the respective g_j values could be fixed in the fitting procedure. Although the g_j factors of both energy levels of the particular transition can be calculated simul-

taneously, the knowledge of the g_j factor of one of these levels significantly increases the precision of the calculations for the other level.

Along with the hyperfine structure (*hfs*) constants, the g_j factors can significantly facilitate the proper assignment of the electronic levels to the particular configurations, as well as provide the essential data for the semi-empirical calculations, which is favourable from the point of view of the theory of complex atoms. Semi-empirical methods are vital for atoms such as terbium, as its placement in the middle of the lanthanides series, along with several open shells electronic configurations, results in difficulties in both experimental investigations and theoretical interpretation. This manifests in high number of levels with very similar energy values, as the mean energies of different configurations are close to each other due to the wavefunction collapse of the 4f orbital. For such cases, the results of ab-initio calculations, concerning the parameters of the energy levels, are highly imprecise and differ from the experimental values. Last but not least, the obtained experimental data may contribute to the development of potential applications, such as laser cooling in magneto-optical traps (*MOT*) or quantum computers and memories. The comprehensive knowledge of the g_j factors and the *hfs* constants is substantial for the determination of the usefulness of terbium in the mentioned applications, as well as any other application as a quantum material.

Despite its significance, the knowledge of the Landé g_j factors for the terbium atom is relatively scarce, which may be the result

* Corresponding author.

E-mail address: marcin.j.suski@doctorate.put.poznan.pl (M. Suski).

of the complexity of its structure due to the aforementioned reasons. Investigations of the odd-parity configurations are even more problematic, in terms of determination of both the hfs A and B constants and the g_j factors; for this level system the semi-empirical description is still difficult, despite the data available. The odd-parity system is much more complex than the even-parity system, because of the particularly strong overlap of various configurations on the energy scale, and the resulting strong configuration mixing.

A brief review of the current state of knowledge on both the hfs A and B constants and the Landé g_j factors was presented in our previous work [2].

Within this work the experimental values of Landé g_j factors for 20 odd-parity energy levels are presented for the first time, determined from 32 spectral lines. For any of the investigated levels, no semi-empirical g_j factor value was predicted. Moreover, the g_j factors' values for 15 even-parity energy levels, reported in other works [2–5], were verified. The investigations were carried out by observation of the laser induced fluorescence (LIF) in a hollow cathode discharge lamp, as in our previous works, concerning determination of the Landé factors [2,6–8].

2. Experimental details

The experimental procedure was the same as applied in our previous work concerning determination of the Landé g_j factors of terbium [2], where the detailed description was provided, and no modifications were introduced. The measurements were performed with the method of laser induced fluorescence in a hollow cathode discharge lamp as the source of free atoms. To ensure the proper Zeeman splitting, the cathode was placed in an external magnetic field, produced by one of the two different sets of neodymium magnets. The transitions between the investigated levels were excited by single-mode tunable dye lasers, and the laser induced fluorescence was recorded for π and σ polarization, individually. To select the desired polarization, a polarization rotator was applied. The employed method is similar to the one frequently applied by the cooperating group of University of Gdansk and Graz University of Technology [9–14].

The magnetic field, actually observed during the measurements, differs from the values estimated for each set of magnets outside the discharge lamp. This screening effect was attributed to the series of magnetic phase transitions in terbium, resulting from the temperature gradient, caused by the non-uniform heating and cooling of the terbium cathode. To determine the actual value of the magnetic field inside the hollow cathode, supplementary spectral lines of argon and terbium were recorded, where the g_j factors of the energy levels, involved in the transitions, are known with high precision.

Two modified frequency-stabilized Coherent CR 699-21 continuous wave ring dye lasers were used to optically excite the investigated transitions, one covering the blue-green region of the spectrum (approx. 490–525 nm) and the another one - the yellow-orange region (approx. 570–610 nm). The wavelength of the exciting beam was precisely controlled by the Burleigh WA-1500 wavemeter, and a mode analyzer was used to verify the single mode operation.

The detection system consisted of an SPM-2 grating monochromator, used for the spectral selection of the fluorescence channels, and a Hamamatsu R-375 photomultiplier with preamplifier, where the photocurrent signal was generated. To ensure the highest possible signal-to-noise ratio, the laser beam was modulated by a mechanical chopper, and a phase-sensitive amplifier was exploited.

The frequency scale, based on the signal from a temperature-stabilized Fabry-Perot interferometer (FSR = 1500 MHz), was obtained by using the "Fitter" program, which has been exploited in our calculations of hfs for many years.

3. Determination of g_j values

At the initial stage of our computational procedures, the energies of Zeeman sublevels, relative to the fine structure energy $E(J)$, for both the upper and the lower level of the studied transition, are determined by means of diagonalization of the Hamiltonian matrix:

$$H_{FM_F, F'M'_F} = \delta_{FF'} \left(A \frac{C}{2} + B \frac{\frac{3}{4}C(C+1) - I(I+1)J(J+1)}{2I(2I-1)J(2J-1)} \right) + \mu_B g_j H_{mag} (-1)^{F-M_F+J+I+F'+1} \sqrt{(2F+1)(2F'+1)J(J+1)(2J+1)} \times \begin{pmatrix} F & 1 & F' \\ -M_F & 0 & M'_F \end{pmatrix} \begin{Bmatrix} F & 1 & F' \\ J & I & J \end{Bmatrix}, \quad (1)$$

where $C = F(F+1) - J(J+1) - I(I+1)$, μ_B is the Bohr magneton and g_j is the Landé factor. The mandatory input data, including the values of the magnetic field H_{mag} , nuclear spin I and electronic shell angular momentum J quantum numbers, the hyperfine structure A and B constants, as well as the initial values of Landé g_j factors for two energy levels involved, are loaded from an appropriate input file. The obtained eigenvalues and eigenvectors are used for determination of the relative positions of the Zeeman components on the frequency scale, and their intensities, separately for σ and π transitions.

The intensity of an individual radiative transition between two Zeeman sublevels M_F and M'_F is proportional to the related transition probability. The line shape observed experimentally is the envelope of all individual Zeeman components, each with a line profile determined by Doppler- and other broadening mechanisms, as well as by instrumental effects. Therefore, in the next stage, the intensity distribution function is derived as a sum of intensities for each abscissa value of the final pattern, with the use of evaluated splitting constants and line profile parameters. In an iterative procedure, this function is fitted to the experimentally observed line profile stored in the digital form, where the values of Landé g_j factors for the upper and the lower levels are adjustable parameters. In the calculations the Marquardt's algorithm [15] is applied. There is also a possibility to fine-tune the values of hfs constants, which is important in particular when these constants were determined earlier with considerable experimental uncertainties.

In order to take into account the saturation effects, an additional parameter A_s (saturation rate) was introduced in the fitting procedure. The calculated decay rate of each Zeeman component (A_ν) of frequency ν was modified according to the following expression [16]:

$$A_\nu^{sat} = \frac{A_\nu}{1 + A_\nu/A_s} \quad (2)$$

4. Results

Altogether 32 spectral lines were investigated for determination of the Landé g_j factors. The results are presented in Table 1.

The calculations, carried out within the scope of this work, concerned the determination of the g_j factors' values of the odd-parity upper energy levels. In such a case, the knowledge of the applied magnetic field value is required. It is also desirable to know the values of the g_j factors for the even-parity lower energy levels, involved in the investigated transitions, as it notably improves the precision of the obtained results.

The method of estimating the value of the magnetic field was described in more detail in the previous work [2]. It required recording of the transitions between the energy levels with precisely known g_j factors in argon and additionally in terbium. For such transitions, the standard procedure had to be reversed, that is the g_j factors were fixed at the given values and the magnetic

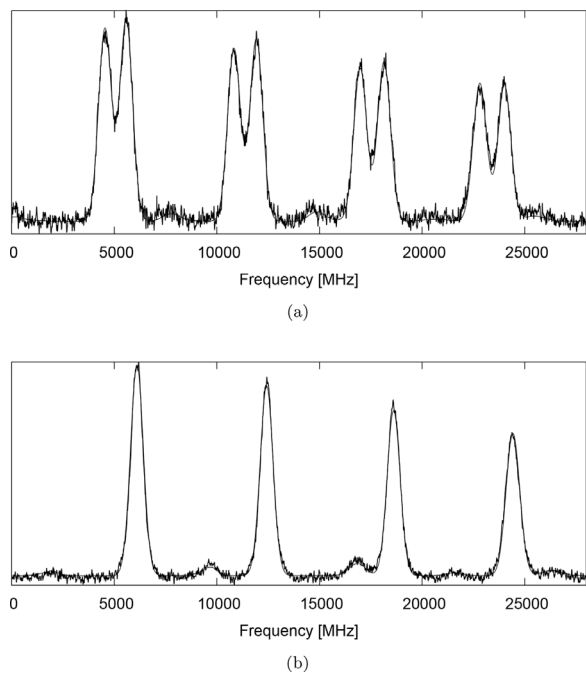


Fig. 1. Recorded Zeeman-*hfs* patterns of the spectral line $\lambda = 514.605$ nm ($k = 19426.97$ cm^{-1} , transition between the levels 15189.26 cm^{-1} , $J = 17/2$ and 34616.23 cm^{-1} , $J = 19/2$) in the terbium atom (Table 1, No 30), along with the least-squares fitted curves for (a) polarization σ , and (b) polarization π at the magnetic field strength 296.7 G.

field value was calculated. For the reasons discussed in Suski et al. [2], only the σ components were taken in the evaluation.

To verify the values of the Landé g_j factors of the even-parity lower energy levels, the mean values of the g_j factors of the upper energy levels, obtained from more than one spectral line, were used. The values of the g_j factors for the upper levels were fixed, and the factors of the lower levels were calculated. The calculations enabled the verification of the Landé factors of 15 even-parity energy levels. The values, obtained in such an approach, are not independent of the used literature values; however, they are provided with a higher precision.

The values of the Landé g_j factors, calculated for the individual lines, are summarized in Table 1. In columns 2 and 3, the wavelengths and wavenumbers, of the investigated transitions are presented. Columns 4–6 provide the data on the even-parity lower levels, that is energies, J quantum numbers and the values of the g_j factors. The values of the Landé factors were taken from the literature, some of them from our previous work [2]. For the levels, where no experimental data was available, semi-empirical predictions were provided. For each value, the literature source is indicated in column 7. Column 8 contains the recalculated g_j factors, obtained for the individual spectral lines, in those cases, where the g_j factors for the respective upper odd-parity levels determined from multiple spectral lines were available, as explained in previous paragraph. The last set of columns contains analogous information, regarding the odd-parity upper levels. The values of the g_j factors, presented in column 11, are the weighted means of the results obtained for the π and σ polarizations. The examples of the spectra with the fitted Zeeman-*hfs* patterns are depicted in Figs. 1–3.

The values of the g_j factors for each of the investigated levels were obtained by averaging the partial values from individual spectral lines involving those levels, wherever possible. The Landé g_j factors for 20 odd-parity levels were calculated, though, for 11 of which from single lines. The results are presented in Table 2.

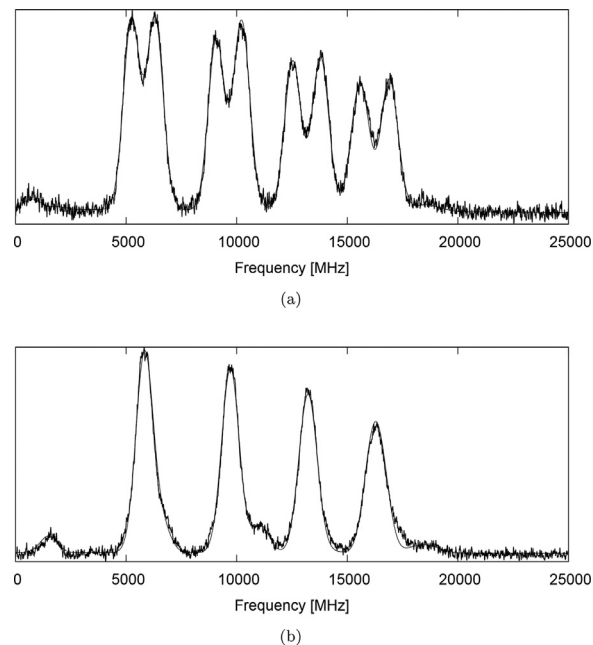


Fig. 2. Recorded Zeeman-*hfs* patterns of the spectral line $\lambda = 506.580$ nm ($k = 19734.70$ cm^{-1} , transition between the levels 11879.20 cm^{-1} , $J = 17/2$ and 31613.90 cm^{-1} , $J = 19/2$) in the terbium atom (Table 1, No 25), along with the least-squares fitted curves for (a) polarization σ , and (b) polarization π at the magnetic field strength 296.7 G.

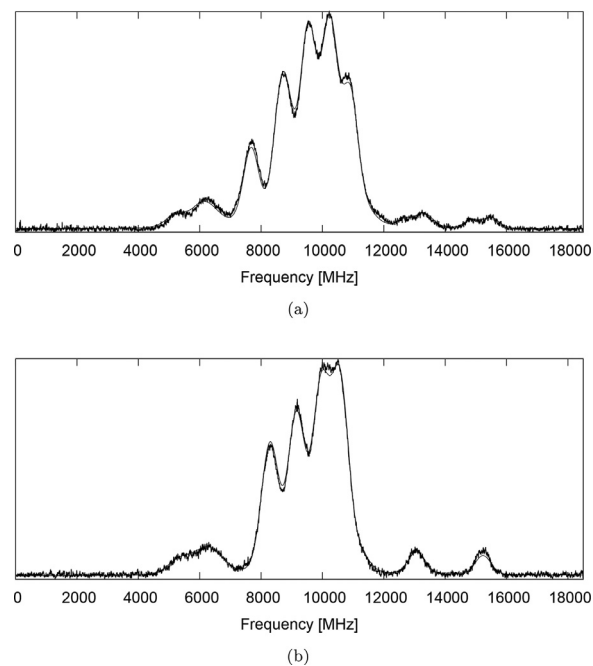


Fig. 3. Recorded Zeeman-*hfs* patterns of the spectral line $\lambda = 578.438$ nm ($k = 17283.16$ cm^{-1} , transition between the levels 9763.02 cm^{-1} , $J = 13/2$ and 27046.18 cm^{-1} , $J = 13/2$) in the terbium atom (Table 1, No 7), along with the least-squares fitted curves for (a) polarization σ , and (b) polarization π at the magnetic field strength 251.9 G.

For any of the investigated levels, no semi-empirically calculated g_j factors are available, since no such description is available due to difficulties mentioned in Section 1. Additionally, for each of the investigated level, the *hfs* constants A and B values are provided, along with the reference sources. Similarly, the recalculated values of the Landé g_j factors for 15 even-parity energy levels, compared with previous literature values, are presented in Table 3.

Table 1

Spectral lines of the terbium atom experimentally investigated in this work for the purpose of determination of the Landé g_j factors. For all lines the g_j factors for the upper odd-parity levels were determined independently.

No 1	Line		Lower level					Upper level		
	λ_{air} (nm) 2	κ_{vac} (cm ⁻¹) 3	E (cm ⁻¹) 4	J 5	$g_{j,lit}$ 6	Ref. 7	$g_{j,recalc}$ 8	E (cm ⁻¹) 9	J 10	$g_{j,av}$ 11
1	595.161	16797.52	5425.06	15/2	1.370(5)	[3]	1.364(21)	22222.58	13/2	1.318(15)
2	592.632	16869.21	5353.37	11/2	1.545(5)	[3]	1.555(20)	22222.58	13/2	1.303(10)
3	574.100	17413.73	5425.06	15/2	1.370(5)	[3]		22838.79	15/2	1.463(16)
4	603.530	16564.59	8646.21	11/2	1.60(2)	[3]	1.590(23)	25210.80	13/2	1.343(23)
5	590.373	16933.76	8277.04	13/2	1.57(2)	[3]	1.579(22)	25210.80	13/2	1.325(23)
6	589.971	16945.30	9763.02	13/2	1.30(2)	[3]		26708.32	15/2	1.437(24)
7	578.438	17283.16	9763.02	13/2	1.30(2)	[3]		27046.18	13/2	1.367(26)
8	579.882	17240.11	11260.41	11/2	1.68(2)	[4]	1.678(15)	28500.52	11/2	1.485(22)
9	571.183	17502.67	10997.85	11/2	1.21(2)	[4]	1.211(20)	28500.52	11/2	1.482(33)
10	566.219	17656.12	11260.41	11/2	1.68(2)	[4]		28916.53	9/2	1.381(45)
11	504.348	17108.36	12283.30	21/2	1.425	[5]	1.423(22)	29391.66	19/2	1.429(16)
12	570.864	17512.46	11879.20	17/2	1.43(2)	[4]	1.440(26)	29391.66	19/2	1.412(26)
13	503.404	19859.21	9867.65	7/2	1.68(2)	[4]		29726.86	9/2	1.678(38)
14	580.186	17231.06	12628.67	15/2	1.447(25)	[2]		29859.73	15/2	1.450(34)
15	578.255	17288.60	13116.48	13/2	1.532(14)	[2]	1.531(17)	30405.08	13/2	1.391(16)
16	572.172	17472.42	12932.66	15/2	1.440(35)	[2]	1.437(14)	30405.08	13/2	1.396(38)
17	566.588	17644.60	12932.66	15/2	1.440(35)	[2]	1.446(28)	30577.26	15/2	1.397(40)
18	565.753	17670.66	12906.60	13/2	1.553(19)	[2]	1.548(23)	30577.26	15/2	1.407(21)
19	578.958	17267.61	13398.40	19/2	1.421	[5]	1.422(31)	30666.01	17/2	1.481(7)
20	517.057	19334.86	11331.14	19/2	1.46(2)	[4]	1.457(13)	30666.01	17/2	1.484(24)
21	515.922	19377.39	11580.68	15/2	1.501(39)	[2]		30958.07	15/2	1.516(51)
22	608.673	16424.64	15189.26	17/2	1.409(5)	[4]	1.391(20)	31613.90	19/2	1.401(12)
23	591.700	16895.79	14718.11	17/2	1.400(5)	[4]	1.386(19)	31613.90	19/2	1.395(9)
24	517.171	19330.60	12283.30	21/2	1.425	[5]	1.436(21)	31613.90	19/2	1.372(13)
25	506.580	19734.70	11879.20	17/2	1.43(2)	[4]	1.454(25)	31613.90	19/2	1.360(29)
26	492.892	20282.76	11331.14	19/2	1.46(2)	[4]	1.458(17)	31613.90	19/2	1.383(32)
27	498.998	20034.58	13116.48	13/2	1.532(14)	[2]		33151.06	11/2	1.336(30)
28	502.145	19909.02	13398.40	19/2	1.421	[5]		33307.42	19/2	1.453(27)
29	493.180	20270.92	13398.40	19/2	1.421	[5]		33669.32	21/2	1.387(12)
30	514.605	19426.97	15189.26	17/2	1.409(5)	[4]		34616.23	19/2	1.385(12)
31	504.638	19810.66	15189.26	17/2	1.409(5)	[4]	1.414(44)	34999.92	19/2	1.424(25)
32	492.915	20281.81	14718.11	17/2	1.400(5)	[4]	1.378(34)	34999.92	19/2	1.453(15)

Table 2

Values of the Landé g_j factors of the odd-parity electronic levels of the terbium atom, determined in this work from the measurements of the Zeeman effect in the hyperfine structure.

No 1	E(cm ⁻¹) 2	J 3	A(MHz) 4	B(MHz) 5	Ref. 6	No of lines 7	$g_{j,mean}$ 8
1	28916.53	9/2	993.3(3.3)	401(32)	[17]	1	1.381(47)
2	29726.86	9/2	441.4(2.2)	210(17)	[17]	1	1.678(44)
3	28500.52	11/2	680.0(2.5)	290.4(9.6)	[17]	2	1.484(10)
4	33151.06	11/2	522.2(2.0)	603(24)	[17]	1	1.336(32)
5	22222.58	13/2	662.6(1.1)	437(12)	[17]	2	1.311(18)
6	25210.80	13/2	572.3(2.7)	448(26)	[17]	2	1.334(20)
7	27046.18	13/2	576.7(1.3)	1084(14)	[17]	1	1.367(26)
8	30405.08	13/2	762.3(1.0)	557(21)	[17]	2	1.394(10)
9	22838.79	15/2	616.6(0.2)	953.6(9.8)	[17]	1	1.463(28)
10	26708.32	15/2	673.3(1.5)	1745(27)	[18]	1	1.437(26)
11	29859.73	15/2	395.3(0.3)	1185.0(3.0)	[17]	1	1.450(34)
12	30577.26	15/2	572.2(0.8)	1266(23)	[18]	2	1.402(17)
13	30958.07	15/2	273.7(0.5)	474.8(8.6)	[17]	1	1.516(62)
14	30666.01	17/2	218.5(3.8)	395.8(6.8)	[17]	2	1.482(10)
15	29391.66	19/2	269.8(0.9)	1128.5(9.5)	[17]	2	1.421(18)
16	31613.90	19/2	331.6(0.7)	1314.0(6.4)	[17]	5	1.382(15)
17	33307.42	19/2	314.2(2.3)	1014(48)	[17]	1	1.453(47)
18	34616.23	19/2	310.9(0.6)	1683(50)	[17]	1	1.385(16)
19	34999.92	19/2	282.1(0.8)	1132(27)	[17]	2	1.438(30)
20	33669.32	21/2	283.6(1.0)	1718(18)	[17]	1	1.387(14)

The experimental uncertainties of the calculated Landé g_j factors of the odd-parity levels consist of mean standard deviation for the g_j factor of the upper level involved in a transition, the uncertainty of the g_j factor of the lower level, and the uncertainty related to the fluctuations of the magnetic field. The mean standard deviation for the average magnetic field value was obtained from the investigation of transitions between levels with known g_j factors, for π and σ components, separately. The total contribution, regarding the fluctuations, was determined to be the differ-

ence between the g_j factors calculated for the underestimated and the overestimated values of the magnetic field, divided by 2. Thus, the total uncertainty for individual levels is calculated as follows:

$$\Delta g_j = \sqrt{(\Delta g_{j,U})^2 + (\Delta g_{j,L})^2 + (\Delta g_{j,B})^2} \quad (3)$$

where $\Delta g_{j,U}$ is the mean standard deviation for g_j factor of the upper energy level, $\Delta g_{j,L}$ is the uncertainty of the g_j factor of the lower energy level, and the last term is the contribution of the magnetic field fluctuation to the total error.

Table 3

Values of the Landé g_j factors of the even-parity electronic levels of the terbium atom, verified in this work, compared to the previous literature values.

No	E(cm ⁻¹)	J	A(MHz) [5]	B(MHz) [5]	No of lines	$g_{j,recalc,mean}$	$g_{j,lit}$	Ref.
1	2	3	4	5	6	7	8	9
1	5353.37	11/2	267.2(1.0)	-448.7(9.8)	1	1.555(20)	1.545(5)	[3]
2	8646.21	11/2	984.255(0.003)	925.956(0.003)	1	1.590(24)	1.60(2)	[3]
3	10997.85	11/2	500.3(2.0)	1262.5(2.5)	1	1.211(20)	1.21(2)	[4]
4	11260.41	11/2	919.9(2.3)	309(13)	1	1.678(15)	1.68(2)	[4]
5	8277.04	13/2	981.2(2.6)	820(24)	1	1.579(22)	1.57(2)	[3]
6	12906.60	13/2	831.0(1.1)	820(17)	1	1.548(24)	1.553(19)	[2]
7	13116.48	13/2	836.6(0.8)	704(15)	1	1.531(17)	1.532(14)	[2]
8	5425.06	15/2	459.627(0.001)	1724.243(0.010)	1	1.364(21)	1.370(5)	[3]
9	12932.66	15/2	294.2(1.8)	406(24)	2	1.441(18)	1.440(35)	[2]
10	11879.20	17/2	757.6(0.4)	1167(24)	2	1.447(16)	1.43(2)	[4]
11	14718.11	17/2	781.5(4.9)	1020(18)	2	1.382(15)	1.400(5)	[4]
12	15189.26	17/2	1025.6(0.7)	682(29)	2	1.403(24)	1.409(5)	[4]
13	11331.14	19/2	876.3(3.8)	1460(20)	2	1.457(7)	1.46(2)	[4]
14	13398.40	19/2	690.6(0.6)	1023(16)	1	1.422(31)	1.421	[5]
15	12283.30	21/2	845.9(0.1)	1906(11)	2	1.430(15)	1.425	[5]

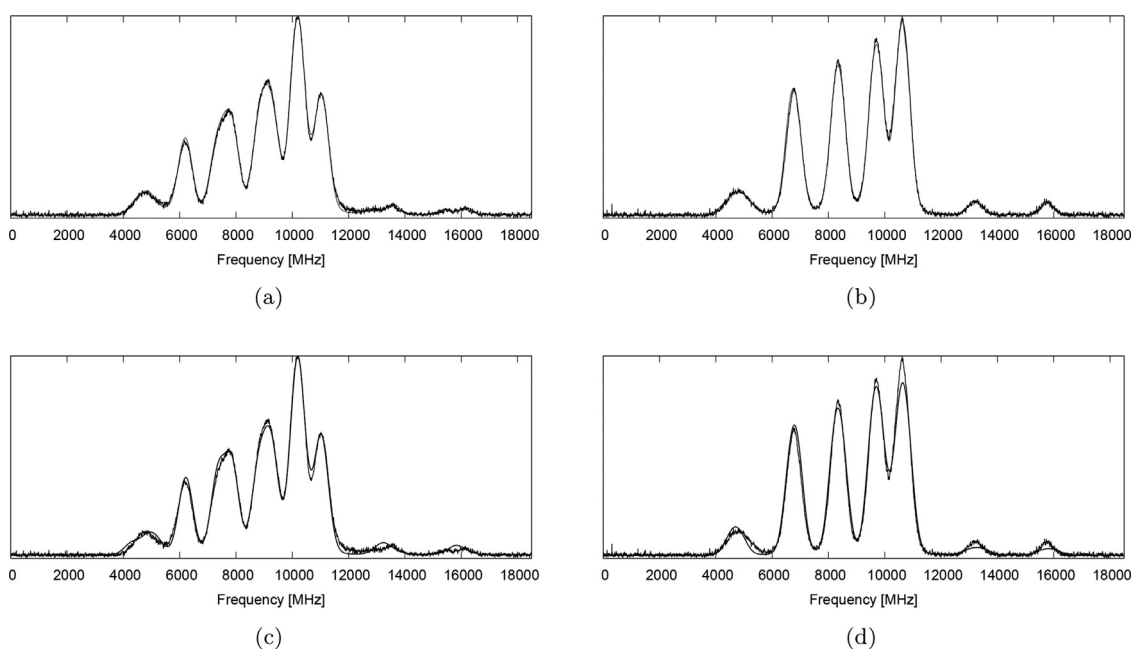


Fig. 4. Recorded Zeeman- hfs patterns of the spectral line $\lambda = 574.100$ nm ($k = 17413.73$ cm⁻¹, transition between the levels 5425.06 cm⁻¹, $J = 15/2$ and 22838.79 cm⁻¹, $J = 15/2$) in the terbium atom (Table 1, No 3), along with the least-squares fitted curves for (a) polarization σ , and (b) polarization π at the magnetic field strength 241.1 G. Pictures (c) and (d) present an attempt to match the value of the g_j factor of 1.295 for the upper energy level for σ and π polarization, respectively. The fit quality is considerably worse than for the correct g_j value of 1.463(16).

5. Discussion

All of the presented Landé g_j factors for the odd-parity levels are determined for the first time, and cannot be compared to any earlier experimental values. Moreover, no semi-empirically calculated values are available for the investigated levels, therefore the consistency of the obtained results cannot be compared.

For 9 levels, where the g_j factors were calculated from more than one line, the values for each line involved (calculated by averaging the results obtained from the π and σ polarizations), are consistent within the uncertainty limits.

For the remaining 11 levels, the average g_j factors' values were calculated from the π and σ components of a single spectral line in each case. Thus, the obtained results may be less accurate.

The recalculated values of the g_j factors for 15 even-parity lower levels are consistent with the previously reported values within uncertainty limits, and no significant deviations were ob-

served. For 9 levels, the g_j factors were obtained from a single spectral line in each case.

For each of the investigated spectral lines, some deviations between the results obtained for π and σ polarizations are observable. This also applies to the average values of the g_j factors of various lines with the same upper level. It is mostly due to the aforementioned screening effect, which decreases the precision of the magnetic field determination, as well as its value itself. This contributes to the reduction of the accuracy of the evaluation of intervals between the split hfs components, as the observed Zeeman effect is weaker. This is particularly true for the π polarization, where the splitting is smaller, compared to σ polarization, resulting in noticeably higher uncertainties.

For the results, where no referential values of g_j factors are available, it is somewhat harder to check whether the obtained value is correct, in particular considering the fact, that the spectrum may be similar for different g_j factor values, within the un-

certainty limits. Therefore, different values of g_j factors can be satisfactorily fitted to the same recorded spectra. For example, for the spectral line 17413.73 cm^{-1} , $\lambda_{\text{air}} = 574.100 \text{ nm}$ (transition between the levels 5425.06 cm^{-1} , $J = 15/2$, $g_j = 1.37$, and 22838.79 cm^{-1} , $J = 15/2$, $g_j = 1.462(31)$), for the upper level, the value 1.295 may be fitted for σ polarization of the experimental spectrum. In such a case, the π component can be used as the determinant. Although the g_j factor value, obtained for π polarization is considered less accurate, as stated in Section 2, the properly fitted spectra for both π and σ polarizations provide an information, that the obtained g_j factor is reliable. The examples of the spectra of the line 17413.73 cm^{-1} , fitted using both of the mentioned g_j factors' values, are presented in Fig. 4. It can be seen, that the fit quality is considerably worse than for the correct g_j value of 1.463(16).

As stated in Section 1, both the Landé g_j factors and the hfs A and B constants are vital for the proper assignment of the electronic levels to the particular configurations. In many cases, it may be done based on only one of those, although, the available information on both is favourable. The g_j factors and the energies of the levels are used to determine the wavefunctions, whereas the hfs constants are calculated on the basis of these wavefunctions. The comparison between the calculated and the experimentally obtained values provides an information, whether the determination is valid. It is significant for the levels, for which the hfs constants' values are very similar with noticeably different values of the g_j factors, and vice versa.

6. Conclusions

Within this work, the experimentally determined values of Landé g_j factors for 20 energy levels, belonging to the odd-parity configurations, are presented. All of the results are obtained for the first time, and neither experimental nor semi-empirically calculated values are available for the comparison. The orders of magnitude of the total uncertainties, dominated by the contribution from the fluctuations of the magnetic field, are similar to those evaluated in our previous work [2], concerning this topic. In any case, the uncertainty does not exceed 5% of the average value of the g_j factor.

Moreover, the Landé g_j factors for 15 even-parity energy levels were verified. The obtained values are consistent with the reference values within uncertainty limits.

The results presented in this work are the extension of the topic, undertaken in the previous work, and may contribute to the extension of the database of the structure of the terbium atom, as well as facilitate its semi-empirical analysis. The comprehensive data, concerning the possible transitions in terbium, may be valuable from the point of view of the further development of the applications, based on both fluorescent and magnetic properties.

Declaration of Competing Interest

The authors declare that they have no known competing financial interests or personal relationships that could have appeared to influence the work reported in this paper.

CRediT authorship contribution statement

M. Suski: Data curation, Investigation, Formal analysis, Writing – original draft, Writing – review & editing. **B. Furmann:** Data curation, Formal analysis, Investigation, Software, Funding acquisition, Writing – review & editing, Supervision. **M. Chomski:** Data curation, Investigation, Formal analysis. **J. Ruczkowski:** Formal analysis, Software, Writing – original draft. **D. Stefańska:** Investigation, Writing – review & editing. **S. Mieloch:** Data curation, Investigation.

Acknowledgements

The authors would like to express their gratitude to Dr. Sci. Magdalena Elantkowska for her valuable remarks concerning the development of the software for g_j factors' calculation, as well as Dr. Andrzej Krzykowski, Dr. Eng. Semir El-Ahmar and M.Sc. Eng. Sebastian Wilman for their professional help in realization of the technical part of the work. Dr. Sławomir Werbowy from the University of Gdańsk is greatly acknowledged for his essential contribution to the transfer of the method of measuring the Zeeman effect of the hyperfine structure to our group.

Financial support of this work by the Ministry of Science and Higher Education, Poland within the projects realized at Poznan University of Technology: 0511/SBAD/2251 at Faculty of Materials Engineering and Technical Physics, (M.S., B.F., M.C., D.S. and S.M.), 0711/SBAD/4560 at Institute of Electric Power Engineering (J.R.) is also acknowledged.

References

- [1] Stone NJ. Table of nuclear magnetic dipole and electric quadrupole moments. At Data Nucl Data Tables 2005;90(1):75–176. doi:10.1016/j.adt.2005.04.001.
- [2] Suski M, Chomski M, Furmann B, Ruczkowski J, Stefańska D. Lande g_j factors of the even-parity electronic levels of the terbium atom. J Quant Spectrosc Radiat Transf 2022;288:108270. doi:10.1016/j.jqsrt.2022.108270.
- [3] Klinkenberg PFA. Structure of the spectrum of neutral terbium, Tb I. Part VI: the sextet system of $4f^8(7F)5d6s^2$. Physica (Utrecht) 1972;57:594–615. doi:10.1016/0031-8914(66)90147-9.
- [4] Martin WC, Zalubas R, Hagan L. Atomic energy levels – the rare-earth elements. Nat. stand. ref. data ser., NSRDS-NBS 60. US: Nat Bur Stand; 1978. <https://nvlpubs.nist.gov/nistpubs/Legacy/NSRDS/nbsnrsds60.pdf>
- [5] Stefańska D, Elantkowska M, Ruczkowski J, Furmann B. Fine- and hyperfine structure investigations of even configuration system of atomic terbium. J Quant Spectrosc Radiat Transf 2017;189:441–56. doi:10.1016/j.jqsrt.2016.10.008.
- [6] Furmann B, Ruczkowski J, Chomski M, Suski M, Wilman S, Stefańska D. Lande g_j factors of the electronic levels of the europium atom. J Quant Spectrosc Radiat Transf 2020;255:107258. doi:10.1016/j.jqsrt.2020.107258.
- [7] Chomski M, Furmann B, Ruczkowski J, Suski M, Stefańska D. Lande g_j factors of the electronic levels of the holmium atom. J Quant Spectrosc Radiat Transf 2021;274:107865. doi:10.1016/j.jqsrt.2021.107865.
- [8] Chomski M, Suski M, Wilman S, Furmann B, Ruczkowski J, Stefańska D. Lande g_j factors of odd-parity electronic levels of the holmium atom. J Quant Spectrosc Radiat Transf 2022;279:108045. doi:10.1016/j.jqsrt.2021.108045.
- [9] Grabowski D, Drozdowski R, Kwela J, Heldt J. Hyperfine structure and Zeeman effect studies in the $6p7p-6p7s$ transitions in Bi II. Z Phys D 1996;38:289–93. doi:10.1007/s004600050093.
- [10] Werbowy S, Güney C, Windholz L. Experimental investigations of the Zeeman effect of new fine structure levels of lanthanum and praseodymium. Spectrochim Acta Part B 2016;116(Supplement C):16–20. doi:10.1016/j.sab.2015.11.003.
- [11] Werbowy S, Güney C, Windholz L. Studies of Landé g_j -factors of singly ionized lanthanum by laser-induced fluorescence spectroscopy. J Quant Spectrosc Radiat Transf 2016;179(Supplement C):33–9. doi:10.1016/j.jqsrt.2016.03.009.
- [12] Sobolewski L, Windholz L, Kwela J. Laser induced fluorescence spectroscopy used for the investigation of Landé g_j - factors of praseodymium energy levels. J Quant Spectrosc Radiat Transf 2017;194(Supplement C):24–30. doi:10.1016/j.jqsrt.2017.03.021.
- [13] Sobolewski L, Windholz L, Kwela J. Determination of Lande g_j - factors of La I levels using laser spectroscopic methods: complementary investigations. J Quant Spectrosc Radiat Transf 2017;201(Supplement C):30–4. doi:10.1016/j.jqsrt.2017.06.030.
- [14] Sobolewski L, Windholz L, Kwela J. Zeeman structure of red lines of lanthanum observed by laser spectroscopy methods. J Quant Spectrosc Radiat Transf 2017;201(Supplement C):180–3. doi:10.1016/j.jqsrt.2017.07.013.
- [15] Marquardt DW. An algorithm for least-squares estimation of nonlinear parameters. J Soc Ind Appl Math 1963;11(2):431–41. <http://www.jstor.org/stable/2098941>
- [16] Sobolewski L, Windholz L, Kwela J. Landé g_j - factors of Nb I levels determined by laser spectroscopy. J Quant Spectrosc Radiat Transf 2020;249:107015. doi:10.1016/j.jqsrt.2020.107015.
- [17] Stefańska D, Furmann B. Hyperfine structure of the odd parity level system in the terbium atom. J Phys B 2017;50(17):175002. doi:10.1088/1361-6455/aa8370.
- [18] Furmann B, Stefańska D, Chomski M, Suski M, Wilman S. Hyperfine structure studies of the odd-parity electronic levels of the terbium atom. J Quant Spectrosc Radiat Transf 2019;237:106613. doi:10.1016/j.jqsrt.2019.106613.



Investigations of the hyperfine structure and isotope shifts in the even-parity level system of atomic europium



B. Furmann*, M. Chomski, M. Suski, S. Wilman, D. Stefańska

Institute of Materials Research and Quantum Engineering, Faculty of Materials Engineering and Technical Physics, Poznan University of Technology, Piotrowo 3, Poznan 60-965, Poland

ARTICLE INFO

Article history:

Received 9 April 2020

Revised 6 May 2020

Accepted 6 May 2020

Available online 21 May 2020

Keywords:

Atomic structure

Laser spectroscopy

Hyperfine structure

Isotope shift

Europium

ABSTRACT

This work presents the measurements of the hyperfine structure constants A and B , as well as the isotope shifts, for 26 electronic levels belonging to the even-parity configurations at the energy range 28000–40000 cm^{-1} in the europium atom. The measurements were performed with the use of laser spectroscopy with a hollow cathode discharge lamp as the source of the atoms and the detection of laser induced fluorescence. Among the results obtained, 10 levels were measured for the first time, in the case of another 3 levels results somewhat more precise than the earlier published ones were obtained. The A and B hyperfine structure constants' values were determined on the basis of the measurements on 73 spectral lines located in two wavelength ranges: 480–560 nm and 625–680 nm.

© 2020 Elsevier Ltd. All rights reserved.

1. Introduction

Europium belongs to the lanthanide series. The presence of 7 4f-electrons situates the europium atom approximately in the middle of this series. Like for other lanthanides, the 4f-electron wavefunction collapse causes that the electronic level structure of europium includes many levels belonging to various configurations with close energy values.

Europium possesses two stable isotopes, ^{151}Eu and ^{153}Eu . The natural abundance of ^{151}Eu amounts to 47.8 %, and this of ^{153}Eu - 52.2 %. Both are odd isotopes and possess equal values of the nuclear spin $I = 5/2$. According to the latest measurements, the magnetic dipole nuclear moment for the isotope ^{151}Eu amounts to 3.4717(6) μ_N , while for the other isotope ^{153}Eu it is 1.5324(3) μ_N . The respective reported values of the electric quadrupole moments exhibit a significant scattering, dependent on the measurement method, while it is consistently assumed, that the ratio $Q(^{153}\text{Eu})/Q(^{151}\text{Eu})$ amounts to 2.5516(12). The physical properties, which can be determined on the basis of precise spectroscopic measurements of the spectral lines of europium, are the hyperfine structure (hfs) constants of magnetic dipole interaction - A , and electric quadrupole interaction - B , for both the lower and the upper levels involved in the transitions studied, as well as the shift between the lines' centers of gravity - the isotope shifts (IS).

In the years 1950–2018 over 100 research works concerned with the spectroscopy of the spectral lines of the europium atom were published. These works can be divided into several topic groups.

The first group covers high-precision measurements of the hyperfine structure on a very limited number of lines (in the extreme case a single line only), with the level-crossing method [1–3], LIF spectroscopy on an atomic beam [4–6], Doppler-free inter-modulation spectroscopy (IMOGS) [7] or laser-microwave double resonance on an atomic beam (ABMRLIRF) [8]. These investigations were aimed mainly at determination of the europium nuclear moments and the hyperfine anomaly.

The second group of works was inspired by the publication of Bauche and Champeau [9], where the authors proposed parametrization of the isotope shifts and investigation of the II order (CSO) effects with the use of the angular coefficients known from the analysis of the fine structure, in particular of those associated with the exchange integral and the spin-orbit interaction integral. A semi-empirical parametrization of the isotope shifts, based on these assumptions, yielded good results for the levels, which are assigned to a single configuration. In the europium atom this assumption is valid to a good approximation for the levels belonging to the configurations $4f^7 5d6s$, $4f^7 6s6p$, $4f^7 5d6p$, $4f^7 6s6d$, relatively low-lying in the energy scale. Indeed, for the levels belonging to the aforementioned configurations, single-configuration CSO parameters obtained were well-determined and consistent with the parameters evaluated for the neighboring elements in the lanthanide series. In the case of the levels, for which a multi-

* Corresponding author.

E-mail address: boguslaw.furmann@put.poznan.pl (B. Furmann).

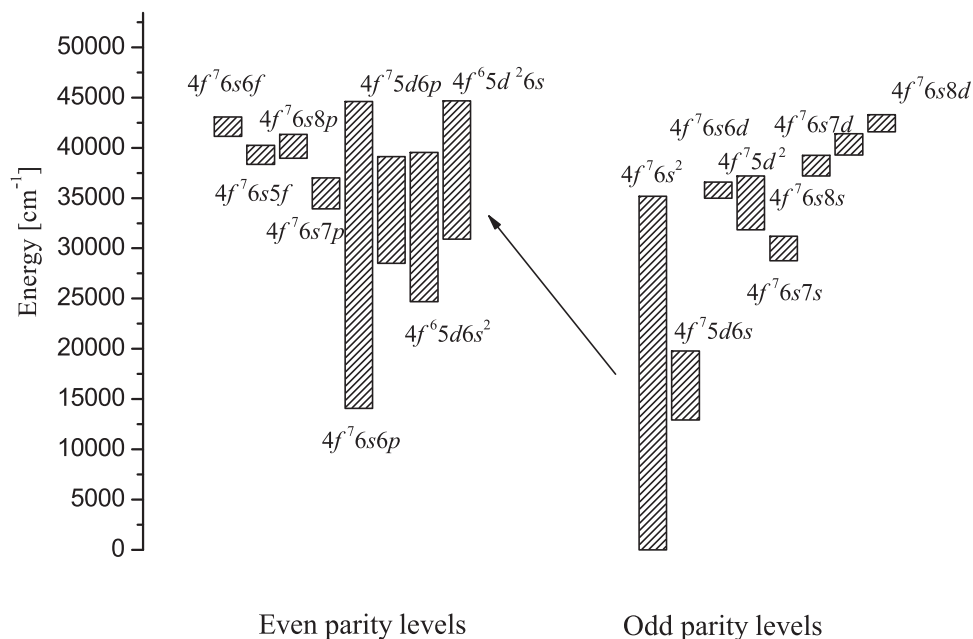


Fig. 1. Layout in the energy scale for the levels belonging to the particular electronic configurations of the europium atom.

configuration description is appropriate, the values of the isotope shifts are influenced to a larger degree by the "abundance" of the particular configurations than by the CSO parameters. In the work [10] we performed an analysis of this influence.

The third group of works concerned with the spectroscopy of the europium atom is related to the investigations of the Rydberg (autoionization) levels [11–13].

Apart from that, also a few works devoted to the particular properties of europium were published. This group involves investigations of the transitions with the change of F quantum number larger than 1 [14–16], as well as the measurements with the use of the unstable europium isotopes [17,18]. The issues of laser cooling and trapping of the europium atoms in magneto-optical traps (MOT) were addressed in the works [19,20].

In many of the works mentioned the hyperfine structure constants were determined in various ways, and with various precision. On this basis Stachowska et al. [21] published the work containing a semi-empirical analysis of the fine- and hyperfine structure of the levels belonging to the odd-parity configurations in atomic europium. The main objective of the present work was an extension of the experimental results database necessary for performing a similar interpretation for the even-parity level system.

The layout of the particular even-parity and odd-parity configurations of the europium atom in the energy scale was depicted in Fig. 1. In the case of the levels belonging to the even-parity configurations, the measurement results of the constants A and B known from the literature include many precise values for the levels assigned to the configuration $4f^7 6s 6p$ [1–4,22–26]. In the works [10,27–29] there are several tens of results for the levels assigned to the configuration $4f^7 5d 6p$, while the works [6,29] contain the results for the levels of the configuration $4f^6 5d 6s^2$. The levels including larger contributions from the remaining configurations appear in the literature much less often, mainly in the works [10,29]. In order to take into account the influence of the configurations $4f^6 5d^2 6s$, $4f^7 6s 7p$, $4f^7 6s 8p$ and $4f^7 6s 5f$ in the semi-empirical calculations, it is necessary - as clearly visible in Fig. 1 - to measure the hyperfine structure of the levels with energy values in the range ca. $30000\text{--}40000\text{ cm}^{-1}$. Moreover, in the course of the investigations reported in the works [10,29] we stated that in the energy range $20000\text{--}30000\text{ cm}^{-1}$ discrepancies between the wave-

functions determined from the semi-empirical interpretation of the hfs constants and the isotope shifts are observed. This inspired us to measure also some levels from this energy range.

2. Experimental details

The method applied in experimental investigations performed in this work was laser induced fluorescence (LIF) in a hollow cathode discharge lamp. The specific feature of the used variant of the method was the spectral resolution of the observed fluorescence. Although this is a Doppler-limited method, with a typical Doppler-broadened linewidth of a few hundreds of MHz, it proved adequate for investigation of the hyperfine structure of europium [10,29]; the achieved degree of precision of the hfs constants A and B was as usually obtained for the elements with single stable isotopes.

As the sources of the exciting radiation tunable single-mode ring dye lasers (modified Coherent CR 699-21) were applied. The spectral lines studied were distributed over two spectral regions:

- ca. 480–560 nm, covered by two dye solutions: Coumarin 498 and binary energy transfer dye mixture (Coumarin 498 + Pyrromethene 556), both optically pumped at $\lambda = 445\text{ nm}$ by a multimode diode laser (Lasever Inc. LSR445SD-4W) - 38 lines,
- ca. 625–680 nm, covered by DCM, optically pumped at $\lambda = 532\text{ nm}$ by a frequency-doubled Nd:YVO₄ laser (Coherent Verdi V-10) - 35 lines.

All the lasers were already used in our earlier works concerning other lanthanide atoms.

Individual decay transitions from the excited upper levels (commonly referred to as the fluorescence channels) were selected by a grating monochromator (SPM-2, Carl Zeiss Jena), in some cases supported by adequate color glass filters. The exciting light was amplitude-modulated by a mechanical chopper and phase-sensitive detection of the resulting LIF signal was applied.

The absolute wavenumbers of the transitions investigated were determined with the use of a wavemeter (Burleigh WA-1500), while the relative frequency scale for the spectra was calculated on the basis of the frequency marker signal (transmission of a stable FP interferometer, FSR = 1500 MHz, wavelength corrected), recorded along with the LIF signal.

As in our earlier works on atomic europium [10,29,30], the hollow cathode with a 4 mm diameter axial bore was used. As a buffer gas argon was applied at a typical pressure of 0.25–0.5 mbar. The applied current values ranged between 10 mA and 50 mA, dependent on the strengths of the excitation and fluorescence transitions; the resultant linewidths, mainly resulting from the Doppler broadening, amounted to 400–650 MHz. It has to be stressed, that because of the overlap of the *hfs* patterns for both stable europium isotopes of comparable abundances we tried to keep the spectral resolution as high as possible.

3. Results

In this work altogether 73 spectral lines in atomic europium were investigated, involving altogether 26 upper even-parity levels (most of them occurring in multiple lines). The spectra were evaluated with the program "Fitter" (developed in the former research group of Prof. Guthöhrlein at the Bundeswehr University of Hamburg), with the option dedicated for multiple isotopes.

The *hfs* constants for both stable isotopes of the europium atom (^{151}Eu and ^{153}Eu), as well as the isotope shifts, were fairly precisely known for all the involved odd-parity lower levels from earlier investigations by other authors [7], with Doppler-reduced intermodulated optogalvanic saturation spectroscopy (IMOGS). Thus the respective *A* and *B* values were fixed in the fitting procedure, and only the constants for the upper even-parity levels were determined. In most cases the constants *A* for both isotopes could be fitted independently, but in three instances it proved necessary to ignore the possible minor contribution from the hyperfine anomaly and apply the relation $A(^{153}\text{Eu}) = 0.44157 A(^{151}\text{Eu})$, resulting from the ratio of the nuclear magnetic dipole moments of both isotopes. On the contrary, for the constants *B* in all cases the constraint $B(^{153}\text{Eu}) = 2.5516 B(^{151}\text{Eu})$, i.e. the ratio of the nuclear electric quadrupole moments, was applied in the fit procedure.

In most cases the spectra were fitted with a Gauss profile, since the Doppler broadening proved to dominate over the natural linewidth. In a few cases a Voigt profile (with a minor Lorentz profile contribution) proved more adequate; however, the differences between the *hfs* constants values obtained in these cases with Gauss and Voigt profiles proved not to exceed the uncertainties limits determined.

In the fitting procedure specific constraints were posed on the relative intensities of the *hfs* components fixed ratios of the intensities of the components within the groups with the same value of ΔF were maintained, while the absolute intensity of the strongest component is fitted independently. This method is aimed to account for the saturation effect, and numerous studies proved that it was sufficient in the case of the hyperfine structure analysis. In the cases of transitions, which were particularly strong and relatively well resolved, the intensities of the components within the main group $\Delta F = \Delta J$ could be fitted independently, thus the (slight) decrease in intensity for the strongest component was directly taken into account.

In Table 1 the results concerning the hyperfine structure and the isotope shifts in the individual spectral lines are collected. The layout of the table is described in what follows. First the information on the transitions studied is provided - the wavenumbers (column 2) and wavelengths (column 3). The data concerning the lower odd-parity levels are limited to their energies (column 4) and *J* quantum numbers (column 5); the literature values of the *hfs* constants *A* and *B* were omitted. Then the data related to the upper even-parity levels, obtained in this work, follow: the energies (column 6), *J* values (column 7), and the *A* and *B* constants for both isotopes (columns 8–11). The last three columns are devoted to the isotope shifts $IS^{151,153}$ observed in the spectral lines: the to-

tal *IS* values, the normal mass shifts (*NMS*), and finally the residual *IS* (columns 12–14, respectively).

All the uncertainties are purely statistical - these are single mean standard deviations directly obtained by averaging the values calculated for the groups of scans of the same line in the cases of the independently fitted constants, or the properly scaled mean standard deviations for the constants related by a fixed ratio.

The literature *hfs* constants for the lower odd-parity levels, fixed in the fitting procedure, could not be incorporated in Table 1; these were compiled separately in Table 2. The layout of the table is as follows: the first two columns include the levels' energies (in increasing order) and their *J* quantum numbers, further the *hfs* constants *A* and *B* for both the isotopes (^{151}Eu and ^{153}Eu) are compiled, and in the last column the residual isotope shifts are listed.

In the initial approach the *hfs* constants for all the lower odd-parity levels, fixed in the fitting procedure, were taken from Seifert's work [7], since they were the most precise, and consistent with the results obtained by other authors. However, one exception was found at the level 19273.24 cm^{-1} , $J = 9/2$. For this level more precise constants *A* and *B* could be found in Klemz's work [31]; moreover, the difference between the values from both sources exceeds the experimental uncertainties limits, in particular the Klemz's constant *A* is higher by more than 3 MHz. Indeed, we found that the *hfs* constants of the upper even-parity levels, determined in the present work from the lines involving the lower level in question, with the Seifert's *hfs* constants values [7], deviated from those obtained from the analysis of other spectral lines. Thus, in the second approach, we decided to adopt the *A* and *B* values for the lower level 19273.24 cm^{-1} from Klemz's work [31] in all the lines where it was involved, and obtained improved *A* and *B* values for the respective upper levels.

In Table 2 both *hfs* constants values sets for the level 19273.24 cm^{-1} , i.e. from [7] and [31], are included; as mentioned, the final results for the upper even-parity levels were obtained with the latter option.

Table 3 constitutes a compilation of the relevant features of the upper even-parity levels of atomic europium, determined in this work. The levels are grouped according to their *J* quantum number values (column 1), and ordered with increasing energies (column 2). Further the final *hfs* constants *A* and *B* for both isotopes determined in the described experiment and known from the literature are listed (columns 3–10). The last two columns (11–12) include the final residual isotope shifts for the levels (the upper-level *RIS* for the individual lines were calculated by addition of the determined line *RIS* from Table 1 to the literature *RIS* values of the respective lower levels from Table 2).

For the majority of the levels, which were investigated in multiple lines, the uncertainties were evaluated as single mean standard deviations reflecting the scattering between the results obtained from the individual lines. For a few remaining levels, which could be observed in single lines only (this concerns mainly the levels with the highest *J* value, 13/2), also an estimate of the possible systematic uncertainties was made, and the final values include both the statistical and systematic contributions.

In Figs. 2, 3, 4, 5, 6 some examples of the recorded spectra are depicted. The selection represents the cases with isotope shifts of various signs and magnitudes.

4. Discussion

In columns 4, 6, 8 and 10 of Table 3 the values of *A* and *B* constants known from the literature were listed for those among the levels investigated within this work, for which any data of this kind were available. In the last column of Table 3 the values of isotope shifts known from the literature were listed. As can be seen, in the case of these levels the differences with respect to the liter-

Table 1

Spectral lines of the europium atom experimentally investigated in this work for the purpose of determination of the *hfs* constants for the upper even-parity levels involved, for both stable isotopes: ^{151}Eu and ^{153}Eu . The respective constants for the lower odd-parity levels were fixed at the literature values [7]. Also the directly observed (and residual) isotope shifts for the spectral lines are listed.

No	Line			Lower level		Upper level				Line $I^{151,153}$			
	k_{vac} 2	λ_{air} 3	E 4	J 5	E 6	J 7	$A(^{151}\text{Eu})$ 8	$B(^{151}\text{Eu})$ 9	$A(^{153}\text{Eu})$ 10	$B(^{153}\text{Eu})$ 11	total 12	NMS 13	RIS 14
1	20686.73	483.267	13222.04	9/2	33908.77	7/2	1298.0(1.0)	69(13)	576.6(1.7)	175(32)	1944.7(8.2)	29.3	1915.4(8.2)
2	20538.29	486.760	13778.68	13/2	34316.97	11/2	913.5(0.4)	130(10)	403.9(0.3)	331(25)	1356.0(0.7)	29.0	1327.0(0.7)
3	19616.15	509.642	19447.19	11/2	39063.29	13/2	602.5(0.8)	-1630(14)	267.5(0.7)	-4146(36) *	325.9(7.7)	27.7	298.2(7.7)
4	19579.21	510.604	19273.24	9/2	38852.45	11/2	977.7(2.3)	-366(13)	434.5(1.4)	-937(52)	4886.0(1.4)	27.7	4858.3(1.4)
5	19405.26	515.181	19447.19	11/2	38852.45	11/2	978.8(0.5)	-346(7)	433.5(0.6)	-881(16)	5292.9(3.3)	27.4	5265.5(3.3)
6	19374.28	516.004	19364.50	7/2	38738.78	5/2	128.7(6.1)	-50(41)	57.1(2.8)	-128(103) *	4161.3(6.1)	27.4	4133.9(6.1)
7	19313.11	517.639	15248.76	5/2	34561.87	7/2	835.0(0.4)	-116(5)	374.6(2.5)	-295(11)	1672.2(0.9)	27.3	1644.9(0.9)
8	19304.56	517.868	15421.25	7/2	34725.81	9/2	-1.4(0.4)	51(5)	-3.1(0.6)	129(13)	857.8(0.7)	27.3	830.5(0.7)
9	19221.19	520.114	19631.26	9/2	38852.45	11/2	978.3(0.4)	-373(3)	433.7(0.2)	-948(7)	5201.2(0.3)	27.2	5174.0(0.3)
10	19140.62	522.304	15421.25	7/2	34561.87	7/2	34561.87	-113(6)	374.8(0.7)	-287(14)	1640.9(0.9)	27.1	1613.8(0.9)
11	19138.59	522.359	19273.24	9/2	38411.83	7/2	356.2(0.4)	-192(16)	157.9(1.2)	-488(42)	1023.8(4.7)	27.1	996.7(4.7)
12	19138.54	522.360	19447.19	11/2	38585.73	13/2	783.3(1.0)	717(16)	377.0(0.8)	1825(41)	2980.0(13.3)	27.1	2952.9(13.3)
13	19086.98	523.771	19447.19	11/2	38534.17	13/2	789.9(0.5)	524(6)	350.0(0.6)	1333(15)	2474.3(5.4)	27.0	2447.3(5.4)
14	19047.33	524.862	19364.50	7/2	38411.83	7/2	354.2(6.2)	-155(46)	147.5(3.2)	-393(116)	915.0(18.8)	26.9	888.1(18.8)
15	19045.53	524.912	15680.28	9/2	34725.81	9/2	0.5(0.2)	21(5)	-2.4(0.3)	54(13)	818.7(0.4)	26.9	791.8(0.4)
16	18975.00	526.863	19763.78	5/2	38738.78	5/2	131.1(1.6)	20(3)	54.4(0.9)	50(8)	4451.8(1.4)	26.8	4425.0(1.4)
17	18949.78	527.564	19462.05	5/2	38411.83	7/2	355.8(9.2)	-227(43)	160.3(4.5)	-578(109)	915.5(26.3)	26.8	888.7(26.3)
18	18944.57	527.709	19794.21	3/2	38738.78	5/2	134.5(1.8)	-39(9)	55.1(0.5)	-99(22)	4505.1(1.3)	26.8	4478.3(1.3)
19	18881.59	529.469	15680.28	9/2	34561.87	7/2	836.8(2.7)	-92(5)	371.5(0.3)	-235(13)	1623.5(1.0)	26.7	1596.8(1.0)
20	18853.02	530.271	15248.76	5/2	34101.78	7/2	-56.7(0.5)	-114(5)	-21.7(2.5)	-290(13)	87.9(1.1)	26.7	61.2(1.1)
21	18844.98	530.498	19447.19	11/2	38292.17	13/2	746.0(0.5)	235(7)	335.0(0.6)	598(16)	5095.7(4.1)	26.7	5069.0(4.1)
22	18699.68	534.620	19712.15	7/2	38411.83	7/2	353.6(1.6)	-165(10)	157.2(1.1)	-420(25)	1325.7(3.0)	26.4	1299.3(3.0)
23	18680.53	535.168	15421.25	7/2	34101.78	7/2	-53.0(0.5)	-89(6)	-21.0(0.6)	-225(13)	87.3(1.1)	26.4	60.9(1.1)
24	18660.01	535.756	15248.76	5/2	33908.77	7/2	1296.2(0.9)	-28(6)	582.7(2.5)	-70(15)	2306.8(3.8)	26.4	2280.4(3.8)
25	18648.83	536.078	15137.72	3/2	33786.55	5/2	-418.8(2.7)	-6(9)	-181.4(0.4)	-15(22)	-895.6(1.6)	26.4	-922.0(1.6)
26	18636.69	536.427	15680.28	9/2	34316.97	11/2	915.7(0.7)	93(7)	405.9(0.5)	235(18)	1883.3(5.0)	26.4	1856.9(5.0)
27	18537.79	539.289	15248.76	5/2	33786.55	5/2	-422.4(0.4)	36(4)	-180.8(2.5)	92(11)	-881.9(0.7)	26.2	-908.1(0.7)
28	18503.89	540.277	13222.04	9/2	31725.93	11/2	-29.1(0.3)	95(4)	-13.0(0.2)	243(8)	-3203.9(0.5)	26.2	-3230.1(0.5)
29	18466.30	541.377	16079.76	11/2	34546.06	9/2	816.9(1.3)	-53(14)	368.3(0.9)	-136(35)	3690.1(3.7)	26.1	3364.0(3.7)
30	18421.50	542.693	15680.28	9/2	34101.78	7/2	-54.6(0.3)	-91(6)	-24.4(0.3)	-231(14)	76.7(2.5)	26.1	50.6(2.5)
31	18365.30	544.354	15421.25	7/2	33786.55	5/2	-419.0(0.5)	28(6)	-189.6(0.6)	72(13)	-896.2(1.9)	26.0	-922.2(1.9)
32	18338.42	545.152	13778.68	13/2	32117.10	13/2	12.2(0.5)	57(10)	4.8(0.4)	145(25)	-3466.2(1.7)	25.9	-3492.1(1.7)
33	18333.71	545.292	13048.90	7/2	31382.61	9/2	-47.1(0.9)	46(9)	-21.5(0.3)	118(22)	-3060.0(0.9)	25.9	-3085.9(0.9)
34	18268.72	547.232	13457.21	11/2	31725.93	11/2	-27.1(0.6)	76(16)	-14.8(0.3)	194(39)	-3253.2(0.6)	25.8	-3279.0(0.6)
35	18214.39	548.864	12923.72	5/2	31138.11	7/2	-9.6(0.7)	37(5)	-2.0(0.3)	94(12)	893.0(0.7)	25.8	867.2(0.7)
36	18192.66	549.520	12923.72	5/2	31116.40	7/2	151.4(0.7)	39(5)	67.2(0.3)	98(12) *	5134.8(0.5)	25.7	5109.1(0.5)
37	18021.35	554.743	12923.72	5/2	30945.07	5/2	-234.5(0.8)	-54(5)	-100.9(0.5)	-138(13)	-2763.0(1.6)	25.5	-2788.5(1.6)
38	17925.40	557.713	13457.21	11/2	31382.61	9/2	-44.1(0.6)	40(16)	-20.6(0.3)	102(39)	-3085.0(1.0)	25.4	-3110.4(1.0)
39	15994.45	625.044	12923.72	5/2	28918.17	7/2	-18.9(0.7)	-28(5)	-7.6(0.3)	-71(12)	1903.0(0.5)	22.6	1880.4(0.5)
40	15961.36	626.340	15421.25	7/2	31382.61	9/2	-49.8(0.4)	53(6)	-21.7(0.6)	134(14)	-2648.3(1.5)	22.6	-2670.9(1.5)
41	15889.35	629.178	15248.76	5/2	31138.11	7/2	-10.5(0.4)	40(4)	-1.8(2.5)	101(10)	1313.0(0.5)	22.6	1290.4(0.5)
42	15869.27	629.975	13048.90	7/2	28918.17	7/2	-17.3(0.9)	-7(9)	-9.1(0.3)	-18(22)	1901.7(0.2)	22.4	1879.3(0.2)
43	15807.35	632.442	15137.72	3/2	30945.07	5/2	-233.7(2.7)	-34(9)	-105.0(0.4)	-86(22)	-2318.7(0.7)	22.4	-2341.1(0.7)
44	15743.67	635.000	12923.72	5/2	28667.39	5/2	-196.1(0.7)	-239(5)	-88.7(0.3)	-609(12)	-3204.6(0.3)	22.3	-3226.9(0.3)
45	15716.86	636.084	15421.25	7/2	31138.11	7/2	-11.0(0.4)	47(6)	-3.5(0.6)	119(13)	-3281.0(0.6)	22.2	-3258.8(0.6)
46	15702.33	636.672	15680.28	9/2	31382.61	9/2	-46.7(0.3)	51(5)	-20.7(0.3)	131(13)	-2650.1(0.9)	22.2	-2672.3(0.9)
47	15696.13	636.924	13222.04	9/2	28918.17	7/2	-18.8(0.3)	-37(4)	-9.1(0.2)	-94(8)	1875.0(0.2)	22.2	1852.8(0.2)
48	15662.99	638.271	15137.72	3/2	30800.71	3/2	-652.4(2.7)	-30(9)	-290.5(0.6)	-76(22)	-3074.1(0.8)	22.2	-3096.3(0.8)
49	15660.34	638.379	15137.72	3/2	30798.06	5/2	-303.2(2.7)	103(9)	-131.7(0.4)	263(22)	-2888.5(0.9)	22.2	-2910.7(0.9)
50	15618.49	640.090	13048.90	7/2	28667.39	5/2	-194.0(0.9)	-252(9)	-84.1(0.3)	-641(22)	-3219.7(0.6)	22.1	-3241.8(0.6)
51	15551.95	642.828	15248.76	5/2	30800.71	3/2	-648.8(0.5)	-33(4)	-288.4(2.5)	-83(10)	-3064.6(0.7)	22.0	-3086.6(0.7)
52	15549.30	642.938	15248.76	5/2	30798.06	5/2	-307.4(0.4)	89(4)	-144.8(2.5)	226(10)	-2931.7(0.6)	22.0	-2953.7(0.6)
53	15523.82	643.993	15421.25	7/2	30945.07	5/2	-237.6(0.4)	-23(5)	-109.6(0.7)	-59(13)	-2345.2(2.5)	22.0	-2367.2(2.5)
54	15457.83	646.743	15680.28	9/2	31138.11	7/2	-9.8(0.2)	34(5)	-4.2(0.3)	86(12)	1245.1(0.4)	21.9	1223.1(0.4)
55	15376.81	650.150	15421.25	7/2	30798.06	5/2	-300.6(0.4)	62(5)	-141.2(0.6)	158(13)	-2867.6(1.0)	21.7	-2889.3(1.0)
56	15361.31	650.806	19364.50	7/2	34725.81	9/2	-1.2(6.1)	-4(41)	-2.2(2.8)	-11(102)	448.1(1.3)	21.7	426.4(1.3)
57	15302.85	653.293	16079.76	11/2	31382.61	9/2	-45.5(1.3)	50(14)	-21.6(0.8)	126(34)	-2713.4(0.8)	21.6	-2735.0(0.8)
58	15288.63	653.900	19273.24	9/2	34561.87	7/2	837.5(0.7)	-103(6)	374.4(0.6)	-263(14)	1240.9(1.2)	21.6	1219.3(1.2)
59	15278.62	654.329	19447.19	11/2	34725.81	9/2	-0.7(0.5)	42(6)	-2.1(0.6)	106(15)	804.0(0.5)	21.6	782.4(0.5)
60	15272.82	654.577	19273.24	9/2	34546.06	9/2	816.3(0.8)	-44(13)	363.3(1.3)	-111(32)	3137.8(0.6)	21.6	3116.2(0.6)
61	15197.37	657.827	19364.50	7/2	34561.87	7/2	837.2(6.1)	-147(41)	373.6(2.8)	-375(102)	1233.0(1.2)	21.5	1211.5(1.2)
62	15138.86	660.369	15680.28	9/2	30819.14	11/2	243.3(0.3)	-135(5)	107.5(0.3)	-344(13)	7866.6(1.4)	21.4	7845.2(1.4)
63	15099.82	662.077	19462.05	5/2	34561.87	7/2	837.8(9.1)	-114(40)	373.2(4.1)	-289(100)	1212.6(0.8)	21.4	1191.2(0.8)
64	15098.87	662.118	19447.19	11/2	34546.06	9/2	812.5(0.5)	-32(6)	370.8(0.6)	-82(15)	3490.1(0.4)	21.4	3468.7(0.4)
65	15092.89	662.381	19273.24	9/2	34366.13	9/2	916.4(1.4)	55(19)	407.6(1.4)	140(47)	2520.5(2.0)	21.3	2499.2(2.0)
66	15001.63	666.410	19364.50	7/2	34366.13	9/2	917.8(6.1)	-33(41)	410.9(2.8)	-83(103)	2491.6(5.7)	21.2	2470.4(5.7)
67	14930.61	669.580	19631.26	9/2	34561.87	7/2	836.6(0.4)	-95(3)	371.9(0.3)	-240(8)	1554.9(2.0)	21.1	1533.8(2.0)
68	14918.94	670.104	19447.19	11/2	34366.13	9/2	916.5(0.5)	38(6)	408.4(0.6)	98(15)	2860.4(0.6)	21.1	2839.3(0.6)
69	14914.80	670.290	19631.26	9/2	34546.06	9/2	811.7(0.4)	-103(4)	364.8(0.4)	-262(9)	3388.9(5.2)	21.1	3367.8(5.2)
70	14849.72	673.227	19712.15	7/2	34561.87	7/2	836.7(1.6)	-97(10)	372.9(0.9)	-246(24)	1525.5(0.8)	21.0	1504.5(0.8)
71	14828.54	674.189	19273.24	9/2	34101.78	7/2	-53.4(2.9)	-55(21)	-22.2(1.4)	-141(53)	-302.0(1.9)	21.0	-281.0(1.9)
72	14739.38	678.267	16079.76										

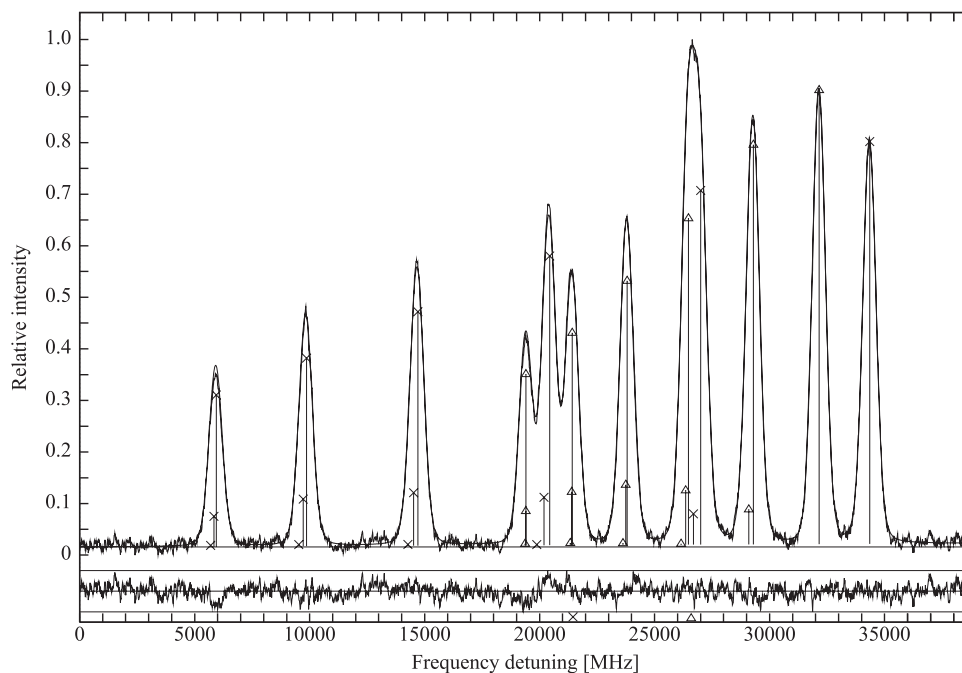


Fig. 2. Recorded *hfs* pattern of the spectral line $\lambda = 520.114$ nm in the europium atom (line 9 in Table 1: 19631.26 cm^{-1} , $J = 9/2 \rightarrow 38852.45 \text{ cm}^{-1}$, $J = 11/2$). The components for both isotopes fitted by program "Fitter" are marked with vertical lines topped by different symbols: crosses for ^{151}Eu and triangles for ^{153}Eu ; the respective symbols marked at the abscissa denote the line centers of gravity for both the isotopes. The lower traces, representing the deviations of the experimental data from the respective theoretical curves, show the quality of the fit, and the horizontal lines at the value of relative intensity close to 0 represent the fitted background.

Table 2

Compilation of the literature values of the hyperfine structure constants *A* and *B* and the residual isotope shifts of the lower odd-parity levels involved in the examined transitions, for both europium isotopes. The values were obtained in Seifert's [7] and Klemz's [31] studies and are quoted after the original works. In the present work, these values were fixed in the fitting procedure aimed at calculation of the respective parameters of the upper even-parity levels. Values from Klemz's work [31] are marked with asterisks; the remaining values were taken from Seifert's work [7]. In the cases where the fixed ratios of the constants for both isotopes were applied in the original works, no uncertainties were quoted for the values concerning the isotope ^{153}Eu .

<i>E</i> (cm^{-1})	<i>J</i>	<i>A</i> (^{151}Eu) (MHz)	<i>B</i> (^{151}Eu) (MHz)	<i>A</i> (^{153}Eu) (MHz)	<i>B</i> (^{153}Eu) (MHz)	<i>RIS</i> (MHz)
15137.72	3/2	-1825.6(2.6)	65.4(8.4)	-810.80(32)	166.84	-4795(30)
19794.21	3/2	654.8(1.7)	22.7(8.4)	291.82(39)	57.91	-4663(18)
12923.72	5/2	1201.93(68)	109.5(4.5)	534.54(25)	279.33	-4375(16)
15248.76	5/2	-959.29(34)	-197.6(3.8)	-424.8(2.4)	-504.08	-4780(27)
19462.05	5/2	323.8(9.0)	-103(39)	142.8	-262.75	-4323(15)
19763.78	5/2	18.0(1.5)	-144.5(2.5)	7.97(78)	-368.62	-4623(32)
13048.90	7/2	906.10(80)	-190.4(8.5)	402.70(20)	-485.71	-4359(19)
15421.25	7/2	-671.34(37)	-157.0(4.9)	-298.03(51)	-400.51	-4764(22)
19364.50	7/2	242.8(6.0)	-42(40)	107.07	-107.14	-4339(10)
19712.15	7/2	-41.4(1.5)	-97.5(9.3)	-18.25(86)	-248.72	-4651(15)
13222.04	9/2	770.22(25)	-185.8(3.0)	342.27(15)	-473.98	-4338(24)
15680.28	9/2	-538.10(19)	28.0(4.7)	-239.69(20)	71.43	-4728(23)
19273.24	9/2	76.8(3.0)	198(24)	33.87	505.10	-4355(20)
19273.24	9/2	80.0(1.0)*	186.9(2.4)*	36.7(2.3)*	505.10*	
19631.26	9/2	40.58(32)	63.5(2.7)	17.98(17)	161.99	-4651(18)
13457.21	11/2	696.99(50)	1.0(15)	308.76(21)	2.55	-4308(24)
16079.76	11/2	-454.2(1.2)	296(13)	-202.43(76)	755.10	-4668(28)
19447.19	11/2	691.17(44)	292.5(5.5)	306.81(54)	746.17	-4713(24)
13778.68	13/2	644.21(35)	286.0(9.6)	286.23(26)	729.59	-4274(24)

ature values usually fall within the experimental uncertainties limits.

As already mentioned, even though europium possesses two stable isotopes exhibiting the hyperfine structure, the *hfs* constants could be determined with the same degree of precision as for the elements with single isotopes. Of course Doppler-limited or Doppler-free methods, e.g. LIF on an atomic beam or saturation spectroscopy in a hollow cathode discharge, could yield more precise results. However, applicability of such methods is much more limited - they require a relatively high population of the lower levels, as well as relatively strong excitation and fluorescence transi-

tions. It is not accidental, that many of the levels reported in the present work were reported for the first time. These levels could not be investigated before by any high-resolution methods, since the spectral lines involving these levels are relatively weak; moreover the thermal population of the lower levels positioned at more than 10000 cm^{-1} is negligible, and remains not very high even with special measures (e.g. an auxiliary discharge in an atomic beam). Nevertheless, for some of the levels investigated obtaining more precise results with high-resolution spectroscopic methods could perhaps be considered, provided other spectral regions become available for excitation.

Table 3
 Compilation of the properties (*hfs* constants *A* and *B* for both stable isotopes: ^{151}Eu and ^{153}Eu , and the residual isotope shifts) of the even-parity levels of the europium atom, investigated in this work and known from the references.

<i>J</i>	Level		<i>hfs</i> constants and $IS^{151,153}$								
	<i>E</i> (cm $^{-1}$)	<i>A</i> (^{151}Eu)	<i>A</i> _{ref} (^{151}Eu)	<i>B</i> (^{151}Eu)	<i>B</i> _{ref} (^{151}Eu)	<i>A</i> (^{153}Eu)	<i>A</i> _{ref} (^{153}Eu)	<i>B</i> (^{153}Eu)	<i>B</i> _{ref} (^{153}Eu)	<i>RIS</i>	<i>RIS</i> _{ref}
1	2	3	4	5	6	7	8	9	10	11	12
3/2	30800.71 ^a	-650.6(1.8)	-654.63(89)[31]	-31(2)	-16.16(30)[31]	-289.4(1.1)	-290.07(15)[31]	-80(4)		-7879(18)	-7898(20)[31]
5/2	28667.39 ^a	-195.1(1.1)	-194.44(42)[31]	-246(7)	-243.3(2.5)[31]	-86.4(2.3)	-86.84(28)[31]	-625(17)		-7601(1)	-7583(24)[31]
	30798.06 ^a	-303.8(2.0)	-304.85(16)[31]	85(13)	80.74(50)[31]	-139.2(4.0)	-136.04(2)[31]	215(31)		-7698(41)	-7714(24)[31]
	30945.07 ^a	-235.3(1.2)	-235.64(28)[31]	-37(10)	-39.6(2.7)[31]	-105.2(2.5)	-103.95(13)[31]	-94(24)		-7144(18)	-7155(24)[31]
	33786.55 ^a	-420.1(1.2)	-419.86(6)[32]	20(13)	22.6(8)[32]	-183.9(2.9)	-186.17(8)[32]	50(33)	52.6(1.2)[32]	-5697(18)	-5660.7(0.6)[32]
	38738.78 ^a	131.4(1.7)	131.4(5.5)[29]	-23(22)	-81(30)[29]	55.5(0.9)		-59(56)		-196(11)	-186(100)[29]
			124.6(3.2)[10]		9(28)[10]						-152(60)[10]
7/2	28918.17 ^a	-18.3(0.6)	-19.24(26)[31]	-24(9)	-41.8[31]	-8.6(0.6)		-61(23)		-2487(8)	-2494(24)[31]
			-14.7(3.4)[10]		-48(9)[10]						-2521(28)[10]
	31116.38 ^b	151.4(3.0)	153.2(1)[6]	38(37)	36(2)[6]	67.2(1.3)	66.23(0.7)[6]	98(94)	107.5(1.1)[6]	734(1)	762(28)[31]
	31138.11 ^a	-10.2(0.4)	-18(9)[33]	-39(3)	-45(45)[33]	-2.9(0.6)		100(7)		-3502(9)	-3519(15)[33]
			-4.4(5.5)[10]		-25(20)[10]						-3462(37)[10]
	33908.77 ^a	1297.1(1.0)	1294.47(10)[32]	21(49)	14.0(9)[32]	579.7(3.1)	575.58(5)[32]	52(123)	55.3(3)[32]	-2461(54)	-2411(0.4)[32]
	34101.78 ^a	-54.5(1.0)		-89(22)		-23.9(1.0)		-227(33)		-4687(10)	
	34561.87 ^a	836.8(0.8)		-110(17)		373.5(1.4)		-277(42)		-3135(9)	
	38411.83 ^a	356.0(2.4)		-154(78)		158.0(1.0)		-390(45)		-3400(50)	
9/2	31382.61 ^a	-46.7(1.0)	-48.14(11)[31]	48(3)	48.2(1.1)[31]	-21.2(0.3)	-21.46(23)[31]	122(6)		-7420(20)	-7417(24)[31]
	34366.13 ^a	917.2(1.0)	916.53(22)[31]	22(33)	50.7(5.4)[31]	407.5(0.4)	407.71(26)[31]	57(72)		-1856(7)	-1869(25)[31]
	34546.06 ^a	815.8(3.8)		-46(12)		362.5(1.9)		-116(30)		-1252(20)	
	34725.81 ^a	-0.7(0.5)		27(13)		-2.5(0.3)		69(32)		-3928(11)	
11/2	30819.14 ^a	243.5(0.2)	242.3(6)[6]	-134(2)	-81(2)[6]	107.1(0.4)	107.18(58)[6]	-341(3)	-326.3(2.0)[6]	3131(20)	3128(25)[31]
			242.3(1.7)[29]		-81(11)[29]						3123(24)[29]
			242.1(0.5)[10]		-82(50)[10]						3092(57)[10]
	31725.93 ^a	-28.1(1.0)	-30.3(6)[29]	86(10)	92(30)[29]	-13.9(0.9)		218(25)		-7578(14)	-7555(24)[29]
			-28.00(57)[31]		104.1(4.1)[31]						-7584(24)[31]
	34316.97 ^a	914.6(1.2)		111(19)		404.9(1.0)		283(48)		-2909(54)	
	38852.45 ^a	978.0(0.3)		-366(13)		434.4(0.1)		-937(52)		521(18)	
13/2	32117.10 ^b	12.2(1.7)	13.04(11)[31]	57(38)	81.7(4.6)[31]	4.8(1.5)	5.56(17)[31]	145(96)		-7766(24)	-7738(24)[31]
			12.3(2.5)[29]		72(20)[29]						-7760(24)[29]
	38292.17 ^b	746.0(1.5)	747.7(3.5)[29]	235(44)	251(25)[29]	335.0(1.7)		598(110)		356(15)	302(24)[29]
	38534.17 ^b	789.9(2.0)		524(57)		350.0(2.1)		1333(145)		-2266(6)	
	38585.73 ^b	783.3(2.5)		718(67)		377.0(2.2)		1825(171)		-1760(14)	
	39063.29 ^b	602.5(1.6)		-1630(41)		267.5(1.0)		-4146(102)		-4415(8)	

^a *hfs* constants *A* and *B*, as well as the residual isotope shifts, determined as the averages from all lines involving this level investigated in the present study ^b *hfs* constants *A* and *B*, as well as the residual isotope shifts, determined from single lines

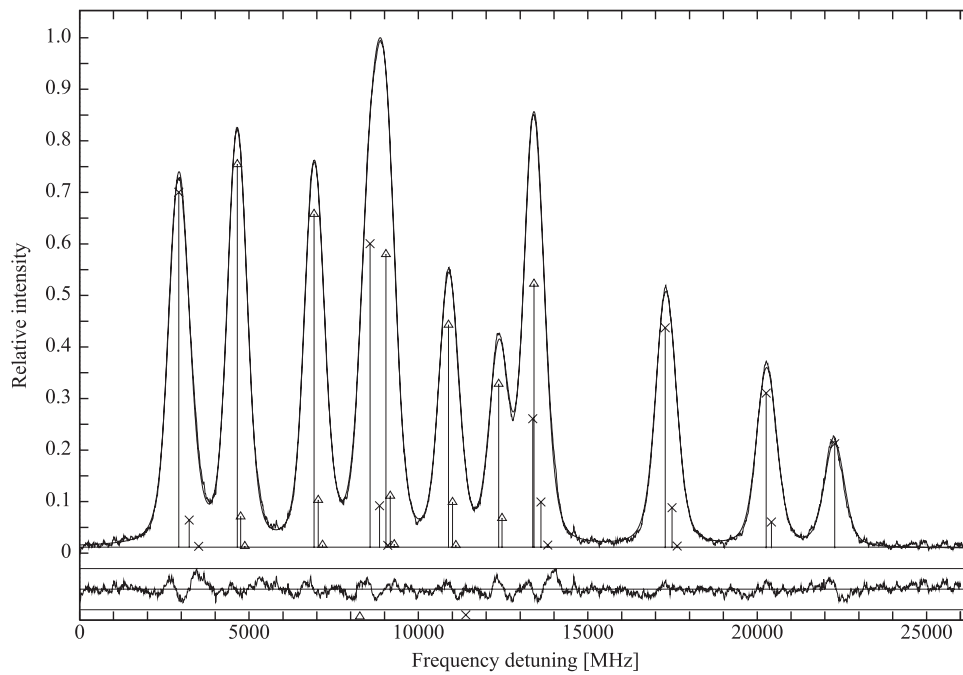


Fig. 3. Recorded *hfs* pattern of the spectral line $\lambda = 545.292$ nm in the europium atom (line 33 in Table 1: 13048.90 cm^{-1} , $J = 7/2 \rightarrow 31382.61$ cm^{-1} , $J = 9/2$). The components for both isotopes fitted by program "Fitter" are marked with vertical lines topped by different symbols: crosses for ^{151}Eu and triangles for ^{153}Eu ; the respective symbols marked at the abscissa denote the line centers of gravity for both the isotopes. The lower traces, representing the deviations of the experimental data from the respective theoretical curves, show the quality of the fit, and the horizontal lines at the value of relative intensity close to 0 represent the fitted background.

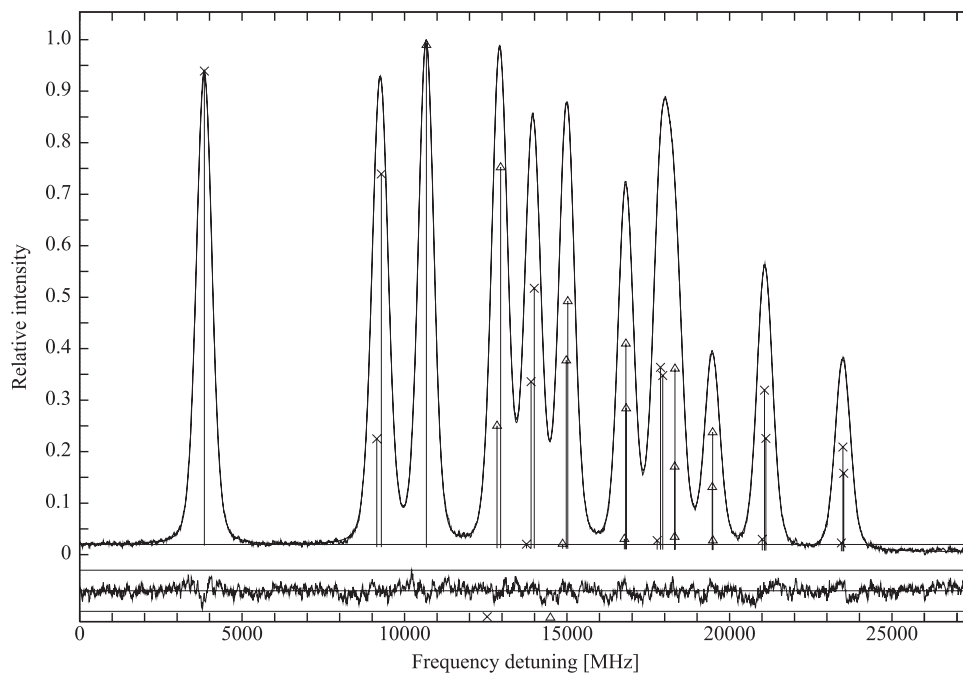


Fig. 4. Recorded *hfs* pattern of the spectral line $\lambda = 636.924$ nm in the europium atom (line 47 in Table 1: 13222.04 cm^{-1} , $J = 9/2 \rightarrow 28918.17$ cm^{-1} , $J = 7/2$). The components for both isotopes fitted by program "Fitter" are marked with vertical lines topped by different symbols: crosses for ^{151}Eu and triangles for ^{153}Eu ; the respective symbols marked at the abscissa denote the line centers of gravity for both the isotopes. The lower traces, representing the deviations of the experimental data from the respective theoretical curves, show the quality of the fit, and the horizontal lines at the value of relative intensity close to 0 represent the fitted background.

Perhaps some comment on the mutual relations of the *hfs* constants for both isotopes would be desired. The constants A were fitted independently in all the cases where it was possible. The exceptions concerned only the cases where the *hfs* for the lower levels were previously unknown and had to be determined from our current investigations. The analysis of the final results indicates that the ratio $A(^{153}\text{Eu})/A(^{151}\text{Eu})$ is in most cases very close

to the ratio of the respective nuclear magnetic dipole moments; for three levels (31138.11 cm^{-1} , $J = 7/2$, 31725.93 cm^{-1} , $J = 11/2$ and 32117.10 cm^{-1} , $J = 13/2$), for which the A values are of the order of some tens of MHz, the difference between both ratios slightly exceeds 10 %. Only for one level - 34725.81 cm^{-1} , $J = 9/2$, for which both A constants are very close to 0, their ratio differs substantially from the ratio of the magnetic dipole moments. For neither

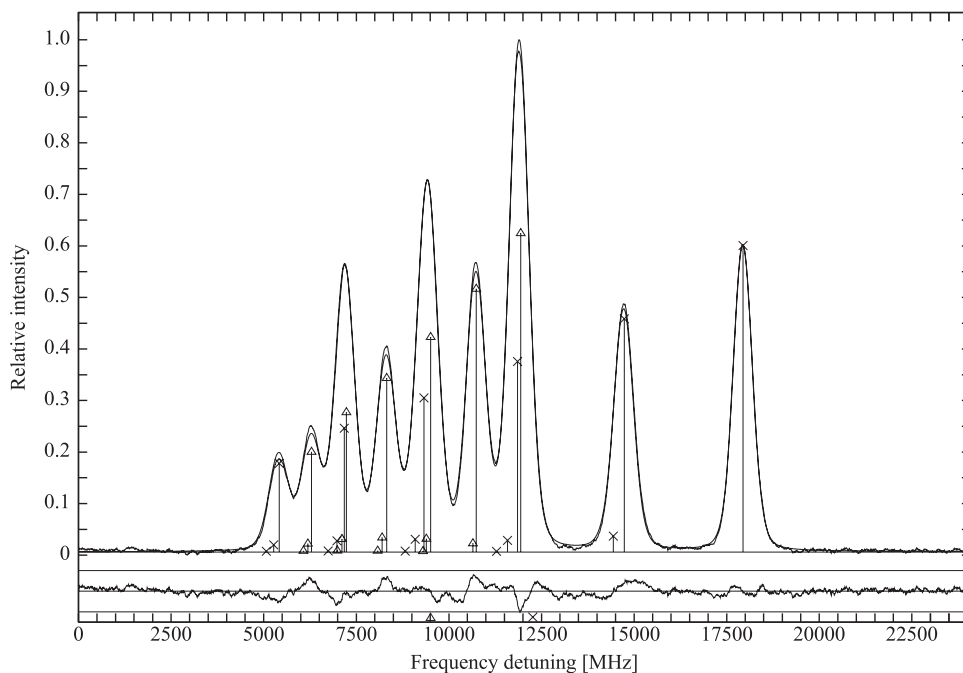


Fig. 5. Recorded *hfs* pattern of the spectral line $\lambda = 653.293$ nm in the europium atom (line 57 in Table 1: 16079.76 cm^{-1} , $J = 11/2 \rightarrow 31382.61$ cm^{-1} , $J = 9/2$). The components for both isotopes fitted by program "Fitter" are marked with vertical lines topped by different symbols: crosses for ^{151}Eu and triangles for ^{153}Eu ; the respective symbols marked at the abscissa denote the line centers of gravity for both the isotopes. The lower traces, representing the deviations of the experimental data from the respective theoretical curves, show the quality of the fit, and the horizontal lines at the value of relative intensity close to 0 represent the fitted background.

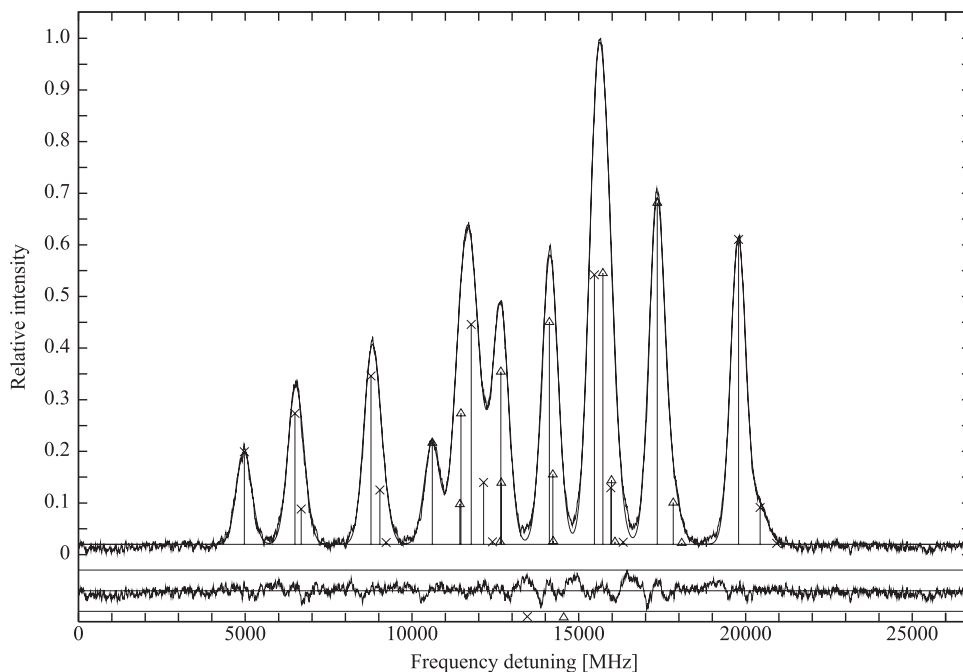


Fig. 6. Recorded *hfs* pattern of the spectral line $\lambda = 653.900$ nm in the europium atom (line 58 in Table 1: 19273.24 cm^{-1} , $J = 9/2 \rightarrow 34561.87$ cm^{-1} , $J = 7/2$). The components for both isotopes fitted by program "Fitter" are marked with vertical lines topped by different symbols: crosses for ^{151}Eu and triangles for ^{153}Eu ; the respective symbols marked at the abscissa denote the line centers of gravity for both the isotopes. The lower traces, representing the deviations of the experimental data from the respective theoretical curves, show the quality of the fit, and the horizontal lines at the value of relative intensity close to 0 represent the fitted background.

of the exceptional cases, where we fixed the ratio between the A constants, their absolute values for $A(^{153}\text{Eu})$ were smaller than 50 MHz; thus we did not expect any substantial deviation from the ratio assumed.

On the other hand, for the constants B , even if the relation between the values for both isotopes, resulting from the ratio of the respective nuclear electric quadrupole moments, is only approxi-

mate, it is not possible to detect any significant differences at the level of precision involved. It has to be emphasized that even in earlier the studies performed by other authors with the use of an atomic beam or saturation spectroscopy the constants B for both europium isotopes were fitted independently only very rarely.

Because of the interference effects occurring for the *hfs* constants for the electronic levels characterized with strong configu-

ration mixing, it is difficult to conclude on the particular configurations related to the levels investigated on the basis of the values of A and B constants obtained from the experiment.

More can be deduced on the basis of the isotope shifts, which constitute the sums of the shifts for the particular configurations, if the second order effects are neglected. As it results from the work [29], the isotope shifts for the pure levels of the configuration $4f^75d6p$ should approximately amount to -7800 MHz, for the pure levels of configuration $4f^65d6s^2$: 6400 MHz, for the levels of configuration $4f^65d^26s$: 700 MHz, and for the levels of configuration $4f^76s7p$: -2500 MHz. On this basis it can be stated, that seven among the measured levels, i.e. the levels $30800.71\text{ cm}^{-1} J = 3/2$, 28667.39 cm^{-1} , 30798.06 cm^{-1} , $30945.07\text{ cm}^{-1} J = 5/2$, $31382.61\text{ cm}^{-1} J = 9/2$, $31725.93\text{ cm}^{-1} J = 11/2$ and $32117.10\text{ cm}^{-1} J = 13/2$ belong to the configuration $4f^75d6p$. Indeed, the contributions from various configurations, presented in [29] predict in these cases more than 90% contribution of the configuration $4f^75d6p$. Another three levels: $31116.38\text{ cm}^{-1} J = 7/2$, $38852.00\text{ cm}^{-1} J = 11/2$ and $38292.17\text{ cm}^{-1} J = 13/2$ can be the levels belonging to the configuration $4f^65d^26s$, although the small isotope shifts values can also result from the mixing of the configurations with positive and negative shifts. On the other hand, the large contribution of the configuration $4f^65d6s^2$ for the levels $28918.17\text{ cm}^{-1} J = 7/2$, $31116.38\text{ cm}^{-1} J = 7/2$ and $30819.14\text{ cm}^{-1} J = 11/2$, predicted in [29], was not confirmed. These levels have the RIS values smaller than 6400 MHz. A large number among the measured isotope shifts is of the order of -2500 MHz. It may indicate, that the respective levels belong to the configuration $4f^76s7p$ or $4f^76s5f$, but it can also be related to the mixing of a larger number of configurations.

5. Conclusions

In the present work we presented the results of the measurements of the hyperfine structure constants and the isotope shifts for 26 electronic levels belonging to the even-parity configurations in the europium atom. These data should considerably extend the experimental results database, and thus facilitate a semi-empirical interpretation of the fine and hyperfine structure. Because of the location of the measured levels in the energy scale, in the region where strong configuration mixing is present, interpretation of the results may be difficult, but this is the only way of determination of the one-configuration parameters for the higher-lying configurations.

Including the results of the present work, the total number of the even-parity levels of the atomic europium, for which the experimental results concerning the A and B constants and the isotope shifts are available, exceeds 110. Since these results are distributed over several tens of publications, we summarized in Table 4 the values known from the experiment of the levels' energies, Landé g_J factors, hfs constants A and B for the isotope ^{151}Eu , and the isotope shifts. We decided not to quote the A and B values for the isotope ^{153}Eu , since in the cases of determination of the hfs constants from weak spectral lines it was not always possible to determine these values independently. The hfs constants for this other isotope were evaluated in such a situation on the basis of the relations resulting from the nuclear moments ratios. In the case of this work this concerns all the determined constants B . In the situation, where for a given electronic level in the literature more than one value of the hyperfine structure constants and the isotope shift could be found, we selected for Table 4 those values for which the authors provided the smallest measurement uncertainty for the constant A .

We hope that Table 4 will prove helpful in semiempirical calculations of the fine and hyperfine structure, also in other ap-

Table 4

Compilation of the relevant parameters for the levels belonging to the even-parity configurations of the atomic europium: the values of energies, Landé g_J factors and the literature values of the hfs constants A and B for the isotope ^{151}Eu , and the isotope shifts between the isotopes ^{151}Eu and ^{153}Eu . The results obtained in this work were marked with [*].

E (cm ⁻¹)	g_J	A^{151} (MHz)	B^{151} (MHz)	RIS (MHz)
J= 1/2				
31735.760		-1274.3(2.8)[27]		-7754(30)[27]
J= 3/2				
17945.490		-2293.8(3.0)[22]	71(6)[22]	-3722.1(9.2)[22]
28519.970		-735.91(18)[31]	117.90(86)[31]	-7489(16)[31]
30800.710	2.800	-654.63(89)[31]	-16.16(30)[31]	-7898(20)[31]
31787.710		-194.96(30)[27]	-236.0(1.4)[27]	-7782(20)[27]
35799.090		-1328(7)[29]	52(5)[29]	-362(42)[29]
35941.510		928.3(4.0)[29]	41(10)[29]	311(12)[29]
36334.520		701.9(1.5)[10]	136(11)[10]	-1104(70)[10]
36501.650		456.4(1.0)[31]	-24.7(3.6)[31]	-4944(30)[31]
36586.350	2.430	120.85(88)[7]	9.7(2.5)[7]	-6747(24)[7]
J= 5/2				
15890.530	2.227	-606.8(4)[4]	65(4)[4]	-3604(2)[4]
17707.420	1.932	-590.7(5)[4]	-354(4)[4]	-3683(2)[4]
21444.580	2.272	-157.2(3)[4]	78(3)[4]	-2834(2)[4]
27852.900	2.009	-196.2(1)[6]	244(4)[6]	5892(22)[6]
28667.390	2.194	-194.44(42)[31]	-243.3(2.5)[31]	-7583(22)[31]
29982.500	2.060	-146.5(1)[6]	-17(1)[6]	5182(24)[6]
30798.060	2.140	-304.85(16)[31]	80.74(50)[31]	-7714(24)[31]
30945.070	2.490	-235.64(28)[31]	-39.59(2.7)[31]	-7155(24)[31]
31107.280	1.954	-69.9(1)[6]	231(1)[6]	5155(26)[6]
31876.090	1.720	-44.91(22)[34]	-254.0(3.2)[34]	-7806(10)[31]
33786.550	2.276	-419.86(6)[32]	22.6(8)[32]	-5660.7(0.6)[32]
35703.650	1.890	-1451.4(7.9)[29]	-127(12)[29]	-3059(13)[29]
36052.710	2.202	454.4(3.8)[29]	-176(38)[29]	-134(26)[29]
36284.820	1.420	31.73(49)[31]	-15.4(6.3)[31]	-7341(18)[29]
36411.020	1.624	29.3(1.5)[10]	-7.5(3.5)[10]	535(36)[10]
36441.770	2.224	-340.6(2.1)[29]	-34(22)[29]	-357(23)[29]
36584.310	1.971	9.35(21)[7]	22(1)[7]	-6097(24)[7]
36736.260	1.103	303.6(3.6)[29]	141(39)[29]	1547(43)[29]
37001.690	1.297	749.0(2.1)[29]	-288(45)[29]	2511(27)[29]
37093.810	1.990	997.0(1.1)[29]	-139(24)[29]	1061(6)[29]
37266.440	2.380	1097.9(1.0)[29]	228(15)[29]	31(32)[29]
38738.780		131.4(1.7)[*]	-23(22)[*]	-196(11)[*]
J= 7/2				
14067.860	2.198	969.15(54)[22]	159.3(3.6)[22]	-3446.5(6.0)[22]
15952.310	1.875	-236.4(2)[4]	-203(3)[4]	-3624(2)[4]
17340.650	1.787	-6.2(1)[3]	132(3)[3]	3640(1)[35]
21605.170	1.929	-219.1(2)[4]	-295(3)[4]	3007(2)[4]
28827.830	1.811	-8.1(1)[6]	165(2)[6]	843(28)[6]
28918.170	1.841	-19.24(26)[31]	-41.8(2.7)[31]	-2494(24)[31]
30783.640	1.551	495.3(5)[6]	-425(1)[6]	5593(27)[6]
30841.990	1.824	-141.20(11)[27]	17.3(1.2)[27]	-7452(24)[27]
31116.380	1.928	153.2(1)[6]	36(2)[6]	762(28)[31]
31138.110	2.006	-10.2(0.4)[*]	39(3)[*]	-3502(9)[*]
32003.240	1.628	-1.45(77)[34]	-191.0(7.2)[34]	-7808(20)[29]
32398.250	2.195	146.15(96)[34]	99(19)[34]	-6422(24)[34]
32681.130	1.729	349.7(2)[6]	27(2)[6]	5527(26)[6]
33245.000	1.483	694.3(7)[29]	306(42)[29]	1060(24)[29]
33908.770	2.180	1294.47(10)[32]	14.0(9)[32]	-2411(0.4)[32]
34101.780		-54.5(1.0)[*]	-89(22)[*]	-4687(10)[*]
34561.870		836.8(0.8)[*]	-110(17)[*]	-3135(9)[*]
35612.470	1.716	-1171.3(0.4)[29]	-131(30)[29]	-3105(120)[29]
36005.730	2.150	656.3(1.5)[10]	150(30)[10]	-531(34)[10]
36081.010	1.426	24.77(81)[31]	108.3(3.0)[31]	-7503(25)[31]
36381.590	1.841	-211.9(2.0)[29]	53(17)[29]	4165(12)[29]
36600.900	1.910	561.9(3)[7]	46(5)[7]	-763(24)[7]
36700.390	1.830	-326.46(45)[31]	-67.3(2.7)[31]	-5798(21)[31]
37301.640	1.311	253.3(7)[29]	48(20)[29]	2288(24)[29]
37812.870	1.820	930.0(3.1)[29]	-241(13)[29]	1157(42)[29]
37851.880	1.650	674.4(8.2)[29]	-293(4)[29]	1356(34)[29]
38411.820	1.598	356.0(2.4)[*]	-154(78)[*]	-3400(50)[*]
38569.480		1091.8(8.0)[29]	18(49)[29]	-1184(27)[29]
38677.340	1.760	676.6(1.5)[29]	59(32)[29]	552(40)[29]
38917.740	1.796	516.9(2.2)[29]	141(42)[29]	-5399(48)[29]
39126.900		804.5(3.2)[29]	24(17)[29]	-4316(90)[29]
39328.300	1.800	384.7(4.5)[10]	-34(15)[10]	124(48)[10]
41335.670	1.775	145(7)[29]	57(5)[29]	-1456(24)[29]
42087.020	1.860	672.3(4.3)[29]	-120(50)[29]	-2782(40)[29]
42147.420	1.642	206.9(3.5)[10]	125(20)[10]	-944(25)[10]

(continued on next page)

Table 4 (continued)

E (cm ⁻¹)	g _J	A ¹⁵¹ (MHz)	B ¹⁵¹ (MHz)	RIS (MHz)
42787.000		541[29]	209[29]	-3228(44)[29]
J= 9/2				
14563.570	1.936	1024.14(24)[23]	-503.7(3.0)[23]	-3466.1(7.5)[22]
16611.790	1.797	664.9(5)[4]	296(7)[4]	-3575(2)[4]
21761.260	1.772	-228.9(2)[4]	226(4)[4]	-3142(2)[4]
29186.320	1.700	48.75(4)[27]	-237.5(0.9)[27]	-7610(24)[27]
29838.590	1.676	140.7(1)[6]	361(1)[6]	5892(22)[6]
30901.840	1.706	-83.76(9)[27]	-15.3(5.7)[27]	-7722(24)[27]
31382.610	1.860	-48.14(11)[31]	48.2(1.1)[31]	-7417(24)[31]
32130.250	1.747	420.9(9)[6]	-153(12)[6]	1356(20)[33]
32184.650	1.615	98.12(37)[34]	-42.1(8.0)[34]	-5731(20)[35]
32596.310	1.930	167.18(24)[31]	-225.0(2.1)[31]	-6008(15)[31]
34366.130	1.803	916.53(22)[31]	50.7(5.4)[31]	-1869(25)[31]
34546.060	1.960	815.8(3.8)[*]	-46(12)[*]	-1252(20)[*]
34725.810	1.719	-0.7(0.5)[*]	27(13)[*]	-3928(11)[*]
35731.620	1.458	107.2(0.3)[29]	289(13)[29]	-5040(7)[29]
36071.710	1.447	232.1(1.4)[29]	294(14)[29]	2980(23)[29]
36504.630	1.793	314.8(29)[7]	40(4)[7]	-3609(24)[7]
36548.940	1.810	242.85(7)[7]	32(4)[7]	-2633(24)[7]
36889.620	1.729	-310.34(69)[7]	-95.2(9.6)[7]	-5690(24)[7]
37126.160	1.795	875.6(1.0)[29]	72(22)[29]	555(17)[29]
37591.310	1.580	290.4(2.5)[29]	-321(30)[29]	-6016(24)[29]
38167.160	1.491	286.4(9)[29]	-237(30)[29]	-2725(24)[29]
38262.980	1.699	930.4(9)[29]	40(10)[29]	685(24)[29]
38360.760	1.804	1064.3(3.2)[10]	-431(60)[10]	-122(32)[10]
39051.760		679.1(2.1)[29]	78(43)[29]	-4236(12)[29]
39192.100	1.700	539.2(9)[29]	235(80)[29]	693(24)[29]
42010.340	1.771	452.2(3.5)[10]	93(25)[10]	-2145(4)[10]
J=11/2				
15581.580		936.0(1.2)[22]	381(12)[22]	-3535(9.1)[22]
29612.690		66.32(49)[31]	-60.2(1.2)[31]	-7716(18)[31]
30819.440		242.3(6)[6]	-81(2)[6]	3128(25)[6]
31014.480		4.50(15)[27]	-25.4(3.2)[27]	-4989(24)[27]
31725.930		-28.00(57)[31]	104.1(4.1)[31]	-7584(24)[31]
32326.730		474.4(5)[6]	-822(13)[6]	4340(24)[6]
32418.380		73.89(25)[27]	40.3(6.1)[27]	-6070(23)[27]
32948.410		180.46(54)[31]	95.6(2.9)[31]	-6601(25)[31]
34316.970		914.6(1.2)[*]	111(19)[*]	-2909(54)[*]
35453.230		113.35(70)[31]	517.9(2.0)[31]	-7762(30)[31]
36867.040	1.662	276.3(2)[7]	16(11)[7]	-5478(24)[7]
37034.830		486.33(27)[31]	220.1(2.4)[31]	-2285(26)[31]
37800.420		425.6(9)[29]	10(20)[29]	-5557(24)[29]
38852.450		978.0(0.3)[*]	-366(13)[*]	521(18)[*]
39040.310		643.5(2.5)[10]	36(20)[10]	-3302(38)[10]
J=13/2				
30211.090		45.97(9)[27]	235.9(4.0)[27]	-7766(24)[27]
32117.100		13.04(11)[31]	81.7(4.6)[31]	-7738(24)[31]
32598.000		346.1(7)[29]	95(20)[29]	5958(24)[29]
32761.740		-2.00(28)[31]	486.3(3.3)[31]	-7583(25)[31]
38292.170		746.0(1.5)[*]	235(44)[*]	356(15)[*]
38534.170		789.9(2.0)[*]	524(57)[*]	-2266(6)[*]
38585.730		783.3(2.5)[*]	718(67)[*]	-1760(14)[*]
39063.290		602.5(1.6)[*]	-1630(41)[*]	-4415(8)[*]
J=15/2				
30923.710		19.88(4)[27]	610.4(2.6)[27]	-7844(24)[27]

plications, as a comprehensive database on the properties of the electronic levels of the even-parity configurations of the europium atom.

Declaration of Competing Interests

The authors declare that they have no known competing financial interests or personal relationships that could have appeared to influence the work reported in this paper.

CRediT authorship contribution statement

B. Furmann: Conceptualization, Investigation, Formal analysis, Writing - original draft, Visualization, Supervision, Funding acquisition. **M. Chomski:** Investigation, Formal analysis. **M. Suski:** Inves-

tigation, Formal analysis. **S. Wilman:** Investigation, Formal analysis. **D. Stefańska:** Investigation, Writing - review & editing.

Acknowledgements

The research was financially supported by the Ministry of Science and Higher Education, Poland within the project realized at Poznan University of Technology at Faculty of Materials Engineering and Technical Physics.

The authors would like to express their gratitude to Prof. Guthöhrlein for making the program "Fitter" accessible.

Many thanks are due to Dr. Magdalena Elantkowska, as well as Dr. Jarosław Ruczkowski (Faculty of Control, Robotics and Information Engineering, Poznan University of Technology), for numerous fruitful discussions.

References

- Champeau RJ, Handrich E, Walther H. The hyperfine structure of the y ⁸p-multiplet of 4f⁷(⁸s)6s6p in eu i. Z Phys 1973;260:361–5. doi:10.1007/BF01397960.
- Lange W. Level crossing investigation of the hyperfine splitting in the z⁶p_{7/2}-level of eu i. Z Phys A 1975;272:223–6. doi:10.1007/BF01438013.
- Pietsch W, Guthöhrlein GH, Jäger H, Windholz L. Hyperfine structure constants of the eu-i level 4f⁷6s6p z⁶p_{7/2}. Z Phys D 1991;21:189–90. doi:10.1007/BF01426370.
- Zaal GJ, Hogervorst W, Eliel ER, van Leeuwen KAH, Blok J. A high resolution study of the transitions 4f⁷6s² → 4f⁷6s6p in the eu i-spectrum. Z Phys A 1979;290:339–44. doi:10.1007/BF01408393.
- Eliel ER, van Leeuwen KAH, Hogervorst W. Hyperfine anomaly in the z ⁶p_{7/2} level of the 4f⁷6s6p configuration of europium i. Phys Rev A 1980;22:1491–9. doi:10.1103/PhysRevA.22.1491.
- Elantkowska M, Bernard A, Dembczyński J, Ruczkowski J. Hyperfine structure constants and isotope shift of the levels of the configuration 4f⁶5d6s² in eu i. Z Phys D 1993;27:103–9. doi:10.1007/BF01426756.
- Seifert P, Weber D-J, Kronfeldt H-D, Winkler R. Parametric analysis of the isotope shift and hyperfine structure in the eu i configuration 4f⁷5d6s. Z Phys D 1989;14:99–106. doi:10.1007/BF01399029.
- Childs WJ. M1, e2 and m3 hyperfine structure and nuclear moment ratios for ^{151,153}eu. Phys Rev A 1991;44:1523–30. doi:10.1103/PhysRevA.44.1523.
- Bauche J, Champeau R-J. Recent progress in the theory of atomic isotope shift. In: Advances in Atomic and Molecular Physics, 12. Academic Press; 1976. p. 39–86. doi:10.1016/S0065-2199(08)60042-1.
- Furmann B, Stefańska D. Experimental verification of isotope shift and hyperfine structure of some even parity levels of neutral eu. Phys Scr 2014;89:095402. doi:10.1088/0031-8949/89/9/095402.
- Nakhate SG, Razvi MAN, Bhale GL, Ahmad SA. New odd-parity high-lying energy levels of the europium atom by resonance ionization spectroscopy. J Phys B: At Mol Opt Phys 1996;29(8):1439–50. doi:10.1088/0953-4075/29/8/009.
- Nakhate SG, Razvi MAN, Connerade JP, Ahmad SA. Investigation of Rydberg states of the europium atom using resonance ionization spectroscopy. J Phys B: At Mol Opt Phys 2000;33(22):5191–202. doi:10.1088/0953-4075/33/22/319.
- Nakhate SG, Razvi MAN, Ahmad SA. New odd-parity energy levels of europium atoms in the 43 200–45 000 cm⁻¹ region by laser photoionization spectroscopy. J Phys B: At Mol Opt Phys 2000;33(2):191–9. doi:10.1088/0953-4075/33/2/305.
- Eliel ER, Hogervorst W. δF = ± 2 transitions in the hyperfine spectrum of the λ = 576.520 nm line in eu i. J Phys B 1981;14:3037–45. doi:10.1088/0022-3700/14/17/011.
- Mei GH, Zhong D, Tan YF, Zhu XW. δF = 2–6 transitions in the hyperfine spectrum of λ = 601.8 nm line of ¹⁵¹eu. Z Phys D 1997;39:115–19. doi:10.1007/s004600050117.
- Jin W-G, Endo T, Wakui T, Uematsu H, Katsuragawa H. Measurements of the hyperfine structure and δf = +2 transitions in eu i by high-resolution diode-laser spectroscopy. J Phys Soc Jpn 2002;71(8):1905–9. doi:10.1143/JPSJ.71.1905.
- Dörschel K, Heddrich W, Hühnermann H, Peau EW, Wagner W, Alkhaov GD, et al. Nuclear moments and isotope shifts of europium isotopes by hyperfine structure investigations with collinear laser – ion beam spectroscopy. Z Phys A 1983;312:269–70. doi:10.1007/BF01412175.
- Gangrsky YP, Karaivanov VD, Markov BN, Zemlyanoi SG, Kokalova TT, Marinova KP, et al. Hyperfine splitting and isotope shift in the optical transition 4f⁷6s²8s_{7/2} → 4f⁷6s6p ⁶p_{5/2} of ^{151,153}eu isotopes and electromagnetic moments of ¹⁵⁵eu. Eur Phys J D 2000;11:341–5. doi:10.1007/s100530070061.
- Kim J, Friedrich B, Katz DP, Patterson D, Weinstein JD, DeCarvalho R, et al. Buffer-gas loading and magnetic trapping of atomic europium. Phys Rev Lett 1997;78:3665–8. doi:10.1103/PhysRevLett.78.3665.
- Inoue R, Miyazawa Y, Kozuma M. Magneto-optical trapping of optically pumped metastable europium. Phys Rev A 2018;97:061607. doi:10.1103/PhysRevA.97.061607.
- Stachowska E, Elantkowska M, Ruczkowski J, Dembczyński J. Reanalysis and semi-empirical predictions of the hyperfine structure of eu i in the odd parity multiconfiguration system. Phys Scr 2002;65:237–47. doi:10.1238/physica.regular.065a00237.

- [22] Kropp J-R, Kronfeldt H-D, Winkler R, Wyart J-F. Parametric analysis of the level-isotope shift in the configuration $4f^7 6s 6p$ in the eu i spectrum. *Physica B+C* 1984;124:105–13. doi:10.1016/0378-4363(84)90038-X.
- [23] Müller W, Steudel A, Walther H. Die hyperfeinstruktur in den $4f^7 6s 6p$ -termen des eu i und die elektrischen kernquadrupolmomente von eu^{151} und eu^{153} . *Z Phys* 1965;183:303–20. doi:10.1007/BF01393264.
- [24] Krüger HD, Lange W. On the magnetic hyperfine splitting in the configuration $4f^7 6s 6p$ of eu i. *Phys Lett A* 1972;42:293–4. doi:10.1016/0375-9601(72)90427-6.
- [25] Acharyulu GVSG, Sankari M, Kumar PVK, Suryanarayana MV. Hyperfine structure and isotope shift measurements of the $4f^7 6s^2(^8S_{7/2})^2 4f^7 6s 6p(^8P_{9/2})$ 601.8154 nm transition in eu i by laser induced atomic beam fluorescence spectroscopy. *J Quant Spectrosc Radiat Transf* 2014;133:251–63. doi:10.1016/j.jqsrt.2013.08.010.
- [26] Kumar P, Saini VK, Purbia GS, Prakash O, Dixit SK, Nakhe SV. Hyperfine structure studies of neutral europium transitions at 601.815 and 580.027 nm by saturation absorption spectroscopy. *Appl Opt* 2017;56:1579–84. doi:10.1364/AO.56.001579.
- [27] Brand H, Pfeufer V, Steudel A. Laser-atomic-beam spectroscopy of $4f^7 5d 6s$ - $4f^7 5d 6p$ transitions in eu i. *Z Phys A* 1981;302:291–8. doi:10.1007/BF01414259.
- [28] Skrok D, Winkler R. Level classification in the configurations $4f^6 5d 6s^2$ and $4f^7 5d 6p$ of $^{151,153}eu$ -i by isotope shift measurements. *Physica B+C* 1977;85:214–18. doi:10.1016/0378-4363(76)90116-9.
- [29] Furmann B, Stefańska D. Isotope shift and hyperfine structure in even configurations of neutral europium. *J Phys B* 2011;44:225005. doi:10.1088/0953-4075/44/22/225005.
- [30] Furmann B, Stefanska D. 6S electron screening in isotope shifts of configurations $4f^7 5d 6s$, $4f^7 6s 6d$ and $4f^7 6s 7d$ in europium. *J Phys B* 2014;47:085001. doi:10.1088/0953-4075/47/8/085001.
- [31] Klemz G.. Thesis. Berlin; 1995.
- [32] Eliel ER, Hogervorst W, van Leeuwen KAH, Post BH. Ultraviolet transitions in europium studied with a frequency-doubled cw ring dye laser. *Opt Commun* 1981;39:41–6. doi:10.1016/0030-4018(81)90451-X.
- [33] Kronfeldt H-D, Kropp J-R, Winkler R. The isotope shift of the $a^{10}d$ -term of the configuration $4f^7 5d 6s$ in eu i. *Physica B+C* 1982;112:138–44. doi:10.1016/0378-4363(82)90139-5.
- [34] Esrom H.. Dissertation. Universitaet Hannover; 1985.
- [35] Brüggemeyer H, Esrom H, Pfeufer V, Steudel A, Bauche J. J and term dependences in the isotope shift of eu i. *Z Phys D* 1986;1:55–64. doi:10.1007/BF01384659.



Landé g_j factors of the electronic levels of the europium atom

B. Furmann^{a,*}, J. Ruczkowski^b, M. Chomski^a, M. Suski^a, S. Wilman^a, D. Stefańska^a

^aInstitute of Materials Research and Quantum Engineering, Faculty of Materials Engineering and Technical Physics, Poznan University of Technology, Piotrowo 3A, Poznan 60-965, Poland

^bInstitute of Robotics and Machine Intelligence, Faculty of Control, Robotics and Electrical Engineering, Poznan University of Technology, Piotrowo 3A, Poznan 60-965, Poland

ARTICLE INFO

Article history:

Received 31 July 2020

Revised 12 August 2020

Accepted 13 August 2020

Available online 15 August 2020

Keywords:

Atomic structure

Laser spectroscopy

Zeeman-hyperfine structure

Landé factors

Europium

ABSTRACT

In the present work measurements of Landé g_j factors for some electronic levels of the europium atom are presented. The measurements were performed with the use of the Zeeman effect of the hyperfine structure, observed with the method of laser spectroscopy in a hollow cathode discharge lamp placed in constant magnetic field, with laser induced fluorescence detection. Investigation of 54 spectral lines of europium in the spectral range 511–662 nm enabled for the first time the determination of g_j factors for 16 levels belonging to the odd-parity configurations of Eu and 4 levels belonging to the even-parity configurations. Moreover, 3 g_j values for levels belonging to the even-parity configurations, previously known from the literature, were corrected.

© 2020 Elsevier Ltd. All rights reserved.

1. Introduction

The element europium possesses two stable isotopes: ^{151}Eu and ^{153}Eu . The natural abundances of these isotopes amount to 47.8% and 52.2%, respectively. The nuclear spin values for both isotopes amount to 5/2, thus the spectral lines of europium atom exhibit hyperfine structure. In our recent work [1] a short outline of the history of research on the hyperfine structure and the isotope shifts in the europium atom was presented, which includes over 50 published articles. On the contrary, there are only a few works concerning investigations of the Zeeman effect and the g_j factors of the europium atom. Practically all the known experimental values of the Landé factors in the europium atom were determined by Smith and Tomkins [2] from the investigations of the Zeeman effect in the absorption spectrum. Since the ground state of the europium atom $4f^7 6s^2 \ ^8S$ possesses the quantum number $J = 7/2$, g_j factors for levels belonging to the even-parity configurations with $J = 5/2$, $7/2$ and $9/2$ could be determined with this method. As a result, g_j values for over 200 levels belonging to the even-parity configurations were evaluated, as well as for the ground level, which has been so far the only level belonging to the odd-parity configuration system with experimentally determined g_j value. The accuracy of the g_j factor for the ground state was improved several times; finally an experimental uncertainty of 0.00007 was reached. All the g_j values known from experiment for the europium atom

are presented in the data collection of Martin et al. [3] and in the web database created by NIST [4].

Somewhat more frequently the effects related to the interaction of the europium atoms with very weak magnetic field were investigated. Among these effects e.g. observation of transitions with the change of the quantum number $\Delta F = 2, 3, 4$ [5] can be named. Such transitions are forbidden by the selections rules without magnetic field. The presence of a field with a magnetic flux as low as ca. 20 G makes it possible to observe such transitions. This results from the fact that the matrix representing the Hamiltonian describing the hyperfine structure is not longer diagonal when the interaction with the external magnetic field is included. Diagonalization modifies the components' intensities in an essential way. Studies of this kind of transitions, apart from [5], were also described in the works [6,7].

In the history of atomic physics Landé factors were routinely applied in interpretation of the physical properties of the electronic levels, obtained as a result of parametrization of the fine structure interactions in an atom, e.g. according to Slater's-Condon theory. Assignment of a level to the specific term and configuration implies a specific g_j value, which can be compared to the value known from the experiment; thus the correctness of the assignment can be tested. A similar test can be performed by comparison of the Landé factors obtained from *ab initio* calculations with the experimental results.

The first results of parametrization for the electronic levels of the europium atom were published by Smith and Wybourne in 1965 [8]. Calculations were performed for the levels belong-

* Corresponding author.

E-mail address: boguslaw.furmann@put.poznan.pl (B. Furmann).

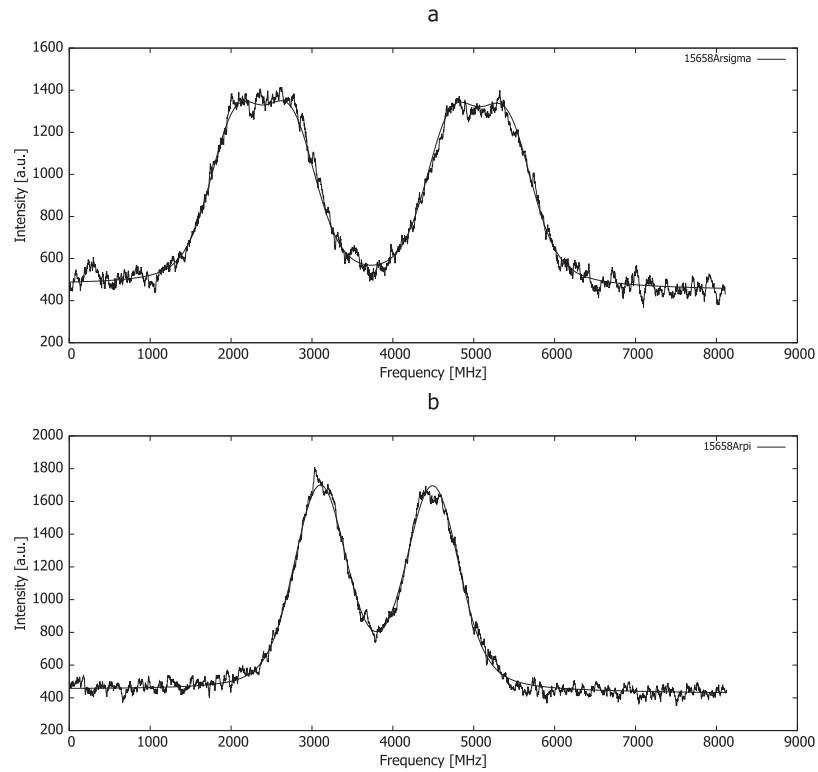


Fig. 1. Recorded Zeeman patterns of the spectral line $\lambda = 638.4717$ nm in the argon atom, along with the least-squares fitted curves for the a) polarization σ at the magnetic field strength 606.1(8)G and b) polarization π at the magnetic field strength 608.7(9)G. The Zeeman splitting of this line was used to measure the magnetic field.

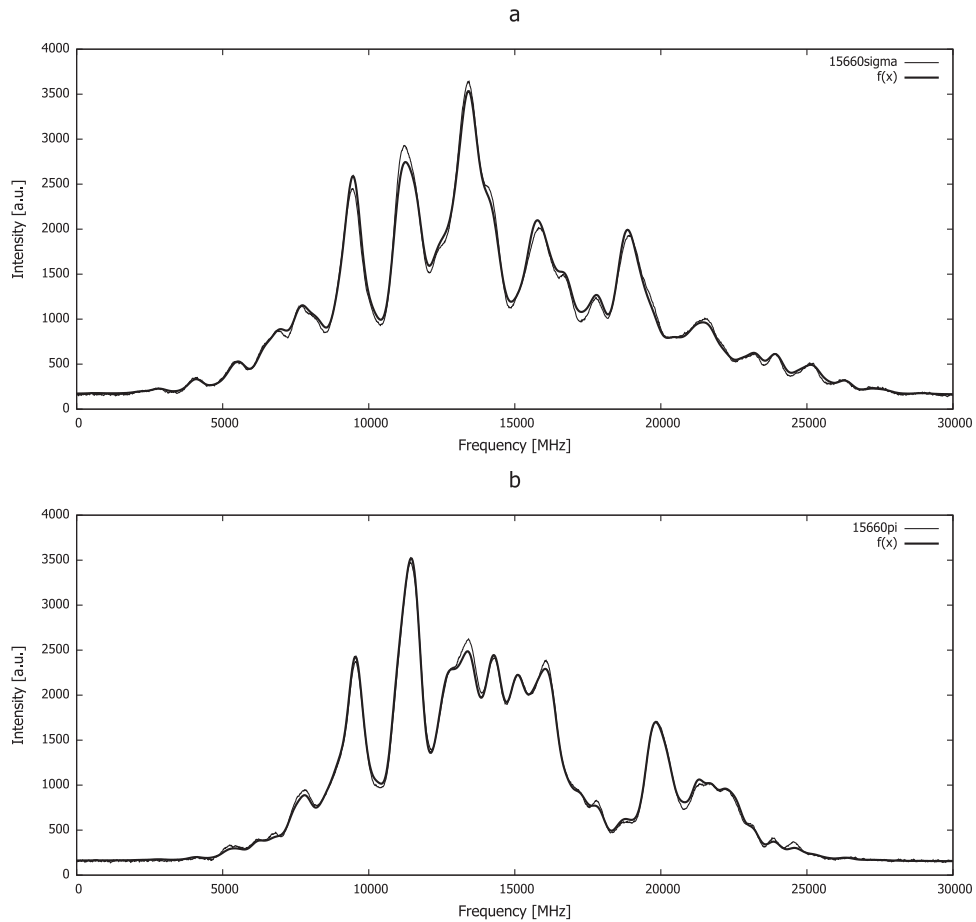


Fig. 2. Recorded *hfs* and Zeeman-*hfs* patterns of the spectral line $\lambda = 638.379$ nm in the europium atom (Table 1, No 43), along with the least-squares fitted curves for the a) polarization σ at the magnetic field strength 608.2(7)G and b) polarization π at the magnetic field strength 609.2(9)G.;

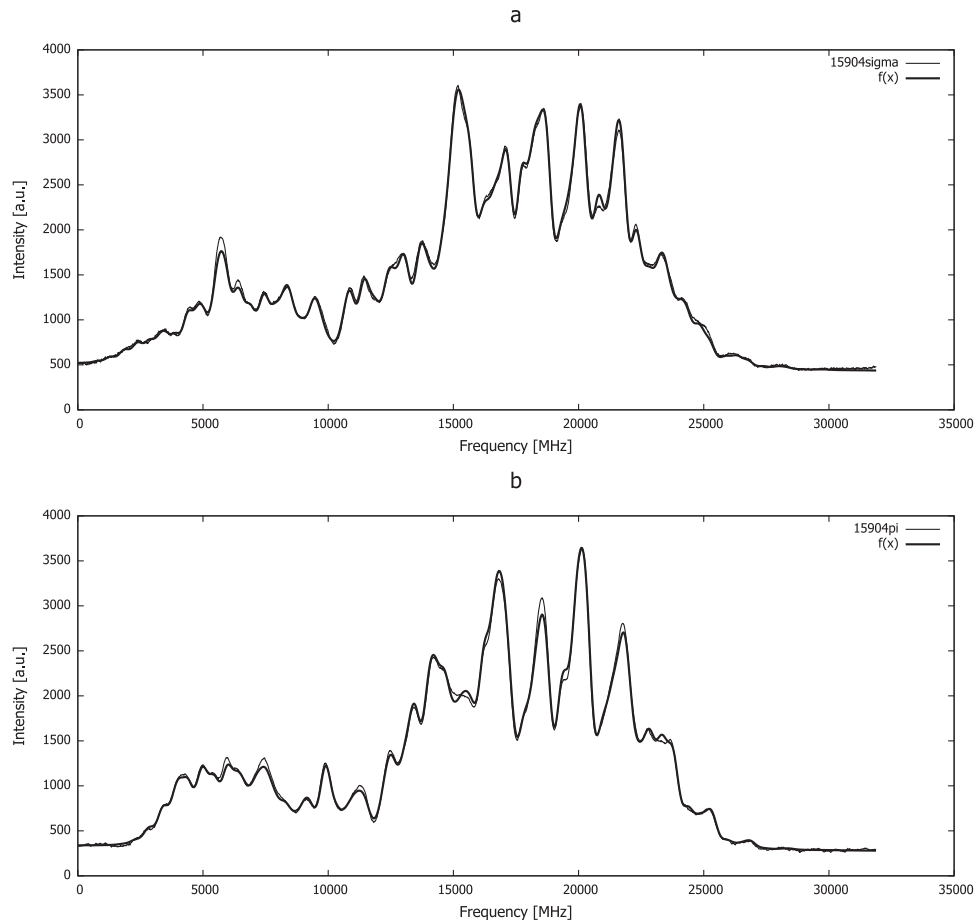


Fig. 3. Recorded *hfs* and Zeeman-*hfs* patterns of the spectral line $\lambda = 628.594$ nm in the europium atom (Table 1, No 36), along with the least-squares fitted curves for the a) polarization σ at the magnetic field strength 605.8(7)G and b) polarization π at the magnetic field strength 607.5(9)G.

ing to 3 even-parity configurations: $4f^7(^8S)6s6p$, $4f^7(^8S)6s5d$ and $4f^7(^8S)5d6p$, as well as 6 odd-parity configurations: $4f^7(^8S)6s7s$, $4f^7(^8S)6s8s$, $4f^7(^8S)6s7p$, $4f^7(^8S)6s5f$, $4f^7(^8S)5d^2$ and $4f^7(^8S)6s6d$. In the calculations the electrostatic and spin-orbit interactions were included, as well as the influence of the interconfiguration interactions. In the cases of relatively low-lying levels the evaluated energy values were in general consistent with the experimental ones. For the higher-lying configurations discrepancies were observed, resulting from the fact that in the calculations no interactions with other levels than those with 8S core, or configurations with 6 *f*-electrons, were included. A somewhat better fit of the energies for the levels belonging to the odd-parity configurations was achieved in the works of Wyart [9] and Stachowska [10], where interactions also with the levels originating from other cores and belonging to a larger number of configurations were taken into account. In the works of Smith and Wybourne [8] and Wyart [9] predicted values of g_j factors are presented.

One of the objectives of the present work was obtaining experimental results, which inclusion may improve the fit quality in the semi-empirical method of interpretation of the fine- and the hyperfine structure of the europium atom. The knowledge of Landé factors for metastable levels should also facilitate interpretation and selection of spectral lines for the experimental investigations of the transitions with change of quantum *F* number greater than 1.

Another objective was to obtain experimental results which might be useful for quantum optics experiments on the europium atom. In 2018 a realization of laser cooling of europium atoms was accomplished [11]. Cooling was achieved with the use of optical

pumping to the metastable levels in a magneto-optical trap. The knowledge of Landé factors of these levels, taking into account the specificity of MOT operation, may facilitate the optimization of the cooling process. One of the perspective applications of the cooled europium atoms is the conversion to molecules. Cooled europium atoms easily form dimers, based on Feshbach resonances. The knowledge of g_j factors may also be advantageous in this context.

2. Experimental details

In the measurements of g_j factors of the electronic levels of the europium atom the method employing the Zeeman effect of the hyperfine structure was used, recently frequently applied by the group from the University of Gdansk in collaboration with the University of Technology Graz [12–16]. This method consists in registration of the hyperfine structure pattern of a spectral line of the atoms in an external magnetic field for two orientations of the polarisation plane of the exciting laser light with respect to the magnetic field direction - perpendicular and parallel. Thus one obtains the scans with only σ or π components present in the Zeeman-hyperfine spectrum.

Recording of the hyperfine structure of the spectral lines of the atoms placed in the magnetic field was performed with the method of laser induced fluorescence with the use of the discharge in the hollow cathode lamp as the source of free atoms.

Because of the wide wavelength range of the spectral lines investigated it was necessary to apply four separate dye lasers as the light sources. In the range 619–662 nm a ring laser constructed on

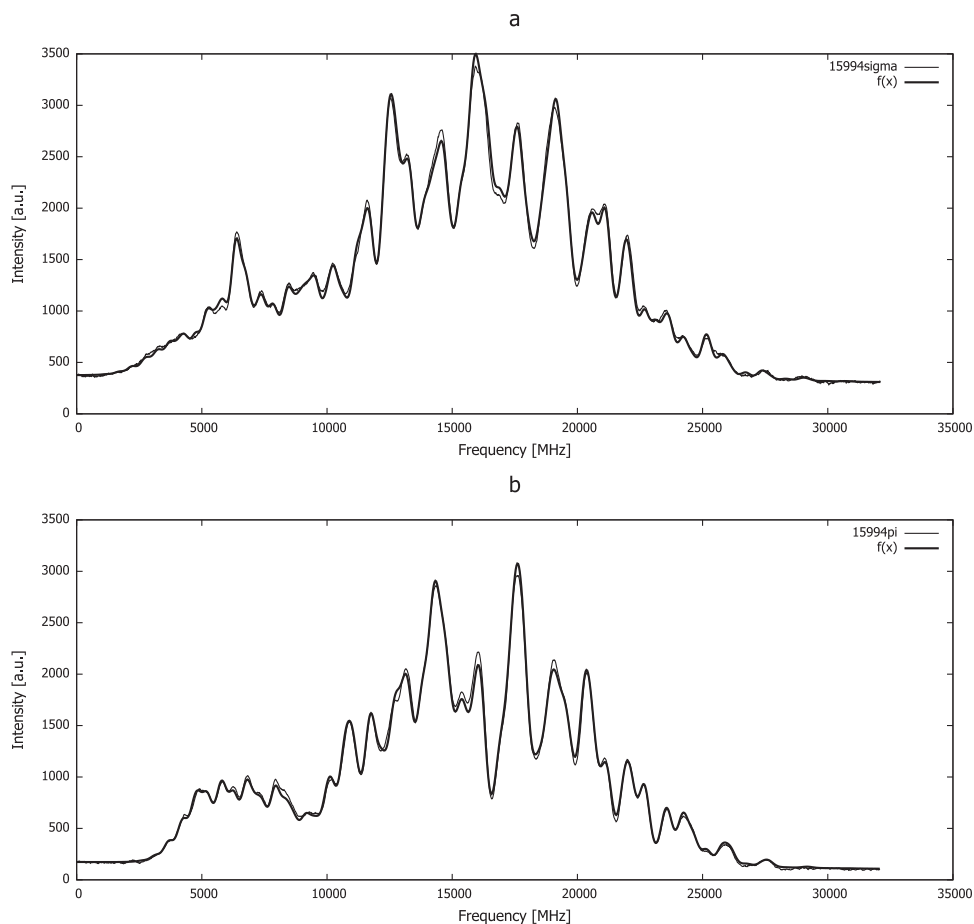


Fig. 4. Recorded *hfs* and Zeeman-*hfs* patterns of the spectral line $\lambda = 625.044$ nm in the europium atom (Table 1, No 34), along with the least-squares fitted curves for the a) polarization σ at the magnetic field strength 605.7(8)G and b) polarization π at the magnetic field strength 607.9(9)G.

the basis of a linear tunable stabilised laser CR 599-21 was applied. This laser was operated on the DCM dye solution and was optically pumped by a frequency-doubled Nd:YVO₄ laser (Coherent, Verdi V-10). In the range 568–612 nm the light source was a modified ring laser CR 699-21 operated on Rhodamine 6G, with the same pump laser. The range 545–559 nm was achieved with a modified CR 699-21 laser with the use of two dyes: Coumarin 498 and Pyrromethane 556, which constituted an energy transfer system, with the former dye as the donor and the latter as the acceptor [17]. The pump laser was a semiconductor laser emitting a wavelength 445 nm (Lasever Inc., China, model LSR445SD-4W). Finally, in the wavelength range 511–530 nm a modified CR 699-21 laser operated on the dye Coumarin 498 was used [18], optically pumped by the same semiconductor laser. Tuning of the laser to the wavelength of the spectral line investigated was accomplished on the basis of the wavemeter readings (Burleigh, WA-1500), while for the monitoring of the single mode operation a mode analyzer was used. In order to create a frequency scale for the scans, along with the laser induced fluorescence signal also the transmission signal of a temperature stabilized FP interferometer with FSR = 1499 MHz was recorded.

Precise resolution of the Zeeman σ and π components requires an ideally linear light polarization. Since the elements steering the laser beam towards the hollow cathode lamp introduce some elliptical polarization, even though the original polarization at the laser exit is linear, in front of the lamp a polarizer was inserted, which restored the linear polarization, and further a polarization rotator was placed, which enabled a smooth regulation of the an-

gle between the polarization plane and the direction of the magnetic flux.

For the purpose of obtaining of free europium atoms the same hollow cathode lamp was applied as in our earlier works concerning investigations of the hyperfine structure of europium and other lanthanides with the method of laser induced fluorescence [1,19–21]. The only essential difference consisted in an additional placement of neodymium magnets, serving for magnetic field creation, in the container for liquid nitrogen (used as coolant for the discharge). The magnets were positioned above the hollow cathode in closest to the discharge center. Preliminary measurements with a Hall probe indicated that the magnetic flux in the discharge center amounts ca. 600 G, which was later confirmed by the Zeeman effect measurements.

Part of the measurement system dedicated to recording of the laser induced fluorescence signal was also very similar to the one used earlier. The fluorescence light was directed to the entrance slit of a grating monochromator SPM-2 through a system of mirrors, lenses and filters. The monochromator was set to the specific (in most cases the strongest) fluorescence channel from the upper level of the transition under study. Behind the exit slit of the monochromator a photomultiplier (Hamamatsu R-375) with preamplifier was placed; its signal was directed to a phase-sensitive amplifier (an amplitude modulation of the exciting beam was applied). The scan recording was accomplished by a computer code, which controlled the scanning of laser frequency and stored the signals from an A/D converter. The code allows recording of over 16,000 measurement points per channel. However, due

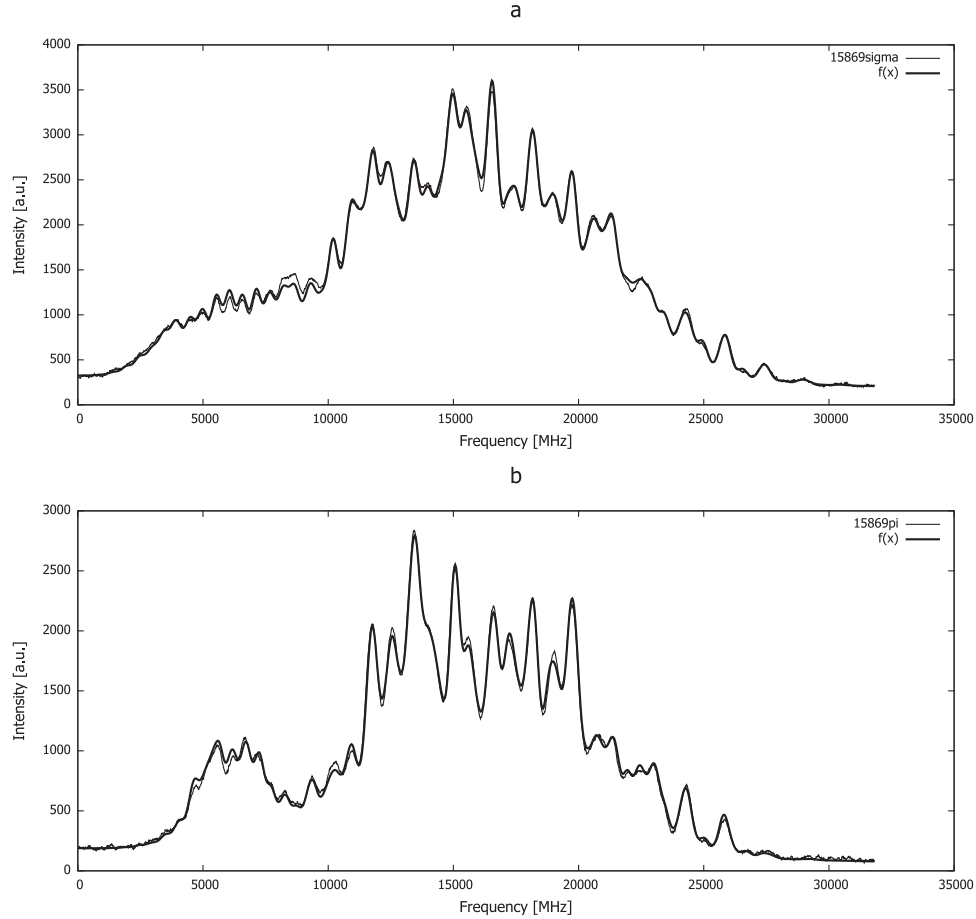


Fig. 5. Recorded *hfs* and Zeeman-*hfs* patterns of the spectral line $\lambda = 629.975$ nm in the europium atom (Table 1, No 37), along with the least-squares fitted curves for the a) polarization σ at the magnetic field strength 607.5(8)G and b) polarization π at the magnetic field strength 609.8(1.2)G.

to severe limitation of the data evaluation speed because of the very large number of Zeeman components, it proved reasonable to record only up to 4096 points.

A fundamental issue in calculation of the Landé factors is the determination and monitoring of the magnetic flux. The influence of the magnetic field on the relative positions of the Zeeman components is strictly correlated with the g_j values, thus these quantities should not be fitted simultaneously. It is also hard to assume that the magnetic field remains constant during the course of measurements. Since the field is nonuniform, even an incremental change of the direction of the beam path through the hollow cathode, e.g. due to the realignment of the laser beam, may cause a change of the magnetic field. For the same reason the field for the vertical and horizontal polarization of the beam may not be the same, due to the change of the beam direction under rotation of the polarization rotator. Preliminary measurements indicated that the changes of the magnetic field related with the above mentioned factors can reach ca. 1%. Much larger changes, up to 7–8%, are observed when the magnets creating the field are removed and re-inserted, or when the beam from another laser is applied. Because of these changes some standard for magnetic field measurement is indispensable. In the case of this work the spectral lines of argon (the buffer gas used in the discharge), with g_j values for both the lower and the upper level known from the literature, served as such standard, see Fig. 1.

The first step in preparation of the recorded scans for the calculations of g_j factors was averaging of groups of 3–4 subsequent scans. This procedure, due to the noise reduction, reduced the calculation time in the least-squares fitting procedure when fit-

ting the theoretical patterns to the spectra recorded. The next step was supplementation of the frequency scale on the basis of the recorded frequency marker (FP interferometer) signal. For this purpose the program “Fitter” [22], routinely used for calculation of hyperfine structure constants, was applied. As a result the files were obtained, where the abscissa consists of points equally spaced in frequency, while the ordinates were normalized laser induced fluorescence intensities. In further evaluation two programs developed in our research group, dedicated for calculations of g_j factors, were applied. The first program, written in FORTRAN, serves for generation of the parametrized function describing the hyperfine structure of a spectral line, split in the magnetic field. The second program, constituting a macro of the program GNUPLLOT, is dedicated to the fit of the parameters’ values with the Marquardt method [23].

3. Determination of g_j values

3.1. Hyperfine structure and Zeeman splitting

The hyperfine structure (*hfs*) atomic states $|\gamma J I F\rangle$ are obtained by diagonalization of H_{hfs} Hamiltonian [24]:

$$H_{hfs} = A \frac{C}{2} + B \frac{\frac{3}{4}C(C+1) - I(I+1)J(J+1)}{2I(2I-1)J(2J-1)}, \quad (1)$$

where $C = F(F+1) - J(J+1) - I(I+1)$ and A, B are the magnetic-dipole and the electric-quadrupole *hfs* constants, respectively.

The probability of the electric-dipole transition between the hyperfine structure sublevels F and F' can be expressed as [24]:

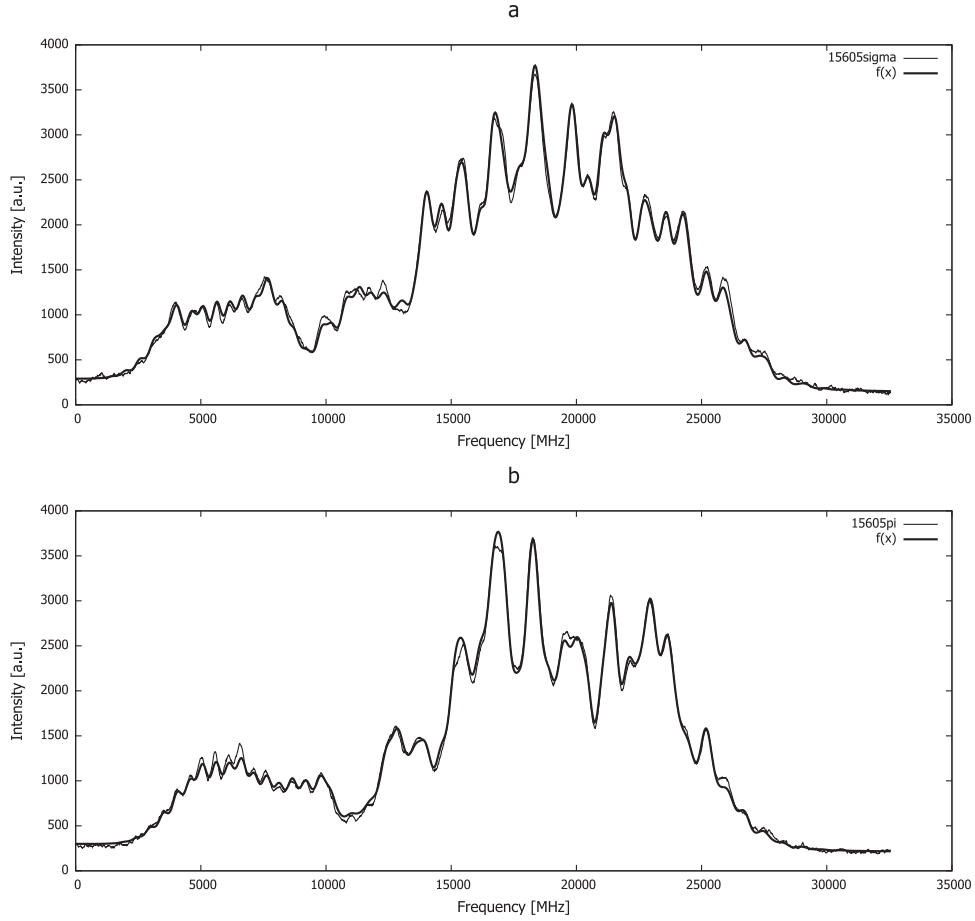


Fig. 6. Recorded *hfs* and Zeeman-*hfs* patterns of the spectral line $\lambda = 640.611$ nm in the europium atom (Table 1, No 45), along with the least-squares fitted curves for the a) polarization σ at the magnetic field strength 606.9(6)G and b) polarization π at the magnetic field strength 608.2(9)G.

$$A_{FF'} \propto (2F+1)(2F'+1) \begin{Bmatrix} J & I & F \\ F' & 1 & J \end{Bmatrix} S_{\gamma J, \gamma' J'}, \quad (2)$$

where $S_{\gamma J, \gamma' J'} = |\langle \gamma J \| \mathbf{P}^1 \| \gamma' J' \rangle|^2$ is the electric-dipole line strength.

In the presence of external magnetic field H_{mag} , when F ceases to be a good quantum number, the atomic eigenstates can be expressed as linear combinations of the form:

$$|\psi M_F\rangle = \sum_F C_{M_F F} |\gamma J F M_F\rangle, \quad (3)$$

and the eigenvector amplitudes $C_{M_F F}$ can be determined by diagonalization of the Hamiltonian matrix [25]:

$$H_{FM_F, F'M_F} = \delta_{FF'} \left(A \frac{C}{2} + B \frac{\frac{3}{4}C(C+1) - I(I+1)J(J+1)}{2I(2I-1)J(2J-1)} \right) + \mu_B g_J H_{mag} (-1)^{F-M_F+J+I+F'+1} \times \sqrt{(2F+1)(2F'+1)J(J+1)(2J+1)} \times \begin{pmatrix} F & 1 & F' \\ -M_F & 0 & M_F \end{pmatrix} \begin{Bmatrix} F & 1 & F' \\ J & I & J \end{Bmatrix}, \quad (4)$$

where μ_B is the Bohr magneton and g_J is the Landé factor.

The observed line intensity of an individual Zeeman component is proportional to the transition probability between two Zeeman sublevels M_F [26]:

$$A_{FM_F, F'M_F} \propto S_{\gamma J, \gamma' J'} \sum_{qFF'} |C_{M_F F} S_{qFF'} C_{M_F' F'}|^2, \quad (5)$$

where $S_{qFF'}$ is the line strength between pure $|FM_F\rangle$ and $|F'M_F'\rangle$ states :

$$S_{qFF'} = (-1)^{F-M_F+J+I+F'+1} \sqrt{(2F+1)(2F'+1)} \times \begin{pmatrix} F & 1 & F' \\ -M_F & q & M_F' \end{pmatrix} \begin{Bmatrix} J & I & F \\ F' & 1 & J \end{Bmatrix}, \quad (6)$$

and $q = M_F - M_F'$ takes values 0 and ± 1 for σ and π transitions, respectively.

The observed line shape is a combination of individual Zeeman components modified by the radiative broadening and instrumental effects.

3.2. Computational procedure

In the first step of the computational procedure, the energy values of Zeeman sublevels, relative to the fine structure level energies $E(J)$, for the upper and lower levels of the transition under consideration, are determined by means of diagonalization of Hamiltonian expressed by Eq. (4). The necessary input data, concerning values of the magnetic field H_{mag} , nuclear spin I , J quantum numbers, the hyperfine structure A and B constants and the initial values of Landé g_j factors for the two energy levels involved, are loaded from the input file.

After obtaining the eigenvalues and eigenvectors, the relative positions in frequency scale and intensities of all the individual Zeeman components are determined with the use of Eqs. (5) and (6), separately for σ and π transitions.

Then the form of the intensity distribution function is determined as a sum of intensities for each abscissa value of the final

Table 1

Spectral lines of the europium atom experimentally investigated in this work for the purpose of determination of the Landé g_j factors. For all lines the g_j factor of the lower odd-parity level was determined, and the respective g_j factors for the upper even-parity levels were fixed at the literature values [3]. In some cases also the g_j factors for the upper even-parity levels were determined independently.

No	Line			Lower level					Upper level			
	λ_{air} (nm)	relative intensity	k_{vac} (cm^{-1})	E (cm^{-1})	J	$g_{J,\pi}$	$g_{J,\sigma}$	$g_{J,average}$	E (cm^{-1})	J	g_j	$g_{J,fit}$ [2,3]
1	2	3	4	5	6	7	8	9	10	11	12	13
1	511.434	170	19547.41	13048.90	7/2	2.0987(12)	2.085(13)	2.0913(67)	32596.31	9/2		1.93(1)
2	513.348	210	19474.53	12923.72	5/2	2.5549(59)	2.5487(82)	2.5511(31)	32398.25	7/2		2.195(1)
3	516.005	270	19374.27	13222.04	9/2	1.870(11)	1.882(12)	1.8759(62)	32596.31	9/2		1.93(1)
4	516.669	210	19349.35	13048.90	7/2	2.0757(49)	2.0917(68)	2.0837(79)	32398.25	7/2		2.195(1)
5	517.639		19313.11	15248.76	5/2	2.038(51)	2.029(51)	2.0336(43)	34561.87	7/2	1.915(5)	1.91(5)
6	521.334		19176.21	13222.04	9/2	1.8718(45)	1.8742(60)	1.8731(12)	32398.25	7/2		2.195(1)
7	522.304		19140.62	15421.25	7/2	1.797(51)	1.777(51)	1.787(10)	34561.87	7/2	1.904(33)	1.91(5)
8	522.345	300	19139.10	13457.21	11/2	1.749(11)	1.755(12)	1.7520(27)	32596.31	9/2		1.93(1)
9	522.437		19135.75	13048.90	7/2	2.0907(53)	2.0890(70)	2.0898(87)	32184.65	9/2		1.615(2)
10	523.926	120	19081.35	13048.90	7/2	2.1035(53)	2.0905(72)	2.0970(64)	32130.25	9/2		1.747(2)
11	527.207	390	18962.61	13222.04	9/2	1.8727(48)	1.8729(63)	1.8728(12)	32184.65	9/2		1.615(2)
12	528.724	55	18908.21	13222.04	9/2	1.8691(48)	1.8779(63)	1.8735(44)	32130.25	9/2		1.747(2)
13	529.469		18881.59	15680.28	9/2	1.675(51)	1.682(51)	1.6784(32)	34561.87	7/2	1.930(4)	1.91(5)
14	545.152	380	18338.42	13778.68	13/2	1.683(52)	1.679(51)	1.6785(54)	32117.10	13/2	1.671(2)	
15	545.292	260	18333.71	13048.90	7/2	2.094(11)	2.0860(73)	2.0891(38)	31382.61	9/2		1.860(2)
16	548.864	120	18214.39	12923.72	5/2	2.572(14)	2.5511(92)	2.560(11)	31138.11	7/2		2.006(5)
17	549.520	45	18192.66	12923.72	5/2	2.558(14)	2.566(11)	2.5626(41)	31116.38	7/2		1.928(5)
18	554.743	200	18021.35	12923.72	5/2	2.583(42)	2.569(41)	2.5759(68)	30945.07	5/2		2.49(4)
19	557.034		17947.25	13778.68	13/2	1.710(11)	1.7015(72)	1.7048(41)	31725.93	11/2	1.746(4)	
20	557.713	200	17925.40	13457.21	11/2	1.7684(88)	1.7554(59)	1.7606(64)	31382.61	9/2		1.860(2)
21	558.003	120	17916.07	13222.04	9/2	1.890(12)	1.8737(76)	1.8802(81)	31138.11	7/2		2.006(5)
22	558.624	90	17896.17	13048.90	7/2	2.101(42)	2.102(41)	2.1018(41)	30945.07	5/2		2.49(4)
23	567.381	60	17619.95	13222.04	9/2	1.858(16)	1.869(14)	1.8643(55)	30841.99	7/2		1.824(3)
24	573.083	60	17444.63	13457.21	11/2	1.746(15)	1.756(13)	1.7514(50)	30901.84	9/2		1.706(2)
25	573.899	60	17419.85	19447.19	11/2	1.629(15)	1.635(12)	1.6323(27)	36867.04	11/2		1.662(3)
26	580.028	60	17235.78	19631.26	9/2	1.693(15)	1.647(13)	1.668(23)	36867.04	11/2		1.662(3)
27	584.577	27	17101.64	19447.19	11/2	1.630(15)	1.636(13)	1.6329(31)	36548.83	9/2		1.810(5)
28	586.094	27	17057.37	19447.19	11/2	1.565(14)	1.585(12)	1.5758(97)	36504.56	9/2	1.770(6)	1.719(2)
29	595.342	27	16792.41	19712.15	7/2	1.762(16)	1.735(13)	1.747(14)	36504.56	9/2	1.782(17)	1.719(2)
30	597.274	170	16738.10	15680.28	9/2	1.6848(38)	1.6805(36)	1.6846(25)	32418.38	11/2	1.571(4)	
31	599.283	240	16681.98	16079.76	11/2	1.636(54)	1.635(53)	1.6359(53)	32761.74	13/2	1.560(2)	
32	611.877	120	16338.62	16079.76	11/2	1.636(14)	1.639(12)	1.6377(13)	32418.38	11/2	1.571(2)	
33	619.506	140	16137.42	13048.90	7/2	2.099(31)	2.077(31)	2.088(11)	29186.32	9/2	1.744(1)	1.70(3)
34	625.044	55	15994.45	12923.72	5/2	2.5636(51)	2.5574(33)	2.5599(31)	28918.17	7/2		1.841(2)
35	626.225	240	15964.28	13222.04	9/2	1.888(31)	1.874(31)	1.8809(67)	29186.32	9/2	1.736(2)	1.70(3)
36	628.594	15	15904.11	12923.72	5/2	2.5629(46)	2.5644(38)	2.5637(72)	28827.83	7/2		1.811(1)
37	629.975	170	15869.27	13048.90	7/2	2.0859(42)	2.0885(28)	2.0874(13)	28918.17	7/2		1.841(2)
38	633.581	75	15778.93	13048.90	7/2	2.0885(38)	2.0898(23)	2.0893(62)	28827.83	7/2		1.811(1)
39	635.000	120	15743.67	12923.72	5/2	2.5579(46)	2.5515(26)	2.5538(32)	28667.39	5/2		2.194(1)
40	635.588	60	15729.11	13457.21	11/2	1.7526(12)	1.7555(6)	1.7536(12)	29186.32	9/2	1.734(2)	1.70(3)
41	636.924	60	15696.13	13222.04	9/2	1.8725(42)	1.8747(28)	1.8738(11)	28918.17	7/2		1.841(2)
42	638.271	55	15662.99	15137.72	3/2	2.763(12)	2.789(11)	2.776(13)	30800.71	3/2		2.80(1)
43	638.379	75	15660.34	15137.72	3/2	2.804(12)	2.795(11)	2.7992(45)	30798.06	5/2		2.14(1)
44	640.090	120	15618.49	13048.90	7/2	2.0853(38)	2.0895(22)	2.0880(21)	28667.39	5/2		2.194(1)
45	640.611	40	15605.79	13222.04	9/2	1.8722(36)	1.8783(21)	1.8760(30)	28827.83	7/2		1.811(1)
46	641.127	140	15593.23	15248.76	5/2	2.0358(48)	2.0274(38)	2.0311(42)	30841.99	7/2		1.824(3)
47	642.828	55	15551.95	15248.76	5/2	2.044(11)	2.038(11)	2.0410(29)	30800.71	3/2		2.80(1)
48	645.792	120	15480.59	15421.25	7/2	1.7946(38)	1.8027(27)	1.7993(40)	30901.84	9/2		1.706(2)
49	648.298	18	15420.74	15421.25	7/2	1.7951(44)	1.7937(37)	1.7944(67)	30841.99	7/2		1.824(3)
50	653.900		15288.63	19273.24	9/2	1.577(51)	1.586(51)	1.5812(45)	34561.87	7/2	1.933(2)	1.91(5)
51	656.781	75	15221.56	15680.28	9/2	1.6873(36)	1.6893(27)	1.6885(10)	30901.84	9/2		1.706(2)
52	657.827		15197.37	19364.50	7/2	1.624(51)	1.635(51)	1.6293(53)	34561.87	7/2	1.933(5)	1.91(5)
53	659.374	45	15161.71	15680.28	9/2	1.6790(43)	1.6827(34)	1.6810(19)	30841.99	7/2		1.824(3)
54	662.077		15099.82	19462.05	5/2	1.703(51)	1.710(51)	1.7068(33)	34561.87	7/2	1.931(6)	1.91(5)

pattern, using estimated values for the splitting constants and line profile parameters. In the iterative procedure, this function is fitted to the experimentally observed line profile stored in the digital form, where values of Landé g_j factors for the upper and lower levels serve as adjustable parameters. In this procedure, the Marquardt's algorithm [23] is applied. It is also possible to fine-tune the values of hfs constants, which is particularly important in cases where these constants are determined with significant measurement uncertainties.

In order to include saturation effects, an additional parameter A_s (saturation rate) was introduced in the fitting procedure. The calculated decay rate of each Zeeman component (A_ν) of frequency ν was modified in accordance with the following expression [16]:

$$A_\nu^{sat} = \frac{A_\nu}{1 + A_\nu/A_s} \tag{7}$$

A version of the program that allows the analysis of overlapping spectra originated from two isotopes, was also developed.

Table 2
Literature values [1,27] of the hyperfine structure constants A and B and residual isotope shifts for the electronic levels of the europium atom involved in the Zeeman- h_f s investigations within this work.

No	E (cm^{-1})	J	$A(^{151}\text{Eu})$ (MHz)	$B(^{151}\text{Eu})$ (MHz)	$A(^{153}\text{Eu})$ (MHz)	$B(^{153}\text{Eu})$ (MHz)	RIS (MHz)
1	2	3	4	5	6	7	8
odd-parity							
1	12923.72	5/2	1201.93	109.5	534.54	279	-4375
2	13048.90	7/2	906.1	-190.4	402.7	-486	-4359
3	13222.04	9/2	770.2	-185.8	342.27	-474	-4338
4	13457.21	11/2	696.99	1	308.76	3	-4308
5	13778.68	13/2	644.21	286	286.23	730	-4274
6	15137.72	3/2	-1825.6	65.4	-810.8	167	-4795
7	15248.76	5/2	-959.3	-197.6	-424.8	-504	-4780
8	15421.25	7/2	-671.3	-157	-298.03	-401	-4764
9	15680.28	9/2	-538.1	28	-239.69	71	-4728
10	16079.76	11/2	-454.2	296	-202.43	755	-4667
11	19273.24	9/2	76.8	198	33.87	505	-4355
12	19364.50	7/2	242.8	-42	107.07	-107	-4339
13	19447.19	11/2	691.17	292.5	306.81	746	-4713
14	19462.05	5/2	323.8	-103	142.8	-263	-4323
15	19631.26	9/2	40.58	63.5	17.98	162	-4651
16	19712.15	7/2	-41.4	-97.5	-18.25	-249	-4651
even-parity							
1	28667.39	5/2	-194.44	-243.3	-86.84	-621	-7583
2	28827.83	7/2	-8.10	165.3	-3.7	421	843
3	28918.17	7/2	-19.24	-41.8	-8.43	-107	-2494
4	29186.32	9/2	48.75	-237.5	21.25	-606	-7610
5	30798.06	5/2	-304.85	80.74	-136.04	206	-7714
6	30800.71	3/2	-654.63	-16.16	-290.07	-41	-7898
7	30841.99	7/2	-141.2	17.3	-62.4	44	-7452
8	30901.84	9/2	-83.76	-15.3	-37.47	-39	-7722
9	30945.07	5/2	-235.64	-39.59	-103.95	-101	-7155
10	31116.38	7/2	153.2	36	67.6	92	762
11	31138.11	7/2	-10.2	39	-2.9	100	-3502
12	31382.61	9/2	-48.14	48.2	-21.46	123	-7417
13	31725.81	9/2	-28.0	104.1	-12.4	266	-7584
14	32117.10	13/2	13.04	81.7	5.56	208	-7738
15	32130.25	9/2	420.9	-153	185.6	-390	1356
16	32184.65	9/2	98.12	-42.1	43.8	-107	-5731
17	32398.25	7/2	146.15	99	65.2	253	-6422
18	32418.38	11/2	73.89	40.3	33.12	103	-6070
19	32596.31	9/2	167.18	-225	74.22	-574	-6008
20	32761.74	13/2	-2	486.3	-0.36	1241	-7583
21	32948.41	11/2	180.46	95.6	80.38	244	-6601
22	34561.87	7/2	836.4	-109	373	-278	-3134
23	36504.56	9/2	314.81	40	138.8	102	-3609
24	36548.83	9/2	242.85	32	107.1	82	-2633
25	36867.04	11/2	276.3	16	122.59	41	-5478

4. Results

Altogether 54 spectral lines were investigated for the determination of Landé factors of the electronic levels of the europium atom. All the lines were presented in Table 1. In order to assure an appropriate precision and reliability of the results, several criteria were taken into account in selection of the lines:

1. the relative line intensity should not be too low - it concerned in particular the lines from the spectral ranges, where the available power of the exciting laser was the lowest (wavelengths below 565 nm),
2. the upper level should possess a g_j factor value known from the literature, with an experimental uncertainty of the order of 0.001 whenever possible,
3. at least one strong fluorescence channel from the upper level to a lower level with the energy differing from that of the start level by at least 20 cm^{-1} should be available,
4. the hyperfine structure constants A and B of both the lower and the upper level should be known from the literature with sufficiently high accuracy - ca. 0.3 MHz for the constant A and ca. 3 MHz for the constants B ,

5. the total hyperfine splitting of the line should not be smaller than 10 GHz.

All the above mentioned criteria have influence on either the signal-to-noise ratio or the precision of the calculated g_j factors.

As can be seen from Table 1, not all the criteria could be met. For instance, for some part of the lines no specified intensities were available in the spectral lines databases. For some of the lines the g_j factors of the upper levels were known from the literature with accuracies only of the order of 0.05, and for some lines the upper level g_j factors were unknown. A similar situation was encountered concerning the fluorescence channels - in some cases they were weak. However, we decided to retain the respective spectral lines with the expectation that their measurement might yield some essential information, in particular in the cases, where the lines nevertheless constituted the best available choice for the lower levels under study. The largest numbers of suitable lines (7–10) were found for 3 lowest-lying levels. The measurements of g_j factors of these levels were considered to be a test of both the experimental setup and the software.

For all the lines 10–15 scans for each polarization were recorded. The scans were averaged in the groups of 3–4 subsequent scans with the use of the program Origin. Then the values

Table 3

Values of the Landé g_j factors of the electronic levels of the europium atom, determined from the measurements of the Zeeman effect in the hyperfine structure, as well as theoretically predicted [8,9].

No	E(cm ⁻¹)	J	(No Lines)	g_{jmean}	g_{jlit} [3]	g_{jpred} [8]	g_{jpred} [9]
1	2	3	4	5	6	7	8
odd-parity							
1	12923.72	5/2	7	2.5611(24)		2.571	2.555
2	13048.90	7/2	10	2.0934(21)		2.094	2.082
3	13222.04	9/2	9	1.8731(7)		1.878	1.868
4	13457.21	11/2	4	1.7557(12)		1.761	1.754
5	13778.68	13/2	2	1.6935(14)		1.692	1.687
6	15137.72	3/2	2	2.793(11)		2.797	2.773
7	15248.76	5/2	3	2.0361(32)		2.054	2.039
8	15421.25	7/2	3	1.7946(18)		1.807	1.795
9	15680.28	9/2	3	1.6846(24)		1.695	1.685
10	16079.76	11/2	2	1.6347(8)		1.636	1.63
11	19273.24	9/2	1	1.5812(45)		1.561	1.58
12	19364.50	7/2	1	1.6293(53)		1.596	1.634
13	19447.19	11/2	3	1.625(14)		1.637	1.631
14	19462.05	5/2	1	1.7068(33)		1.670	1.727
15	19631.26	9/2	1	1.668(23)		1.694	1.665
16	19712.15	7/2	1	1.747(14)		1.803	1.756
even-parity							
1	29186.32	9/2	3	1.7368(15)	1.70(3)	1.749	
2	31725.81	9/2	1	1.7462(38)		1.735	
3	32117.10	13/2	1	1.6708(20)		1.635	
4	32418.38	11/2	2	1.5707(16)		1.591	
5	32761.74	13/2	1	1.5602(24)		1.597	
6	34561.87	7/2	6	1.9239(52)	1.91(5)		
7	36504.56	9/2	2	1.7728(64)	1.719(2)		

of g_j factors for the lower levels, or for both the lower and the upper levels, wherever required, were calculated with the method described in the preceding section. Even though the program allows for calculation of the hyperfine structure constants and the isotope shifts, because of the very large number of the components and the limited computing power we abandoned this possibility, regarding the values known from the literature [1,27] presented in Table 2 as sufficiently precise. Initial value of the magnetic flux was calculated on the basis of the measurements of the Zeeman effect for the argon lines (an example of the spectrum is presented in Fig. 1). As expected, the magnetic flux in the case of the change of the laser light source, laser beam re-alignment, or removing and re-inserting the magnets, varied within the range 586–628 G.

Examples of the recorded spectra for the europium atom without the magnetic field, as well as with magnetic field for both σ and π polarizations, are presented in Figs. 2–6. The g_j values of the lower levels for both polarization directions and the mean values are listed in Table 1. These values are the averages of the ones obtained for individual groups of scans. The experimental uncertainties were calculated according to the formula:

$$\Delta g_{jL} = \sqrt{(SD)^2 + (\Delta g_{jU})^2 + (\Delta B/B * g_{jL})^2} \quad (8)$$

where SD is the mean standard deviation for g_{jL} obtained from the individual groups of scans, Δg_{jU} is the uncertainty of the g_j value of the upper level, and the last term represents the estimation of the influence of the magnetic flux uncertainty.

The averaged g_j values for the particular levels were compiled in Table 3. In this case the experimental uncertainty was taken as the standard deviation of the weighted mean. Apart from the g_j factors for the lower levels belonging to the odd-parity configurations of the europium atom, also the g_j values for 4 levels belonging to the even-parity configurations were determined for the first time. These values were also included in Table 3. Moreover, it proved that for 3 levels the values of g_j factors quoted in the work [2] required correction. In the case of the levels 29186.32 cm⁻¹ and 34561.87 cm⁻¹ the corrections fall within the experimental uncertainties given in Smith's work, while in the case of the level 36504.56 cm⁻¹ it is likely that a misprint occurred in [2], since the

corrected value would be close to the literature one if the last two digits were reversed.

5. Discussion

Results presented in this work are the first published results of the measurements of the g_j factors obtained with the method of investigation of the Zeeman effect in the hyperfine structure for an element possessing more than one odd isotope. The presence of two isotopes increases the computation time, but does not essentially influence the accuracy.

The main factors determining the accuracy of the results include the accuracy of the g_j values of the upper levels involved in the transitions studied, as well as the temporal stability of the magnetic flux. A very important issue is to avoid saturation of the laser induced fluorescence signal. Introducing the factor described by Eq. (3.2) allows accounting for the saturation effect, but it is strictly valid for a two-level system only, while in europium usually multi-level systems are encountered. Thus, in the case of strong saturation, a correction introduced by Eq. (3.2) is not sufficient.

Another effect impairing the accuracy of the calculations is the presence of the "minority" components, i.e. the components σ and vice versa. This effect results from the imperfect parameters of the polarizer and the polarization rotator. Every system has a limited contrast, i.e. it transmits some light with polarization which should be blocked. In the case of strong spectral lines and strong exciting laser beams transmission of ca. 0.1% of parasitic light is sufficient for the "minority" components to be observed.

In Table 3, apart from the experimental results, also the g_j values predicted by semi-empirical calculations by Smith [8] and Wyart [9] are presented. As can be seen, the experimental values usually fall between the ones predicted in two models. Somewhat better consistency with the Wyart's results can be observed, which is not unexpected because of taking into account of the higher cores and more configurations in Wyart's work [9].

6. Conclusions

In this work results of the determinations of Landé g_J factors for 20 electronic levels of the europium atom are presented, including 16 levels belonging to the odd-parity configurations and 4 levels belonging to the even-parity configurations. Moreover, g_J values for 3 levels belonging to the even-parity configurations were corrected. All the results were obtained for the first time. The values are close to those predicted by the semi-empirical calculations, but generally deviate from them by more than the experimental uncertainty limits. It was proved that the method of investigation of the Zeeman effect in the hyperfine structure can be applied not only to the elements with one stable isotope, but also to those which possess more odd isotope.

Declaration of Competing Interest

The authors declare that they have no known competing financial interests or personal relationships that could have appeared to influence the work reported in this paper.

CRedit authorship contribution statement

B. Furmann: Conceptualization, Investigation, Formal analysis, Writing - original draft, Visualization, Supervision, Funding acquisition. **J. Ruczkowski:** Conceptualization, Software, Writing - original draft. **M. Chomski:** Investigation, Formal analysis. **M. Suski:** Investigation, Formal analysis. **S. Wilman:** Investigation, Formal analysis. **D. Stefańska:** Investigation, Writing - review & editing.

Acknowledgments

The authors would like to express their gratitude to Dr. Sci. Magdalena Elantkowska for her valuable remarks concerning the development of the software for g_J factors' calculation, as well as Dr. Andrzej Krzykowski and Dr. Eng. Semir El-Ahmar for their expert help in realization of the technical part of the work. Dr. Sławomir Werbowy from the University of Gdańsk is greatly acknowledged for his essential contribution to the transfer of the idea of measuring the Zeeman effect of the hyperfine structure to our group.

Financial support of this work by the Ministry of Science and Higher Education, Poland within the projects realized at [Poznan University of Technology: 0511/SBAD/2053](#) at Faculty of Materials Engineering and Technical Physics, (B.F., M.C., M.S., S.W. and D.S.) and [0214/SBAD/0219](#) at Institute of Robotics and Machine Intelligence (J.R.) is greatly acknowledged.

References

- [1] Furmann B, Chomski M, Suski M, Wilman S, Stefańska D. Investigations of the hyperfine structure and isotope shifts in the even-parity level system of atomic europium. *J Quant Spectrosc Radiat Transf* 2020;251:107070. doi:10.1016/j.jqsrt.2020.107070.
- [2] Smith G, Tomkins FS, Stephen GWR. The absorption spectrum of europium. *Phil Trans R Soc A* 1976;283:345–65. doi:10.1098/rsta.1976.0089.

- [3] Martin WC, Zalubas R, Hagan L. Atomic energy levels - The rare-earth elements. NSRDS-NBS, vol. 60. U.S. Department of Commerce, National Bureau of Standards; 1978. <https://nvlpubs.nist.gov/nistpubs/Legacy/NSRDS/nbsnsrds60.pdf>
- [4] Kramida A, Ralchenko Yu, Reader J, NIST ASD Team. NIST Atomic spectra database (ver. 5.7.1). In: National institute of standards and technology, Gaithersburg, MD; 2019. [Online]. Available: [https://physics.nist.gov/asd\[2020, July 23\]](https://physics.nist.gov/asd[2020, July 23])
- [5] Fechner B, Rinkliff R-H, Steudel A. Magnetic field-induced $\Delta F = \pm 2, 3, 4$ transitions in the Eu I-spectrum. *Z Phys D* 1987;7(2):125–8. doi:10.1007/BF01384576.
- [6] Mei GH, Zhong D, Tan YF, Zhu XW. $\Delta F = 2-6$ transitions in the hyperfine spectrum of $\lambda = 601.8$ nm line of ^{151}Eu . *Z Phys D* 1997;39:115–19. doi:10.1007/s004600050117.
- [7] Jin W-G, Endo T, Wakui T, Uematsu H, Katsuragawa H. Measurements of the hyperfine structure and $\Delta F = +2$ transitions in Eu I by high-resolution diode-laser spectroscopy. *J Phys Soc Jpn* 2002;71(8):1905–9. doi:10.1143/JPSJ.71.1905.
- [8] Smith G, Wybourne BG. Energy levels of the first spectrum of europium (Eu I). *J Opt Soc Am* 1965;55:121–5. doi:10.1364/JOSA.55.000121.
- [9] Wyart JF. Interprétation paramétrique des configurations impaires de l'europium (Eu I). *Phys Scr* 1985;32(1):58–63. doi:10.1088/0031-8949/32/1/007.
- [10] Stachowska E, Elantkowska M, Ruczkowski J, Dembczynski J. Reanalysis and semi-empirical predictions of the hyperfine structure of Eu I in the odd parity multiconfiguration system. *Phys Scr* 2002;65:237–47. doi:10.1238/physica.regular.065a00237.
- [11] Inoue R, Miyazawa Y, Kozuma M. Magneto-optical trapping of optically pumped metastable europium. *Phys Rev A* 2018;97:061607. doi:10.1103/PhysRevA.97.061607.
- [12] Sobolewski Ł M, Windholz L, Kwela J. Laser induced fluorescence spectroscopy used for the investigation of Lande g_J - factors of praseodymium energy levels. *J Quant Spectrosc Radiat Transf* 2017a;194:24–30. doi:10.1016/j.jqsrt.2017.03.021.
- [13] Sobolewski Ł M, Windholz L, Kwela J. Zeeman structure of red lines of lanthanum observed by laser spectroscopy methods. *J Quant Spectrosc Radiat Transf* 2017b;201:180–3. doi:10.1016/j.jqsrt.2017.07.013.
- [14] Sobolewski Ł M, Windholz L, Kwela J. Magnetic splitting of lines of Pr I. *J Quant Spectrosc Radiat Transf* 2018;219:399–404. doi:10.1016/j.jqsrt.2018.09.003.
- [15] Sobolewski Ł M, Windholz L, Kwela J. Laser spectroscopy used in the investigation of the Zeeman - hyperfine structure of vanadium. *J of Quant Spectrosc Radiat Transfer* 2020a;242:106769. doi:10.1016/j.jqsrt.2019.106769.
- [16] Sobolewski Ł M, Windholz L, Kwela J. Landé g_J - factors of Nb I levels determined by laser spectroscopy. *J Quant Spectrosc Radiat Transf* 2020b;249:107015. doi:10.1016/j.jqsrt.2020.107015.
- [17] Stefańska D, Suski M, Zygmunt A, Stachera J, Furmann B. Tunable single-mode cw energy-transfer dye laser directly optically pumped by a diode laser. *Opt and Laser Tech* 2019;120:105673. doi:10.1016/j.optlastec.2019.105673.
- [18] Stefańska D, Suski M, Furmann B. Tunable continuous wave single-mode dye laser directly pumped by a diode laser. *Laser Phys Lett* 2017;14(4):045701. doi:10.1088/1612-202X/aa5f00.
- [19] Furmann B, Stefańska D. Isotope shift and hyperfine structure in even configurations of neutral europium. *J Phys B* 2011;44:225005. doi:10.1088/0953-4075/44/22/225005.
- [20] Furmann B, Stefańska D. 6s electron screening in isotope shifts of configurations $4f^7 5d6s$, $4f^7 6s6d$ and $4f^7 6s7d$ in europium. *J Phys B* 2014a;47:085001. doi:10.1088/0953-4075/47/8/085001.
- [21] Furmann B, Stefańska D. Experimental verification of isotope shift and hyperfine structure of some even parity levels of neutral Eu. *Phys Scr* 2014b;89:095402. doi:10.1088/0031-8949/89/9/095402.
- [22] Guthöhrlein GH. Program package "Fitter". Hamburg: Universität der Bundeswehr, Helmut-Schmidt Universität; 1998.
- [23] Marquardt DW. An algorithm for least-squares estimation of nonlinear parameters. *J Soc Ind App Math* 1963;11(2):431–41. doi:10.1137/0111030.
- [24] Cowan RD. *The theory of atomic structure and spectra*. Berkeley: Berkeley University of California Press; 1981.
- [25] Grabowski D, Drozdowski R, Kwela J, Heldt J. Hyperfine structure and Zeeman effect studies in the $6p^7p-6p^7s$ transitions in Bi II. *Z Phys D* 1996;38. doi:10.1007/s004600050093.
- [26] Werbowy S, Kwela J, Drozdowski R, Heldt J. M1-E2 interference in the Zeeman effect of the 461.5 nm line of Bi I. *Eur Phys J D* 2006;39(1):5–12. doi:10.1140/epjd/e2006-00066-6.
- [27] Seifert P, Weber D-J, Kronfeldt H-D, Winkler R. Parametric analysis of the isotope shift and hyperfine structure in the Eu I configuration $4f^7 5d6s$. *Z Phys D* 1989;14:99–106. doi:10.1007/BF01399029.